Modelling climate change impacts on the water regimes of the river-wetland systems in the data-scarce transboundary Upper Meghna River Basin (Bangladesh and India)

A thesis submitted for the degree of Doctor of Philosophy at
University College London (UCL)

Mohammed Mizanur Rahman

Wetland Research Unit
UCL Department of Geography

October 2016

Declaration

I, Mohammed Mizanur Rahman, confirm that the work presented in this thesis is my own. Where information has been derived from other sources, I confirm that this has been indicated in the thesis with an appropriate reference.

Mohammed Mizanur Rahman
13 October 2016

Abstract

Many regions are likely to be increasingly exposed to water related problems due to climate change-driven modifications to the hydrological cycle. Flooding is the major long-term problem in the haor wetlands of the transboundary (Bangladesh and India) Upper Meghna River Basin (UMRB). Past studies of haor wetlands and changes due to climate change have provided conflicting results. Many studies either ignore the role of haors on local hydrology or do not correctly represent haor hydraulics.

In order to address the above issues, this study first develops a modified version of the Soil and Water Assessment Tool (SWAT) for riparian wetlands (SWATrw). This model better represents bidirectional hydraulic interactions between wetlands, rivers and aquifers. A case study for the comparatively data rich Hakaluki haor shows that SWATrw outperforms the original SWAT in the simulation of haor hydrology including flash flooding from adjacent rivers and the persistence of water through the dry season haor which is sustained by aquifers.

A SWATrw model for the entire UMRB is developed and manually calibrated and validated against 21 years (1990–2010) of observed streamflow and river stage at 18 gauging stations. The model is forced with projections from four CMIP5 GCMs for the RCP4.5 scenario. An improved Quantile Mapping (QM) based approach is developed to remove biases from raw GCM data as well as adjusting dry day (coldest day for temperature) frequency.

Compared to the baseline (1981–2000), monsoonal streamflows are projected to increase by up to 12% for 2021–2040 and 42% for 2061–2080. Dry season low flows decrease by as much as 58%. The average flooding risk in haors in April is likely to decrease which will likely benefit Boro rice cultivation. However, flooding risk in May is considerably higher compared to the baseline.

Acknowledgements

First, I would like to express my sincere gratitude to my principal supervisor Dr. Julian R. Thompson for his prudent guidance and academic supports in conducting this research work. At the culmination of four years intensive study when I look back my past time I realise how greatly he has stewarded me to be succeeded in accomplishing this tumultuous journey. This has academically owed me to him for the rest of my life. I would also like to acknowledge my co-supervisor Dr. Roger J. Flower for mentoring me with his long-term research experience on ecohydrology. I am grateful to both of them for their tremendous supports regarding academic writing with proper English usage.

At this stage, I would like to take the opportunity to acknowledge the contribution of Dr. Jon French who worked as an external examiner during my upgradation to PhD candidate status. The thesis has greatly benefitted from his valuable comments while assessing the upgrade report. I thank to Dr. Mohammad Shamsudduha for providing valuable suggestions and some important data. A number of PhD students (Mandy Robinson, Darryl Price, Miriam Fernandez-Nunez and Charlotte Wheeler) deserve heartiest thanks for sharing their academic experiences with me.

More importantly, without getting financial support from the prestigious Ted Hollis Scholarship in Wetland Hydrology and Conservation, it was not possible for me to study in the world renowned University College London (UCL).

Finally, I thank my wife Afroza Akter so much for understanding my situation and for her supports. Her patience throughout my PhD study would be an unforgettable memory in my life.

Table of contents

List of Figures

List of Tables

Chapter 1
Catchment hydrology and rationale of the study

1.1. Introduction

This introductory chapter first discusses the importance of catchment-scale hydrological modelling (Section 1.2) and then the rationale of the present study (Section 1.3). Section 1.3 chronologically provides a brief description of regional water characteristics with emphasising the socio-economic importance of the study area (Section 1.3.1) and existing water issues (Section 1.3.2). A critical review of previous research undertaken to address these issues is provided in Section 1.3.3. Section 1.3.4 identifies potential research gaps in the past studies and Section 1.4 presents the aims and objectives of the present study. Finally, Section 1.5 gives a brief description of research design adopted for this study.

1.2. Necessity of catchment-scale hydrological modeling

Globally the hydrological cycle experiences significant disturbances through the changes of its components (e.g. precipitation, evapotranspiration, river flows, soil water storage) in quantity, quality, space and time (Harding et al., 2014; Palmer et al., 2008; Sophocleous, 2004; Sterling et al., 2013; Tang and Lettenmaier, 2012). Many nations and communities across the world have been experiencing intensified water related problems such as floods, drought and associated water scarcity for the last few decades (Hirabayashi et al., 2013; Tang and Lettenmaier, 2012; World Bank, 2013; Zevenbergen et al., 2013). Water related disasters killed more than 290,000 and affected more than 1.5 billion people worldwide during the period of 2000–2006 (UN Water, 2014a). About 1800 million people will suffer from water scarcity by 2025 (UN Water, 2014b). On one hand, increasing population pressure, unsustainable developmental activities and industrialization are together increasing pressure on the Earth's finite useable water resources (Junk et al., 2013; Molden et al., 2001; UNESCO, 2013). On the other hand, climate and land use changes have been found to be the dominant causes of frequent and intense flooding in many regions of the world (Arnell, 1999; Guo et

al., 2008; Kumar et al., 2010; Raneesh and Thampi Santosh, 2011; Turner and Annamalai, 2012; UNESCO, 2013; Wohl et al., 2012). Sophocleous (2004) stated that water related problems are more visible at local scales (e.g. river catchment) than at the global scale. This is because the overall water turnover between Earth's atmosphere and land systems remains almost the same at the global scale but at more local scales this turnover varies in space and time. For this reason catchment-scale water analysis has been one of the key approaches in the development of sustainable water management plans (Borah and Bera, 2003; Lund et al., 2010; Singh and Woolhiser, 2002).

Generally, a catchment is a portion of Earth's surface that collects runoff and concentrates it at its furthest point (the outlet) (Ponce, 1996). A catchment may vary from less than 1 km^2 to hundreds of thousands of km^2. Each catchment drains its generated surface runoff through a river or channel, which is developed along the lowest altitudinal points of catchment's surface and terminates at extreme lowest elevation point (catchment outlet). A watershed is often taken to mean smaller catchment whereas basin is usually referred to a larger catchment (Ponce, 1996). However, today in the literature and academic usages, no specific distinction is made between catchment and watershed. According to this definition, a river basin needs not be confined within a political boundary but may rather cross multiple national borders (commonly termed a transboundary or international basin).

1.2.1. Importance of catchment hydrology

Commonly hydrology is defined as a branch of science that deals with the dynamics of water in the earth system. As quoted by Singh & Woolhiser (2002) from Penman (1961), hydrology seeks the answers to the question "What happens to the rain". Sometimes hydrology is defined as the processes between any form of precipitation (rain, snow, hail, sleet, etc.) touching the earth surface and when water leaves the earth through the processes of evaporation, transpiration, and/or evapotranspiration (Calver, 2009). The hydrological cycle is generally described as having the following major constituent processes (Ojha et al., 2008; Raghunath, 2006): precipitation (falling of water from the atmosphere to the earth's surface); interception (trapping of precipitated water before it

reaches the earth surface by vegetation canopies or other land cover); infiltration (the entry of precipitated water into the soil); surface runoff (overland flow of excess precipitated water that cannot be infiltrated into the soil system and accommodated in surface depressions); evapotranspiration and sublimation (evaporation from canopy, soil and open water bodies such as rivers, pond, and lakes, sublimation from snowpack in cold regions, and transpiration through plant system); percolation (downward movement of soil water beyond field capacity, this percolated water ultimately contributes to underlying aquifers); interflow (horizontal flow of water through soil horizons); and base or groundwater flow (flow of water from aquifer to nearby rivers or other drainage systems). A typical representation of the hydrological cycle is shown in Figure 1.1. The component processes of the hydrological cycle are sometimes categorized as one-dimensional (e.g. precipitation, evaporation, infiltration), two-dimensional (e.g. surface runoff) and three-dimensional (e.g. ground water flow) (Binley and Beven, 1992; Gibson and Pasternack, 2016). Surface runoff, interflow, and base flows are the major sources of inland river flows. The interactions between the components of the hydrological cycle are such that impacts on one component may lead to the other components being impacted and consequently, the hydrological balance will shift to a new state (Murray et al., 2012).

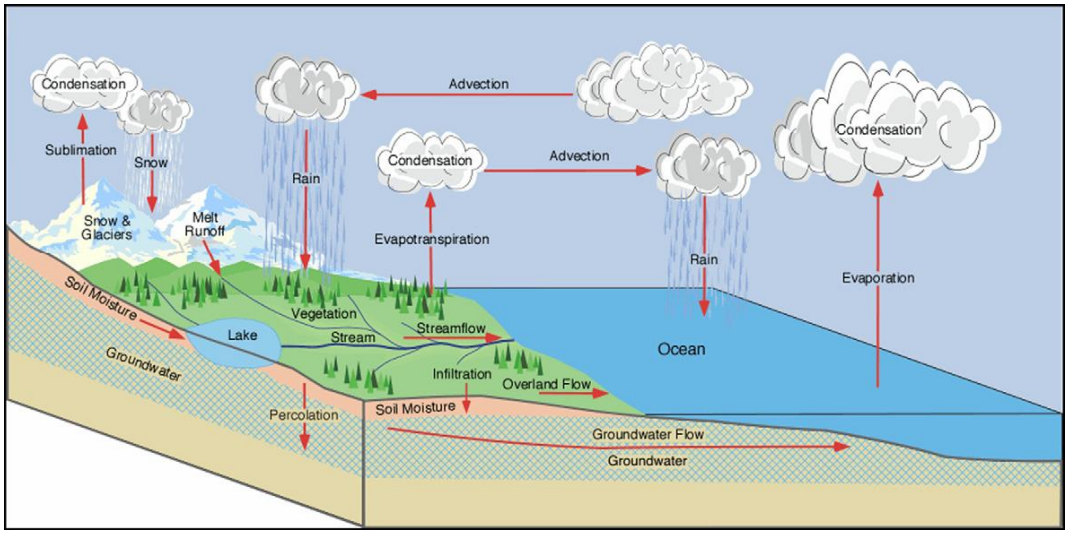

Figure 1.1. Representation of a typical hydrological cycle. Source: Yeh et al., 2011

With increasing spatial extent, hydrological systems become more complicated due to a wider range of variability in climate, land use and land cover, soil, geology, topography and anthropogenic activities as well as a larger number of interactions between different component processes which will occur at varying temporal and spatial scales (Borah and Bera, 2003; Gentine et al., 2012; Guo et al., 2008; Paz et al., 2010; Xiaomeng Song et al., 2011; Stisen et al., 2008). The spatial scaling extent for developing, assessing, analyzing, and modelling terrestrial water resources may span from the field to global scale (Kite and Droogers, 2000) depending on the specific problems being addressed, financial support, and interests of water managers, practitioners, planners, modellers, scientists, and policy makers.

Figure 1.2 shows that most of world's land surface is occupied by transboundary river basins and that the majority of world's people live within these basins. For example, the Mekong, the 8th largest river basin of the world in terms of annual flow (475 km^3) and 21st in terms of drainage area (795,000 km^2), is central to the economic development of the region supporting about 500 million people (Kite 2001; Kiem et al., 2008 cited by Thompson et al. 2014). Another Asian river basin the Ganges-Brahmaputra-Meghna (GBM) supports more than 600 million people on its 1.6 million km^2 area. It is one of the most densely populated basins on the earth (Akanda, 2012; FFWC, 2011) with many of the people being amongst the poorest in the planet (Yang et al., 2011).

Figure 1.2. Distribution of population density in world's international or transboundary river basins.

Source: http://www.transboundarywaters.orst.edu/index.html

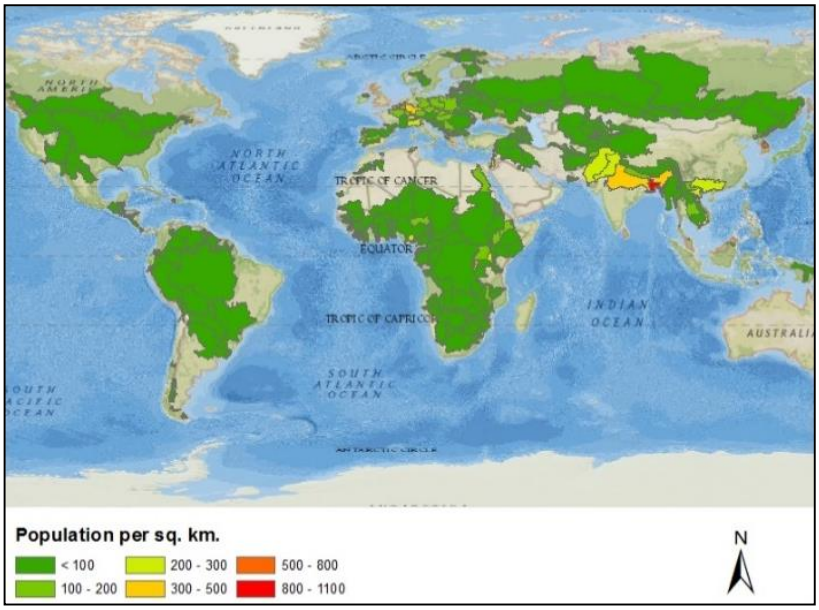

Despite providing enormous services to human beings, today the world's river basins are prone to many hydrological (Guo et al., 2008; Lai et al., 2013; Nishat and Rahman, 2009; Paiva et al., 2011) and non-hydrological problems (Ahmadi et al., 2006; Betrie et al., 2011a; Niraula et al., 2012; Flanagan et al., 2013a). Increased and uneven population pressure, ecologically damaging human activities, and climate and land use changes are the major causes of water related problems such as flood, drought, pollution, conflict among different stakeholders, and even between nations within transboundary basins (Bakker, 2009; Nishat and Rahman, 2009; Sood and Mathukumalli, 2011). Realizing the necessity of better water management, the UN conference on Environment and Development in 1992 promoted the concept of "Integrated Water Resources Management (IWRM)" that is now being followed by many world policy makers, water regulatory organizations, and regional water planners. Catchment models provide potentially invaluable tools in the development of integrated water resource management.

1.2.2. Catchment modelling: scope and applications

Since the development of the first digital Stanford Watershed Model (Crawford and Linsley, 1966) in late 1960s, larger-scale hydrological studies have gained momentum throughout the world (Kampf and Burges, 2007; Singh and Woolhiser, 2002). The most dominant reasons for this have been: (i) the necessity to quantify the effects of environmental change, particularly caused by climate and land use changes and anthropogenic activities, on basin's water resources (Guo et al., 2008; Lai et al., 2013; Nishat and Rahman, 2009; Paiva et al., 2011) and (ii) growth in the capabilities of modern computing power to take on larger scale hydrological modelling problems (Senarath et al., 2000 cited by Lai 2009; Singh & Woolhiser 2002; Kampf & Burges 2007).

Unlike a smaller experimental field site, instrumenting a larger catchment or fitting its hydrological behaviour to a statistical regression model in order to assess the basin's hydrology is often inappropriate and impractical (Kite and Droogers, 2000). Therefore, numerous catchment-scale hydrological models, ranging from simple conceptual lumped to comprehensive physics-based distributed models, have been developed and employed throughout the world to simulate river basin

hydrological and hydraulic dynamics (Borah and Bera, 2003; Daniel et al., 2010; Singh et al., 2005; Singh and Woolhiser, 2002; Yamazaki et al., 2011). A catchment or basin model may be defined as a model that can represent a basin's hydrology with significant statistical confidence (Moriasi et al., 2007). Undoubtedly, the foremost and immediate objective of developing a catchment model is to understand the complex and interactive dynamics of catchment hydrology. However, the biggest implication of such models is to quantify catchment's response to various potential or hypothetical perturbations such as climate change (Andersen et al., 2006; Raneesh and Thampi Santosh, 2011; Singh et al., 2010; Thompson et al., 2014b; L. Wu et al., 2012), land use/land cover change (Githui et al., 2009; Öztürk et al., 2013; Rahman et al., 2014; L. Wu et al., 2012) and anthropogenic activities that could include the development of water management infrastructure (such as dams) as well as water abstractions or returns (Jankowfsky et al., 2014; Pokhrel et al., 2012; M. Wang et al., 2010). Some of the particular application areas that are often evaluated by catchment models are quantitative and qualitative analysis of streamflows and groundwater, interaction between rivers and other water bodies (floodplains, lakes, wetlands, and groundwater), reservoir operation, flood forecasting and drought monitoring.

Modelling at the catchment scale has two advantages over other non-catchment scale assessments such as political domains. The first advantage is a realistic representation of a catchment's surficial boundary by its borderline or ridgeline or drainage divide, which may be found from topographic survey data or generated from digital elevation data. The second advantage is the comparatively readily available observed runoff or streamflow time series data at the outlet of catchment. As surface water cannot cross the ridgeline, the frontier line between two adjacent catchments, water mass balance within the modelled catchment suffers less uncertainty due to improper boundary conditions unless significant subsurface hydrological interaction exists between adjacent catchment (Gonçalves et al., 2013). Runoff or streamflow at the catchment's outlet reflects the basin's overall hydrological response to different influencing factors such as climate, land use, soil and man-made activities (Ivanov et al., 2004). For this reason, many catchment models, whether lumped or distributed, are calibrated and validated against observed streamflow data with the hypothesis that once a model's performance is statistically significant in resembling streamflows at the

catchment's outlet then other hydrological processes are assumed to be captured well by the model (Bulygina et al., 2007; Krysanova and Arnold, 2008).

Growing demand for water and developmental activities not only create stresses in terms of the volume of hydrological flows but also impose a great threat to water quality. Therefore, recent decades have witnessed enhanced capability of many catchment models by incorporating non-hydrological process modules, for instance, erosion and sedimentation, nutrient and pollution transport, and ecological responses (Flanagan et al., 1995; Neitsch et al., 2011; Zi et al., 2016). The presumption behind the application of a catchment model to simulate other non-hydrological processes is that if a well-calibrated model is able to mimic catchment's water mass balance and water dynamics spatially and temporally then such a model may be an auxiliary tool to simulate other processes having correlation with hydrological dynamics (Connolly et al., 1997; Narasimhan et al., 2010). For example, some widely used catchment models such as SWAT (Arnold et al., 1993), ANSWERS (Dabral and Cohen, 2001; Dillaha et al., 2014), WASH123D (Yeh et al., 1998), AGNPS (Bingner et al., 2011; Young et al., 1989), KINEROS-2 (Woolhiser et al., 1990), CASC2D-SED (Julien et al., 1995; Rojas et al., 2003), and WEPP (Flanagan et al., 2013b; Flanagan and Nearing, 1995) are capable of modelling a basin's erosion and sedimentation and/or pollutant processes alongside the core hydrological simulation. A few sophisticated models even include plant simulation module not only for modelling biological yield but also for reducing model's uncertainties in hydrological simulation. For example, the Soil and Water Assessment Tool (SWAT) model has a crop/plant simulation module, which is used to estimate plant growth with time and its effects on other relevant processes.

1.3. Rationale of the present study

This section first describes the importance of hydrological cycle on the socio-economic conditions of the present study area, the Upper Meghna River Basin. A number of problems associated with water in the lower floodplain of the area are examined using findings of past studies.

1.3.1. Importance of the study area

The present study focuses on the hydrological dynamics of Meghna River Basin, one of the three basins making up the Ganges, Brahmaputra, and Meghna (hereafter referred to as GBM) River Basin system (Figure 1.3a). The world's highest annual precipitation (>= 11,500 mm reported by Dash et al., 2012; Dhiman, 2012; FFWC, 2011; IFAD, 2011) receiving area Cherrapunji lies within the boundaries of Meghna River Basin (Figure 1.3b) whilst the region experiences severe spatial rainfall variability. The occurrence of rainfall in this region is caused by both convective and orographic phenomena (Hofer and Messerli, 2006; Knight and Shamseldin, 2005). Such characteristics in humid tropical regions including the studied basin are behind the greater spatial variation in rainfall (Wohl et al., 2012). Previous research has demonstrated that the hydrological response to highly variable rainfall is extremely difficult to explain, and different studies have provided variable results (Hofer and Messerli, 2006; Mirza et al., 2001). The hydrological behavior of Meghna River Basin is often represented by the Upper Meghna River Basin (hereafter referred to as UMRB) with the outlet at Bhairab Bazar (Figure 1.3b) which is about 50 km upstream of the confluence of rivers Padma (Ganges River in India) and Meghna (see Figure 1.3a). The prime focus of the present study is therefore the UMRB.

The geographical extent of the UMRB (Figure 1.3b) is 90.03° E to 94.31° E and 22.83° N to 25.77° N. The approximate area of the basin is 63,746 km^2, of which 20,099 km^2 (31.5% of the basin) is within Bangladesh territory and remaining lies in northeastern forested hilly region of India, except a tiny portion in Myanmar. Based on topographic and climatic characteristics, the UMRB can be divided into four distinct regional subbasins namely the Barak River Basin with high-frequency wave shaped rugged hills, the Meghalaya Basin with steep hill slopes and the world's highest rainfall area Cherrapunji, the Tripura Basin with some drought prone areas, and floodplains and wetlands dominated the lower Sylhet Basin of Bangladesh. Sometimes the Sylhet Basin is called as Surma-Kushiyara River Basin according to the name of its two major rivers, the Surma and Kushiyara (see Figure 1.3b). Being located downstream of the other three Indian basins (Barak River, Meghalaya, and Tripura), the hydrology of the Sylhet Basin is highly vulnerable to any changes in upstream basins such as climate and land use changes, river flow regulations by diversions, dams or other artificial withdrawals of river water beyond minimal flow. After flowing through the three

upper basins, all the rivers draining the hilly uplands enter the lower Sylhet Basin of Bangladesh. This is crisscrossed by numerous rivers forming a very complex network with distributaries and tributaries.

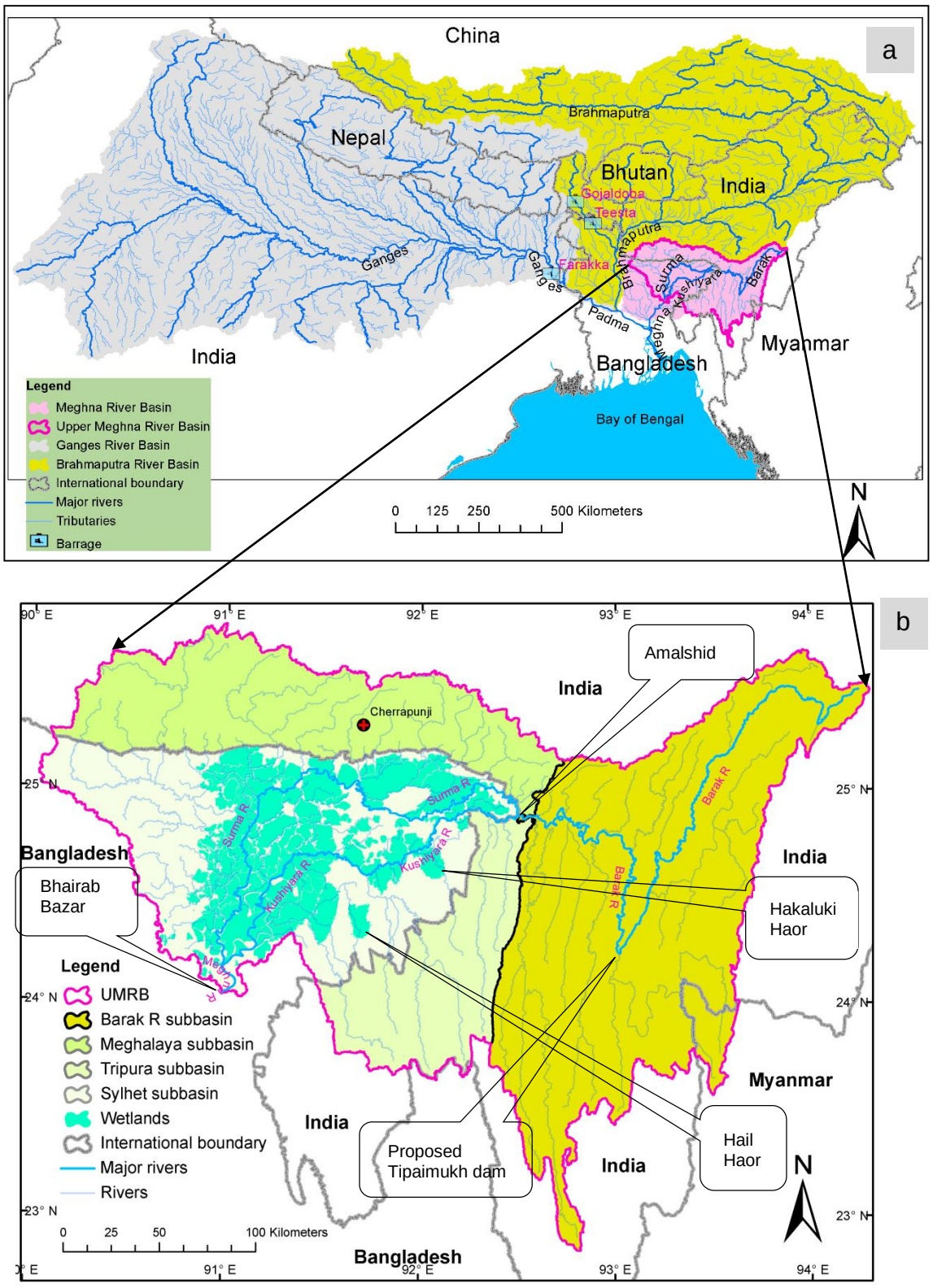

Figure 1.3. Geographical position of the (a) Ganges-Brahmaputra-Meghna (GBM) River Basin and (b) Upper Meghna River Basin (UMRB) with its four constituent regional subbasins (Barak R, Meghalaya, Tripura and Sylhet).

Figure 1.4 depicts the spatial distribution of population density over the UMRB, which is created from the district wise population census of 2011 (BBS, 2011; Office of the Registrar General & Census Commissioner India, 2011). It demonstrates that the Sylhet Basin is much more populous compared to the other three upper Indian basins.

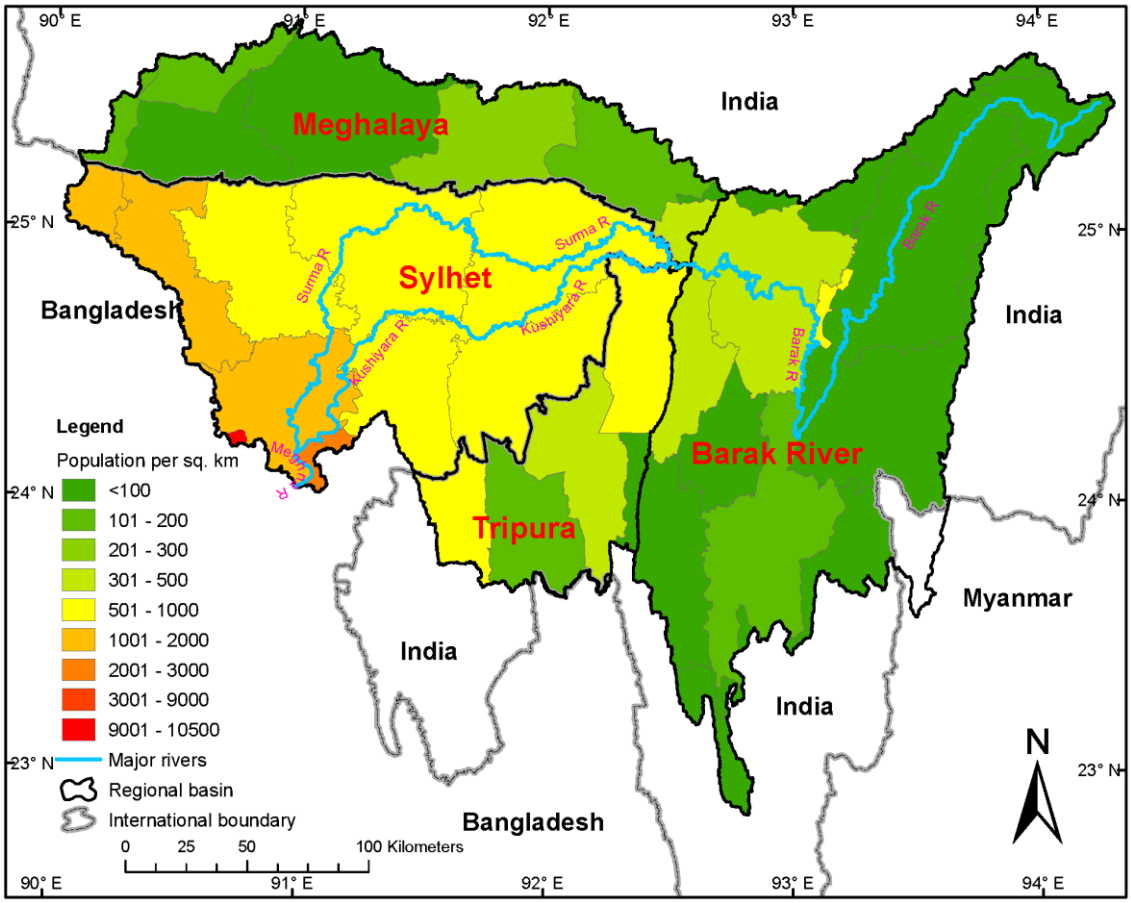

Figure 1.4. Spatial distribution of population density in the UMRB.

The motivation of this study is firstly related to the long-term and growing flooding problems in the lower UMRB or the Sylhet Basin where 12.91% of Bangladesh's 150 million people are presently living. This basin is within the Northeast (NE) hydrological region as categorized by Bangladesh Water Development Board (BWDB) according to hydro-meteorological characteristics. Along with the very dense system of river channels, the presence of numerous riparian depressional wetlands in the Sylhet Basin not only plays an important role within the national

economy (agriculture and fisheries – see below) but sustains diverse ecological resources. In Bangladesh, according to the Ramsar Convention (Ramsar Convention Secretariat, 2013), wetlands may include rivers, haors (saucer shaped depression), baors (oxbow lakes), beels (the deepest area in a haor), ponds, reservoirs and lakes (Figure 1.5). The Sylhet Basin has about 370 haor wetlands (see Figure 1.3b), the dominant category of wetland having an combined area of about 8573 km^2 i.e. ~43% of the basin area when all are full of water (CEGIS, 2012a; Islam, 2010). Due to the existence of huge numbers of haor wetlands, the Sylhet Basin is sometimes called the Haor Basin.

Almost all haor wetlands in the Sylhet Basin are traversed by or connected to rivers and thus have a strong interaction with the river system. The hydrology of these haor wetlands depends on seasonal rainfall; in the wet season (April–November) haor wetlands are hydraulically connected with rivers due to the rise of water levels while in the dry season (December–March) they are isolated from the river system as water levels fall through drainage, evaporation, and seepage. At this time these shallow haor wetlands turn into massive arable lands for Boro rice cultivation. Boro is an intensively irrigated rice variety planted in December/January and harvested in April/May followed by Aus rice with the growing period April/May–July/August and Aman rice with the growing period June/July–November/December. Agriculture and fisheries are the two major driving sectors of the Haor Basin's economy. Containing 16% of the country's 10.57 million ha of rice growing area, the region produces about 18% of the country's total rice production (CEGIS, 2012a). Moreover, haor wetlands are a sanctuary of 260 fish species, 259 species of birds, 40 reptiles, 29 mammals and amphibians, and 300 flowering plants (Byomkesh et al., 2009; CEGIS, 2012a). Haor wetlands are the main breeding and feeding habitats for fish species; currently these wetlands produce about 0.432 million tons of fishes that is projected to increase to 0.468 m tons in 2030 (CEGIS, 2012a).

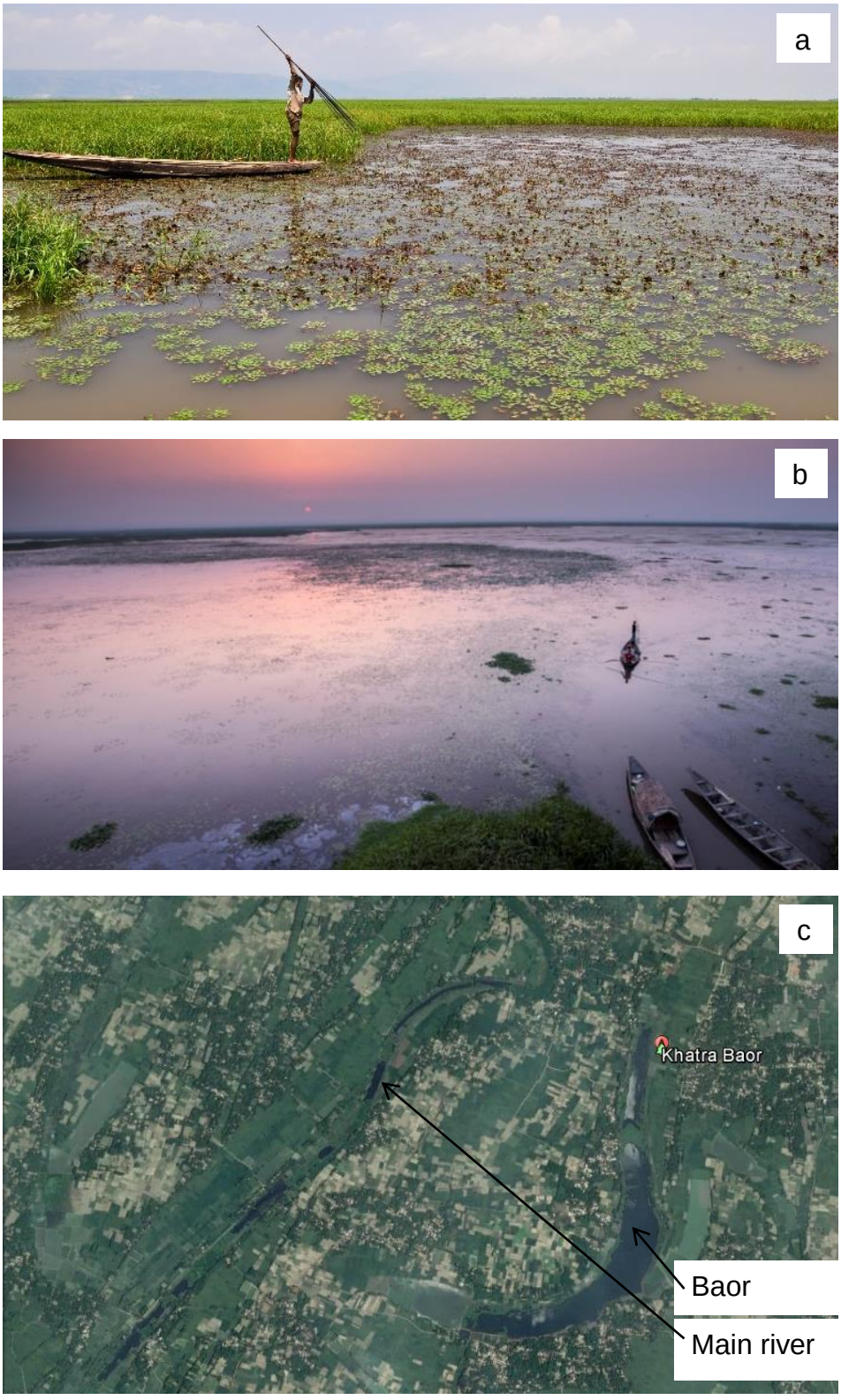

Figure 1.5. Special wetlands in the Sylhet Basin: (a) Haor wetland (b) Beel in dry season (c) Oxbow lake or baor.

Sources: (a) https://commons.wikimedia.org/wiki/File:Fishing_by_spear_in_a_haor_of_Sunamganj,_Bangladesh.jpg; (b) https://scottspixels.wordpress.com/2013/02/24/30/; (c) Google Earth

To meet the food demands of the country's increasing population and to improve the overall economy, identifying the sectors and areas that have potential to be further developed is always one of the important priority areas of the Government of Bangladesh. Recent surveys in order to develop the Master Plan of Haor Areas show that the haor region has the potential to increase its existing contribution (2%) to Gross Domestic Product (GDP) by tenfold. The Master Plan of Haor Areas (CEGIS, 2012a) has proposed 153 projects to a value of ~3495 million USD, to be accomplished in short, middle and long term phases, under the 17 major sectors alphabetically agriculture, biodiversity and wetland management, education, fisheries, forest, health, housing and settlement, industry, institution, livestock, mineral resources, pearl culture, power and energy, social facilities, tourism, transportation and communication, water resources, and water supply and sanitation. These multi-organization integrated projects are expected not only to improve overall socio-economic conditions of poor people and biodiversity of the haor region but also to benefit the country's overall economy.

1.3.2. Hydrological issues in the lower UMRB (or Sylhet Basin)

Despite having enormous potential, as discussed in the previous section, the lower UMRB or Sylhet Basin has been suffering from some severe hydrological problems: flash floods in the pre-monsoon season (April–May), prolonged inundation of floodplains and haor wetlands due to heavy monsoonal (June–September) rainfalls so that the period of inundation is longer than experienced in the past, and water shortage in the dry season (December–March) when the main crop (Boro rice) is grown (BWDB, 2012; CEGIS, 2012a; Khan et al., 2005; Rahman et al., 2005). These key factors have led to the loss of haor wetlands' functioning, thus directly impacting the socio-economic condition of local people who live on haor resources. Very large runoff, generated from unpredictable early pre-monsoonal torrential rainfall in the Meghalaya Basin, causes devastating flash floods in the Sylhet Basin, which often damage nearly ripened Boro rice awaiting to be harvested (BWDB, 2012; CEGIS, 2012a; Khan et al., 2005, 2012). Due to its steep terrain and close proximity to downstream floodplains, the wettest Meghalaya Basin is thought to be the pivotal factor in creating such flash floods even though the drainage area of this basin is only 17.5% of the entire UMRB.

To protect Boro rice from being damaged by early flash floods, the BWDB, a Government organization which oversees the country's water resources, builds submersible earthen dykes along the periphery of some haor wetlands and sluice gates across the connecting channels between wetlands and main rivers. However, most wetlands and connecting channels are beyond the project area of the BWDB and are not dyked and lack sluice gates. Earthen made submersible dykes or embankments are generally 1–1.5 m above the floodplain and are completely submerged under water during deep or monsoonal flooding. A dyked wetland with sluice gates allows farmers a transitional buffer time to harvest their crops until floodwater overtops or breaches the dykes. However, recent field surveys reveal that the people of the haor region and their agriculture are now more exposed to frequent flash flooding than 30–40 years ago (Ahmed, 2014; CEGIS, 2012a). Increased erratic precipitation is mainly blamed for such frequent flash flooding.

In addition to pre-monsoonal flash floods, recurrent monsoonal (June-September) flooding is a common scenario in the Sylhet basin, like other parts of Bangladesh. During this flooding period, millions of rural people reliant on agriculture and fisheries are marooned in their houses and have miserable conditions due to shortages of food and employment. This monsoonal floodwater may stagnate in the haor basin for up to six months (Hofer and Messerli, 2006). Figure 1.6 shows the inundated area of Bangladesh during the devastating flood in 2007 whilst the severity of floods and difficulties of rural life in haor areas during the flood season are illustrated in Figure 1.7.

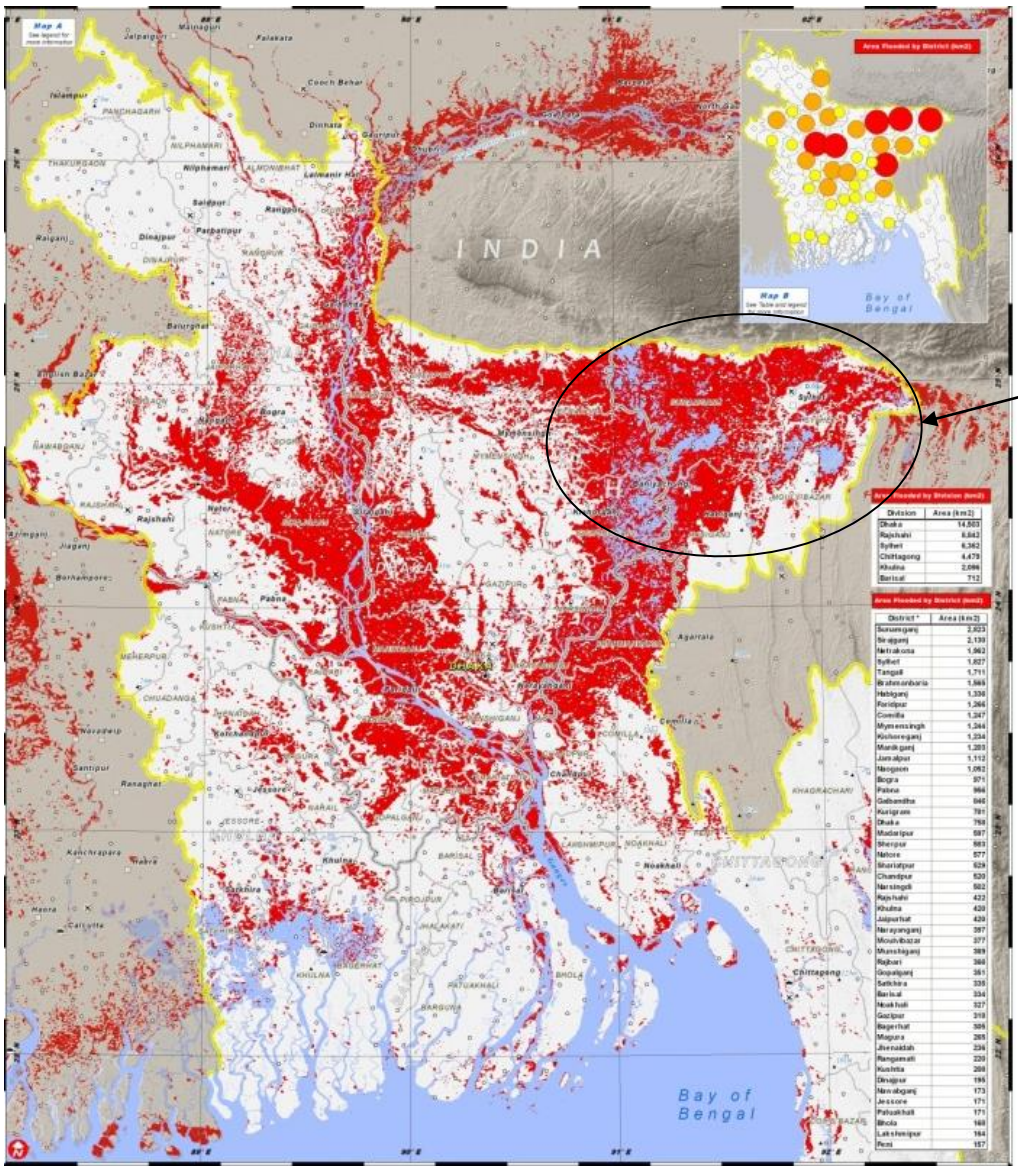

Figure 1.6. Inundated area (red coloured) after devastating flood of 2007 in Bangladesh.

Source: http://www.unitar.org/unosat

(a) Aerial view of a flooded haor wetland during the monsoon season. Along with runoff water, huge sediment is carried out by the river as reflected by its muddy water.
Source: The Daily Prothom-Alo (5 September 2014).

(b) Difficulties of rural life during flooding of haor wetlands.
Source: http://commons.wikimedia.org/wiki/File:Flooded_haor.jpg

Figure 1.7. Haor wetland scenarios during periods of flooding.

Timing, duration and direction of hydrological interaction through a connecting channel between a haor wetland and an adjacent main river play a crucial role in haor water management. A connecting channel turns into a distributary during the early monsoon season when water level in the associated main river starts to rise faster than that of connected wetland(s). The direction of flow reverses and the connecting channel acts as a tributary during the receding period of monsoonal flooding when river water level starts to drop. As the end of the monsoon approaches (September/October), a rapid natural drainage of haor wetlands is highly desirable so that Boro rice can be planted in the newly drained land. However, any delay in the fall in water levels within the main river impedes gravitational drainage of haor wetlands leading to the late planting of Boro rice (CEGIS, 2012a, 2012b). This delay increases the chances of Boro crop damage due to early flash flooding during the next harvesting period.

In addition to flooding problems, water scarcity in the dry period, usually in mid-dry season (January–February), imposes a great threat to irrigated Boro rice in the Sylhet Basin. Both surface and groundwater irrigation are practiced in haor agriculture. Rivers and beels (the deepest potholes in a haor that often receive water from groundwater seepage) are sources for surface water irrigation. However, this surface water is insufficient to meet the demands of Boro rice water requirements; consequently, about 50% of irrigation demand is subsequently supplied from the groundwater sources (CEGIS, 2012b).

1.3.3. Review of past research works and attempted approaches to combat the water problems in the study area

According to the Master Plan of Haor Areas (CEGIS, 2012a, 2012b), failing to combat the evident problems in the Sylhet Basin described in the previous section would deprive the country from achieving an estimated GDP of approximately $8.43 billion by 2030 against the current $3.12 billion generated from the haor areas. Given the socio-economic importance of Sylhet Basin, the Master Plan of Haor Areas developed under the auspices of Ministry of Water Resources (Bangladesh) formulated short- and long-term water resource development strategies that include construction of more new embankments along the main

rivers and around periphery of wetlands. These strategies are formulated based on statistical analysis of historical hydro-meteorological (river flow, stage, rainfall) records from within the Sylhet Basin and information collected from affected people within the basin through several field surveys. In addition to historical data based evidence, another key argument behind the suggested strategies was that the existing water problems will be further aggravated by climate change. It has been a general consensus among the people of Bangladesh that in common to the other two mega basins, the Ganges and Brahmaputra, flooding in the Meghna River Basin is mainly caused by heavy rainfall in the upper basin situated in India (Allison et al. 1998; Mirza et al. 2001; WARPO 2001; Gupta et al. 2005; Hofer & Messerli 2006; Islam et al. 2006; Islam et al. 2010; Babel & Wahid 2011; FFWC 2011; Hoque et al. 2011; Sood & Mathukumalli 2011; Akanda 2012). However, Hofer and Messerli (2006) stated that causes of floods in this region are numerous, heterogeneous, and complex; and should not be attributed to a single cause.

In terms of flooding in the lower delta of the GBM basin (i.e. in Bangladesh), and in particularly in the lower UMRB (or the Sylhet Basin), most research has either concentrated on identifying the degree and trends of flooding with support of statistical analysis of historical hydro-meteorological data (Hofer and Messerli, 2006; Hoque et al., 2011; Islam et al., 2010, 1999; Metcalfe, 2003; Mirza et al., 2001; Sood and Mathukumalli, 2011), or on small-scale studies, for instance, on specific wetlands of the basin (Oka et al., 2013; TEEBcase by P. Thompson and T. Balasinorwala, 2010; Thompson, 2014). However, little research has been undertaken that involves basin-scale model based studies (Hofer and Messerli, 2006; Khan et al., 2005; Liong et al., 2000). Statistical trend analysis of discharge data showed that flows at the intakes of the two major rivers (Surma and Kushiyara) of the Sylhet Basin (Figure 1.3) were increasing since the middle of 20th Century. This was linked to increased rainfall in their headwater basin of Barak River (Hofer and Messerli, 2006; Mirza et al., 2001). However, flow trends at the outlet (Bhairab Bazar) of the Sylhet Basin are contentious. With four different statistical trend treatments, Mirza et al. (2001) found no significant trends in annual peak flows at Bhairab Bazar since 1950 whereas Hofer and Messerli (2006) showed a prominent upward trend in monsoonal peak flows, thus annual peaks, at this station over the same period. Flow characteristics at the outlet of

UMRB are strongly impacted by highly variable rainfall pattern in the northern Meghalaya Basin, numerous haor wetlands in the Sylhet Basin, and backwater effect due to tidal flow through the confluence of Padma (Ganges in India) and Meghna Rivers (Chowdhury and Salehin, 1997; Chowdhury and Ward, 2004; Rahman et al., 2005). Some researchers tried to establish the specific causes of the most devastating flood experienced by the UMRB in 2004 (Hoque et al., 2011; Islam et al., 2010). Analysing multi-source rainfall [local and TRMM (Tropical Rainfall Radar Mission)] and remotely sensed image (LANDSAT and RADARSAT) data reveals that heavy rainfall in the Sylhet Basin rather than in the three upper Indian basins was the key factor of the 2004 devastating flood (Hoque et al., 2011; Islam et al., 2010).

Although statistical analysis of historical time series data collected from several point stations in a basin may identify the trend and correlation of interested variables, for example, rainfall and river discharge, results from such analyses for a larger basin cannot be confidently relied upon to develop a regional water resources management plan. Statistical regression models are methodologically not suitable to represent numerous complex processes of catchments (McIntyre et al., 2007; Steinschneider et al., 2015). In addition, remotely sensed image data can produce the extent of flooded area but not the underlying physics of the flooding process. A basin's response at its outlet is the result of hundreds of interactive processes. Therefore, catchment modelling is becoming an indispensable tool to capture the dynamics of and to assess the response of catchment to many forcing factors such as climate change, land use change, human interventions (Borah and Bera, 2003; Collischonn et al., 2007; Daniel et al., 2010; Downer et al., 2002; Marsik and Waylen, 2006; Singh and Woolhiser, 2002; Thompson, 2004; Yamazaki et al., 2011). With the support from and involvement of multiple organizations (core organizations including United Nations University, Tokyo; Swiss Agency for Development and Corporation, Bern and Dhaka; University of Bern; Food and Agriculture Organization (FAO)), Hofer and Messerli (2006) investigated the mechanism of flooding processes in the floodplain of lower delta of the GBM Basin. They developed a two parameter simple rainfall-runoff model for the entire GBM River Basin. One parameter, the discharge factor, is analogous to runoff coefficient that determines how much rainfall is converted to surface runoff, and the second one, relevance of potential

runoff, is related to travel time of surface runoff which reflects the properties of subbasin's resistance to runoff water movement and relative distance from basin's outlet. The entire GBM River Basin was manually delineated into 11 subbasins by considering factors that included topography, political administrative boundary, rainfall, and documented watershed boundaries. Due to the lack of representative observed flow data at the Meghna River Basin outlet, the model was first parameterized using flow data of the Ganges River; later these calibrated parameters were adapted for the three subbasins of Meghna River basin. Notably, their manual catchment delineation did not include the Barak and Tripura basins that encompass 57.47% of entire UMRB. Since numerous haor wetlands in the Sylhet Basin (north-eastern Bangladesh, subbasin number 11 within their model) are usually full of water in the monsoon season, Hofer and Messerli (2006) assumed higher discharge factors for the four monsoonal months of June–September (0.7, 0.8, 0.9, and 0.9, respectively) which implies that haor wetlands are capable of converting 70% to 90% of rainfall to surface runoff. This assumes that in contrast to baseflow, surface runoff has a greater control on flooding process in the wetland dominated Sylhet Basin (Islam et al., 2010; Rahman et al., 2005). For the same basin, however, Masood et al., 2015 found contradictory results from the conceptual H08 model (Hanasaki et al., 2008a, 2008b) where baseflow was found to be dominant over surface runoff in haor wetlands. Nishat and Rahman (2009) employed a MIKE BASIN model to represent the hydrology of the entire GBM Basin which was spatially discretized into 148 sub-basins using Shuttle Radar Topographic Mission (SRTM) topographic data. Of the 148 subbasins, only five encompass the entire Meghna River Basin. For the latter, the model was calibrated and validated against measured daily flows from 2005–2007 at Amalshid (see Figure 1.3b), the outlet point of Barak River Basin, and the calibration parameters were constant over each of the subbasins. Therefore at subbasin scale the characteristics of the GBM basin were in fact lumped within the MIKE BASIN model. In general, the model was able to simulate monthly flow volumes at Amalshid within a range of -15 to 19% of observed monthly observations. The correlation coefficient for daily simulated discharges was 0.71. Although in general the model appeared to be a good predictor it suffered from some serious limitations: (i) the model was parameterized for flow data at Amalshid which is situated at the upstream end of the Sylhet Basin, thus the flow simulation performance of the model in the lower

wetlands dominated Sylhet Basin is unknown, (ii) a three year simulation period may not be sufficient for the highly spatial and temporal variable rainfall of Meghna River Basin, (iii) the reliability of a catchment model should not be judged with only graphical and one statistical performance indicator (Jain and Sudheer, 2008; Moriasi et al., 2007), (iv) effects of land use and soil data were ignored, and (v) there was lack of hydro-meteorological data from upper riparian country, India.

With the North East Regional Model (NERM), Khan et al. (2005) studied the impact on the water resources of Sylhet Basin of the proposed Tipaimukh Dam to be built across the Barak River in India ~70 km upstream of the Amalshid border point and where the Barak River bifurcates into Surma and Kushiyara Rivers (Figure 1.3b). The NERM is an ensemble hydrologic-hydrodynamic model developed from the lumped rainfall-runoff model NAM (Nedbør-Afstrømnings-Model) (DHI, 2009a) and the river hydrodynamic model MIKE11 (DHI, 2009a). Since the early 1990s the NERM model has been used and updated periodically by the Flood Forecasting and Warning Centre (FFWC), a wing of the BWDB, to forecast river water stage and flooding in the northeast region of Bangladesh (FFWC, 2011; Liong et al., 2000). In the NERM modelling platform, each river within a subbasin receives surface runoff, generated from the prior calibrated lumped rainfall-runoff NAM model, and headwater inflows, if any, from upper tributaries. Observed river flows and stages at about 20 gauge stations established along the frontier of Bangladesh and India were used as boundary conditions of the NERM model. Upon receiving boundary observed flow data, the model can predict water stages of the Meghna River at Bhairab Bazar with a maximum lead time of three days (Islam et al., 2010). Although this model can satisfactorily produce hydraulics of river's water in the Sylhet Basin its prediction ability is highly subjected to boundary flow conditions along the frontier. Moreover, use of such a model in assessing the catchment's response to different forcings such as climate and land use change is restricted as about 68% of the entire UMRB, lying in India, is not explicitly modelled but is instead represented by observed water levels/flows as boundary inputs to the model.

The role of numerous depresional haor wetlands in the Sylhet Basin on flooding processes has rarely been explored. Oka et al. (2013) developed a numerical

inundation model to understand the role of Hakaluki haor wetland (Figure 1.3b), one of the major haor wetlands in the Sylhet Basin, during the flooding period. This wetland is drained by eight rivers and connects Kushiyara River, one of the two major rivers in the Sylhet Basin. With a case study of the 1988 devastating flood, it was found that at the beginning of the flooding season a substantial amount of water entered into the Hakaluki haor from the adjacent Kushiyara River when water level in the haor is relatively lower than that of Kushiyara River; the reverse process occurs during flood recession time. However, this story may not be replicated for all hoar wetlands because the interception ability of a depressional wetland from adjacent rivers depends on specific factors such as the degree of hydraulic connectivity (which is influenced by factors such as the presence and dimensions of channels that link rivers with wetlands), hydraulic gradient, and available storage capacity.

1.3.4. Research gaps

An effective water management plan for the Sylhet Basin of the UMRB which incorporates assessment of the impacts of potential future modifications in hydrological conditions such as those associated with climate change, cannot be synthesised from the past studies, reviewed in Section 1.3.3 due to their multifaceted limitations. For example, the simple linear rainfall-runoff regression model based study of Hofer and Messerli (2006) can detect the overall trend and correlation of relevant variables to some extent but cannot be recommended for decision making processes. Such a simple approach masks many crucial underlying processes taking place across the space-time dimension between the predictor (rainfall) and predictand (runoff). Although some studies have been conducted with some elements of the more sophisticated MIKE model platform, their shortcomings restrict the application of those models. These include coarser spatial resolution input data, limited data (mainly for the upper basin in India), and lack of explicit inclusion of the role of wetlands within basin hydrological processes. For instance, results from the conceptual catchment model H08 (Hanasaki et al., 2008a, 2008b) that overlooks wetland hydrology indicate that rainfall falling over the haor wetland area of UMRB contributes to streamflows via baseflow (Masood and Takeuchi, 2016) rather than surface runoff as modelled by Hofer and Messerli (2006).

Many researchers argue that India's reluctance to share hydro-meteorological data with the lower co-riparian country of Bangladesh is the main hurdle to develop a realistic water resources management plan for downstream Bangladesh (FFWC, 2011; Hofer and Messerli, 2006; Khan et al., 2005; Nishat and Rahman, 2009). For instance, while analysing the impact of the proposed Tipaimukh Dam Khan et al. (2005) had to synthesise historical flow data at the dam site from a simple linear regression model that is a function of downstream flows at Amalshid. Similarly, while studying the international GBM River Basin Islam et al. (2010) used remotely sensed TRMM rainfall data rather than station records which are more likely to more accurately represent rainfall.

The existing water problems within the Sylhet Basin of the UMRB might be further exacerbated due to the effects of climate change. The potential impacts of climate change on the hydrological cycle have been studied worldwide (e.g. Bronstert 2006; Immerzeel 2008; Kumar et al. 2010; Raneesh & Thampi Santosh 2011; Wohl et al. 2012; Wu et al. 2012; Wu et al. 2013). The GBM River Basin and its surrounding areas are reported as being one of the most vulnerable regions to adverse effects of climate change (CCC, 2009; Dash et al., 2012; Ghosh et al., 2012; Gupta et al., 2011; Kumar et al., 2010; Pattanaik, 2007; Revadekar et al., 2011). From a rainfall-runoff modelling study, Gupta et al. (2011) showed that the potential annual runoff of the Brahmaputra-Barak River basin would decrease by 65 BCM (billion cubic meters) in 2080 from normal annual value (1951–1980) of 410 BCM, mainly due to a rainfall reduction in the region. However, contrary to this study, several other investigations have predicted increased precipitation in pre-monsoon and summer monsoon seasons in the 21st Century which might increase runoff (Revadekar et al., 2011; Turner and Annamalai, 2012). Complex spatial physiographic characteristics of the basin make this region one of the world's most spatial variable and least predictable climate zones (Hirabayashi et al., 2013; Revadekar et al., 2011).

1.4. Aims and objectives of the study

The main aim of this study is to develop a catchment-scale wetland model that is capable of realistically simulating hydraulic interactions between rivers, wetlands

and aquifers as seen in the haor wetlands of the UMRB. The second aim is to project future shifts in the current haor flash flooding conditions with reference to the latest climate change signals predicted under the Coupled Model Intercomparison Project Phase 5 (CMIP5) (Taylor et al., 2012).

To achieve the above aims, the study is accomplished through the following specific objectives:

(i) To prepare a database of climate, topography, soil, land use, and hydrology for the UMRB;
(ii) To develop an enhanced version of SWAT's existing wetland module to more accurately represent hydraulic interactions between wetlands, rivers and aquifers;
(iii) To build a SWAT model (enhanced version) of the UMRB which can reliably be used to simulate the water regime of river-wetland system in the lower part of the basin;
(iv) To analyse the water regime responses of the river-wetland system to changing climate;
(v) To formulate a risk-based wetland hydroperiod map in order to mitigate the current crop loss in haor areas of the UMRB.

1.5. Research design

While designing the research approach to achieve the above objectives, a rigorous literature review on existing catchment modelling approaches is undertaken to contrast the comparative capability, usability and availability of alternative models (Chapter 2). Rather than merely discussing the comparable aspects of these models in a descriptive manner, the review is sythesised by investigating their discretization approach of a catchment and mathematical representation of different hydrological processes.

Although a number of catchment models, with varying capacity and complexity, have been developed over the years, a handful of them have the ability to model wetlands (see Section 5.2). However, there are a series of issues with the ability of these models to represent the bidirectional hydraulic interactions between rivers, wetlands and aquifer that characterize the UMRB. Since SWAT is an open

source code model and can be run in data scarce region such as the UMRB, this model is finally selected for this study. Chapter 3 elaborates the structural configuration of SWAT and its mathematical representation of different hydrological processes.

A thorough investigation of the UMRB in light of its physio-graphic and hydro-meteorological characteristics was necessary so as to develop a catchment model for the basin. This is detailed in Chapter 4. The socio-economic characteristics of the region, specifically the lower part of the UMRB in Bangladesh, have already been discussed while justifying the rationale of the study (see Section 1.3).

To address existing limitations of SWAT in the representation of wetlands such as the haors of the UMRB the wetland code in SWAT is redefined and tested for a comparatively data rich haor in the basin (Chapter 5). The testing process includes parameterization (calibration and validation) of both models (SWAT and redefined SWAT) against monthly river flow data at six gauging stations and daily rive stage data at three gauging stations. This follows a comparative analysis of simulation performance in representing haor wetland hydrology by the models. Later, the redefined SWAT model that was found to be better than the original SWAT in simulating haor wetland hydrology is calibrated and validated for the whole UMRB (Chapter 6).

To achieve the last objective, the redefined SWAT model is employed to simulate the future water regimes of river-wetland systems in the lower UMRB for the Intergovernmental Panel on Climate Change (IPCC) RCP4.5 climate scenario used in the Coupled Model Intercomparison Project Phase 5 (CMIP5) (Chapter 7). This chapter begins with a concise review on climate change impacts on hydrological process, particularly river-wetland water regimes before describing the generation of future climate data from projections derived from the latest state-of-the-art Global Climate Model (GCMs). These scenarios are subsequently used to force the model and the resulting changed hydrological conditions (streamflows and wetland hydroperiods) are assessed. Moreover, possible shifts in current flash flooding risk of haor wetlands due to altered climate are discussed based on simulated results.

Finally, some specific conclusions are drawn based on the results of this study (Chapter 8). This follows limitations of the study and recommendations for further research.

Chapter 2
Catchment modelling

2.1. Introduction

This chapter provides a detailed review of catchment-scale hydrological modelling including the approaches that can be used to classify catchment models and represent the different hydrological processes within a catchment.

Hundreds of catchment (or watershed) models have been developed and are being employed in thousands of catchments across the world. Catchment modelling allows better understanding of water dynamics in the atmosphere-land system continuum and therefore allows assessments of the vulnerability and response to many driving forces, and the formulation of best water management plans (Andersen et al., 2006; Bingeman et al., 2006; Borah and Bera, 2003; Daniel et al., 2010; Githui et al., 2009; Öztürk et al., 2013; Rahman et al., 2014; Raneesh and Thampi Santosh, 2011; Singh et al., 2010, 2005; Singh and Woolhiser, 2002; Thompson et al., 2014b; L. Wu et al., 2012; Yamazaki et al., 2011).

A model, whatever its robustness, can never mimic reality exactly because we still do not fully understand the complex and inherently chaotic behavior of nature (Beven, 1996; Bingeman et al., 2006). Moreover, none of the existing catchment models is equally applicable to all catchments since many models are developed for specific regions to predict some specific processes (Jing and Chen, 2011; Kalin and Hantush, 2006). Nonetheless, today use of many catchment models is not confined to the regions where they were developed but instead models are applied to regions for which they may not have been originally intended. For example, the SWAT model was first developed in the early 1990s for smaller agricultural watersheds of the USA to predict impacts of land management on runoff. Today this model is being applied in numerous catchments around the world of different sizes (e.g. 0.0039 – 444185 km^2 (Douglas-Mankin et al., 2010))

and for different purposes (Liu et al. 2008; Xie & Cui 2011; van Griensven et al. 2012).

Before employing a watershed model in a particular region or catchment, a modeller must know the model's capabilities, structural configurations, and limitations. For this reason, having a thorough understanding of the model's class, structure, process equations and limitations will certainly help model selection and adaption for the watershed of interest.

2.2. Classification of catchment models

Many studies have classified catchment hydrological or rainfall-runoff models (Clarke, 1973; Plate, 2009; Refsgaard, 1996; Singh, 1995; Todini, 1988). Rather than employing any of the available classification schemes, here catchment models are discussed under the following major categories (i) mode of process representation (ii) discretization of a catchment and (iii) time scale.

2.2.1.Mode of process representation

Depending on how a hydrological model represents different component processes of hydrological cycle, three types of models can be identified: (i) empirical (i) conceptual and (iii) physics-based. An empirical model is also termed metric or black-box model as it does not represent and so cannot explain internal hydrological processes of a catchment. Instead such a model converts rainfall into runoff through a linear parametric equation (Rochester, 2010; Xu, 2002) or a transfer function (Mutlu et al., 2008; Rochester, 2010). The simplest empirical rainfall-runoff model is perhaps the single parametric runoff coefficient based model. Runoff coefficient is the ratio of effective rainfall i.e. runoff to total rainfall falling over a catchment during a particular time period. In other words, runoff coefficient defines the water retention ability of a catchment (Giudice et al., 2014, 2012). Where detailed characteristics of a catchment are sparse such models may be used to estimate design flood peaks (Giudice et al., 2014, 2012).

Models based on the Artificial Neural Network (ANN) approach are another family member of empirical rainfall-runoff models. The working principle of ANN models

is analogous to the nervous system of human being (Dowla and Rogers, 1995). A biological nervous system is an architecture of millions of inter connected cells or neurons, which upon receiving an input signal generates output signal(s). A typical ANN based rainfall-runoff model will have one input layer, many hidden intermediate layers, and one output layer (Figure 2.1). Each layer may contain one or several neurons. Each neuron at input layer receives a particular input (e.g. rainfall); later this input is transformed into output(s), passing through a transfer function that is a graphically hidden layer.

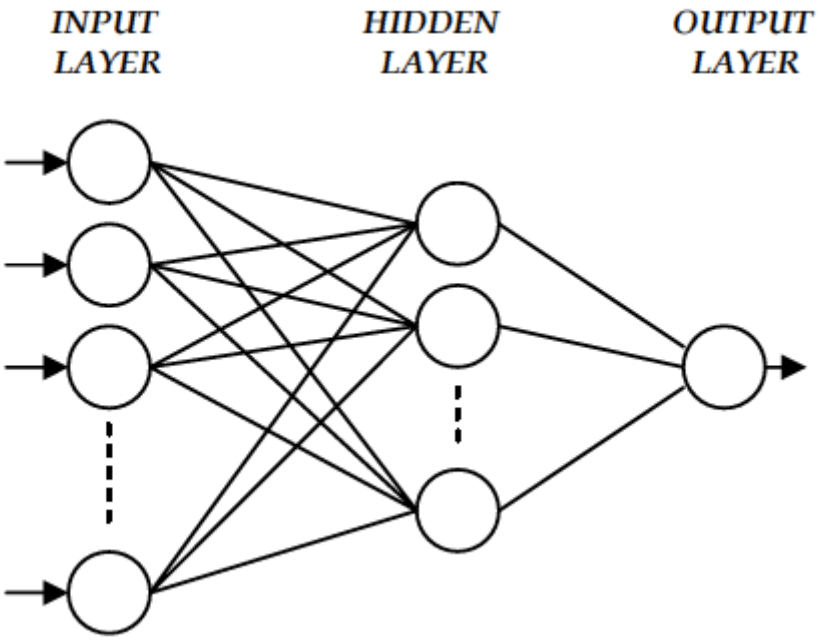

Figure 2.1. Typical architecture of an ANN model. Source: Kalteh, 2008

ANN rainfall-runoff models can be fast and robust tools where little is known about the physical characteristics of a catchment (Jeong and Kim, 2005; Mutlu et al., 2008). For example in a data scarce catchment, Mississippi, Hsu et al. (1995) showed that their ANN model even outperformed the conceptual Sacramento Soil Moisture Accounting (SAC-SMA) model. In another study conducted by Rezaeianzadeh et al. (2013), compared to the conceptual HEC-HMS model, the multiple layer perceptron (MLP) ANN rainfall-runoff model showed better performance for simulated peaks and annual runoff volumes for the Khosrow Shirin catchment in Iran. Wilby et al. (2003) made a major breakthrough to tackle criticism of ANN models that their intermediate hidden layers are unable to

explain the internal processes of catchment hydrology as done by conceptual and distributed models. The authors compared the simulated outputs from an ANN model with three nodes in a hidden layer and from a conceptual model with 12 parameters, employed in the Test River Basin of southern England. Results indicated that each of the three nodes corresponded respectively to quickflow/surface runoff, baseflow, and soil moisture simulated by the conceptual model. Mutlu et al. (2008) argued that an ANN model can take precedence over a distributed model if the experimental catchment lacks minimum required data by the distributed model. These authors developed an ANN model for the Eucha watershed of Oklahoma, USA (Figure 2.2) and found that daily streamflow simulation performance was very satisfactory.

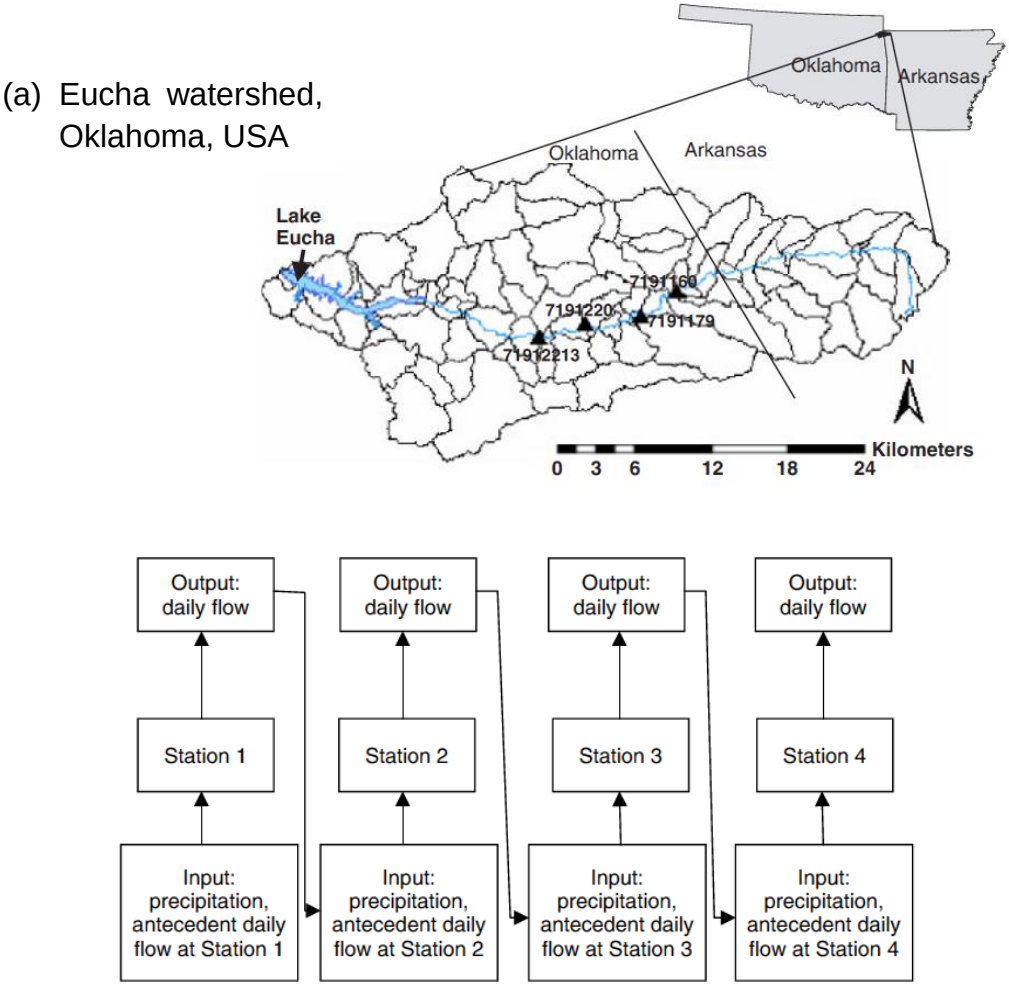

Figure 2.2. An example of real world application of ANN model. Source: Mutlu et al., 2008

Conceptual models, also termed grey-box models, are generally recognized as superior to empirical rainfall-runoff models since they emulate the major component processes of hydrological cycle rather than lumping those processes empirically. In conceptual modelling, precipitation/snow melt water is cascaded through some linear storage reservoirs such as surface, soil, and groundwater. In conjunction with few physical properties of each storage reservoir, necessary parameters are incorporated to determine the water retention ability of each reservoir and to route/transfer water from one reservoir to another or from reservoir to channel. Most conceptual rainfall-runoff models maintain the conservation of mass law and use simpler physical expressions for water movement in the system (Xu, 2002). Moreover, in data scarce environments, conceptual model may be the better alternative to more physics-based approaches with their higher data demands. Figure 2.3 shows a typical schematic diagram of a conceptual rainfall-runoff model where only two storage reservoirs are used and two different transfer functions are employed to route water over the hillslopes and channel networks. Practical applicability of a conceptual rainfall-runoff model is subject to how well its parameters are calibrated. According to Wilby et al. (2003), a conceptual model can be treated as a black-box type because parameterization of this model does not account for spatial variability of heterogeneous catchment's characteristics. In order to take the influence of spatial variation into account, conceptual models can be applied separately in each subbasin of a discretized basin and then runoffs from all subbasins are routed to the lowest outlet of the basin (Abebe et al., 2010; Thompson et al., 2015). With a conceptual model of the Inner Niger Delta Thompson et al. (2015) demonstrated how such a discretization approach can be employed to take the spatial variability of catchment including those associated with dams and floodplain inundation.

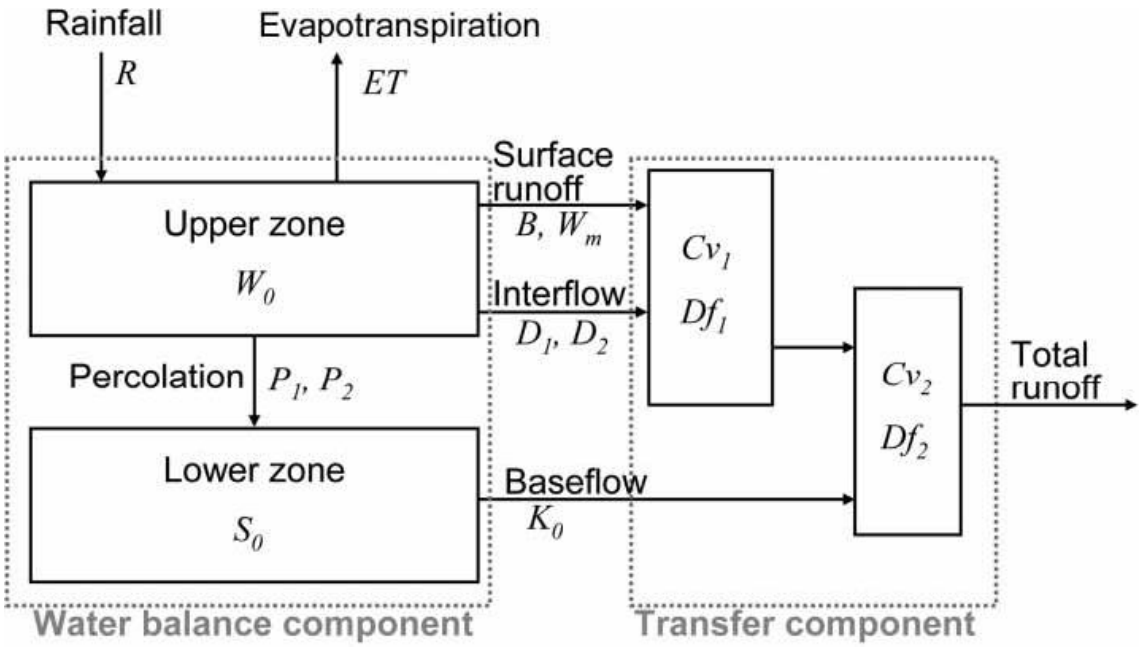

Figure 2.3. Example of a simple conceptual rainfall-runoff model. W_m is average storage capacity of the upper zone, B is shape parameter of the storage capacity probability distribution, D_1 is maximum interflow value, D_2 is shape parameter of the interflow curve, P_1 is maximum percolation value, P_2 is shape parameter of the percolation curve, K_0 is depletion rate constant of the reservoir representing base runoff, Cv_1 is convection coefficient of the parabolic hydrograph for transfer along hillslopes, Df_1 is diffusion coefficient of the parabolic hydrograph for transfer along hillslopes, Cv_2 is convection coefficient of the parabolic hydrograph for transfer along the river network, and Df_2 is diffusion coefficient of the parabolic hydrograph for transfer along the river network. Source: Alvisi et al., 2013

Physics-based rainfall-runoff models express major hydrological processes in the form of fundamental mathematical equations of conservation of mass, momentum, and energy (Freeze and Harlan, 1969; Valerity Y. Ivanov et al., 2004; Kavvas et al., 2004; Krysanova and Arnold, 2008; Meselhe et al., 2009). However, sometimes this definition of physics-based model is reduced to only laws of mass conservation. For instance, SWAT, one of the world's most frequently used catchment models, is often termed a physics-based model though it does not strictly consider the conservation of momentum and energy (Spruill et al., 2000). The major hydrological processes which are commonly used to identify a model if it is a physics-based are infiltration, evapotranspiration,

overland and channel flows, and groundwater dynamics (Kampf and Burges, 2007). However, many physics-based models do not use the state-of-the-art one dimensional (1D) Richard's soil water equation for estimating actual evapotranspiration as suggested by Kampf and Burges (2007). For example, MIKE SHE, one of the robust physics-based watershed models, estimates actual evapotranspiration based on empirical equation developed by Kristensen & Jensen (1975).

The identified three major distinctive characteristics of physics-based models are their inclusion of overland flow, channel flow, and groundwater dynamics which will be discussed in later sections (Sections 2.3.5, 2.3.6 and 2.3.7). Usually physics-based models, if they completely follow their governing principles, use less parameters than those of conceptual models and these parameters can be determined from field observations; therefore, they have specific physical meaning as well. Wong (2006) stated that the outstanding feature of a physics-based model is that the required parameters can be determined *a priori*, unlike many conceptual models that are to be calibrated against observed data, for example, time series of discharge data at the basin's outlet. In spite of these advantages, reliability of a physics-based model in simulating catchment response is not beyond questions (Krysanova and Arnold, 2008; Meselhe et al., 2009). Most of the physics-based governing equations to represent hydrological processes are derived from field scale studies. Using such an equation in a gridded heterogeneous catchment-scale model might not be as appropriate as it is for field scale (Dehotin and Braud, 2008). Moreover, many processes particularly those outside the purely hydrological category (e.g. dynamics of sediment, nutrients, and pollutants) are expressed as empirical forms; therefore, modelled results are highly subject to model structure. Despite having been developed with physics-based process equations, today many physics-based rainfall-runoff models are being parameterized against observed measurements (Ivanov et al., 2004); the principal reason is perhaps the inability to satisfy the complete data requirements throughout the catchment for a physics-based model. An excellent example can be demonstrated from the work of Panday & Huyakorn (2004). While developing a physics-based fully distributed catchment model, the authors modified the concept of "depth of water", generally represented as h or d, used in the St. Venant hydrodynamic equations for

overland and channel flows. Commonly, many physics-based watershed models treat “h” as excess rainfall or ponded surface runoff in overland flow equation and as water depth in channel flow equation. Panday & Huyakorn (2004) argued that ignoring the effects of micro-topographic depressions and exclusion of obstruction storage (e.g. vegetation in channels) will misrepresent real water depth; thus simulation results will not be accurate even though using a physics-based model.

2.2.2. Spatial discretization or representation of a catchment

Based on spatial representation, catchment models can be classified into (i) lumped and (ii) distributed categories. In lumped model, a catchment is considered as a unique system or a single computational unit i.e. all state variables (climate, land use, soil etc.) and parameters are invariant across the catchment (Daniel et al., 2010; Kling and Gupta, 2009; Meselhe et al., 2009; Shih and Yeh, 2011). The calibrated parameters of a lumped rainfall-runoff model thus reflect the average hydrological characteristics of the catchment. It is therefore often inappropriate to employ such lumped models where spatial variability of state variables is significant (Ivanov et al., 2004; Kalin and Hantush, 2014). This spatial variability is likely to increase with the increase of catchment size. To take spatial variability in the characteristics of a basin and in turn hydrological processes, into account, a basin can be spatially divided into several subbasins; a lumped model is separately applied in and calibrated for each subbasin (Meselhe et al., 2009; Thompson et al., 2015). Finally, the hydrological responses of individual subbasin are integrated to yield basin’s overall response. With an experiment on 49 catchments in Austria, Kling and Gupta (2009) showed that even though a lumped model is well calibrated its parameters still contain substantial noise due to neglecting the spatial variability of catchment’s physical properties thus has less confidence to simulate ungauged catchments.

In contrast to the lumped model, a distributed catchment model accounts for spatial variability of state variables across the basin by discretizing it into many smaller spatial elements/segments and consequently parameters of a distributed model vary from space to space. Kampf and Burges (2007) stated that a distributed model is one that “simulates pathways of water through XY or XYZ

surface-subsurface space" (Figure 2.4). A distributed model is thought to be a more robust and informative simulator than lumped model (Kampf and Burges, 2007; Kouwen, 2013; Shih and Yeh, 2011). Examples of some widely used distributed models include SWAT (Arnold et al., 1993), MIKE SHE (DHI, 2009b; Kristensen and Jensen, 1975), VIC (Liang et al., 1994), and MODFLOW (McDonald and Harbaugh, 1988). In the last three decades, application of distributed models has gained great attention in basin-scale hydrological modelling, specifically in assessing interactions among different hydrological processes, in assessing impacts of climate change and land use change on basin's water resources, in quantifying non-point source pollution, and in simulating erosion and sedimentation (Andersen et al., 2006; Öztürk et al., 2013; Rahman et al., 2014; Raneesh and Thampi Santosh, 2011; Singh and Woolhiser, 2002; Thompson et al., 2014b; L. Wu et al., 2012).

How a basin is discretized depends on several factors including the purpose of the modelling, data availability, catchment topography, model's structure and computational facilities. Different discretization approaches are used in distributed catchment modelling and include regular grid, Triangulated Irregular Network (TIN), hillslope zoning, and subbasins (Arnold et al., 2010; Kampf and Burges, 2007; Tucker et al., 2001) as shown in Figure 2.4. Among the different discretization configurations, the rectangular grid based approach is frequently used in many distributed catchment models, for instance, MIKE SHE (DHI, 2009b), CASC2D (Julien et al., 1995), GSSHA (Downer et al., 2002), KINEROS2 (Woolhiser et al., 1990) and WATFLOOD (Kouwen, 2013). Some of the reasons for the popularity of grid based discretization are readily available raster/pixel form spatial data (elevation, land use, soil, and climate variables) and easier representation of flow path direction in grid based models and computational simplicity when numerical solution techniques are applied for different process equations. Due to significant advancement of technology, today numerous remotely sensed information on the atmosphere and land systems are being retrieved by space borne satellites, RADAR and LiDAR; and these data are widely being used in distributed catchment modelling (Gupta et al., 2008; Kouwen, 2013; Rahman et al., 2014; X. Song et al., 2011; Stisen et al., 2008).

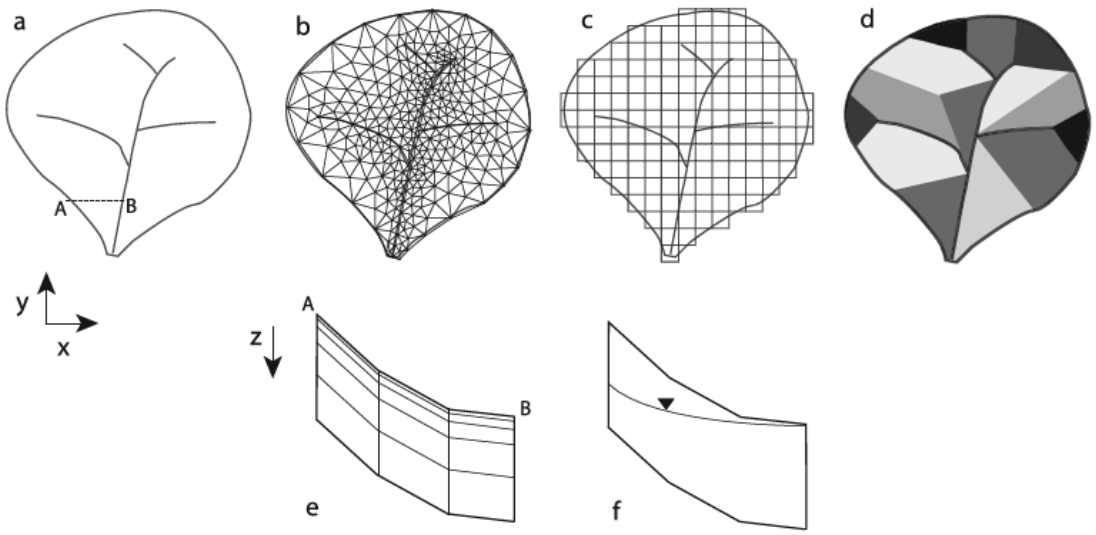

Figure 2.4. Different discretization configurations used in distributed watershed models: (a) hypothetical catchment (b) TIN discretization (c) rectangular or grid discretization (d) planes and channel segments (e) explicit discretization of depth Z and (f) discretization of Z into unsaturated and saturated zones. Source: Kampf and Burges, 2007

Usually in the rectangular grid based approach, different variables are computed at each grid and then routed from grid to grid (Figure 2.5). Such models, whose smallest computing unit is each individual grid, are often classified as fully distributed (Todini, 1988). However, in many distributed catchment model platforms, although the land surface and upper soil zone are discretized into XYZ directions, the lower soil zone/aquifer/groundwater zone is not explicitly discretized as it is seen in groundwater modelling with MODFLOW (McDonald and Harbaugh, 1988), for example. Reasons for not modelling a groundwater system in a fully distributed manner are the lack of availability of geological and observed groundwater level data, computational burden and negligible interaction between surface and groundwater systems.

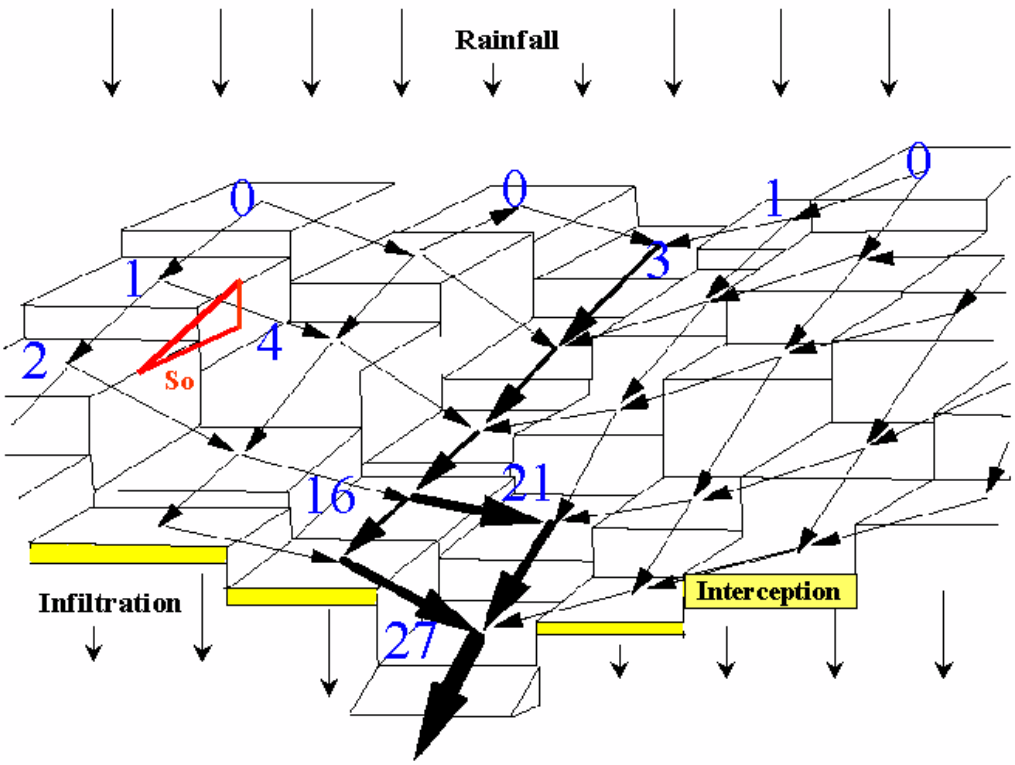

Figure 2.5. Routing process in rectangular grid based distributed catchment model. Source: Rojas et al., 2003

In gridded distributed modelling, there are two types of algorithms by which hydrological components are routed or moved from grid to grid, namely, D4 and D8 methods. In the former approach, hydrological components (for example, runoff) generated from a grid can move to any of the surrounding four grids depending on steepness of topographic slope or elevation of water surface between two adjacent grids. On the other hand, D8 method works in the same principle except runoff can be routed through any of the surrounding eight grids. To compare the relative performance of these two algorithms, Kalin & Hantush (2014) employed two catchment-scale models GSSHA (Gridded Surface Subsurface Hydrologic Analysis (GSSHA) model (Downer et al., 2002)) and KINEROS-2 (Kinematic Runoff and Erosion-2 (KINEROS-2) model (Woolhiser et al., 1990)) in the USDA experimental watershed W-2, Treynor, Iowa. The GSSHA model uses the D4 approach whereas the KINEROS-2 model uses the D8 approach. Results reveal that the cause of the underestimated and retarded peak

streamflows by the D4 based model is the longer travel path for overland flow and thus longer travel time than that of D8 approach.

In spite of having some distinctive advantages, regular grid based discretization schemes create the following problems: (i) constant resolution of the grid unnecessarily requires many grids for a homogeneous region, thus high demand for computational cost, if large spatial variability in other parts of a catchment are to be accurately represented, and (ii) coarser grids lack accurate terrain information, for example, slope (Ivanov et al., 2004; Ivanov et al., 2004; Tucker et al., 2001; Vivoni et al., 2004). To overcome these problems, Ivanov et al. (2004a) developed the TIN-based Real-time Integrated Basin Simulator (tRIBS) distributed model [a modified version of original RIBS (Real-time Integrated Basin Simulator) model developed by Garrote & Bras (1995)] where the watershed is discretized into many Voronoi polygons/regions (Tucker et al., 2001) generated from TIN digital elevation data. Figure 2.6 depicts a real world watershed discretized into several Voronoi polygons. While employing tRIBS model in three US watersheds, Ivanov et al. (2004b) showed that the number of computational elements decreased by 3-7% compared to the original regular gridded DEM data.

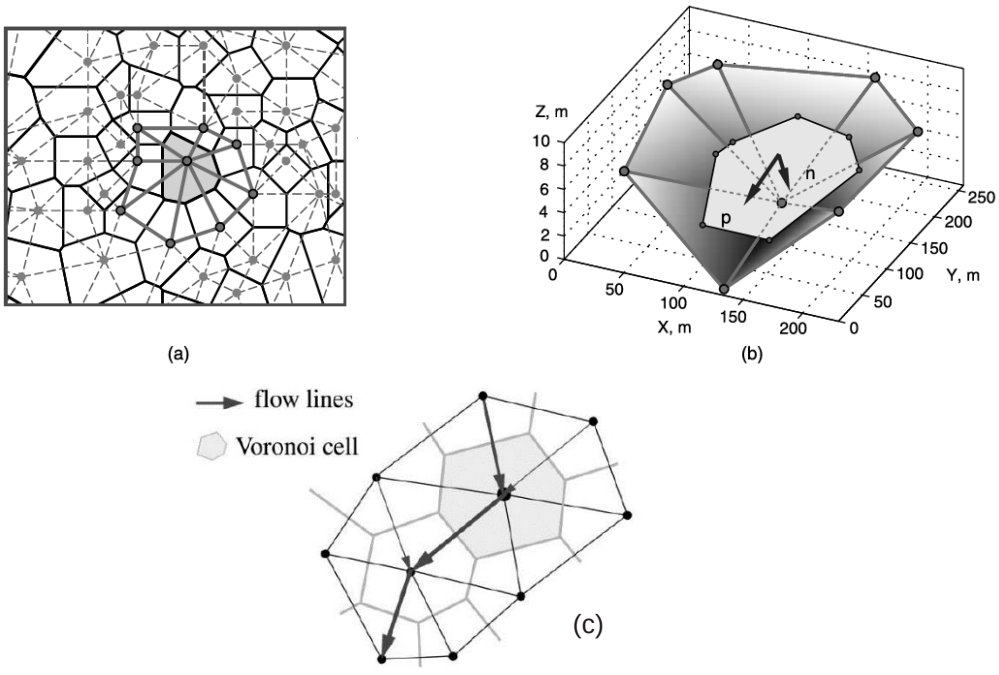

Figure 2.6. (a) Spatial discretization of a watershed into Voronoi polygons/cells where each dot point indicates node of TIN, dashed grey line indicates edge line of TIN data and polygon indicates Voronoi cell (b) 3D view of Voronoi cell where “p” indicates direction along steepest slope plane and “n” normal direction to “p” (c) interconnected Voronoi cells according to flow direction lines. Source: Tucker et al., 2001 and Ivanov et al., 2004

Semi-distributed catchment modelling is a trade-off between the computationally expensive but spatially informative fully distributed models and the computationally efficient lumped models, in expense of losing significant catchment's spatial information. There is no generalised definition or framework for semi-distributed models. A catchment model with a fully distributed surface water module and a lumped groundwater module can be categorized in semi-distributed family. Even though some models simulate vertical hydrological processes (e.g. precipitation and infiltration) at each grid of a sufficiently discretized catchment, horizontal processes (e.g. overland flow) are often lumped instead of routing through grids. This phenomenon can be better explained by exemplifying two different discretization approaches used in some semi-distributed models: (i) Hydrologic Response Units (HRUs) (Arnold et al., 2010) and (ii) Grouped Response Units (GRUs) (Bingeman et al., 2006; Kouwen, 2013). In the HRU approach, a catchment is first spatially divided into the required number of sub-catchments/subbasins. This depends on the purpose of project and on natural river networks. In the second step, each subbasin is further discretized into smaller units (HRUs). Each HRU within a subbasin is unique and homogeneous with respect to surface slope, land use and soil data. With this approach, many pixels having identical information/properties are aggregated into a single HRU regardless of their spatial position within a subbasin and all vertical hydrological components are computed separately for each HRU. The SWAT (Arnold et al., 1998, 1993; Neitsch et al., 2011) and SLURP (Kite, 2001) models use the HRU approach for watershed discretization. A detailed description of the HRU based discretization process is presented in Section 3.2.2 when describing the development of the SWAT model of the UMRB. In the GRU approach (Figure 2.7), a catchment is divided into several regular grids rather than into subbasins as used in HRU based SWAT and SLURP models. Later, within each grid boundary, all pixels having the same land cover are grouped into one GRU (Bingeman et al., 2006; Kouwen, 2013). So a grid may have several GRUs depending on the spatial variability of land use/land cover. Here pixel means the spatial unit (or resolution) of original land use/land cover data that is often retrieved from remotely sensed data. In these approaches (HRU and GRU) horizontal processes (e.g. overland flow and baseflow) from a smallest computational unit are directly transferred to downstream river/channel by some

time-constant based routing equations instead of explicitly routing through all linked computational units. The first approach is more robust as it takes into account spatial distributions of land use, soil, and topography whilst the latter only considers land use. However, the goal of both approaches is identical- reduction of computational time without losing spatial information, especially when a large catchment is to be modelled (Bingeman et al., 2006; Jing and Chen, 2011; Kouwen, 2013). Arnold et al. (2010) pointed out that a 100-m resolution grid based model of the Upper Mississippi River Basin of 500,000 km^2 (No. of grids = 50000000) would take 13 computational days to simulate only 1 year on a 2.6 GHz machine whilst the equivalent time was less than $1/500^{th}$ of the original time for HRU based modelling.

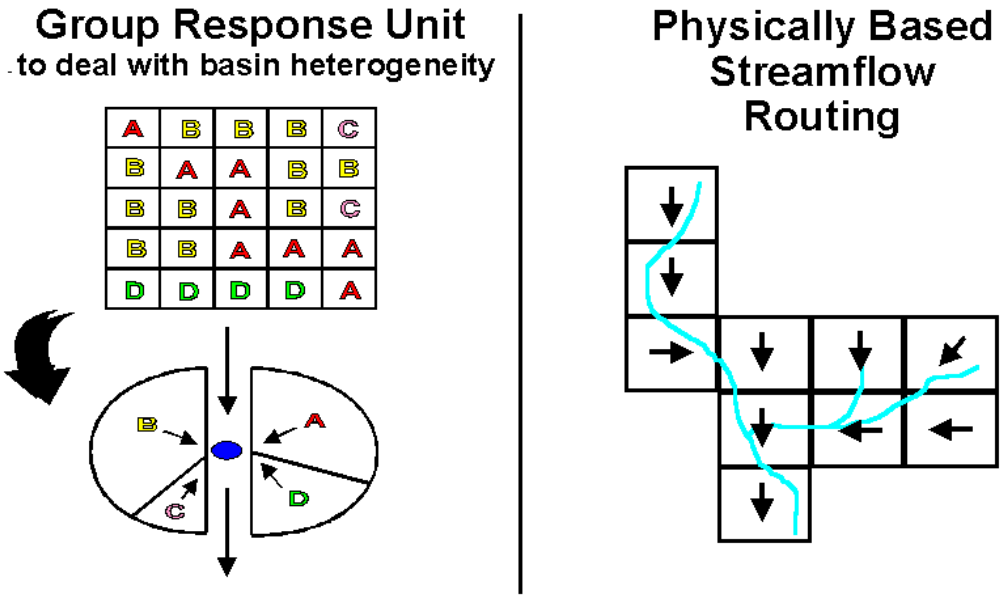

Figure 2.7. GRU based watershed discretization and water routing. Here, the top sketch of the left panel indicates a pixel based land use data and bottom sketch represents how similar pixels are grouped together. The sketch at right panel shows the routing concept adopted in GRU based watershed model. Source: Donald, 1992 cited in Kouwen, 2013

The HRU and GRU discretization approaches are computationally more efficient in catchment modelling. However, ignoring spatial interactions amongst HRUs within a subbasin or amongst GRUs within a grid might undermine the actual

response of different landscapes within a catchment (Arnold et al., 2010). For this reasons, the “catena” approach has been proposed to discretize a subwatershed/subbasin into three landscape units namely divide/edge, hillslope, and valley bottom/floodplain (Figure 2.8). As shown in Figure 2.8a, a subbasin is divided into three landscapes depending on the surface slope of the topography. This concept is further elucidated in Figure 2.9 where routing of hydrological components through different landscapes, discretized by catena method, is shown. Arnold et al. (2010) argued that if a rainfall-runoff model discretizes a basin in the following chronological order basin, subbasin, landscape units (catena) and HRUs, then the modelled results will be more reliable than that of only HRU or GRU based discretization.

Although many discretization approaches have been developed and incorporated in catchment modelling, there are no universal guidelines for catchment discretization (Migliaccio and Chaubey, 2008). However, discretization of a catchment should preserve some fundamental requirements: the size of elements should be computationally efficient without losing significant spatial information and should contain natural feature of the catchment, should be appropriate for numerical treatment if the differential forms of catchment’s flow equations such as the St. Venant equation are solved numerically (Voinov et al., 1998).

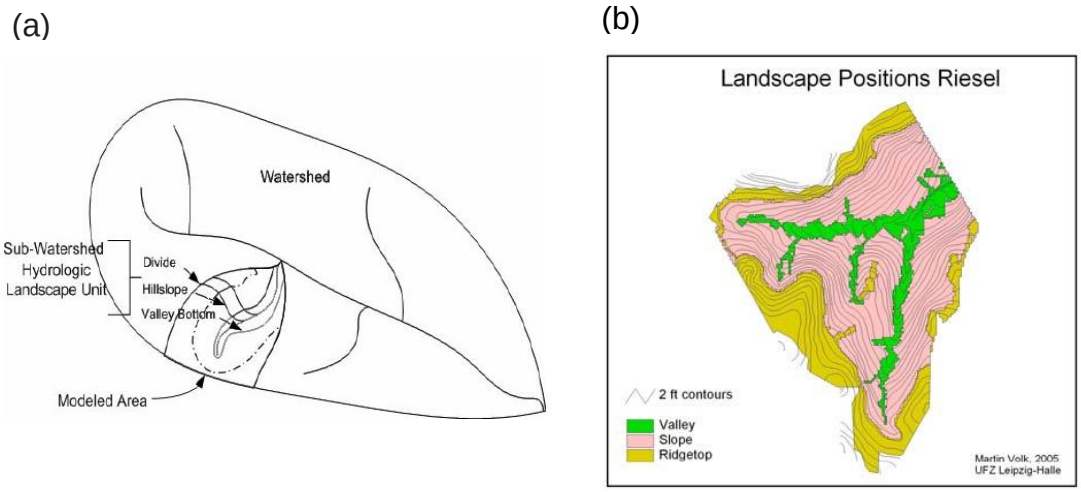

Figure 2.8. Delineation of a watershed using catena approach. Source: Volk et al., 2007

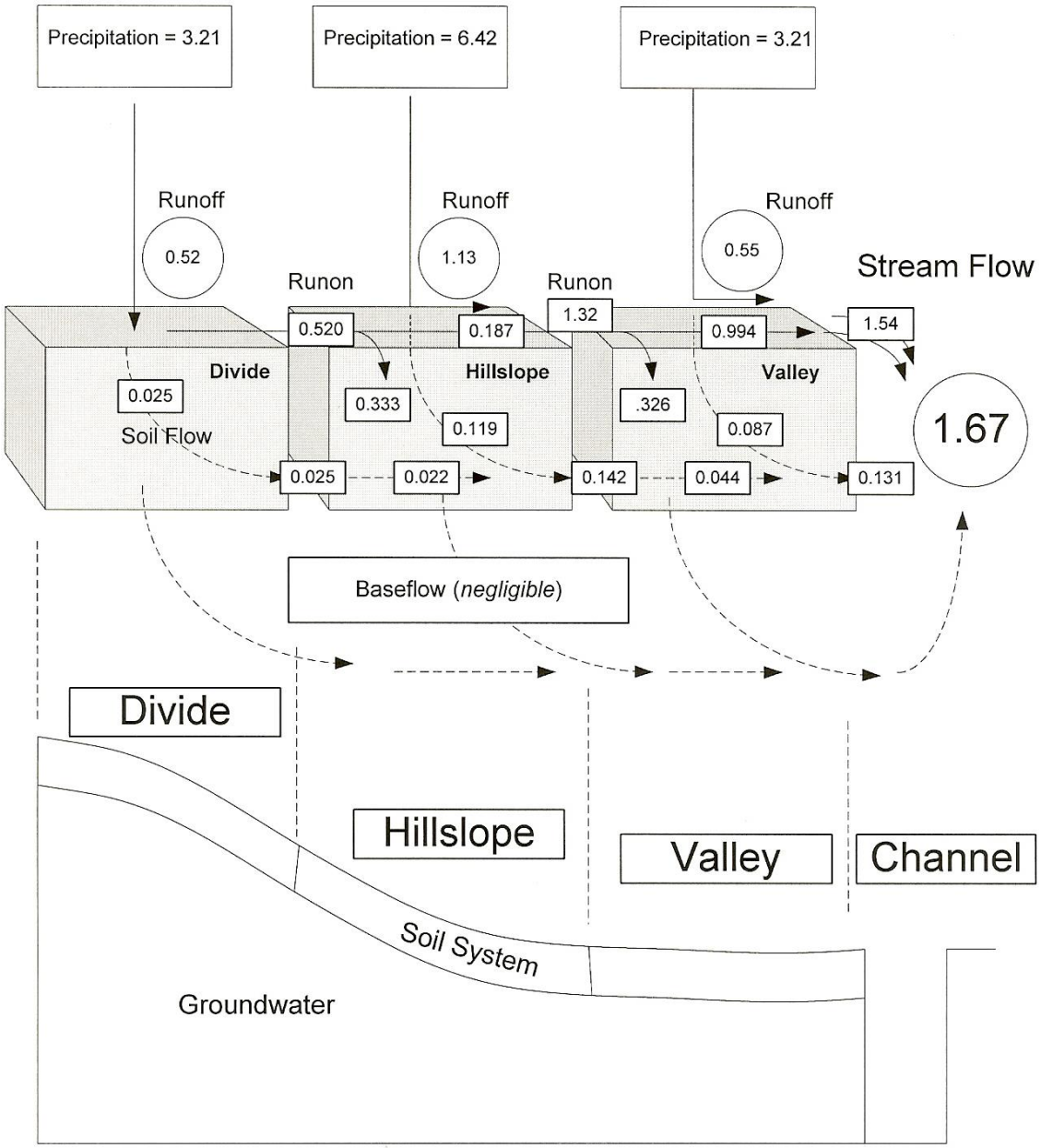

Figure 2.9. Routing of land-phase hydrologic components through different landscapes in the catena approach. Source: Arnold et al., 2010

Although a catchment is said to be a fully distributed one when discretization occurs across XYZ space (Singh and Woolhiser, 2002) many distributed models keep the saturated or groundwater zone lumped at Z space. This is the case for instance with SWAT, GSSHA and WATFLOOD models. Generally, such a semi-distributed model vertically divides the entire subsurface soil profile underlying each spatial model units (grid, HRU, or GRU) into three major zones upper (root

zone), intermediate (vadose zone), and lower (groundwater zone or aquifer system). However, given the importance of upper soil zone that predominantly influences all land phase hydrological components (surface runoff, ET, percolation and recharge to GW, baseflow, soil water), this zone might be further discretized into several subzones or layers as adapted in the SWAT model (see Section 3.3.3). The lack of adequate aquifer information (e.g., lithology, hydraulic characteristics, and time series of groundwater level) is probably the most significant reason behind the z-directional lumped groundwater modelling. For example, within the fully distributed MIKE SHE model, if modelling of the groundwater system with the 3D saturated zone module is prevented by data limitations, then conceptual linear reservoir models (interflow and baseflow) can be used to simulate the groundwater dynamics (DHI 2009; Thompson et al. 2013).

2.2.3. Time scale

With regard to time scale, rainfall-runoff models are divided into two basic classes (i) event and (ii) continuous (Chu and Steinman, 2009; Singh, 1995). Event hydrological models typically simulate a watershed's response, particularly discharge at the outlet, to a single rainfall event. Simulation of all major hydrological components, maintaining the laws of mass conservation, is not a concern here (Berthet et al., 2009) rather converting a single rainfall event into direct hydrograph at the outlet of catchment is the focal objective of the event model. To convert a rainfall event into direct hydrograph, the unit hydrograph approach is commonly practiced in event rainfall-runoff models (Chu and Steinman, 2009). Parameterization of an event hydrological model should come from the integrated performances of that model calibrated for various rainfall events because model reliability is highly subjected to spatial and temporal characteristics of rainfall event. Moreover, initial soil moisture conditions are another important factor that can severely impact the performance of event models (Coustau et al., 2012). However, despite relying on such subjective conditions, event rainfall-runoff modelling is still preferably being used in real-time operational applications like in flash flood forecasting (Coustau et al., 2012).

Unlike event types, continuous models have the capability to simulate a basin's hydrological states and responses continuously, from hours to many years (Bengtson and Padmanabhan, 1999; Coustau et al., 2012; Valerity Y. Ivanov et al., 2004; Kalin and Hantush, 2006; Neitsch et al., 2011; Pathiraja et al., 2012; Plate, 2009). The most distinguishable feature of a continuous model is its Soil Moisture Accounting (SMA) module that consistently updates catchment's wetness status by considering different influxes (infiltration, capillary) and outfluxes (evapotranspiration, percolation, lateral flow). The applications of this modelling approach include long-term impact analysis of climate and land use changes on water resources and estimating hydrological conditions (for example, river flows) of an ungauged catchment where regular monitoring are not possible or available.

2.3. Representation of different hydrological processes in catchment models

The major components of the hydrological cycle have been described in Section 1.2.1. This section describes how the major hydrological processes are commonly represented in distributed catchment models. A review of distributed models, whether they are conceptual or physics-based, shows that the dynamics of hydrology in a watershed are commonly represented by the following processes initial abstraction (interception of rainfall and depression storage), separation of rainfall into infiltration and surface runoff, evapotranspiration, overland flow, channel flow, and subsurface flow or groundwater flow.

2.3.1. Initial abstraction

Initial abstraction refers to how much rainfall is retained by different surficial storage reservoirs, for example, vegetation and surface depressions, before commencing surface runoff. Improper estimation of initial abstraction might lead the model to improperly predict all other subsequent land-phase hydrological components (Vegas Galdos et al., 2012). Depending on spatial coverage and characteristics of intercepting objects such as vegetation, the intensity and energy of ground-bound rainfall might drastically change. Rainfall intensity is one of the dominant factors causing flash-floods in foothill floodplains/valley regions

and soil erosion. For this reason, rainfall-runoff models must accurately account for initial abstraction. In distributed modelling, generally two basic approaches are applied to represent initial abstraction: (i) considering the effects of surface depressions and (ii) neglecting the effects of surface depression. In the former technique, one or two parametric simple linear or exponential equations are used to estimate gross initial abstraction (interception plus storage in surface depressions and infiltration before surface runoff) as a function of maximum storage capacity of surface depressions or land use/land cover (DHI, 2009a; Kouwen, 2013; Neitsch et al., 2011). To estimate initial abstraction, for example, the SWAT model (Neitsch et al. 2011) uses USDA's Soil Conservation Service Curve Number (SCS-CN, (USDA, 2004)) method that is a function of land use/cover, antecedent soil moisture, and hydrologic soil group, shown in equation 2.1. On the other hand, WATFLOOD (Kouwen, 2013) uses an exponential equation (see equation 2.2) as a function of rainfall and of depression storage:

$$I_a = 0.2 * S = 0.2 * \left[25.4\left(\frac{1000}{CN} - 10\right)\right] \quad 2.1$$

$$I_a = (1 - \mathrm{e}^{-kR_c}) * S_d \quad 2.2$$

where, I_a is the initial abstraction, S is the maximum surface retention, CN is the SCS's curve number, R_c is the accumulative rainfall, S_d is the depression storage given by the users, and k is a constant. The main criticism of the SCS-CN method is its arbitrary assumption that 20% of maximum surface retention is to be considered as initial loss (many references cited by Tedela et al. (2012)). Another weakness of this model is that it ignores the effects of temporal dynamics of foliage on interception thus on initial abstraction, rather either soil moisture or rainfall is the time variable in the equations. In a region where leaf dynamics is significantly seasonal, an interception model that accounts for such effects would certainly reduce the uncertainty in the rest of hydrological components compared to time-invariant foliage models. Therefore, interception models that relate "storage capacity of canopy", a one-dimensional (L) physical property of vegetation to express its maximum rainfall retention ability, to the temporal variation of land cover, are incorporated in many physics-based distributed models, for example, MIKE SHE, GSSHA, SWAT and CASC2D. However, this

type of approach does not often explicitly consider surface depression storage. To account for temporal variability, interception might be expressed as a function of leaf area index (LAI) and/or rainfall, in addition to canopy storage capacity. For example, the interception model shown in equation 2.3 is used in the MIKE SHE model which overlooks the effects of canopy wetness on interception. However, usually rate of interception decreases with the degree of canopy wetness and may even reach "0" when canopy reaches at its storage capacity (maximum limit). For this reason, some models (for example, GSSHA, CASC2D, KINEROS-2) express interception as a function of canopy wetness as well (see equation 2.4):

$$I_a = C_{mx} * LAI \qquad 2.3$$

$$i(t) = \begin{cases} b * R(t) & if\ I < C_{mx} \\ 0 & if\ I > C_{mx} \end{cases} \qquad 2.4$$

where $i(t)$ indicates interception rate, $R(t)$ indicates rainfall rate, I indicates cumulative interception, and C_{mx} indicates canopy storage capacity (maximum storage). In all of the interception models, the common postulation is that intercepted water can only be removed by evaporation, but some researchers (Pitman, 1989; Rutter et al., 1975, 1971) show that drainage is another considerable components in surficial water mass balance of canopy as shown in equations 2.5 and 2.6 that are used in tRIBS catchment model (Ivanov et al., 2004):

$$\frac{dC}{dt} = (1 - P)R - D - \frac{C}{C_{mx}} E_p \qquad 2.5$$

$$D = ke^{g(C - C_{mx})} \qquad 2.6$$

where P, k, and g are parameters, C is canopy storage at time t, and E_p is potential evaporation.

2.3.2. Separation of rainfall into surface runoff and infiltrated water

Separation of ground-bound rainfall (rainfall less initial abstraction) into surface runoff and infiltrated water is the most crucial part of any rainfall-runoff model. Turner (2006) argued that infiltration, the entrance of rainfall into top soil, and redistribution, water movement through soil horizon, cannot be separated as these two processes are interactively dependent on each other. Many factors influence the processes of infiltration and movement of water through the soil profile. The factors can be grouped as soil properties (texture, water content and field capacity, hydraulic conductivity, macro-pores, diffusivity, temperature), topography (surface slope), land cover, rainfall intensity, and depth of ponded water. A detailed description of how these factors influence infiltration was presented in the work of Turner (2006).

In separating rainfall into runoff and infiltrated portions, generally two modelling approaches are followed: (i) Hortonian and (ii) soil saturation or non-Hortonian (Downer and Ogden, 2004; Kirkby, 1988; Putty, 2009; Weill et al., 2009). In the former method, how much rainfall water can be infiltrated into the soil depends on soil infiltration capacity that is a time variant exponential decaying characteristic of soil. Until the rainfall rate exceeds infiltration capacity, water keeps entering the soil system. Whenever rainfall rate exceeds infiltration capacity of soil, excess water will be ponded on the surface and available for surface runoff and evaporation. In the second approach, moisture content status of a soil system determines whether rainfall can enter into the soil system and if then, how much. If a specific soil system is completely saturated with water, then no water, whatever the rate of rainfall, cannot be infiltrated into the soil system rather rainfall is ponded on the ground surface and is available for surface runoff. Based on the process representation, Mishra et al. (1999) and Mishra et al. (2003) classified infiltration models into three groups: (i) physics-based/mechanistic models that are developed based on laws of mass conservation and their parameters have clear physical meaning and can be determined from field data, (ii) empirical models that are developed from experimental data and their parameters are to be calibrated, and (iii) semi-empirical that lies in the intermediate position of first two categories i.e., neither explicitly physical nor explicitly empirical. Although there are many infiltration

models, only a few of them are frequently incorporated in distributed catchment models. Perhaps, this is because of their applicability in different environments, smaller data demands, and most importantly their mass balance principle which is essential for continuous hydrological modelling of a catchment. However, whatever their developmental basis (mechanistic or empirical), almost all infiltration models are originated from laboratory-scale and/or field-scale studies using standard conditions. For example, a horizontal land surface is one of the commonest assumptions for which these infiltration models are developed; their ability to model hillslope infiltration is rarely verified (Philip, 1991).

The one dimensional Richard's (Richards, 1931) flow equation (equation 2.7), which is originally developed from Darcy's flow model through porous media, is successfully incorporated in many physics-based distributed models such MIKE SHE (Refsgaard and Storm, 1995), GSSHA (Downer and Ogden, 2006, 2004), and WASH123D (Yeh et al., 1998).

$$C(h)\frac{\partial h}{\partial t} = \frac{\partial}{\partial z}\left[K(h)\frac{\partial h}{\partial z}\right] + \frac{\partial K(h)}{\partial z} - S \qquad 2.7$$

Where $C(h)$ is the specific water holding capacity or gradient of pressure head vs moisture content curve, h is the pressure head, $K(h)$ is the hydraulic conductivity of soil at h, z is the elevation from a datum, and S is the source/sink term. The prominent features of this equation are preservation of the mass conservation law, appropriateness for use in both unsaturated and saturated soil conditions, easy integration with other hydrological components through source/sink terms (e.g., plant water uptake/evapotranspiration), and numerically solvable for discretized/layered soil profile (Cortis and Montaldo, 2013; Downer and Ogden, 2006, 2004; Weill et al., 2009). When equation 2.7 is applied for the top soil layer (see Figure 2.10) it estimates infiltration rate for a particular time step. Initially an arbitrary infiltration rate or ponded water depth (h) on the soil surface is assumed as part of upper boundary condition and then the numerical form of equation 2.7 is solved iteratively until water mass balance is achieved for the top soil layer. Final infiltration rate for a specific time step is the one for which the equation satisfies the laws of mass conservation. At the end of the time step, any surface

water excess to infiltrated amount is considered as ponded water that is available for overland flow or other process like surface evaporation.

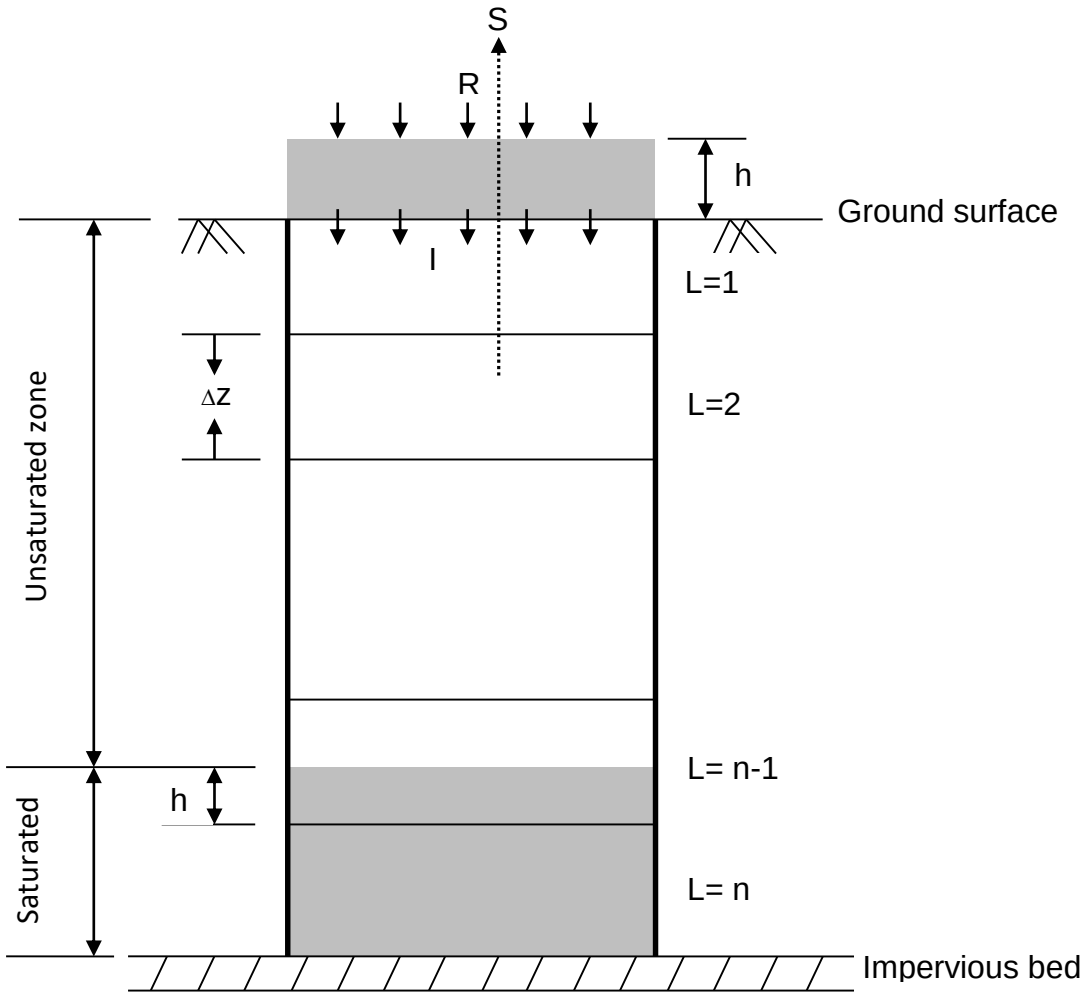

Figure 2.10. A typical schematic diagram of a vertically discretized soil profile (saturated and unsaturated zones). R is the rainfall rate, I is the infiltration rate, h is the pressure head either saturated or unsaturated condition, Δz is the vertical length of discretized unit, grey colour indicates ponded water on soil surface or saturated zone, L is the layer, n is the number of layer, and S indicates source/sink for a particular grid.

Although having many outstanding features, the application of Richards' 1D vertical flow equation for porous media has been reported as problematical for some specific cases (Zaslavsky & Sinai 1981 cited by Downer & Ogden 2006; Zhang et al. 2011). Since flow within a soil column is restricted to the vertical

direction, regions where lateral flow from a perched water table or from an inclined impermeable geologic formation in unsaturated zone is significant cannot be simulated (Zaslavsky & Sinai 1981 cited by Downer & Ogden 2006). Specifically, in many hillslope areas lateral flow is one of the prominent hydrological components (Zhang et al., 2011). Moreover, Downer and Ogden (2006) showed that resolution of vertically discretized soil profile near the surface should be kept very fine, as low as 1 cm, to obtain a better simulation from a numerical solution of Richards' equation irrespective of watershed types. This created large computational demands and the need to have fine vertical discretization. Although preferential/macropore flow might play a major role in forested areas (Cheng et al., 2007; Noguchi et al., 1997), none of the distributed models reviewed in the present study explicitly incorporates macropore flow in Richard's equation as used in PREFLO model (Workman and Skaggs, 1990).

The Green-Ampt (Green and Ampt, 1911) physics-based infiltration model has been widely used at the field and laboratory scales (Mirzaee et al., 2014; Mishra et al., 2003). Many distributed catchment models (SWAT, tRIBS, ANSWERS (Beasley et al., 1982), HEC-HMS (Scharffenberg, 2013), CASC2D, WEPP (Flanagan et al., 1995)) incorporate the Green-Ampt (GA) infiltration model, because of its physically measureable parameters (Brakensiek et al., 1981; King et al., 1999; Ogden and Sagafian, 1997). Equation 2.8 is the generalized mathematical form of the GA infiltration model. Its validity is subject to some assumptions: (i) infiltrated water moves downward with a sharp wetting front as shown in the right panel of Figure 2.11, (ii) soil remains under completely saturated condition above the wetting front, (iii) a pool of ponded water exists on the soil surface, and (iv) soil is homogeneous.

$$I = K_e\left[1 + \frac{h + h_{wf}}{z}\right] = K_e\left[1 + \frac{\Delta\theta * h_{wf}}{F}\right] \qquad 2.8$$

Where I is the infiltration rate, K_e is the effective hydraulic conductivity of soil, h is the depth of ponded water, h_{wf} is the pressure head at wetting front or capillary pressure, z is the depth of soil profile, $\Delta\theta$ is the change in volumetric water content of soil, and F is the cumulative infiltrated water.

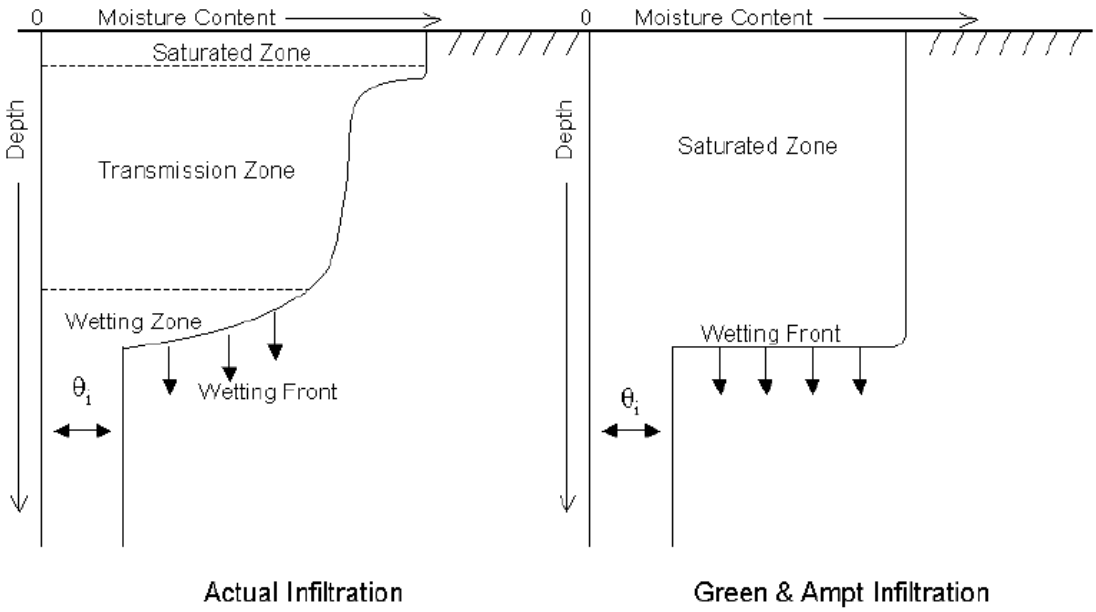

Figure 2.11. Depth-wise distribution of moisture content by the Green-Ampt (GA) model and a typical observation. Source: Neitsch et al., 2011

Because of its strict assumptions, application of the original GA infiltration model (equation 2.8) to reproduce real world soil hydraulics has been the subject of numerous discussions. Consequently this model has been modified and configured in different ways to be applied in multifarious environments (Childs and Bybordi, 1969; Downer and Ogden, 2006; Ivanov et al., 2004; Ma et al., 2011; Mein and Larson, 1973; Ogden and Sagafian, 1997). For example, the term “effective hydraulic conductivity” used in equation 2.8 must not always be for saturated condition since an unsaturated transition zone overlying the wetting front is a common phenomenon in many situations. To account for this effect, “effective hydraulic conductivity” is expressed as a function of depth and surface slope (Ivanov et al., 2004), land use, and antecedent soil moisture content (Dabral and Cohen, 2001; Neitsch et al., 2011). While developing the distributed tRIBS model, (Ivanov et al., 2004) used five different forms of the GA equation to represent distinct infiltration mechanisms that might occur in the real world, depending on the status of soil moisture (saturated i.e. when water is ponded on the surface and unsaturated) and rainfall intensity. Without violating the assumption of homogeneity of soil properties, the integral form of the GA equation, as shown in equation 2.9, has successfully been used in layered soil

distributed models such as SWAT (Neitsch et al., 2011) and GSSHA (Downer and Ogden, 2006).

$$F^t = F^{t-1} + (K_e * \Delta t) + (h_{wf} * \Delta\theta) \ln\left[\frac{F^t + h_{wf} * \Delta\theta}{F^{t-1} + h_{wf} * \Delta\theta}\right] \quad 2.9$$

Where t indicates time that advances with time step Δt. The time derivative of equation 2.9 yields infiltration rate which, in turn, is used to decide surface ponding potentiality of a rainfall event. Any rainfall that cannot be infiltrated during a time step is ponded over the soil surface and available for surface runoff. Although the GA equation is a well-known and widely used infiltration model for Hortonian watersheds, it cannot simulate a non-Hortonian watershed's response i.e. where exfiltration, due to soil saturation or higher groundwater level, may generate overland flow (Dabral and Cohen, 2001; Ivanov et al., 2004). This issue is clearly addressed by Ivanov et al. (2004) where they modified the configuration of the original GA model to account for non-Hortonian watershed's behavior. In the SWAT model, this problem is tackled by using a mass-balance based soil water routing algorithm to move water from one layer to another, rather GA equation is used only to calculate infiltrated water in the top soil layer (Neitsch et al., 2011).

There are other physics-based infiltration models including Philip (1957), Parlange (1971) and Smith & Parlange (1978). The Parlange infiltration model is embedded in the Kinematic Runoff Erosion (KINEROS, KINEROS-2) and HEC-HMS (Scharffenberg, 2013) models whereas WATFLOOD uses Philip's infiltration model. These infiltration models are the generalized form of the GA model and they require almost the same input data, for example, initial and saturated moisture content, ponding depth, and capillary pressure at wetting front (Kalin and Hantush, 2006; Mishra et al., 2003).

Among many semi- and empirical infiltration models, the SCS-CN method has been the most widely used model across the world either as an standalone surface runoff simulator or as an integral part of another distributed catchment model (King et al., 1999; McCutcheon, 2003; Mishra and Singh, 2004; Putty,

2009; Rozalis et al., 2010; Soulis et al., 2009; Tedela et al., 2012). The US Soil Conservation Service, now the National Resources Conservation Services (NRCS), developed this surface runoff/infiltration model in 1954, based on a huge experimental data set of 199 watersheds from across the country (Tedela et al., 2012). The SCS-CN method uses water mass balance and proportionality equations, respectively 2.10 and 2.11, to develop final surface runoff formula as shown in equation 2.12:

$$P = I_a + F + Q_s \tag{2.10}$$

$$\frac{Q_s}{P - I_a} = \frac{F}{S} \tag{2.11}$$

$$Q_s = \begin{cases} \dfrac{(P - I_a)^2}{(P - I_a + S)} & if\ P > I_a \\ 0 & if\ P \leq I_a \end{cases} \tag{2.12}$$

where P, I_a , F, S, and Q_s are the precipitation, initial abstraction, cumulative infiltration, maximum retention, and surface runoff, respectively. Generally initial abstraction is assumed as some fraction, in most cases 0.2, of maximum retention (S) which is a function of Curve Number (CN), a numerical scaling value to represent catchment's water retention capacity (S) based on land use, soil type and soil moisture content. Rainfall water less generated surface runoff and initial abstraction is allowed to infiltrate into the soil system. From the findings of their extensive research works, the NRCS developed the tabular and graphical forms of CN which is used to estimate maximum retention of a catchment as shown in Equation 2.13 for SI unit mm.

$$S = 25.4\ (\frac{1000}{CN} - 10) \tag{2.13}$$

A detailed explanation on SCS-CN method is provided in Section 3.3.2 in the context of model development for the UMRB. Although since its development the SCS-CN method has been employed in different catchments, many investigations unveil a number of limitations of this approach (Ponce & Hawkins 1996; McCutcheon 2003; Mishra & Singh 2004; Putty 2009; Soulis et al. 2009;

Rozalis et al. 2010; Tedela et al. 2012). Some researchers found that the SCS-CN method was not able to reproduce surface runoff from forested watersheds as accurately as from agricultural watersheds (McCutcheon, 2003; Mishra and Singh, 2004; Ponce and Hawkins, 1996; Tedela et al., 2012). The common argument behind this limitation is that values of CN are determined from the results of agricultural watersheds; thus this tabulated CN is likely to be biased. Because runoff generation processes in agricultural and forested watersheds are different, therefore, original tabulated values of CN should be readjusted or calibrated for other types of watersheds (Mishra and Singh, 2004). Putty, (2009) demonstrated that forested watersheds, where subsurface or slow flow (base flow and interflow) is a major contributor of total runoff/streamflow, cannot be modelled with SCS-CN.

In addition to the characteristics of catchments, applicability of the SCS-CN model has also been proved highly conditional on rainfall characteristics (Mishra and Singh, 2004; Rozalis et al., 2010). Rozalis et al. (2010) employed this model to simulate high intensity short-duration rainfall driven flash flood and moderate/low intensity long-duration rainfall driven normal flows in the agriculture dominated Mediterranean catchment of Merhavia, Israel. They concluded that the reason behind poorly simulated runoff for longer duration rainfall events was the model's inability to take account of temporal variation of soil moisture, thus maximum retention parameter, although the catchment was dominated with agricultural land use. Unless any change in land use/cover, soil, or initial moisture status occurs, the value of maximum retention parameter (S) remains constant over the time when modelling with original SCS-CN method. However, these limitations of the SCS-CN model were overcome in some continuous catchment models that simultaneously update CN depending on soil moisture status at each time step and previous CN value (Neitsch et al., 2011; Putty, 2009). For example, in the SWAT model which uses SCS-CN method, daily soil moisture is updated with soil water balance algorithm and accordingly CN is also updated for new soil moisture content (Neitsch et al., 2011).

Unlike parametric empirical infiltration models, physics-based models depend on initial soil water content and soil properties, and in most cases have been developed at the laboratory scale in controlled environment. Therefore, superior

performance of physics-based models over empirical ones for real world catchment-scale application may not be guaranteed as insufficient data are most likely at larger spatial scales. Mishra et al. (2003) compared the performance of 14 infiltration models, ranging from physics-based to empirical, with 243 sets of observed infiltration data collected from field and laboratory experiments conducted in India and USA. When ranking in order of their performance, the first three models were from the family of empirical or semi-empirical whilst the physics-based Smith-Parlange model jointly took 4th place with another empirical model. In another experiment, King et al. (1999) showed that streamflow simulation at the outlet of larger watersheds was better for empirical SCS-CN infiltration model than that of physics-based Green-Ampt Mein Larson (GAML) model. However, they found that GAML outperforms SCS-CN in simulating flood hydrograph that is mainly generated due to high rainfall intensity i.e. where Hortonian infiltration process is dominant.

2.3.3. Evapotranspiration (ET)

Evapotranspiration is an important component of the hydrological cycle. About 60% of global annual precipitation returns to atmosphere through ET (Oki & Kanae 2006 cited in Jung et al. 2010). Therefore, unrealistic representation of ET process in hydrological model will greatly impact overall model performance (Zhao et al., 2013). Zhao et al. (2013) conducted an excellent review of how hydrological models represent ET. After studying 16 most commonly used hydrological models, they identified two major approaches of ET simulation in hydrological models: (i) the classification gathering method and (ii) the integrated converting method. In the former method, evaporation from open water and soil, and transpiration through plant system are separately estimated before integrating them to obtain total ET. On the other hand, in the later approach, potential evapotranspiration (PET) is first estimated with a standard formula, for example, Priestley-Taylor method (Priestley and Taylor, 1972), and then PET is downscaled to actual ET by including the effect of soil moisture status. Zhao et al. (2013) argue that many conceptual hydrological models preferably use “integrated converting method” because of its easier adaptability and less data requirement.

2.3.4. Soil moisture redistribution in unsaturated zone

After infiltration and redistributed in the surface soil layer, soil water moves downwards if it has sufficient energy gradient (sum of elevation and hydraulic gradients). In distributed models, the movement of soil water is generally simulated in a cascading way between adjacent vertically discretized soil cells/layers as shown in Figure 2.10. Physics-based models that use 1-D Richard's equation update hydraulic head and flux of each cell at every time step (Downer and Ogden, 2006, 2003). How much water percolates out of bottom layer, which is ultimately recharge to the saturated zone or groundwater aquifer, is estimated using the boundary conditions at the lower and upper layers of the unsaturated and saturated zones, respectively. Some Richard's equation based models, for example GSSHA, interactively and simultaneously simulate the unsaturated zone (UZ) and saturated zone (SZ) where these two zones are interfaced by the water table. On the other hand, some models separately simulate these two zones before coupling them for mass transfer, for example in MIKE SHE (DHI, 2009b). In distributed conceptual models, soil water distribution and movement from one layer to another are usually simulated based on a storage routing method (Bingner et al., 2011; Connolly et al., 1997; Neitsch et al., 2011). This method requires physical characteristics of soils to estimate hydraulic conductivity, field capacity, wilting point, porosity, and air-entry value. Whenever water content in a soil layer is above field capacity, then excess water is routed into lower layer with some lag time parameters based equations. Percolated out water from the lowest soil layer is transferred either directly to aquifer or through an intermediate vadose zone to aquifer as recharge. For example, in the SWAT model, a virtual vadose zone is assumed to be sandwiched by the bottom soil layer of soil profile and lower shallow aquifer; therefore, percolated water is routed through this zone using some lag time parameters. Such an approach might be appropriate where depth to water table over the year is too high to have a chance to cause saturation excess runoff. However, where a shallow water table rapidly responds to seasonal rainfall such a conceptualization will not be appropriate. A few distributed models (e.g. WATFLOOD, ANSWERS) consider whole soil profile as a unique unit/cell/layer rather than distributed, probably these models are developed particularly for Hortonian overland flow where saturation excess is unlikely and groundwater contribution is insignificant.

2.3.5. Overland flow

In a distributed catchment model, the overland flow module transfers ponded surface water between adjacent cells/grids or other spatial discretized units. Many overland flow equations, spanning from physics-based to empirical types, have been incorporated into distributed models. Kampf and Burges (2007) stated that the 2D St. Venant equations, based on the conservation laws of mass and momentum, are commonly used to simulate overland flow in physics-based distributed watershed models. The simplified forms of St. Venant equations are represented as:

2D continuity equation of mass

$$\frac{\partial h}{\partial t} + \frac{\partial}{\partial x}(uh) + \frac{\partial}{\partial y}(vh) = S \qquad 2.14$$

2D momentum equation

$$\frac{\partial u}{\partial t} + u\frac{\partial u}{\partial x} + v\frac{\partial u}{\partial y} = g(S_{0,x} - S_{f,x} - \frac{\partial h}{\partial x}) \qquad 2.15$$

$$\frac{\partial v}{\partial t} + u\frac{\partial v}{\partial x} + v\frac{\partial v}{\partial y} = g(S_{0,y} - S_{f,y} - \frac{\partial h}{\partial y}) \qquad 2.16$$

where u and v are the average velocities of water at x and y directions respectively, h is the depth of ponded water, S is the source (+)/sink (-), t is the time, g is the gravitational acceleration, S_0 and S_f are the bed slope and friction slope. Some investigators (Dunne et al., 1991; Kampf and Burges, 2007; Panday and Huyakorn, 2004) emphasized that the depth “h” should be estimated by taking account the storage effect of depressions and obstructions where their influence is significant. For example, in a dense forest of large trees, the depth of a fixed volume of ponded water will be considerably greater than that if there were no trees; this phenomenon has been shown in Figure 2.12. The term “S” is the net amount of water on a particular grid during specified time step. Usually it is the difference of rainfall rate and infiltration rate but other significant influx and outflux should also be included, for instance, if the time step in the numerical solution is comparatively large, then ignoring evaporation may violate the mass

conservation principle. To convert all differentiable variables of above equation into single variable “h”, velocity term (u and v) is often expressed as Manning’s formula (equations 2.17 and 2.18), where n is the roughness of coefficient.

$$u = \frac{1}{n} h^{5/3}\left(S_{0,x} \; or \; S_{f,x}\right)^{1/2} \qquad 2.17$$

$$v = \frac{1}{n} h^{5/3}\left(S_{0,y} \; or \; S_{f,y}\right)^{1/2} \qquad 2.18$$

The 2D overland flow equations (2.14, 2.15 and 2.16) cannot be solved analytically; therefore, various numerical schemes are usually employed to solve them and are used in grid based distributed watersheds models. The three most commonly used solutions are fully dynamic, diffusive, and kinematic wave approximation methods. As each solution technique is based on some assumptions, a modeller must judge beforehand the applicability of the model in light of catchment characteristics and logistic supports (Rousseau et al., 2012; Shih and Yeh, 2011). In the fully dynamic wave (FDW) approach, rather than omitting any elements of momentum equations, all component effects are taken into account. However, this approach demands high computational cost and is not suitable for steep hillslopes (Kampf and Burges, 2007; Shih and Yeh, 2011). While solving with diffusive wave approximation (DWA) approach, force terms at the left hand side of the momentum equations are neglected; therefore, the final forms of formulae look like equations 2.19 and 2.20. The main advantages of the simplified DWA technique are less computational burden compared to FDW and capability to take backwater effect on flows over different landscapes (DHI, 2009a; Huang, 2006; Lai, 2009; Shih and Yeh, 2011; Yamazaki et al., 2011). The simplest form of the original momentum equation is kinematic wave approximation (KWA). This ignores all force and pressure head terms as represented by equations 2.21 and 2.22. This approximation assumes that the slope line of water surface is parallel to the bed slope i.e., the backwater effect is then completely neglected. Although KWA-based models can be applied in moderate sloped catchments, use of such models in low relief areas, for example, floodplains and valley areas, is strongly discouraged (Huang, 2006; Jain and Singh, 2005; Shih and Yeh, 2011).

$$\frac{\partial h}{\partial x} = S_{0,x} - S_{f,x} \quad 2.19$$

$$\frac{\partial h}{\partial y} = S_{0,y} - S_{f,y} \quad 2.20$$

$$S_{0,x} = S_{f,x} \quad 2.21$$

$$S_{0,y} = S_{f,y} \quad 2.22$$

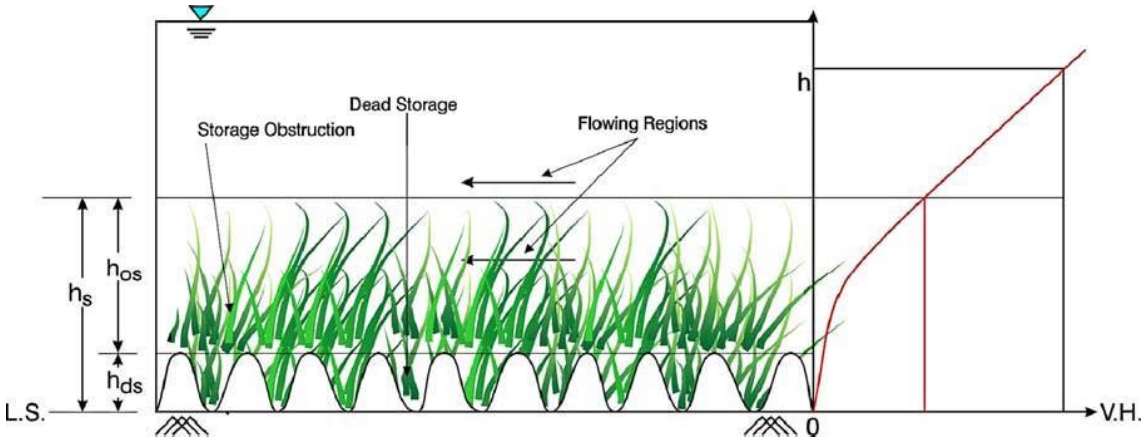

Figure 2.12. Effect of depressions and obstructions on the relationship between ponded surface water depth and volume. H_{ds}= height of depression storage or dead storage as at this height no overland flow can occur, h_{os}=height obstruction, h_s=height beyond which depression and obstruction effects are negligible, h=height of water from land surface (L.S.) and V.H.= volumetric height from L.S. of equivalent volume of water without depressions and obstructions. Source: Panday and Huyakorn, 2004

Although physics-based models are commonly recognized as the most robust modelling platform (Kalin and Hantush, 2014) they may not maintain their superiority in all types of catchment (Pechlivanidis et al., 2011). Therefore, Shih and Yeh (2011) insisted that a physics-based distributed model should include three numerical solution schemes so that it can reliably simulate different parts of catchment. Jaber & Shukla (2012) stated that where natural orientation of surface

topography is severely deviated from the one on which various governing equations are originally developed to represent associated processes in a physics-based model then such a model suffers from many uncertainties.

Apart from using the 2D St. Venant overland flow equations, the Manning's formula based simpler flow equation is also successfully applied in some gridded distributed model, for instance, in the GSSHA model (Downer and Ogden, 2006) and the semi-distributed overland flow model in MIKE SHE (DHI, 2009b). However, models that do not explicitly discretize catchments into regular grids in the XY plane generally use lag time parametric storage routing techniques to route ponded water over the land surface to transfer into a river system (Ivanov et al., 2004; Kouwen, 2013; Neitsch et al., 2011). The distinct feature of this overland flow module is that it can be used in any topography through careful calibration of parameters.

2.3.6. Channel flow

The channel or river flow module is one of the most important components of distributed catchment models because in many cases the entire model's performance is justified based on its ability to simulate observed flow, water stage and sediment movement within channels. What type of data being used for model fitting depends on the overall project objectives. If a project intends to quantify the water potential of a river basin to develop a sustainable water management plan or to assess the impact of climate change on river flows, then calibration of a model against observed river flows is preferable than water stages. Conversely, if flood forecasting or inundation mapping is the main goal of a project then simulation against river stage is more appropriate. In contrast to physics-based watershed models, many conceptual counterparts, which are based on laws of mass conservation, may produce an equivalent or even more than equivalent performance in simulating streamflows but not water stage in a river as this variable is greatly influenced by the energy and momentum of water. Therefore, a modeller must be aware of which river flow algorithm is suitable for his project.

In distributed catchment modelling, generally a channel flow module is used to route channel/river flow from upstream to downstream. A review of the literature

(Elbashir, 2011; Valerity Y. Ivanov et al., 2004; Kouwen, 2013; O'Sullivan et al., 2012; Paiva et al., 2011) shows that the river/channel flow routing is divided into two types: (i) hydraulic/hydrodynamic routing that is based on the physics-based 1D St. Venant hydrodynamic equation, and (ii) hydrological/storage/reservoir routing that is based on an empirical equation, most commonly Muskingum (McCarthy, 1939) or its descendent routing methods, for example, Muskingum-Cunge (Collischonn et al., 2007; Cunge, 1969). Fully distributed models where each tributary or distributary component of the river network is divided into several reach sections should preferably incorporate 1D St. Venant hydrodynamic equations (2.23 & 2.24) to route water from node to node.

1D continuity equation of mass

$$\frac{\partial A}{\partial t} + \frac{\partial Q}{\partial x} = S_r \qquad 2.23$$

1D momentum equation

$$\frac{\partial u}{\partial t} + b\frac{\partial u}{\partial x} = g(S_{0,x} - S_{f,x} - \frac{\partial h}{\partial x}) \qquad 2.24$$

Where A represents the cross sectional area of flowing water, Q is the flow rate, S_r is the source/sink flux along the reach length (∂x), b is the top width of water cross section, and all other terms are explained in previous section. Here term S_r may include several influxes and outfluxes occurred along the reach length, for example, later inflow, channel loss due to seepage, evaporation etc. As discussed for overland flow (Section 2.3.5), these equations can be solved with an appropriate numerical scheme for three approximations, namely, fully dynamic, diffusive wave and kinematic wave. The relative merits and demerits of these approximations, discussed for 2D overland flow equations, are equally applicable for 1D hydrodynamic channel routing. However, it should be highlighted that the greatest obstruction to use of the 1D hydrodynamic channel routing technique arises from its requirement of substantial accurate geometric information at each nodal point of the entire river network (Elbashir 2011; O'Sullivan et al. 2012; Saleh et al. 2013). Henceforth, employing this method in a basin having either longer rivers or higher drainage density (length of rivers per unit basin area) suffers from severe uncertainty as the necessary high spatial

resolution channel's geometric data (cross section, depth, width, and slope) are very scarce at larger scales although utilization of secondary data retrieved from remotely sensed imagery has been successful (Paz and Collischonn, 2007; Thompson et al., 2014b; Wu et al., 2012).

Distributed models that divide a catchment into subbasins usually transfer water and other loads from upstream to downstream of the river network using hydrological routing techniques (Kouwen, 2013; Neitsch et al., 2011; Scharffenberg, 2013). Each subbasin contains a river/channel having uniform geometry throughout the length; therefore, a hydrological routing method is more appropriate in data scarce environment compared to hydraulic routing (Singh, 1988 cited by O'Sullivan, Ahilan and Bruen, 2012). The commonly used hydrological routing method is Muskingum or its derivatives where channel's storage effect on hydrograph is expressed by appropriate parameters. Equations 2.25 and 2.26 are the two basic founding relationships of the Muskingum method where the former equation represents continuity of flow and latter represents storage behavior of the experimental channel.

$$\frac{dS_t}{dt} = I_t - O_t \qquad 2.25$$

$$S_t = K[xI_t + (1-x)O_t] \qquad 2.26$$

Here, S_t, I_t, and O_t respectively indicates storage volume, inflow and outflow rates at time t of a predefined channel section; K and x are the two parameters of the model. Parameter K having the unit of time dimension is called the storage coefficient or travel time constant which actually accounts for storage effect on travel time of inflow hydrograph and x is a dimensionless weighting factor. While using the final routing algorithm (equation 2.27) derived from above two equations in a watershed models, parameters K and x are to be calibrated appropriately to resemble the real system.

$$O_t = C_1 I_t + C_2 I_{t-\Delta t} + C_3 O_{t-\Delta t} \qquad 2.27$$

$$C_1, C_2, \& C_3 = f(K, x, \Delta t) \quad 2.28$$

The greatest advantage of using the lumped storage based routing method is its reduced dependence on high resolution channel geometrical information unlike the hydraulic routing method (Singh, 1988 cited by O'Sullivan, Ahilan and Bruen, 2012). However, this type of routing model cannot represent the effect of backwater on flow hydraulics in a channel (Neitsch et al., 2011; Paiva et al., 2011). Previous research has showed that the flood hydrographs are not as well simulated for gently sloping river as for steeply sloping channels (Elbashir, 2011). Elbashir (2011) further strengthened the conclusion that Muskingum method works better for longer rivers but not for shorter rivers.

2.3.7. Groundwater flow/saturated zone flow

Groundwater modules are an integral part of many catchment models; especially models that are developed to be used in analyzing interaction between surface and groundwater systems. Basically two types of groundwater models have been incorporated within catchment models: (i) fully distributed grid based model, and (ii) lumped reservoir based model or conceptual model. In the former model type, the geology or aquifer overlaid by an unsaturated zone or vadose zone of a catchment is discretized into regular grids (horizontally and vertically) as used in MIKE SHE (DHI, 2009b), GSSHA (Downer and Ogden, 2006), MODFLOW (McDonald and Harbaugh, 1988) or into finite volume elements as used in WASH123D (Yeh et al., 1998). In lumped or reservoir-based approach, an aquifer is represented by a series of conceptual linear reservoirs as used in the linear-reservoir module of MIKE SHE and the SWAT model. The two greatest limitations of reservoir-based approach are its presumption that the spatial extent of the underlying aquifer is identical to its overlaid subbasin area and there is no interaction between the aquifers of adjacent subbasins. However, in reality, the spatial extent of an aquifer might not be exactly coincident with the drainage area of the subbasin. Most available catchment models are mainly developed to simulate surface water dynamics (river flow, stage, extreme events) and its response to various environmental changes (climate, land use); these models poorly resemble the groundwater dynamics and their interactions with surface

water. In an intensive effort to evaluate the integrated surface and groundwater modelling tools, conducted by the Camp Dresser and McKee (CDM) Inc., only nine from a pool of 75 contemporary hydrological models were found to have modelling ability for surface-groundwater interaction (CDM, 2001). These nine models were MIKE SHE, HMS (Hydrologic Model System (Yu and Schwartz, 1998), FHM-FIPR (Florida Institute of Phosphate Research Hydrologic Model (Ross et al., 1997)), SWATMOD (named after combing SWAT and MODFLOW models (Sophocleous et al., 1999)), MODFLOW (the USGS Modular Three-Dimensional Finite-Difference Ground-Water Flow model (McDonald and Harbaugh, 1988)), DYNFLOW (constituent groundwater simulator of DYNSYSTEM finite element model developed by Camp Dresser and McKee Inc. in 1982), MODBRANCH (named after combing USGS BRANCH and MODFLOW models (Swain and Wexler, 1996)), SWMM (Storm Water Management Model (Metcalf & Eddy Inc., 1971)), and HSPF (Hydrologic Simulation Program-FORTRAN (Bicknell et al., 2001).

The form of equation 2.29 is widely used to describe 3-D groundwater flow dynamics in fully distributed physics-based groundwater models (DHI, 2009b; McDonald and Harbaugh, 1988):

$$\frac{\partial}{\partial x}\left(k_x \frac{\partial h}{\partial x}\right) + \frac{\partial}{\partial y}\left(k_y \frac{\partial h}{\partial y}\right) + \frac{\partial}{\partial z}\left(k_z \frac{\partial h}{\partial z}\right) - W = S\frac{\partial h}{\partial t} \qquad 2.29$$

where k indicates saturated hydraulic conductivity along three Cartesian axes, W source or sink, for example, percolated water from unsaturated zone is treated as source and pumped water from aquifer is treated as sink, and S is the storage coefficient of the aquifer. Where interaction between groundwater and surface water is very active, using the above equation in distributed models is preferable to simulate real time water table position. The major limitation of fully distributed groundwater models is their demand for relatively fine spatio-temporal resolution aquifer data (geologic and hydrological). On the other hand, reservoir based models store and route water from one reservoir to another or to nearby water bodies maintaining the mass balance principle. Parameters of these model can be grouped as capacitance related parameters for each reservoir, threshold

values that determine starting and culmination times of flow exchange between water bodies (reservoir-reservoir, reservoir-river, reservoir-wetland), and routing coefficients.

The primary source of incoming water into a groundwater reservoir is percolated water out from upper soil zone. Since capillary fringe from a shallow water table may play a considerable role in water mass balance in the land phase of the hydrological cycle, some reservoir based models conceptually relate the water table in the top reservoir with the upper soil zone (DHI, 2009b; Neitsch et al., 2011). Despite being simple and computationally efficient, the inability of water table modelling at real time and across the catchment is the greatest disadvantage of reservoir based catchment models. For example, Kim et al. (2008) attempted to improve the existing SWAT model by replacing its simpler groundwater module with a sophisticated MODFLOW groundwater model. They concluded that the integrated SWAT-MODFLOW model was successful in simulating spatio-temporal dynamics of groundwater and its interaction with surface water.

2.4. Justification for selecting SWAT for the study

Since one of the aims of the study is to model haor wetlands in the UMRB, the first criteria for selecting a catchment model was its ability to simulate wetlands of the type found within the basin. Although this chapter has not discussed the wetland simulation abilities of different catchment models, this aspect is detailed in Section 5.2. Unlike conceptual models, although fully-distributed models do not explicitly include a wetland module they can be employed or adapted for such applications (see Section 5.2). However, these models require very high resolution elevation data not only for conforming to their governing equations but also for preserving wetlands' shape, specifically for depressional wetlands. Where detailed investigation of individual wetland's water regimes (e.g. water depth and areal extent, fluxes) is sought, any modelling platform must be able to maintain the geometry of the wetland. In some cases, fully-distributed models consider riparian wetlands as a part of their floodplain in order to properly account for the effect of the floodplain on river water regimes (e.g. downstream flows) rather than focusing on the water regime (e.g. wetland inundation) of individual

wetlands (Karim et al., 2012). Furthermore, representing the connectivity between a wetland and river in fully-distributed platforms is limited by a number of factors which are detailed in Section 5.2. Therefore, this study excluded fully-distributed catchment models for the UMRB and instead focused on conceptual semi-distributed models.

Among the previously reviewed semi-distributed models that are capable of simulating wetlands, SWAT has some important distinguishing features: (i) it has been widely used for diverse catchments and wetlands across the world which helps better understand its parameters behaviour, (ii) a large number of hydrological processes associated with different catchment features, particularlry wetlands, are embedded in the model, (iii) the large database of physiological characteristics for different plants lessens the input crop data demands by the model, and (iv) because it is an open source code model, users have the ability to re-define the model if necessary.

2.5. Summary

This chapter has reviewed the different aspects of catchment modelling. Models differ not only in their discretizing approach of a catchment but in representing the various hydrological processes. Although physics-based fully distributed models can preserve the spatial variability of catchment's physio-graphic and climatic properties, their high demand for input data and computational burden limits their wider usability compared to lumped and semi-distributed modelling approaches. Moreover, since fully distributed models are restricted to uniform grid size throughout the modelling domain, they experience a range of issues when they are used to represent varying sized features such as the haor wetlands which feature in the current study.

While reviewing wetland simulation algorithms of different catchment models it is found that none of the reviewed models is useful to simultaneously represent the hydraulic interactions between wetlands, aquifers and rivers as seen in the haor wetlands of the UMRB. Therefore SWAT is considered to be the right candidate for the study subjecting its existing wetland module to be improved to overcome the current limitations (see Chapter 5).

Chapter 3
The SWAT model

3.1. Introduction

This chapter describes the SWAT model, the model code selected for use in the current study. It is divided into three major subsections, firstly (Section 3.1), a brief overview of the model and its history is provided. Section 3.2 describes how SWAT conceptualises the modelled basin whilst process representation within SWAT is described in Section 3.3.

The Soil and Water Assessment Tool (SWAT), a continuous, conceptual, semi-distributed, catchment scale model developed by Dr. Jeff Arnold for the Agricultural Research Service (ARS) of United States Department of Agriculture (USDA) (Arnold et al., 1998, 1993; Neitsch et al., 2011), has been successfully employed throughout the world to simulate the dynamics of water (Vazquez-Amábile & Engel 2005; Spruill et al. 2000; Li et al. 2010; Wagner et al. 2011; Mishra & Kar 2012; Kushwaha & Jain 2013), sediment (Rostamian et al. 2008; Niraula et al. 2012; Betrie et al. 2011; Nejadhashemi et al. 2011), pollutants and nutrients (Nejadhashemi et al. 2011; Mishra & Kar 2012; Parajuli 2012; Zhang et al. 2014) within river basin systems. SWAT is the descendant of the SWRRB (Simulator of Water Resources in Rural Basins) model (Arnold et al., 1990) that was developed in the 1980s by integrating many structural concepts from the CREAMS (Chemicals, Runoff, and Erosion from Agricultural Management Systems) (Knisel, 1980), GLEAMS (Groundwater Loading Effects on Agricultural Management Systems) (Leonard et al., 1987), and EPIC (Erosion-Productivity Impact Calculator) (Williams et al., 1984) models (Gassman et al., 2007; Krysanova and Arnold, 2008; Neitsch et al., 2011). In the early 1990s the model was named as SWAT after merging SWRRB, ROTO (Routing Outputs to Outlet), a more robust routing model for larger and complex basin, and a GIS interface developed from GRASS (Geographic Resources Analysis Support System) (Srinivasan and Arnold, 1994). Figure 3.1 illustrates the developmental history of the SWAT model.

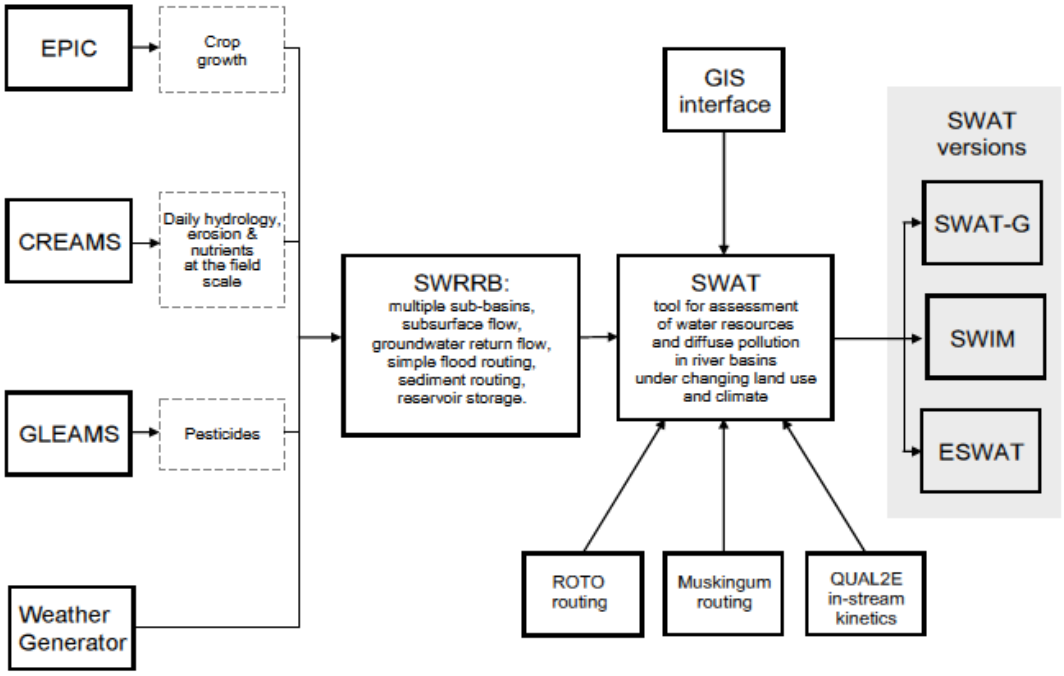

Figure 3.1. Developmental history of the SWAT model (adapted from Krysanova and Arnold, 2008 that was modified from Gassman et al., 2007).

Although the SWAT model was primarily developed to assess management impacts on agricultural watersheds in the USA, its application has spread over the entire world (Gassman et al., 2007; Krysanova and Arnold, 2008). After reviewing more than 250 peer-reviewed papers, Gassman et al. (2007) provided an excellent portfolio of SWAT's applications. The versatility of SWAT model is demonstrated by the website "https://www.card.iastate.edu/swat_articles/", maintained by the Center for Agricultural and Rural Development (CARD), Iowa State University, USA, where approximately 2500 peer-reviewed journal papers using SWAT are identified. SWAT is probably the most widely used catchment model because of a number of distinguishing features: it is distributed, and process-based, it enables trade-offs between structural simplicity and complexity that makes the model useful for larger basin without compromising spatial variability, it is freely available and open source code which enables the model to be modified as required, it has an extensive and active user community, and the code has undergone continuous improvement. This model interfaces with several GIS (Geographic Information Systems) platforms, for example, GRASS, ArcGIS,

MapWindow, and QGIS. Table 3.1, adapted from Gassman et al. (2010), shows different GIS interfaces developed for the SWAT model. SWAT is an integral component of BASINS (Better Assessment Science Integrating point and Nonpoint Sources), a multipurpose environmental analysis system, developed by US Environmental Protection Agency (EPA) to analyze water and water quality at basin scale (Saleh and Du, 2004).

Table 3.1. GIS interfaces developed to support applications of SWAT (adapted from Gassman et al., 2010)

Interface	GIS platforms	Source(s)
SWAT/GRASS	GRASS	Srinivasan and Arnold, 1994
InputOutputSWAT (IOSWAT)	GRASS	(Haverkamp et al., 2005)
ArcVIEW SWAT (AVSWAT)	ArcVIEW 3.x	http://swatmodel.tamu.edu/software/avswat; (Di Luzio et al., 2004)
BASINS*	ArcVIEW 3.x	http://www.epa.gov/waterscience/basins/; (Di Luzio et al., 2002)
ArcGIS-SWAT (ArcSWAT)	ArcGIS 9.x	http://swatmodel.tamu.edu/software/arcswat; (Olivera et al., 2006)
ArcGIS-APEX (ArcAPEX)	ArcGIS 9.x	(Tuppad et al., 2009)
SWATP	ArcVIEW 3.x	(Saleh and Gallego, 2007)
AGWA*	ArcVIEW 3.x & ArcGIS 9.x	http://www.tucson.ars.ag.gov/agwa/; (Miller et al., 2007)
CRP* -DSS	ArcIMS/ArcGIS	(Rao et al., 2007)

*BASINS, AGWA, and CRP stand for Better Assessment Integrating Point and Nonpoint Sources, Automated Geospatial Watershed Assessment, and Conservation Reserve Program, respectively.

Because of its distributed nature and the open source code model, SWAT has been modified and coupled with other models for use in many regions of the world (Betrie et al., 2011b; Sophocleous et al., 1999). Sophocleous et al. (1999) integrated MODFLOW, a robust finite difference based modular groundwater model, with SWAT to enhance SWAT's simulating capabilities by replacing its lumped groundwater module with a distributed groundwater model. To take account of backwater effects on flow and sedimentation onto the river bed, Betrie et al. (2011b) coupled SOBEK (Deltares, 2016), a river hydrodynamic model, with

SWAT through the Open Modelling Interface (OpenMI). It was concluded that the coupled model's performance was superior to that of SWAT alone. Table 3.2 shows a number of hybrid SWAT models.

Table 3.2. Different modified SWAT models (adapted from Gassman et al., 2010 with modification)

Modified model	Description	Source(s)
ESWAT	Extended SWAT including a sub-hourly time step, and enhanced hydrology and in-stream components	(van Griensven and Bauwens, 2005)
$SWAT_{BF}$	Modified SWAT to better simulate processes within forested watersheds in the Canadian Boreal Plain	(Watson et al., 2008)
SWATMOD	Interface between SWAT and the MODFLOW groundwater model	(Sophocleous et al., 1999)
SWAT-DEG	Improved version of SWAT for simulating the time rate of channel degradation in watersheds	(Allen et al., 2008)
SWAT-G	Modified SWAT99.2 for improved flow predictions for typical conditions in low mountain ranges in Germany	(Eckhardt et al., 2002)
SWAT-K	Multiple modified modules for Korean conditions; includes interfaces with the MODFLOW and SWIM models	http://www.swat-k.re.kr/; (Kim et al., 2009)
SWAT-M	Improved subsurface tile drainage routines; has since been incorporated in standard SWAT model	(Du et al., 2005)
SWAT-N	Modified SWAT2000 nitrogen cycling routine by incorporating algorithms from the DNDC model	(Pohlert et al., 2007)
SWAT-VSA	Re-conceptualized model that simulates overland flow in ways consistent with variable source area hydrology	(Easton et al., 2008)
SWAT-WH	Modified SWAT model designed to simulate effects of two water harvesting systems in southeast Tunisia	(Ouessar et al., 2009)
SWIM	Comprehensive water quality model that was developed from SWAT and the MATSALU models	(Krysanova et al., 2005)
SWAT-IRRIG	Suitable for intensive irrigated watershed where source of irrigation water is outside the watershed	(Dechmi et al., 2012)
SWAT-WB	More robust soil moisture accounting model instead of original CN model	(White et al., 2009)

3.2. Basin conceptualization in the SWAT model

This study uses SWAT version 627 (rev. 627); so hereafter any reference to SWAT means rev. 627 unless otherwise stated. As discussed in Chapter 2, any distributed catchment model, whether it is fully-distributed or partially-distributed, may be described from two major points of view (i) delineation of basin and (ii) representation of different processes. As discussed in Section 2.2.2, basin delineation means how a model represents the catchment's landscape based on topographical information (for example, Digital Elevation Model (DEM) data, Triangulated Irregular Network (TIN) data, contour map). In addition to containing river networks, a basin may contain large floodplains, different artificial and natural impoundments (ponds, wetlands, reservoirs). On the other hand, numerous processes (those of the hydrological cycle, vegetation dynamics, sediment and pollutant transports) that take place within a basin may be represented by fully mathematical equations, empirical equations, regression based fittings, or any combination of them. The approaches used to delineate a basin and represent processes are described in the following sections.

3.2.1. Basin delineation in the SWAT model

Luo et al. (2011) stated that successful and accurate watershed delineation is the precondition for accurate runoff, sediment, and water quality modelling. In SWAT, there are two options to represent a basin, namely, automatic watershed delineation from Digital Elevation Model (DEM) data and user supplied GIS shape file of watersheds. In the former approach, the user provides a raster elevation dataset, commonly termed as DEM data, having sufficient spatial extent to cover the basin area. A high resolution and accurate DEM data is desirable to generate more realistic stream networks and watersheds (Lindsay and Creed, 2005). Once a DEM data set is provided in the GIS interface, SWAT first fills artifact cells or grids of DEM data followed by the operation of "flow direction and flow accumulation" for each raster cell (Luo et al., 2011). SWAT follows the D8 method to generate flow direction from and flow accumulation to each grid where runoff generated in an individual grid cell will flow to the lowest of its surrounding eight grid cells (Fairfield and Leymarie, 1991) (see Section 2.2.2). To generate river networks, a threshold or critical area value is defined which is the minimum

upslope area to initiate a river reach; hence, the smaller threshold area the lengthier the resulting river reach and more complex the river network. However, accuracy and precision of the DEM based automatic watershed delineation approach depends highly on the quality of DEM data. Using substandard DEM data is the most likely principal cause of unrealistic representation of river networks (da Paz et al., 2008; Li and Wong, 2010; Poggio and Soille, 2011). However, SWAT has the capability to avoid such limitation by using the Burn In function prior to employing flow direction and flow accumulation process. The premise of using the Burn In function is that a pre-defined realistic digital river network data (shape file), provided by the user, can be superimposed onto the DEM. With this approach, the model is forced to delineate the river reach along the given networks and so the actual location of river networks is preserved. Figure 3.2 shows an example how the Burn In and Threshold or critical area functions influence DEM based river network delineation. In spite of using the Burn In function with real river network (red coloured), the automatic delineation approach generates some longer and smaller rivers (blue coloured) compared to real ones; moreover, some unrealistic rivers are also evident (Figure 3.2). Therefore, manual editing is required to produce final river networks. After successful delineation and editing of the river network, the model will generate a subbasin for each component river. The number of subbasins to be generated can be specified by the user and can be further reduced by deleting tributaries from dendritic river network. Figure 3.3 shows, as an example, a basin with 31 subbasins delineated by the SWAT model.

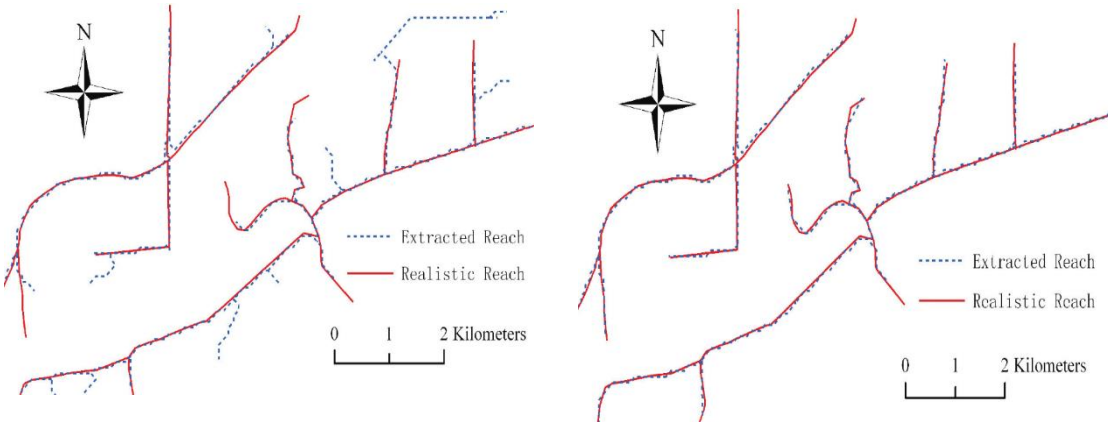

(a) Before manual editing (b) After manual editing

Figure 3.2. Effect of threshold or critical area in DEM based watershed delineation. Source: Luo et al., 2011

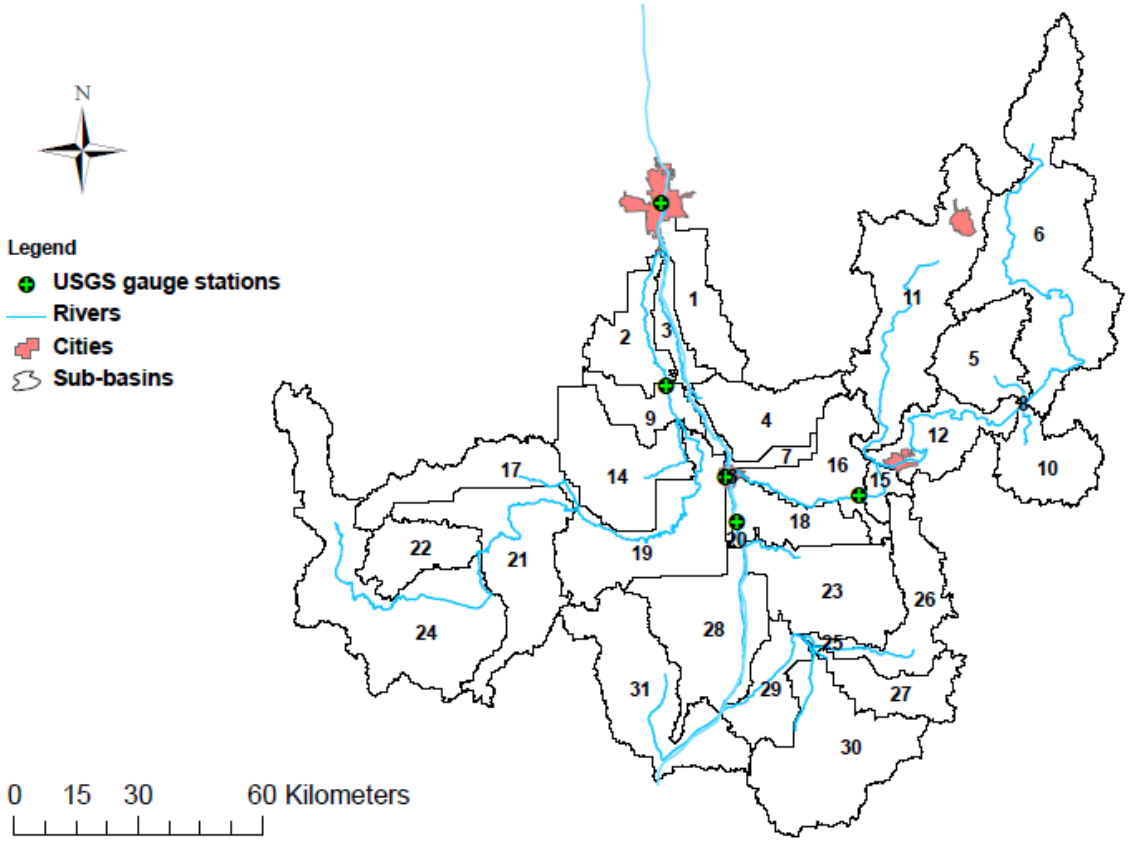

Figure 3.3. Rivers and subbasins delineated by ArcSWAT interface. Source: Rahman, 2011

Although automatic watershed delineation is a widely accepted approach in creating river networks, its reliability is subject to the availability of high quality, fine resolution DEM data of the basin (da Paz et al., 2008; Li and Wong, 2010; Poggio and Soille, 2011). Furthermore, in low relief flat areas, for instance, floodplains and deltaic areas, automatic watershed delineation is found to be very ineffective (Luo et al., 2011; Neitsch et al., 2011; Rahman et al., 2010). In addition, if the natural river network of a basin is modified by human activities, automatic delineation cannot take these changes into account. For example, man-made diversion channels are commonly seen in low relief areas that intercept a portion of main channel's water to serve different purposes such as flood control or irrigation. In the cases where DEM based automatic delineation cannot produce real river network and subbasins, SWAT allows users to provide

pre-defined digital map (shape file) of those objects (rivers and subbasins) with their linking order from upstream to downstream of the basin.

Another distinguishing feature of the SWAT model is its ability to calculate the geometry of a river reach from DEM data. Geometric attributes of a river, particularly cross sectional profile, play an important role in flow hydraulics. Determination of river geometry in-situ is limited by a number of factors such as cost and time constraints, and site accessibility, a particularly important constraint in large, mountainous and forested basins. In such situations, generation of river geometric properties from a DEM-based algorithm is a more realistic option. SWAT assumes the cross section of a river within a subbasin is trapezoidal and constant along the subbasin-scale river reach. The ESRI's ArcHydro tool is used to compute the geometrical dimensions of river. Whenever the volume of water in a river exceeds its full capacity then excess water spreads over the floodplain. The width of the floodplain running along each side of river is considered as 2.5 times of river width.

3.2.2. Computational approach in the SWAT model

As described above, SWAT firstly spatially discretizes an entire basin into smaller subbasins where each subbasin has a main river (see Figure 3.3). Each subbasin is further divided into a number of hydrologic response units (HRUs) obtained from the information of gridded land use, soil, and surface slope data. The HRU is the model's basic computational unit for all processes. Each HRU within a subbasin is a unique combination of land use, soil, and surface slope. The SWAT model has three options to disaggregate a subbasin into smaller spatial computing HRU units: (1) dominant land use, soil and slope, (2) dominant HRU, and (3) multiple HRUs. These options are explained with the following example. Suppose, a basin is delineated from DEM data and it generates three subbasins (Figure 3.4). We assumed one of the generated subbasins is a regular square shown with gridded mesh in Figure 3.4. To discretize a subbasin into different HRUs, three gridded data sets of land use, soil, and slope are overlain in the GIS interface of SWAT model. Three subplots in Figure 3.5 represent the (a) land use, (b) soil, and (c) slope data for the square subbasin. After overlaying these three data sets, each cell of resultant data will contain the combined spatial information

of land use, soil, and slope as shown in Figure 3.6. The information of Figure 3.6a is summarized in Table 3.3 that shows there are nine unique combinations of land use, soil, and slope for the square subbasin. The rightmost column of Table 3.3 depicts the number of cells under each combination i.e. HRU.

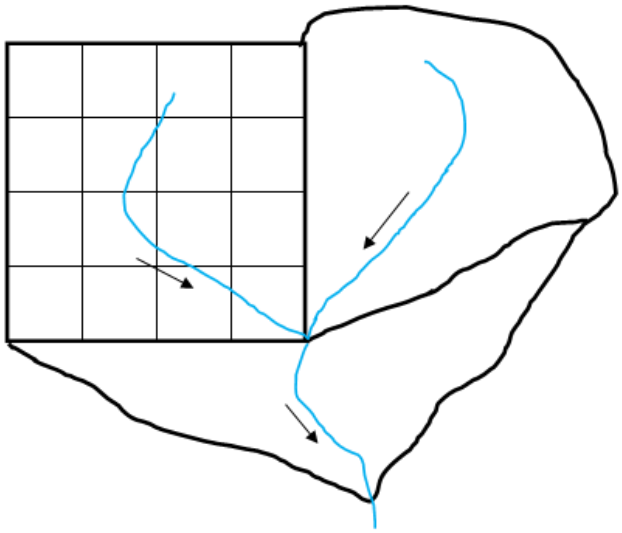

Figure 3.4. A dummy basin with 3 subbasins, delineated from gridded or raster data where one subbasin is like a regular square shown with gridded mesh. Blue colored lines indicate the river reach and corresponding arrow shows the flow direction.

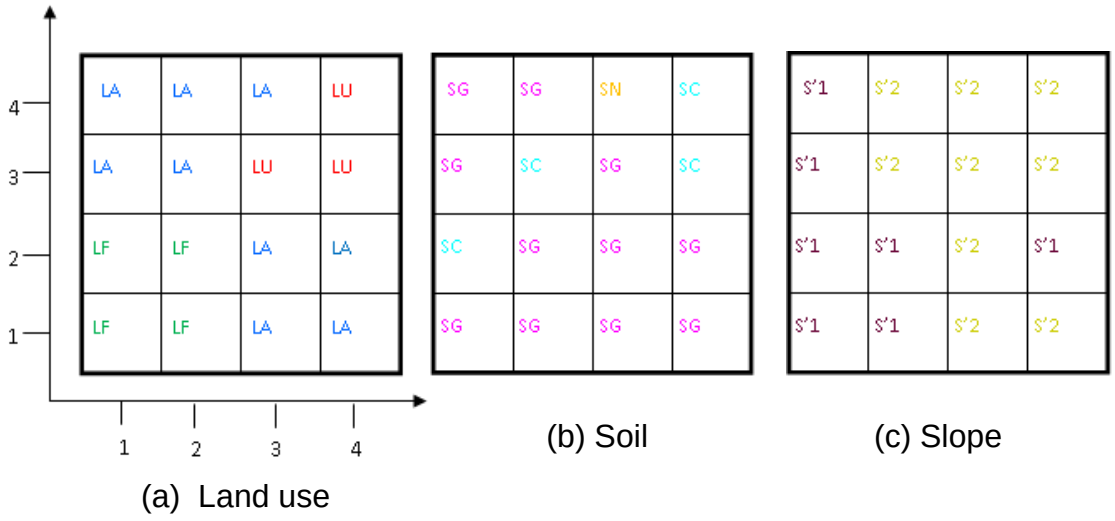

Figure 3.5. Spatial distribution of land use (a), soil (b), and slope (c) in the square subbasin. In Figure 3.5a, an arbitrary scale has been shown to reference the cell or grid ID. The symbols shown in each grid cell represent the names of land use, soil, and slope, where first letter for data category (L for land use, S for soil and S' for slope) and 2nd letter for specific types under a category. For example, in Figure 3.5a, top left cell (ID: 1, 4) indicates an agricultural (A) land use. A-Agriculture, U- Urban, F- Forest; G- Glaysols, N- Nitosols, C- Cambisols; 1- slope 0 – 1%, 2- slope 1-2%.

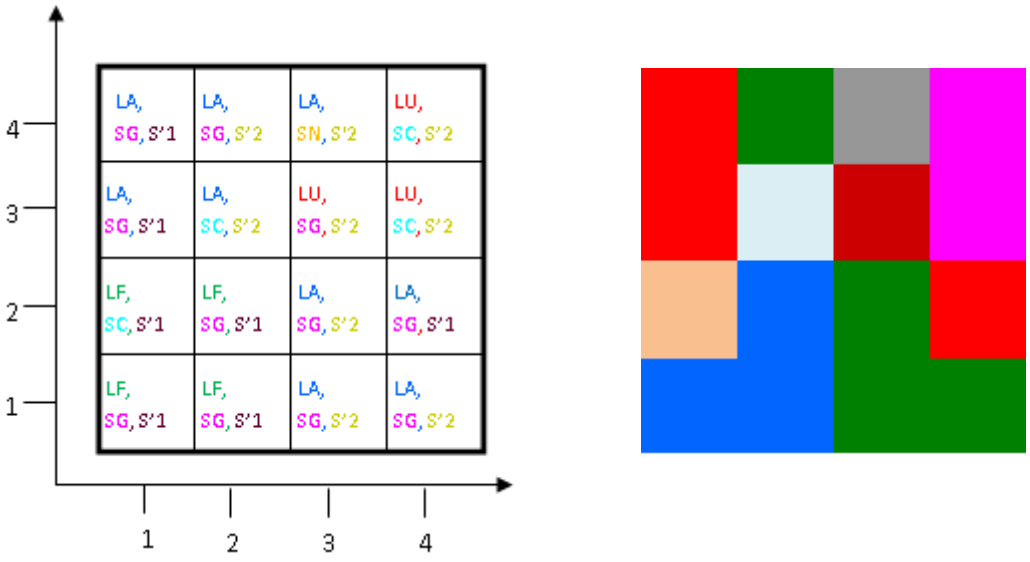

(a) (b)

Figure 3.6. Cell/pixel properties after overlying land use, soil, and slope data. Figure “a” shows alphabetically each cell and figure “b” shows specific HRUs with unique colours.

Table 3.3. Summarized HRU information extracted from Figure 3.6a

Serial number	HRUs (Unique combination of land use, soil and slope)	Cell ID (x, y)	Number of grids or cells
1	LA, SG, S’1	1,4; 1,3; 4,2	3
2	LA, SG, S’2	2,4; 3,1; 4,1; 3,2	4
3	LA, SN, S’2	3,4	1
4	LA, SC, S’2	2,3	1
5	LU, SC, S’2	4,4; 4,3	2
6	LU, SG, S’2	3,3	1
7	LF, SC, S’1	1,2	1
8	LF, SG, S’1	1,1; 2,1; 2,2	3
Total			16

During HRU definition in a SWAT model, if a user chooses option-1 i.e. dominant land use, soil, and slope method, then for the entire subbasin, the model will create only one HRU having LA, SG, and S’2 attributes for land use, soil and

slope, respectively. Of the 16 cells in each raster data set of subbasin, the highest numbers of cells are 8, 11, and 9 for LA (Figure 3.5a), SG (Figure 3.5b), and S'2 (Figure 3.5c), respectively. Selecting option-2 (dominant HRU) will also generate only one HRU for the entire subbasin. The highlighted row in Table 3.3 shows that the dominant HRU is LA, SG, S'2 as it contains maximum number (4) of unique combinations of land use, soil, and slope. However, in this example, both options (1 & 2) fortuitously create identical HRU. This is generally unlikely for real world subbasin due to higher variability in land use, soil, and slope. In principle, both options (1 and 2) do not consider spatial variability in land use, soil and slope within a subbasin; therefore, HRU definition with these options results in homogeneous land use, soil and slope over the subbasin. The third option, multiple HRUs, is the most robust among the three HRU definition approaches offered by SWAT model. In this option multiple HRUs can be created within a subbasin depending on the spatial variability and resolution of input data, spatial extent of a subbasin, and a user defined threshold value. Generation of multiple HRUs is a 3-steps process. In the first step, the area of a subbasin is proportioned to its different land use types based on user given threshold value that is a minimum area to decide whether a land use will be considered or omitted in the HRU definition. For example in this case, LA, LU, and LF occupy 56.3, 18.8 and 25.0% of subbasin area respectively (see column 3 of Table 3.4). If a threshold value of 10% is selected, then each land use category will be used in the model. However, a threshold value of 20% will ignore urban land use (LU) as its coverage (18.8%) is less than the threshold value (20%). Due to phasing out of land use(s), remaining land uses are reapportioned over the subbasin area. For the current example, new areal coverages of LA and LF over the subbasin are 69.25% [56.3/(56.3+25.0)] and 30.75% [25.0/(56.3+25.0)] respectively. In the second step of multiple HRU definition, soils are proportioned to each of land use types, generated after the first step, based on soil threshold value. While overlaying the percentage of each soil coverage over a specific land use area is computed. For example, Table 3.4 shows that soils SG, SN, and SC occupy 77.8, 11.1, and 11.1% of LA land use, respectively. Therefore, selecting a soil threshold value of 15% phases out SN and SC soils for land use LA leaving only one HRU but for the remaining land use 'LF' two HRUs are generated (Figure 3.7). Similarly in the third step, a threshold slope of 30% over land use and soil, as shown in Table 3.5, retains the original spatial distribution. Figure 3.7 depicts the whole process

of HRU creation as discussed here. In this example, finally only four HRUs are created from the subbasin, although initially there were eight unique combinations of land use, soil, and slope (Table 3.3). HRUs within a subbasin do not preserve their spatial location rather they are unique cohort of land use, soil and slope.

Table 3.4. Numeric distribution of land use over subbasin and soil over land use

Land use	Distribution of land use over subbasin area		Distribution of soil over land use area							
			SG		SN		SC		Total	
	Area (unit)	% of subbasin area	Area	% of Land use area	Area	% of Land use area	Area	% of Land use area	Area	% of Land use area
(1)	(2)	(3)	(4)	(5)	(6)	(7)	(8)	(9)	(10)	(11)
LA	9	56.3	7	77.8	1	11.1	1	11.1	9	100
LU	3	18.8	1	33.3	-	-	2	66.7	3	100
LF	4	25.0	3	75.0	-	-	1	25.0	4	100
Total	16	100	11	-	1	-	4	-	16	-

Table 3.5. Numeric distribution of surface slope over soil

Combination land use and soil in the subbasin		Distribution of surface slope over land use and soil					
		S'1		S'2		Total	
Symbols	Area	Area	% of soil area	Area	% of soil area	Area	% of soil area
LA + SG	7	3	42.9	4	57.1	7	100
LA + SN	1	-	-	1	100.0	1	100
LA + SC	1	-	-	1	100.0	1	100
LU + SC	2	-	-	2	100.0	2	100
LU + SG	1	-	-	1	100.0	1	100
LF + SC	1	1	100.0	-	-	1	100
LF + SG	3	3	100.0	-	-	3	100
Total	16	7	-	9	-	16	-

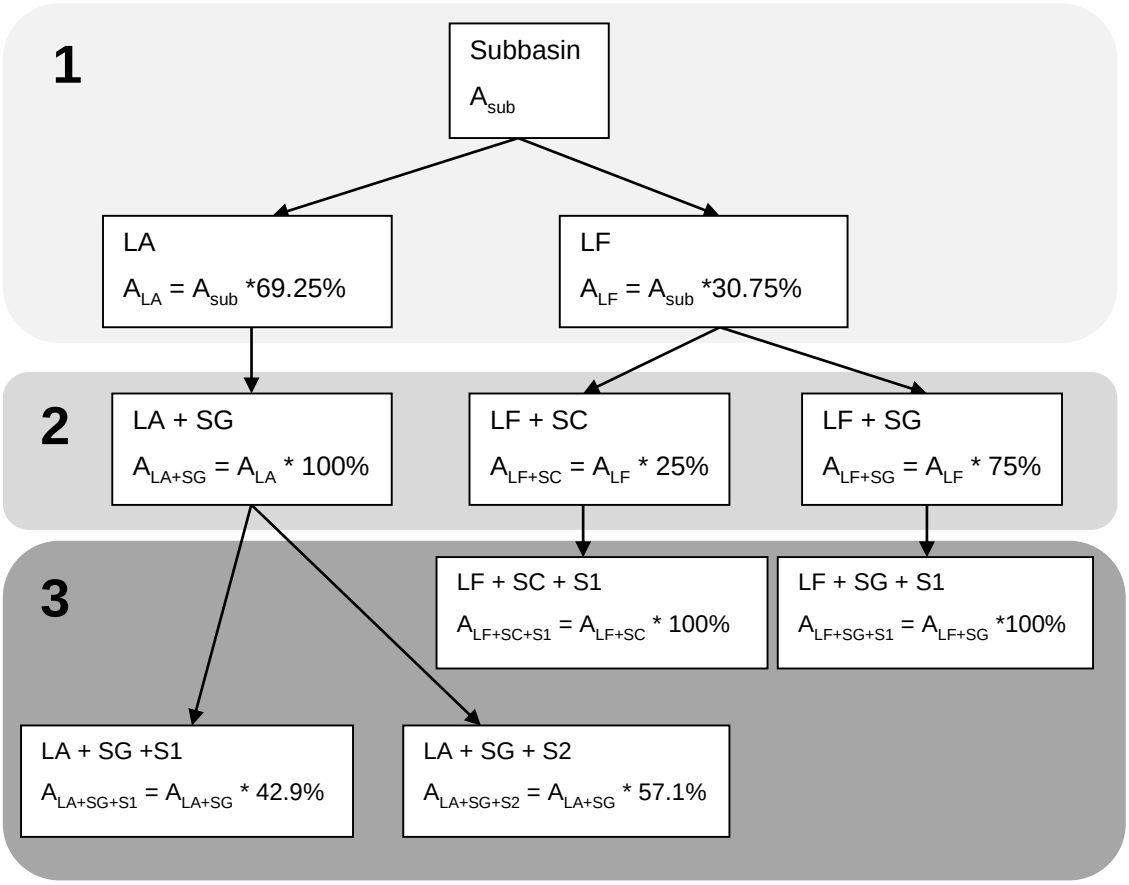

Figure 3.7. 3-steps discretization process of a subbasin into HRUs. Shaded boxes under step-3 indicate final HRUs created from the subbasin.

SWAT computes all processes at HRU level. In the case of hydrological simulations, different components (surface runoff, infiltration, evapotranspiration, base flow, soil moisture storage) of the hydrological cycle are computed first during the time step (hour, day, month, or year) for each HRU of a subbasin. Later loads for a particular component, say runoff, produced from different HRUs are summed to yield total corresponding load of the subbasin. The same procedure is followed for other components such as sediment. Water yield of a subbasin is the total amount of surface runoff, lateral flow, base flow or groundwater flow, released from all HRUs and available to a stream reach during a time step. However, water generated from a HRU in a time step may not reach the stream within that time period because of resistance offered by a subbasin. SWAT routes HRU generated loads to the river reach by introducing some exponential equations (see Equation 3.4 for surface runoff) with lag time parameters. The greatest advantage of HRU based modelling is less computing time for larger

watersheds and so it represents a trade-off between fully distributed grid-based and lumped models.

3.3. Representation of different processes in the SWAT model

This section provides an overview of the different processes modelled in SWAT. Since SWAT is a process-based model; many real processes associated with climate, hydrology, plant growth, erosion and sedimentation, nutrient and pollutant, and microbes are incorporated into the model providing a robust standalone watershed modelling platform. The intention of this section is to discuss those processes which are related to the present study.

3.3.1. Climate: the forcing elements of land surface hydrology

Climatic variables (precipitation, temperature, relative humidity, wind speed, and solar radiation) are the principal driving force of hydrological cycle. Therefore, representing the real world climate in a catchment model significantly influences its performance (Fonseca et al., 2014). In particular, the limitations of a simple rainfall-runoff regression or lumped model for a catchment with diverse climate are mostly overcome by distributed/semi-distributed models due to their capability to take account for spatial climatic variability across the basin (Ajami et al., 2004; Lobligeois et al., 2013). The SWAT model, being distributed in structure, accounts for the effect of spatial variability in climatic variables on a basin's response. As a subbasin is the lowest spatial discretized units, the ability to represent spatial climatic variability depends on the number of subbasins and the number of climate stations and their distribution across the basin. Climate time-series data are considered as a point data for each subbasin which implies that climatic variable is invariant over the subbasin for a particular time step i.e. climatic treatment for all HRUs within a subbasin is identical. Users need to supply spatial location of weather stations within and around the basin. The GIS interface of SWAT determines the closest weather station to the centroid of each subbasin. Although this approach is not directly suitable for gridded climate data, for example, remotely sensed data, aggregating all grids information within a subbasin can be an alternative way to use such data.

A SWAT model can be run with only two main climate variables, time series of daily precipitation, and maximum and minimum temperature data. However, providing other climate data such as daily relative humidity, wind speed, solar radiation, can improve model performance. Using all of these climatic variables in estimating potential evapotranspiration, for example by the Penman-Monteith method, reduces the uncertainty although. Many SWAT applications have been found to produce acceptable results using only precipitation and temperature data (Benaman et al., 2005; Cohen Liechti et al., 2014; Guo et al., 2008; Rahman et al., 2014). If the Green-Ampt (GA) infiltration model (Green and Ampt, 1911) is used to estimate surface runoff, then sub-daily or hourly precipitation is required whilst the SCS-CN method (USDA, 2004) requires daily time series. A stochastic weather generator WXGEN (Sharpley and Williams, 1990) enhances SWAT's ability to handle missing climatic data. If an observed station contains missing data, then WXGEN generates a corresponding value taking average monthly climatic information from the closest station in the user defined database of the WXGEN model.

3.3.2. Separation of precipitation into surface and infiltrated waters

The two infiltration models incorporated in the present SWAT model are the SCS-CN and GA methods. The requirement for sub-daily or hourly precipitation data constricts the use of later approach, which can be problematical especially for large basins and even more so for those in less developed countries. Therefore, we limit our discussion to the SCS-CN approach. This method has been widely used across the world because of its structural simplicity and minimal data requirement (Rozalis et al., 2010). Equation 3.1 expresses the fundamental form of SCS-CN method:

$$Q_s = \begin{cases} \dfrac{(P - I_a)^2}{(P + 0.8S)} = \dfrac{(P - 0.2S)^2}{(P + 0.8S)} & if\ P > I_a \\ 0 & if\ P \leq I_a \end{cases} \qquad 3.1$$

where Q_s is cumulative runoff, P is depth of precipitation for the day, I_a is initial abstraction that includes interception, surface storage, and infiltration before commencement of runoff, and S is maximum retention parameter. Although this

equation is not exactly a physically based approach, it maintains the law of mass conservation (USDA, 2004). The maximum retention parameter is determined from the information of curve number as following:

$$S = 25.4(\frac{1000}{CN} - 10) \quad 3.2$$

where CN represents curve number for antecedent soil moisture condition. Figure 3.8 illustrates the relationship between rainfall and surface runoff using the SCS-CN model.

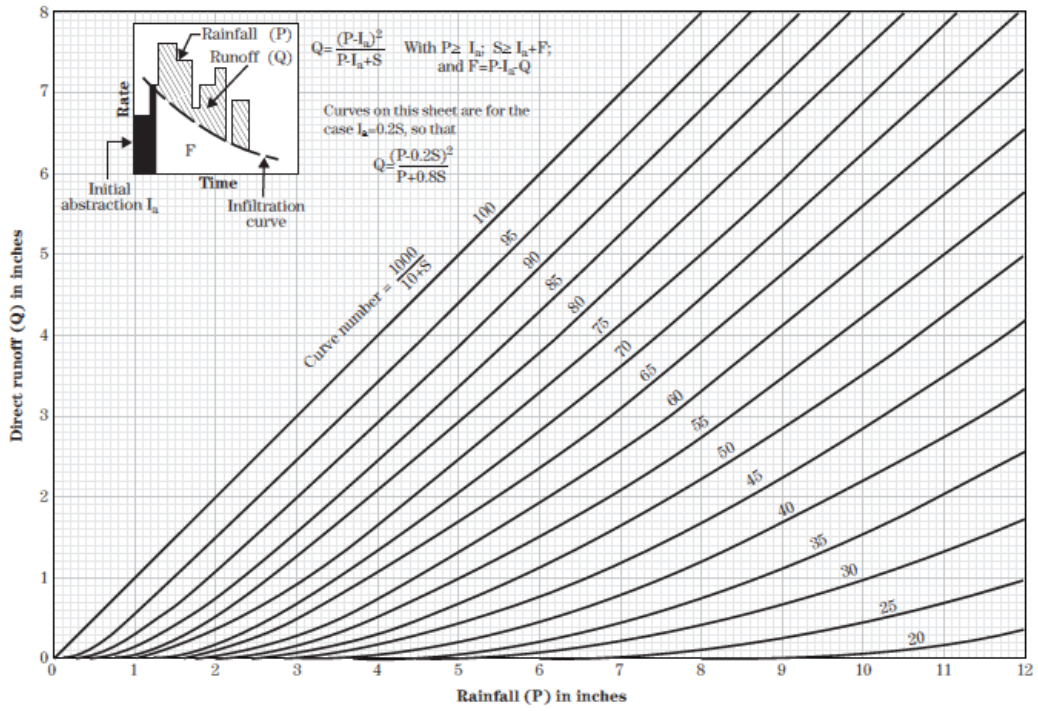

Figure 3.8. Monograph of SCS-CN based rainfall and surface runoff (adapted from USDA, 2004).

In SCS-CN based rainfall-runoff models, CN is frequently found to be one of the important influential parameters. However, identification of an appropriate CN number for a specific region is crucial to develop a reliable model. Usually typical values of CN are determined from the SCS developed standard table (Neitsch et al., 2011) where CN is expressed as a function of land use, antecedent soil moisture condition, and hydrologic soil group, a classification of soil depending on its hydraulic properties. Three types of antecedent moisture are: dry i.e. wilting

point (condition-I), medium (condition-II) and wetter or field capacity (condition-III). To be more realistic in continuous modelling, rather than using these three fixed moisture conditions, SWAT updates daily CN based on diurnal simulated soil water content and surface slope. A wetter soil generates larger value of CN that leads to increased surface runoff. Once the surface runoff is determined then infiltrated water into the soil profile is calculated from the mass balance equation. Surface runoff or infiltrated water modeled by SWAT can be expressed as the following equation:

$$\text{Surface runoff or infiltrated water} = f(LULC, SlP, SHP, \& SWC) \quad 3.3$$

where $LULC$, SlP, SHP, and SWC respectively stand for land use and land cover, surface slope, soil hydraulic properties, and daily soil water content. The first three variables are mostly associated with spatial characteristics of a HRU and fourth variable indicates temporal dynamics of soil water for that HRU.

After vertical separation of surface runoff from precipitation, generated surface runoff is routed horizontally to stream with the following equation:

$$Q_{sr,i} = \left(Q_{s,i} + Q_{st,i-1}\right) \times \{1 - e^{-(\frac{SURLAG}{T_c})}\} \quad 3.4$$

where Q_{sr} represents routed surface runoff (mm), Q_s represents daily generated surface runoff, Q_{st} previously stored surface runoff, SURLAG indicates surface runoff lag coefficient, T_c for time of concentration (hrs), and i represents time step number. A larger value of SURLAG releases more stored surface runoff to the stream and vice-versa. An instantaneously responding watershed (e.g., steep slope watershed) to precipitation should have larger SURLAG value than that of having opposite characteristic (e.g., flat terrain). Unless the land use is an open water body (river, wetlands), precipitation left after initial abstraction and surface runoff infiltrates into the soil system.

3.3.3. Soil water dynamics

SWAT divides the entire soil system/geology into four distinct zones, namely in downward order: soil profile, vadose zone, shallow groundwater system or unconfined aquifer, and deep confined aquifer. The entire soil profile may be further vertically discretized into up to maximum ten layers based on physical (texture, hydraulic conductivity) and chemical (organic carbon, salinity, soil pH) properties of the soil. Each soil layer is homogeneous with regard to its physicochemical properties and all soil layers need not to have an identical thickness. Daily water mass balance in soil zone is expressed by the following equation:

$$SW_i - SW_{i-1} = (P_i - Q_{s,i} - I_{a,i}) - ET_{a,i} - S_i - Q_{g,i} \quad 3.5$$

where SW, P, Q_s, I_a, ET_a, S, and Q_g, respectively represent soil water storage, precipitation, surface runoff, initial abstraction, actual evapotranspiration, seepage, and groundwater flow. Suffix i is for time step (here day). All dimensions are expressed in mm. The term in parenthesis amounts the daily infiltrated water into the top soil layer and subsequent bottom soil layers receive percolated water from its immediate upper layer.

3.3.4. Evapotranspiration

Evapotranspiration (ET) is a dominant component of soil water mass balance especially where crops/plants are growing. Like other contemporary watershed models, SWAT estimates actual evapotranspiration (ET_a) from the information of potential evapotranspiration (ET_p), which may be estimated by any of the three available methods Penman-Monteith (P-M) (Monteith 1965 cited by Neitsch et al. 2011), Priestley-Taylor (Priestley & Taylor 1972 cited by Neitsch et al. 2011), and Hargreaves (Hargreaves et al. 1985 cited by Neitsch et al. 2011). In addition, an alternative ET_p method can be used with time series being calculated externally to the model. In this study, the P-M method was employed since during calibration of the model this method found to give better results than the other two ET methods. This is generally suggested to be the superior approach over other five alternative ET models studied by Thompson et al., 2014a. The P-M method separately calculates potential evaporation (ET_{pev}) (see equation 3.6) and

potential transpiration (ET_{pt}) (see equation 3.7), considering the principle of energy conservation and resistance offered by aerodynamic process and plant canopy, and ignoring the influence of soil heat flux:

$$E_{pev} = \frac{1}{\lambda} \times \left[\frac{\Delta \times H_{net} + \rho_{air} \times c_p \times \frac{(e_z^0 - e_z)}{r_a}}{\Delta + \gamma \times (1 + \frac{r_c}{r_a})} \right] \quad 3.6$$

$$E_{pt} = \frac{1}{\lambda} \times \left[\frac{\Delta \times H_{net} + \left\{ \gamma \times K_1 \times \left(0.622 \times \lambda \times \frac{\rho_{air}}{P} \right) \right\} \times \frac{(e_z^0 - e_z)}{r_a}}{\Delta + \gamma \times (1 + \frac{r_c}{r_a})} \right] \quad 3.7$$

where E_{pev} is the potential evaporation rate (mm d^{-1}), λ is the latent heat of vaporization (MJ kg^{-1}), Δ is the gradient of saturation vapour pressure-temperature curve (kPa $°C^{-1}$), H_{net} is the net radiation (MJ m^{-2} d^{-1}), ρ_{air} is the air density (kg m^{-3}), c_p is the specific heat at constant heat pressure (MJ kg^{-1} $°C^{-1}$), e_z^0 and e_z are the saturation vapour pressures and vapour pressure of air at height z (kPa), γ is the psychrometric constant (kPa $°C^{-1}$), r_c and r_a are the canopy and aerodynamic resistances (s m^{-1}), respectively; in equation 3.7, E_t is the potential transpiration rate (mm d^{-1}), K_1 is a dimension coefficient, and P is the atmospheric pressure (kPa). Equation 3.8 defines the aerodynamic resistance to sensible heat and vapour transfer, which finally simplifies to equation 3.9 using necessary information from alfalfa crops:

$$r_a = \frac{\ln\left[\frac{(z_w - d)}{z_{om}}\right] \times \ln\left[\frac{(z_p - d)}{z_{ov}}\right]}{k^2 \times u_z} \quad 3.8$$

$$r_a = \frac{114}{u_z} \quad 3.9$$

where z_w is height of wind speed measurement in cm, z_p is height of humidity and temperature measurement in cm, d is the zero plane displacement of the

wind profile in cm, z_{om} is the roughness length for momentum transfer in cm, z_{ov} is the roughness length for vapour transfer in cm, k is the von Kármán constant, and u_z is the wind speed (m s^{-1}) at height z_w. Considering the inverse relationship between atmospheric CO_2 concentration and conductance of transpired water through the leaf's stomata (Morison, 1987), potential canopy resistance for alfalfa crops is calculated by equation 3.10:

$$r_c = \frac{49}{\left(1.4 - 0.4 \times \frac{CO_2}{330}\right)} \qquad 3.10$$

where CO_2 is the concentration of atmospheric concentration in ppmv (parts per million by volume). This equation is thought to be appropriate for impact analysis of climate change as CO_2 is the major concerned element of atmosphere (Neitsch et al., 2011). The P-M method separately estimates potential evaporation and transpiration unlike other methods that usually do not disintegrate evapotranspiration into evaporation and transpiration.

Evapotranspiration at the potential rate is only possible in ideal conditions i.e., ET from an actively grown alfalfa crop with no water shortage. However, in reality this ideal condition is seldom present and therefore potential ET (PET) needs to be reduced to actual evapotranspiration. Many commonly used models reduce potential ET to actual ET by multiplying the former value by a crop coefficient (k_c) and a soil water stress factor. Because the SWAT model separately estimates potential evaporation and transpiration, their potential values are also reduced separately. Potential evaporation (E_{pev}) is downscaled by using soil cover index that represents soil surface bareness; later, this downscaled potential evaporation is apportioned among different soil layers based on the exponential Equation 3.11. Since the rate of soil evaporation is not homogeneous down through the depth of a soil layer, SWAT uses Equation 3.12 to take the variability of soil evaporation along soil depth.

$$E_{pev,z} = E_{pev} \times \frac{z}{z + e^{(2.374 - 0.00713 * z)}} \qquad 3.11$$

$$E_{pev,ly} = E_{pev,zl} - ESCO * E_{pev,zu} \quad 3.12$$

Where $E_{pev,ly}$ is the potential evaporation from a soil layer (ly), zl and zu indicate the depths at lower and upper boundary of the soil layer, and $ESCO$ is the soil evaporation compensation factor that can vary from 0.0 to 1.0. Estimated potential soil evaporation is further downscaled depending on available soil water to obtain actual soil evaporation from a soil layer.

Before estimating actual transpiration (E_{pt}), SWAT allocates total potential transpiration (E_{pt}) to different soil layers within the depth of current plant root (z_{root}) as follows:

$$E_{pt,ly} = \frac{E_{pt}}{[1 - e^{-B_w}]} \times \left[e^{-B_w \cdot \frac{z_u}{z_{root}}} - e^{-B_w \cdot \frac{z_l}{z_{root}}}\right] \quad 3.13$$

where $E_{pt,ly}$ represents amount of potential transpiration from a soil layer having thickness ly which is the difference of depths (z_l and z_u) at lower and upper boundary of the layer and B_w is a water use distribution pattern within root zone. SWAT sets the value of B_w to 10 which ensures 50% of transpiration demand will be met up from upper 6% of root zone depth. If an upper soil layer does not have sufficient water to meet the layer's potential transpiration ($E_{pt,ly}$) then the lower layer may supplement the upper layer according to equation 3.14:

$$E'_{pt,ly} = E_{pt,ly} + E_{pt,demand} \times EPCO \quad 3.14$$

where $E'_{pt,ly}$ is the adjusted potential transpiration, $E_{pt,demand}$ is the amount of potential transpiration demand not met by upper soil layer, and $EPCO$ is the plant uptake compensation factor which varies between 0.0 and 1.0. As $EPCO$ approaches to 1.0, more water will be transpired from lower layers. The meaning of $EPCO$ is somewhat like the diffusion process of soil moisture from higher concentration to lower concentration zone. To take the effect of soil water stress on transpiration into account, the following modifications are further applied:

$$E''_{pt,ly} = \begin{cases} E'_{pt,ly} \times e^{\left[5.\left(\frac{SW_{ly}}{0.25 \times AWC_{ly}} - 1\right)\right]} & if\ SW_{ly} < \left(0.25.AWC_{ly}\right) \\ E'_{pt,ly} & if\ SW_{ly} \geq \left(0.25.AWC_{ly}\right) \end{cases} \quad 3.15$$

where $E''_{pt,ly}$ is the potential transpiration after soil water stress, SW_{ly} is the soil water in the layer ly, and AWC_{ly} is the available water capacity of the layer measured from the difference of field capacity (FC), and wilting point (WP). Finally total actual transpiration ($E_{a,t}$) is calculated by following equation:

$$E_{a,t} = \sum_{ly=1}^{n} min\left[E''_{pt,ly}, \left(SW_{ly} - WP_{ly}\right)\right] \quad 3.16$$

3.3.5. Percolation and lateral flows in soil profile

SWAT estimates soil water content for each layer in the soil profile. If a soil layer contains more water than its field capacity, then free or excess water ($SW_{ly,excess}$) may either percolate to a lower layer or be ponded in the soil layer. Excess water is calculated according to equation 3.17:

$$SW_{ly,excess} = \begin{cases} SW_{ly} - FC_{ly} & if\ SW_{ly} > FC_{ly} \\ 0 & if\ SW_{ly} \leq FC_{ly} \end{cases} \quad 3.17$$

where FC_{ly} is the field capacity of soil layer. Depending on existence of seasonal water table (WT) in the soil profile, excess water of a soil layer is percolated to the next lower layer with the following routing equations:

$$W_{per,ly} = \begin{cases} SW_{ly,excess} \times \left[1 - e^{-\frac{\Delta t}{TT_{per,ly}}}\right] & when\ No\ seasonal\ WT\ exists\ in\ lower\ layer \\ 0 & when\ seasonal\ WT\ exists\ in\ lower\ layer \end{cases} \quad 3.18$$

$$TT_{per,ly} = \frac{SAT_{ly} - FC_{ly}}{K_{sat,ly}} \quad 3.19$$

where $W_{per,ly}$ is the percolated water during time step in mm H_2O, Δt is time step (day), TT_{per} is the percolation travel time through soil layer in hours, and $K_{sat,ly}$ is the saturated hydraulic conductivity in ms^{-1}. As can be seen from equation 3.19, the value of TT_{per} is unique for each layer. The existence of an impervious layer either in the soil profile or the vadose zone may create a perched water table by restricting water movement further down towards the shallow aquifer. If an impervious layer is present in the vadose zone then water percolated out of bottom soil layer is routed as following:

$$W_{per,btm\_ly\_imp} = W_{per,btm\_ly\_org} \times \frac{D_{imp-solpr}}{D_{imp-solpr} + e^{[8.833-2.589* D_{imp-solpr}]}} \quad 3.20$$

where W_{per,btm_ly_imp} is the modified percolated water from bottom soil layer in mm H_2O, W_{per,btm_ly_org} is the water percolated out soil profile with original equation, and $D_{imp-solpr}$ is the vertical distance between impervious layer and bottom of soil profile. All amounts are calculated for time step.

An area with sufficient soil hydraulic conductivity, hydraulic head gradient, and a perched water table has the potential to generate lateral flow. SWAT uses the kinematic model (Sloan, Morre, Coltharp and Eigel, 1983; Sloan and Moore, 1984 cited by Neitsch et al., 2011) to model lateral flow. If a soil has significant macropore or crack or preferential flow, then this can also be represented from the information of soil's potential crack volume.

3.3.6. Groundwater system

Accurate simulation of groundwater dynamics is often essential especially where a strong interaction between surface (e.g., streamflow) and groundwater is evident and where water consumption by different users (agriculture, industry, public water supply) depend on regional groundwater resources. SWAT simulates two types of aquifer, namely, shallow aquifer/unconfined aquifer and deep confined aquifer. Equation 3.21 represents the water mass balance of shallow aquifer:

$$W_{sh,i} = W_{sh,i-1} + R_{sh,i} - Q_{gw,i} - E_{revap,i} - W_{pump,i} \quad 3.21$$

where $W_{sh,i}$ and $W_{sh,i-1}$ is the amount of stored water in the shallow aquifer on i and i-1 day, respectively; $R_{sh,i}$ is the recharge to the shallow aquifer, $Q_{gw,i}$ is the baseflow/groundwater flow, $E_{revap,i}$ is the capillary flow, and $W_{pump,i}$ is the pumping out water. All dimensions are in mm H_2O and i indicates day. SWAT employs an exponential decay function to estimate total aquifer recharge (unconfined and confined) (equation 3.22):

$$R_i = \left(1 - e^{-\frac{1}{GW\_DELAY}}\right) \times W_{per,btm\_ly} + \left(e^{-\frac{1}{GW\_DELAY}} \times R_{i-1}\right) \quad 3.22$$

where R indicates recharge, W_{per,btm_ly} indicates percolated water from lowest soil layer including crack flow (if any), GW_DELAY is the travel time through the vadose zone which depends on permeability and saturation of overlying geology, and suffix i indicates day. The same approach is also adopted in the SWIM model (Hattermann et al., 2006). Once total recharge is calculated then the “aquifer percolation coefficient” partitions total recharge between shallow and deep aquifers. Finally exponential equation 3.23 is used to generate baseflow:

$$Q_{gw,i} = \begin{cases} Q_{gw,i-1} \times e^{-ALPHA\_BF*\Delta t} + R_{sh,i}.\left(1 - e^{-ALPHA\_BF*\Delta t}\right) & if\ W_{sh,i} > GWQMN \\ 0 & if\ W_{sh,i} \leq GWQMN \end{cases} \quad 3.23$$

where Q_{gw} indicates groundwater flow in main channel, R_{sh} is shallow aquifer recharge, $ALPHA\_BF$ is baseflow recession constant, $GWQMN$ is threshold water depth in shallow aquifer and $\boldsymbol{i}$ is for days. Although all simulated water depths in the shallow aquifer are not referenced with any datum (for example, ground surface or aquifer’s base), a properly calibrated value of $GWQMN$ results in accurate simulated baseflows.

3.3.7. Water routing through river networks

The SWAT model uses two different types of hydrological routing methods (i) variable storage and (ii) Muskingum rounting. In the former method, the influence of channel's hydraulic and physical characteristics (flow depth, water cross sectional area, roughness, and slope) on flows is ignored whereas the latter takes these effects into account. In this study, the Muskingum method was used and a detailed description of this method has been provided in Section 2.3.6. Like many other contemporary catchment models, there is no mathematical basis to simulate distributaries in river networks. However, specified fractions of water from a main river can be manually transferred to another river branch.

3.4. Summary

This chapter has systematically described how SWAT conceptualises a catchment and represents the major hydrological processes within the catchment. A number of algorithms are embedded in the ArcSWAT interface to automatically delineate a catchment. Although such tools can expedite the delineation process, successful application of this approach is subject to DEM data accuracy. In particular, this is problematical for the low relief flat topography where publicly available DEM data (e.g. SRTM) show less confidence in representing actual topography of the area. The provision of manual catchment delineation in SWAT is of a great advantage to overcome such limitations. Each hydrological process is discussed with necessary mathematical equations. While simulating any hydrological processes SWAT preserves the conservation of mass although the conservation of energy is overlooked unlike some comprehensive physics-based models.

Chapter 4
Study Area: The Upper Meghna River Basin and Database Development for Hydrological Modelling

4.1. Introduction

This chapter provides a detailed description of study area, the Upper Meghna River Basin (UMRB). The basin is described in light of necessary data, to build a SWAT model for the UMRB, including topography, land use, soil, and climate. Since in a data scarce region, input data are probably the primary source of uncertainty in catchment modelling (Fonseca et al., 2014), each of the following sections, where necessary, begins with a detailed description of data source and quality prior to description of the basin with respect to those data.

4.2. Physiographic and hydro-meteorological properties of the UMRB

The geographical position and some hydrographic characteristics of the UMRB have been introduced in Chapter 1. This section describes in detail the physiographic and hydro-meteorological properties of the basin. As discussed in Section 1.3.4, this study encountered problems in retrieving measured hydro-meteorological data for the Indian part of the basin. For example, several requests were sent to the Indian Meteorological Department (IMD) in order to acquire observed time series of hydro-meteorological data but no cooperation was developed. Therefore, most of the required data for the three Indian regional basins (Figure 1.3b) of UMRB come from different sources as secondary data which can be obtained at no cost.

4.2.1. Topography

In order to describe the topography of the UMRB, information were gathered from available research articles, published documents by various Government and non-Government organizations, and from the repository of Shuttle Radar Topographic Mission (SRTM) (Farr et al., 2007) digital elevation data. In this

study HydroSHED processed SRTM DEM (Lehner, 2005) were used. HydroSHED is a global DEM database (90 m resolution) that was developed from the original SRTM-1 data set (30 m resolution) by the Conservation Science Program of the World Wildlife Fund US, in collaboration with the US Geological Survey, the International Center for Tropical Agriculture, The Nature Conservancy, and the Center for Environmental Systems Research of the University Kassel, Germany. This DEM data set is particularly suitable for distributed catchment modelling as many other ancillary data (land use and land cover, digital river networks, lakes and wetlands) were used to remove various artifacts (e.g., unrealistic high and low values, void data) in the SRTM-1 data.

Based on these topographic data (Figure 4.1), the boundary of the UMRB can be defined as: (i) the northern divide line of the Meghalaya basin defined by the Garo hills, Shillong plateau, and Jaintia hills, (ii) the Barail range along the northern border of Barak River Basin; this, in combination with the northern Meghalaya divide line, separates the entire UMRB from the adjacent Brahmaputra Basin (see Figure 1.3a), (iii) the north-eastern tip of the Barak River Basin is bordered by Lushai hills, where the Barak River originates, (iv) the Bhuban and Manipur hills demark the eastern drainage divide of the Barak River Basin whereas the southern border line is formed by Mizoram (Laskar and Phukon, 2013) or Indo-Burma fold belt (Mukherjee et al., 2009), (v) the southern part of Tripura Basin is formed by Tripura and Chittagong hills, and (vi) according to Mukherjee et al. (2009) the western basin divide line is the cause of tectonic depression of the Sylhet basin which ultimately separate the Meghna River Basin from the adjacent old Brahmaputra River Basin.

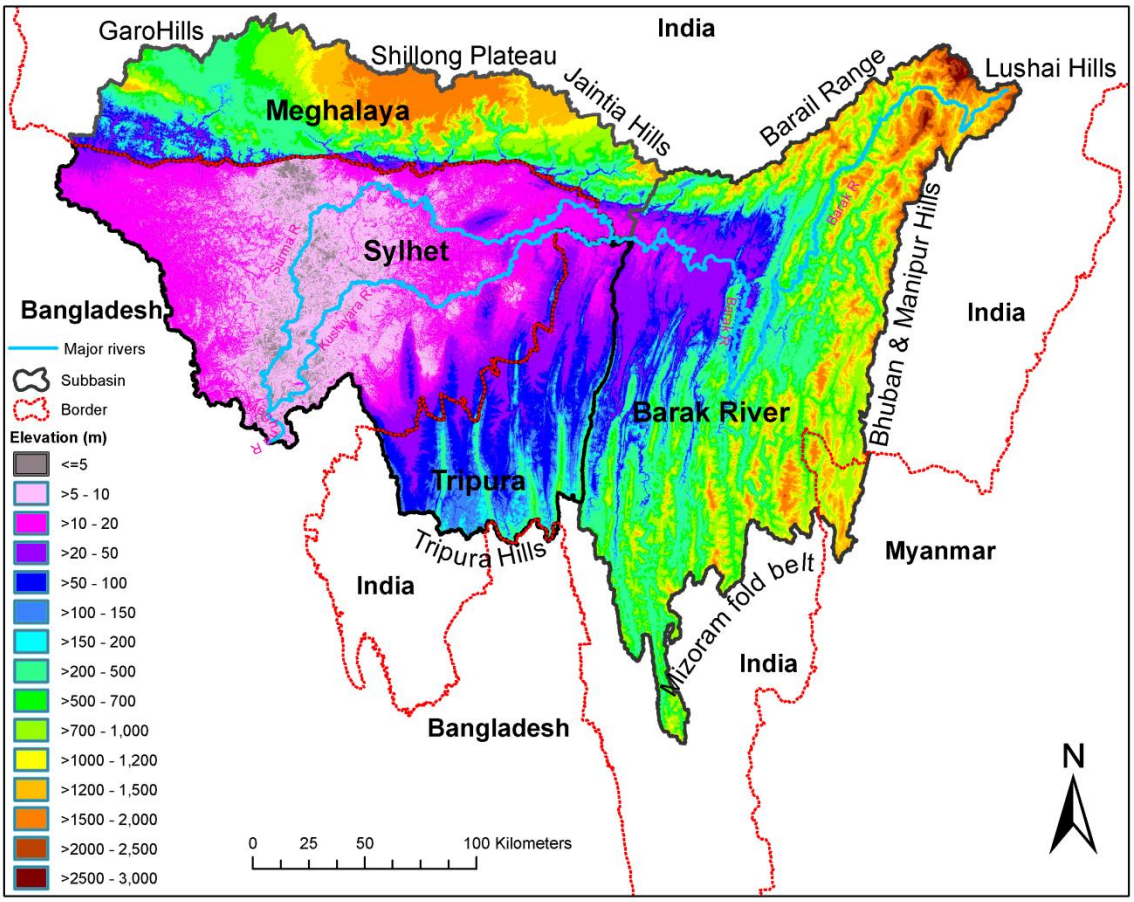

Figure 4.1. Topography of the UMRB. SRTM DEM data were collected from the HydroSHED database (http://hydrosheds.cr.usgs.gov/index.php).

The topographic features of the UMRB are extremely diverse. The elevation range of the UMRB spans from less than 5 m above or below mean sea level (m. s. l.) along the oblique north-southward central line zone of the Sylhet Basin to a maximum of ~3000 m above m. s. l. at the Lushai hills where the Barak river originates (Figure 4.1). DEM data derived surface slope of the UMRB ranges from less than 2% in the floodplain of the Sylhet Basin to more than 150% in Shillong plateau of the Meghalaya basin and along the north and east border of the Barak Basin. The terrain of the Meghalaya Basin is characterised by rugged hills and mountains with the highest elevated Shillong Plateau (up to 1950 m above m. s. l.) being at the centre of the basin. The presence of many ravines and gorges makes this basin a picturesque landscape (Dhiman, 2012) (Figure 4.2). According to Laskar and Phukon (2013), there are six different landscapes in the Barak River Basin: (i) anticlinal hills found in the vicinity of highest relief, (ii) ridge and strike valleys formed from anticlinal hills due to long-term erosional process,

(iii) denudational hills (remnants of ridge hills), (iv) fluvial terraces, (v) alluvial plains along the synclinal troughs between consecutive anticlines, and (vi) active floodplains at the lowest elevations. The low relief Sylhet Basin is bordered by the high relief Meghalaya Basin in the north and by the moderate relief Tripura Basin in the east (Figure 4.1). The topography of the Sylhet Basin is extremely flat except for a few hillocks in the vicinity of the eastern border of Sylhet District (see Figure 4.1 and Figure 4.3).

Figure 4.2. A picturesque landscape of the Meghalaya Basin.
Source: http://placeforvacations.com/shillong-hill-station-india-shillong-tourism

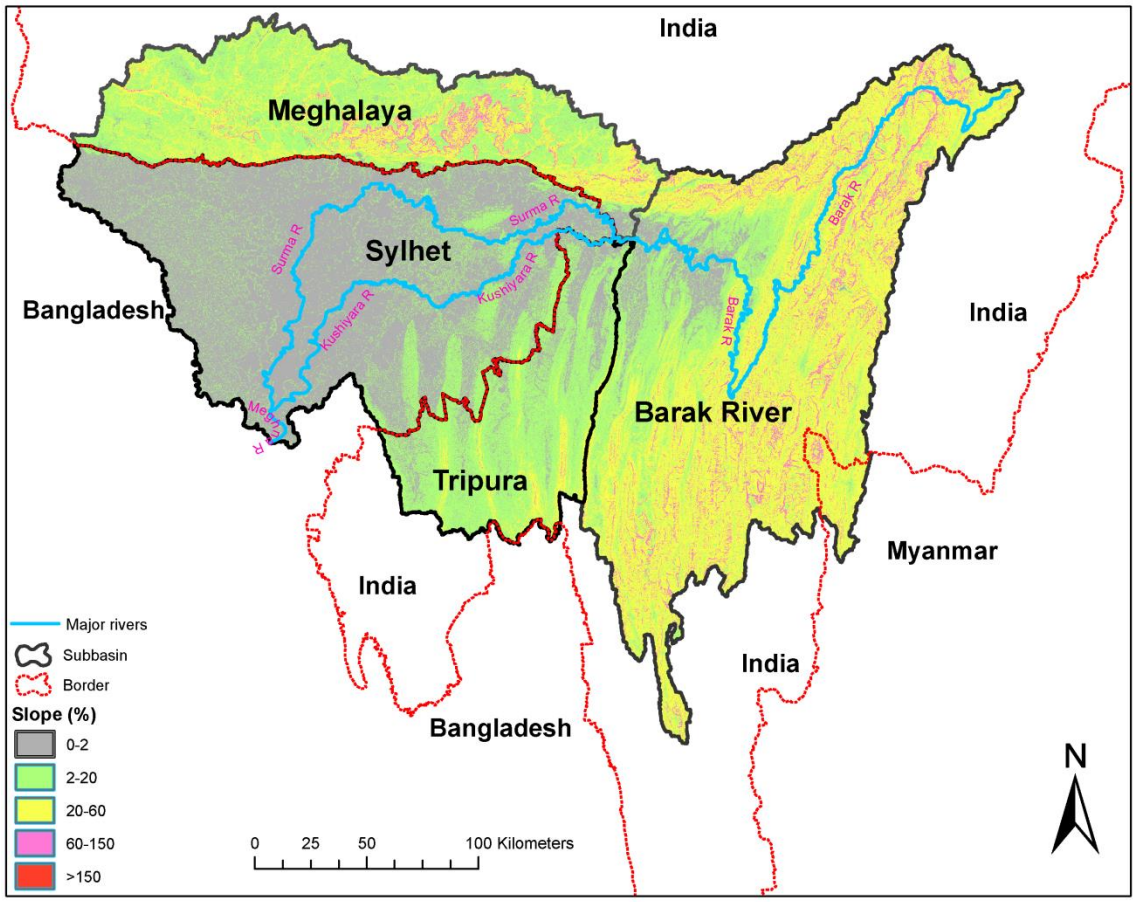

Figure 4.3. Surface slope of the UMRB derived from the HydroSHED DEM data.

4.2.2. Land use and land cover

Land use over the UMRB was derived from the Global Land Cover (GLC) data classified by the Department of Geography, University of Maryland (UMD), from the imagery of Advanced Very High Resolution Radiometer (AVHRR) satellite (Hansen et al., 2000). The images were collected during the period 1981–1994; hence the generated GLC data is an average representation of global land cover for that period. Out of a total of 14 different land cover classes in the GLC database, there are 12 classes in the UMRB (Figure 4.4a). However, the original GLC data were further reclassified to conform with the actual land cover of the study area (Figure 4.4b). For example, the “crop” and “grass” land cover classes in the original GLC data were replaced by “rice” since the region under these two classes is, in fact, intensively rice cultivated which is justified by author’s experience on local land use and by Google Earth. As confirmed by imagery available within Google Earth and some documented reports, all shrubs (open

and closed) and wooded grass land covers were considered to be tea crop whereas deciduous forest and woodlands were merged to form one land cover class (deciduous forest). Both types of evergreen forests (broad leaf and needle leaf) were also merged to provide a single evergreen forest land cover. Figure 4.4 shows therefore that the original land cover classes were finally reduced to six different classes after reclassification. The four major land covers are respectively deciduous forest (30%), evergreen forest (29%), rice (29%), and range (11%). A very small proportion (1%) of the UMRB is classed as non-vegetational i.e. water and urban. The three Indian hilly basins Meghalaya, Tripura, and Barak River are mainly covered by forest whereas the land use of the Sylhet Basin is dominated by rice. The rangelands are generally seen at the low altitudinal hills of subbasins.

(a) Before Reclassification

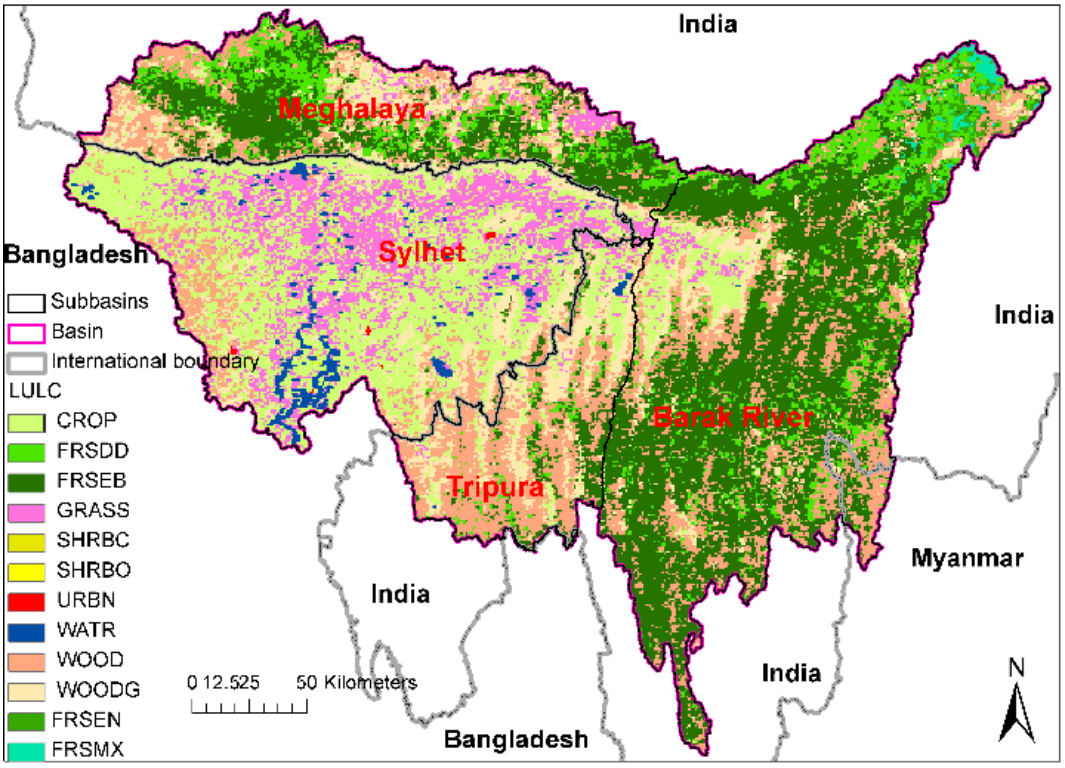

(b) After Reclassification

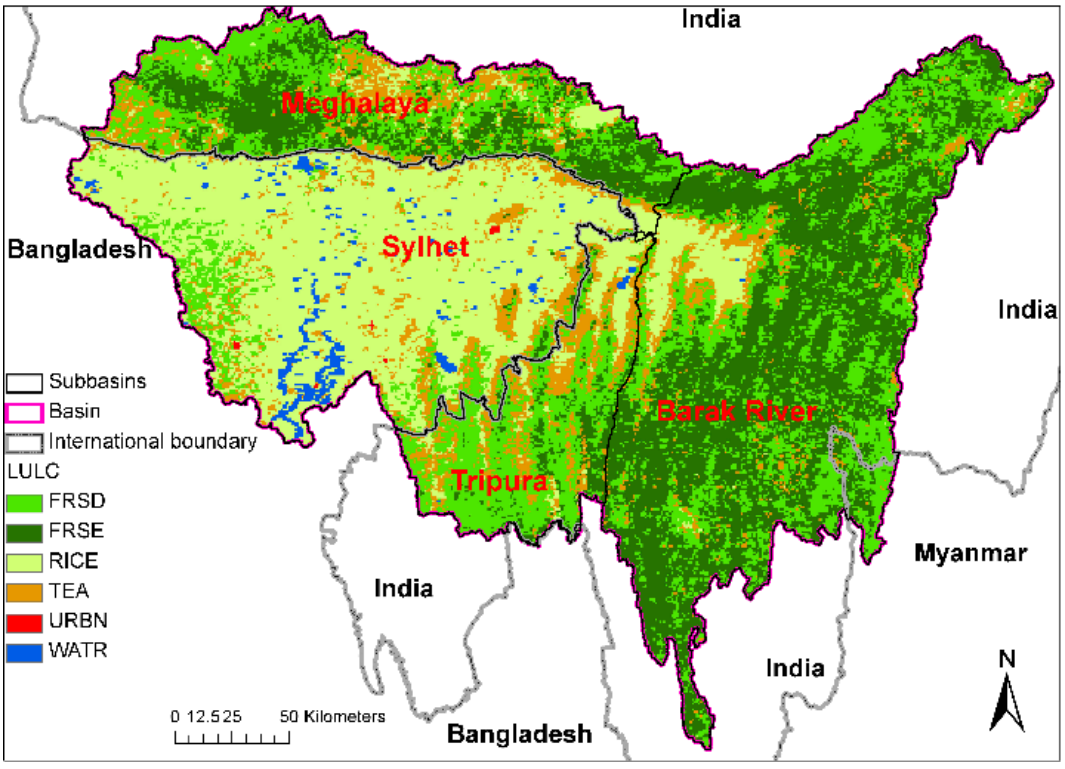

Figure 4.4. Land use/land cover of the UMRB, before and after reclassification of GLC data developed by Hansen et al. (2000). FRSDD=forest deciduous, FRSEB=forest evergreen broad leaf, FRSEN=forest evergreen needle leaf, FRSMX=forest mixed, SHRBC=shrub closed, SHRBO=shrub opened, URBN=urban, WATR=water, WOOD=woodland, and WOODG=wooded grass.

4.2.3. Soil

Soil data are an important prerequisite in many catchment models. Therefore, high spatial resolution (in both horizontal and vertical directions) soil data are desirable for realistic catchment simulation. Singh et al. (2011) , for example, compared runoff and sediment simulation performances of a SWAT model for two different sets of USA soil data, namely, state-level coarser resolution State Soil Geographic (STATSGO) data and finer resolution county-level Soil Survey Geographic (SSURGO) data. They employed the model in the Fish River watershed of Alabama State. The finer SSURGO soil data was found to provide a much better simulation of runoff and sediment compared to the coarser STATSGO soil data.

In this study, soil data were collected from the Harmonized World Soil Database (HWSD), recently developed by the FAO-UN (Food and Agriculture Organization of United Nations) and the International Institute for Applied Systems Analysis with other partner organizations (IIASA) (FAO/IIASA/ISRIC/ISS-CAS/JRC, 2012). The HWSD was compiled from four different soil databases namely FAO-UNESCO Soil Map of the World (FAO-Unesco, 1971-1981 cited in FAO/IIASA/ISRIC/ISS-CAS/JRC, 2012), Soil and Terrain database (Sombroek, 1984 cited in FAO/IIASA/ISRIC/ISS-CAS/JRC, 2012), updated soil database of Europe and northern Eurasia (ESB, 2004 cited in FAO/IIASA/ISRIC/ISS-CAS/JRC, 2012), and the Soil Map of China (Shi et al., 2004 cited in FAO/IIASA/ISRIC/ISS-CAS/JRC, 2012). The spatial resolution of HWSD is 1 km (30 arc seconds). The reliability of HWSD is not homogeneous for all regions of the world. Regions whose soil data were compiled based on only old FAO-UNESCO Soil Map of the World data (e.g. South Asia, North America, and Australia), generally recognized as FAO-74 soil data, are considered less accurate. Since the UMRB lies in South Asia, some uncertainty from HWSD soil data is therefore likely. Although for the newly developed HWSD the entire world's soils are grouped into 28 different main soil classes, the UMRB is found to have four main soil groups Acrisols (AC), Cambisols (CM), Gleysols (GL), and Nitisols (NT). However, as in the FAO-74 soil database the main soil group can have

several soil subgroups based on a “qualifier”, formative elements for naming of soil units. The characteristics of qualifier are defined by the properties of diagnostic soil horizon. The final soil data for the UMRB contains six different soil types (Figure 4.5 and Table 4.1).

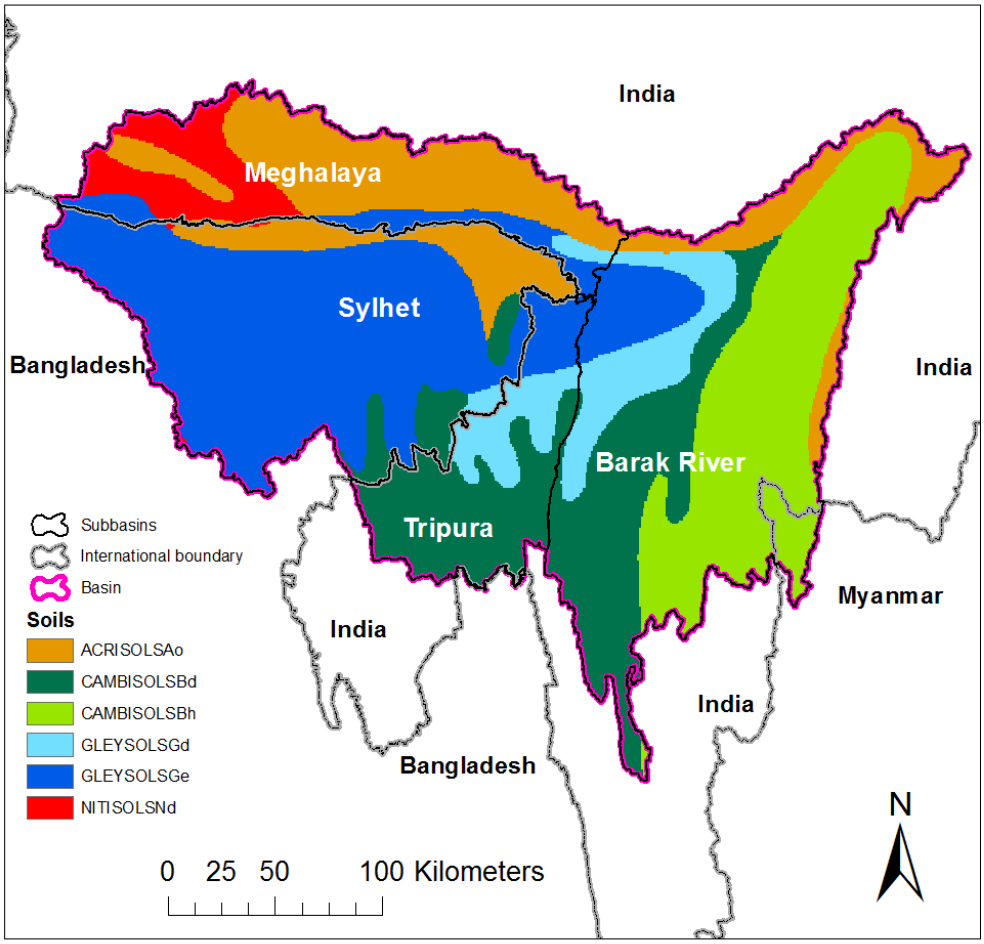

Figure 4.5. Soil map of the UMRB. Source: Harmonized World Soil Database (FAO/IIASA/ISRIC/ISS-CAS/JRC, 2012)

For each soil map unit, reference soil depth is set of 1000 mm from the soil surface where depth of top soil is 0–300 mm and corresponding value for subsoil is 300–1000 mm. Many important physical and chemical soil properties are provided for both top- and subsoils. These include percentage of soil particles (sand, silt, clay), gravel, organic matter, bulk density, cation exchange capacity, and pH. Saturated hydraulic conductivity of soil layers exerts a major influence upon a catchment’s hydrological behavior and is a key requirement within many hydrological models including SWAT (see Section 3.3.3). Therefore, the Soil-

Plant-Air-Water (SPAW) model developed by Saxton and Willey (2005) was used to generate saturated hydraulic conductivity (Table 4.2) from the relative percentage of soil particles (sand, silt, and clay). Moreover, this programme also includes the effect of organic matter, compaction, and gravel while estimating saturated hydraulic conductivity.

Table 4.1. Characteristics of soils existed over the UMRB.

Main soil group	Qualifier	Soil name	Characteristics
ACRISOLS	Orthic	Orthic Acrisols (ACRISOLSAo)	• comparable to Alfisols and Ultisols of USDA Soil Taxonomy • having ochric horizon • found in hilly or undulating topography of wet tropical/subtropical or warm temperate climate regions • susceptible to erosion • soil in lower elevation is subject to periodic saturation • shift cultivation is a common agricultural practice
CAMBISOLS	Dystric	Dystric Cambisols (CAMBISOLSBd)	• comparable to Inceptisols of USDA Soil Taxonomy • found in level and mountainous terrains under all climates • erosion and deposition of soil in mountainous regions exist • loamy to clayey soil texture
	Humic	Humic Cambisols (CAMBISOLSBh)	
GLEYSOLS	Dystric	Dystric Gleysols (GLEYSOLSGd)	• comparable to Inceptisols and Mollisols of USDA Soil Taxonomy • found in depression areas and low landscape positions with shallow groundwater table • soils can remain under saturated condition for long time unless drainage
	Eutric	Eutric Gleysols (GLEYSOLSGe)	
NITISOLS	Dystric	Dystric Nitisols (NITISOLSNd)	• comparable to kandic groups of Alfisols and Ultisols of USDA Soil Taxonomy • found in level to hilly land under tropical rain forest or savannah vegetation • deep (>150 cm) and stable soil • erosion resistant • higher porosity, well drained, and water retention capacity is low • soils can remain under saturated condition for long time unless drainage

Source: Summarized information from the soil report by FAO/IIASA/ISRIC/ISS-CAS/JRC (2012)

Table 4.2. Saturated hydraulic conductivity of soils in the UMRB.

Soil name	Saturated hydraulic conductivity of soils (mm hr^{-1})	
	Top soil layer (0–300 mm bgl*)	Bottom soil layer (> 300–1000 mm bgl*)
Orthic Acrisols (ACRISOLSAo)	7.54	1.73
Dystric Cambisols (CAMBISOLSBd)	10.54	7.55
Humic Cambisols (CAMBISOLSBh)	7.46	7.19
Dystric Gleysols (GLEYSOLSGd)	10.27	5.69
Eutric Gleysols (GLEYSOLSGe)	7.61	3.96
Dystric Nitisols (NITISOLSNd)	7.32	0.78

*bgl (below ground level)

4.2.4. Hydrography

For modelling a catchment, accurate representation of river networks and other water bodies is required. Unless ground survey based river network data are available, a suitable GIS algorithm can be used to generate the river network of an experimental catchment from gridded digital elevation data, for example, raster DEM data. However, such an approach may not be appropriate for low relief topographic area such as floodplains and deltas due to the relatively higher noise in freely available coarse resolution DEM data (although today more precise but expensive LiDAR (Light Detection And Ranging) elevation data can being used to reduce the uncertainty in coarser DEM data if they are available (Charrier and Li, 2012; Murphy et al., 2008).

To prepare a realistic river network for the UMRB, multi-source information were used: SRTM 90 m resolution DEM data, different imageries (Basemap imagery by ESRI, Google Earth), published documents (Baki et al., 2008; Khan et al., 2005), and digital river network of the Sylhet Basin collected from Centre for Environmental and Geographic Information Systems (CEGIS), Bangladesh. Firstly, by using automatic delineation tool of ArcSWAT platform (a SWAT

interface for ArcGIS), an approximate digital river network of the UMRB was generated from the SRTM DEM data. When overlaying the DEM generated river network on the imagery of the UMRB, it was found that the delineated river network was accurate for the three hilly basins (Meghalaya, Barak River, and Tripura) but not for the flat Sylhet Basin. For this reason, the river network within the Sylhet Basin was re-digitized using CEGIS provided river network data (acquired as a shape file) along with the ESRI Basemap and Google Earth imagery. The original river network data, provided by CEGIS, contained many small channels, locally known as khals that in most cases act as connecting channels between rivers and wetlands. The resultant final river network of the UMRB is shown in Figure 4.6. The validity of this river network was confirmed with Google Earth imagery. The final river network is of total 8990 km running length and 0.14 km km^{-2} river density. The major rivers of the UMRB are the Barak, Kushiyara, Surma, and Meghna (Figure 4.6). Originating in the Lushai Hills (see Figure 4.1), the south-westerly flowing Barak River meets Tuvai River at Tipaimukh before running in an almost opposite direction (Figure 4.6). The river changes its direction to west at Lakhipur (93.01° E, 24.78°N) which is the transition point between the floodplain and hilly regions of Barak River catchment. The river meanders through the Barak floodplain until it reaches the border between Bangladesh and India at Amalshid where the River Barak bifurcates into two rivers, the Kushiyara and Surma. The Kushiyara River flows about 42 km along the border before entering Bangladesh and the right sided Surma River flows about 28 km along the border. Flowing through the depressional wetland dominated Sylhet Basin, these two major rivers join at Bajitpur, just 20 km upstream of outlet of UMRB. All other rivers in the UMRB feed the major rivers as tributaries.

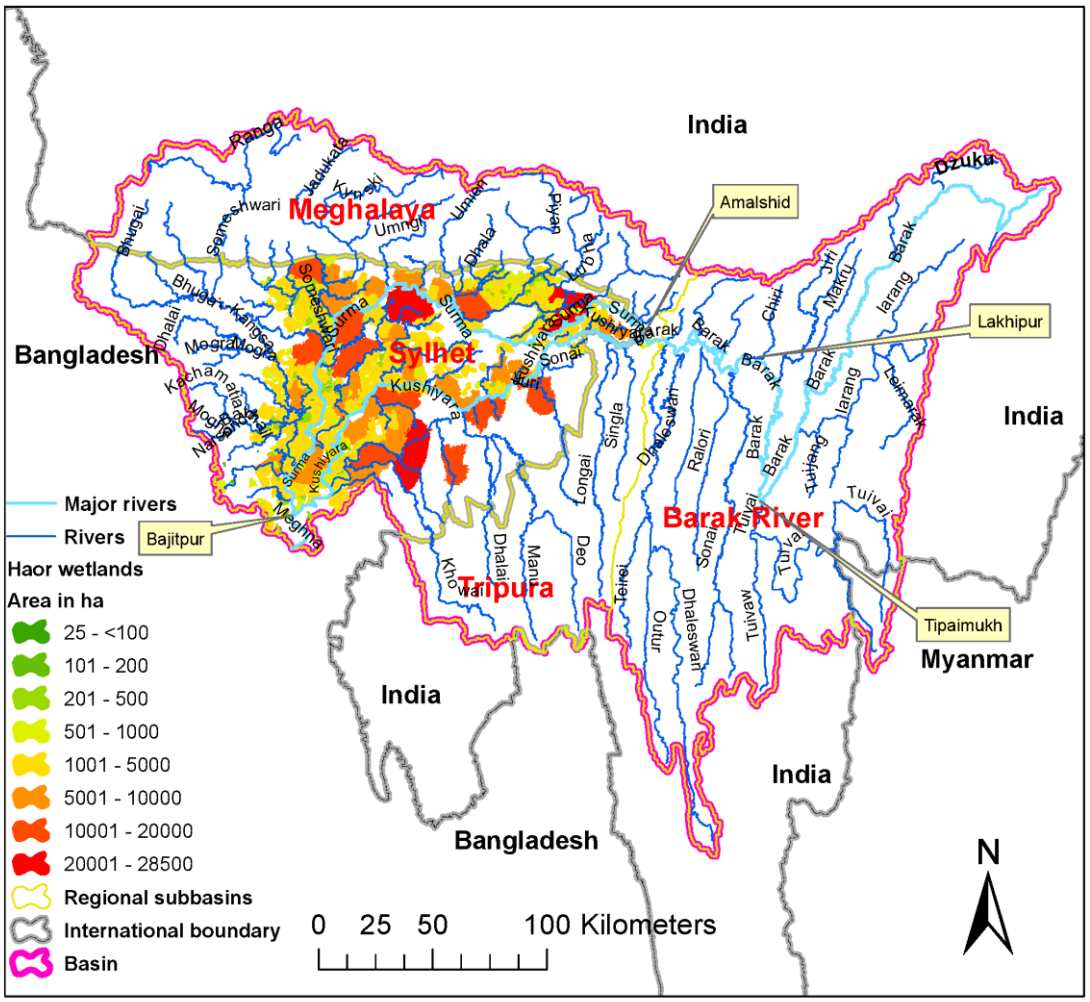

Figure 4.6. Rivers and haor wetlands in the UMRB. The areal extent of haor wetlands represents their maximum inundation.

The hydrological and non-hydrological responses of a catchment can be strongly influences by the presence of wetlands (Hattermann et al., 2008; Hayashi and van der Kamp, 2000; Lindsay et al., 2004). However, this influence depends on the wetlands' position, their morphometric properties (size, shape, depth), soils, antecedent soil moisture and surface water content, interaction with other water bodies and anthropogenic modifications and management of wetlands (Heimann and Krempa, 2011; Ogawa and Male, 1986; Quinton and Roulet, 1998). Therefore, accurate representation of wetlands in catchment modelling is important (see Chapter 5). As described in Chapter 1, the Sylhet Basin of the UMRB contains numerous depressional wetlands that are hydraulically connected with their adjacent rivers during high flow period. In this study, the GIS data of the maximum areal extent of wetlands were collected from the CEGIS,

Bangladesh (Figure 4.6). About 370 haor wetlands, having a range of maximal areal water surface area of 25–28500 ha, are located in the Sylhet Basin. However, this database does not contain any other morphometric characteristics of the wetlands such as shape and depth.

4.2.5. Climate

Climate data (precipitation, temperature, humidity, wind speed, and solar radiation) are the main driving force of any hydrological model. For this reason, quality and resolution (spatial and temporal) of climate data are two major sources of uncertainties that may affect a model's performance. Daily precipitation and temperature (maximum and minimum) data over the modelled period are the two minimum required climatic data for many catchment models such as SWAT. However, an additional three climatic data time series, if available, daily relative humidity, wind speed, and solar radiation, can be used to reduce uncertainty in characterizing meteorological conditions. In particular these data are necessary for estimating PET using the Penman-Monteith method, the method which is generally preferred (Thompson et al., 2014b).

4.2.5.1. Precipitation

To develop a reasonable rainfall database for this study, a range of different sources of rainfall data were employed. Rainfall data either measured at weather stations or estimated at the centre of regular grids in and around the boundary of the UMRB (Figure 4.7) were used. There are total 43 stations and grids which were the principal rainfall data source for model development. Although a grid does not in fact represent a point weather station, here it is considered as a weather station for the sake of simplicity. The eight weather stations within Bangladesh territory (four managed by the Bangladesh Meteorological Department – BMD and four by the Bangladesh Water Development Board – BWDB) provided daily observed rainfall for the period 1987–2010. Among the remaining 35 stations which were within India, 20 stations' daily rainfall data (1990–2005) were obtained from the 50 km gridded all India rainfall database (http://swat.tamu.edu/software/links/india-dataset/) prepared by IMD and rest 15 stations' district wise average monthly rainfall data (2004–2010) were obtained

from the website of IMD. For the sake of simplicity, hereafter these data are referred to as BMD, BWDB, IMDgrid and IMDdist rainfall data, respectively, to indicate their sources/forms (BMD, BWDB, gridded IMD and district wise average IMD).

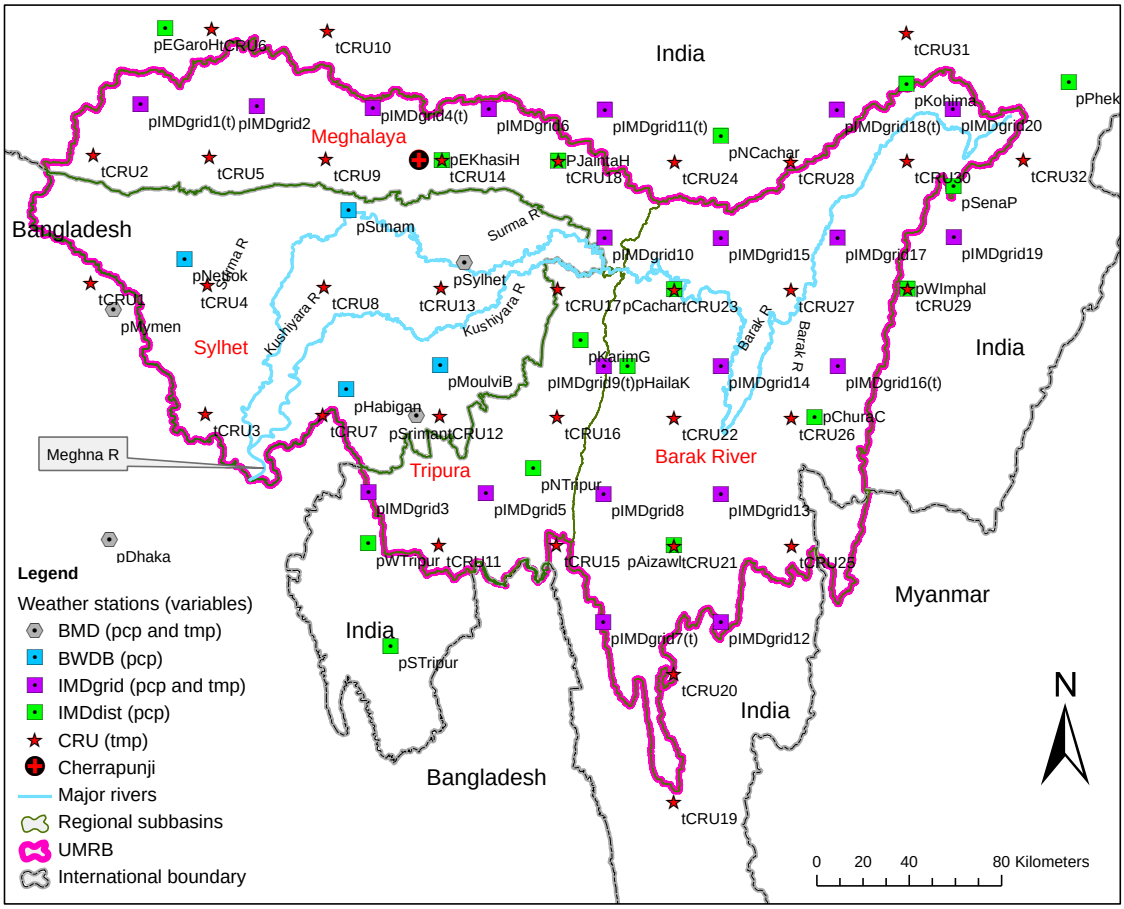

Figure 4.7. Spatial distribution of weather gauge stations or grid points in and around the UMRB. In station or grid name, first character ‘p’ and ‘t’ respectively indicate precipitation and temperature; and remaining characters indicate shortened station name. IMDgrid stations that have both precipitation and temperature data are indicated with a ‘t’ character in a parenthesis at the end of the station’s name. BMD means Bangladesh Meteorological Department; BWDB means Bangladesh Water Development Board; IMD means Indian Meteorological Department.

IMD originally derived both sets of rainfall data (IMDgrid and IMDdist) from the daily time series of observed rainfall recorded at many weather stations across India. However, IMD makes available only the most recent 5 years of IMDdist

data on its website. Figure 4.8 illustrates the availability of rainfall data during the period (1990–2010) for each station and appendix A.1 gives the complete time series of rainfall from which this figure is generated. A station with no records for all the days in a month indicates a missing month (red colour). In general, the BMD and BWDB records are more complete whilst the IMDdist data contains more missing data. IMDgrid data have no missing data during the period 1990–2005.

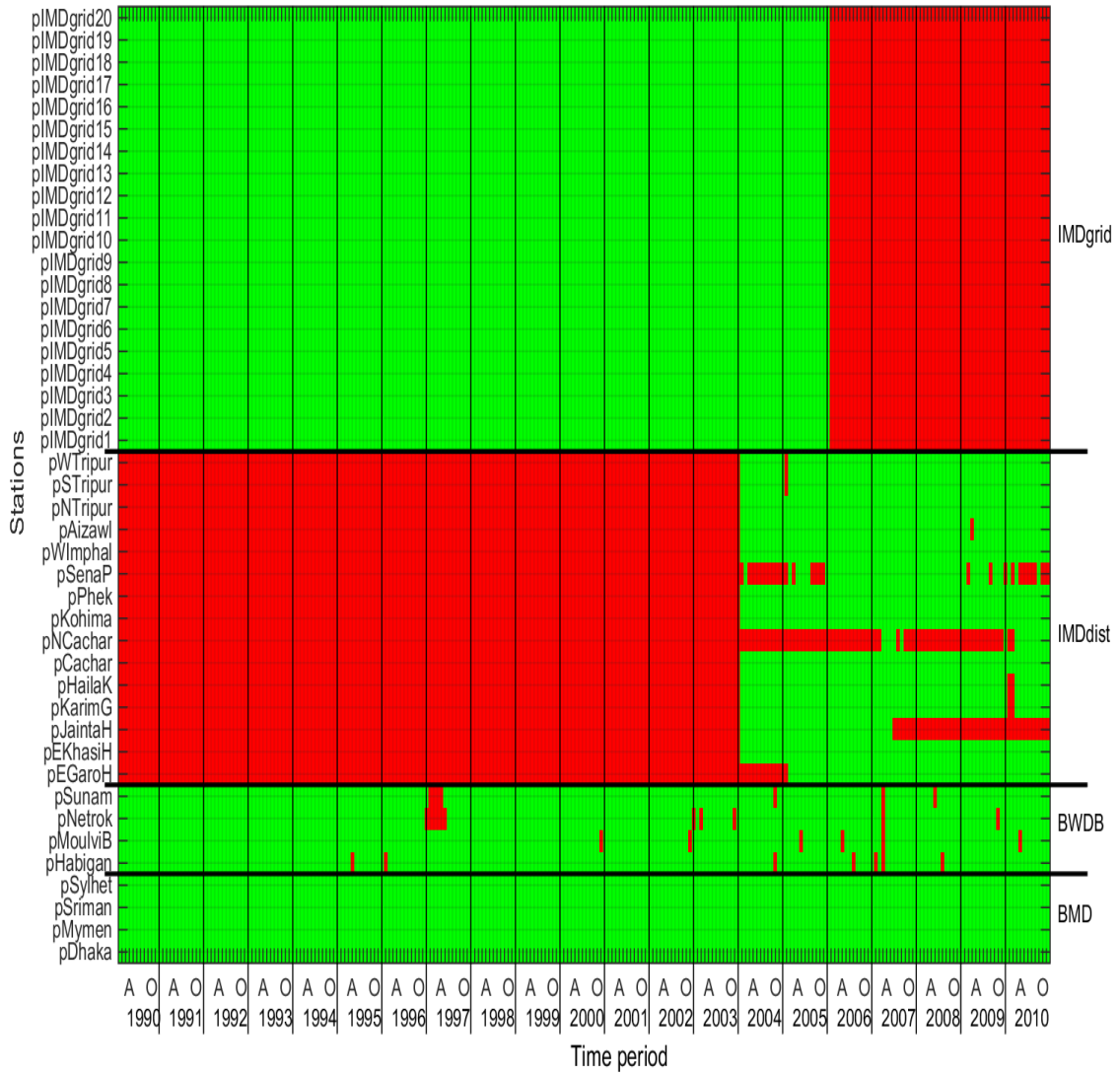

Figure 4.8. Quality of BMD and BWDB monthly rainfall data where red indicates missing data and green indicates no-missing data. Here A=April and O=October.

The form of precipitation in the UMRB is rainfall with the exception of some hail during early monsoon storms. The hydrological year (April–March) of the region can be divided into four seasons: (i) hails and thunderstorms dominated pre-

monsoon (April–May), (ii) monsoon (June–September), post-monsoon (October–November), and dry winter season (December–February) (Khan et al., 2005). Figure 4.9 and Figure 4.10 present the spatial distribution of mean monthly and annual rainfall in the UMRB respectively for the period of 1990–2003 and 2004–2010. Since the period of rainfall time series for all stations is not the same, data are grouped into these two time slices. Over the entire period, basin average annual rainfall varies from 2500 to 3000 mm consisting of 5, 21, 66 and 8% contribution from the four seasons (dry, pre-monsoon, monsoon and post-monsoon). The region in and around Cherrapunji in Meghalaya annually received about 6000–8350 mm rainfall during the period 1990–2003 (Figure 4.9). However, this maximum annual rainfall reduced to 7000 mm for the period of 2004–2010 (Figure 4.10). From the on-set of the pre-monsoon (April), rainfall begins to concentrates towards Cherrapunji and reaches its highest monthly value of 1800–2000 mm in June/July. In the case of the IMDgrid, however, this spatial pattern of rainfall concentration is not exactly towards Cherrapunji rather slightly westward from Cherrapunji.

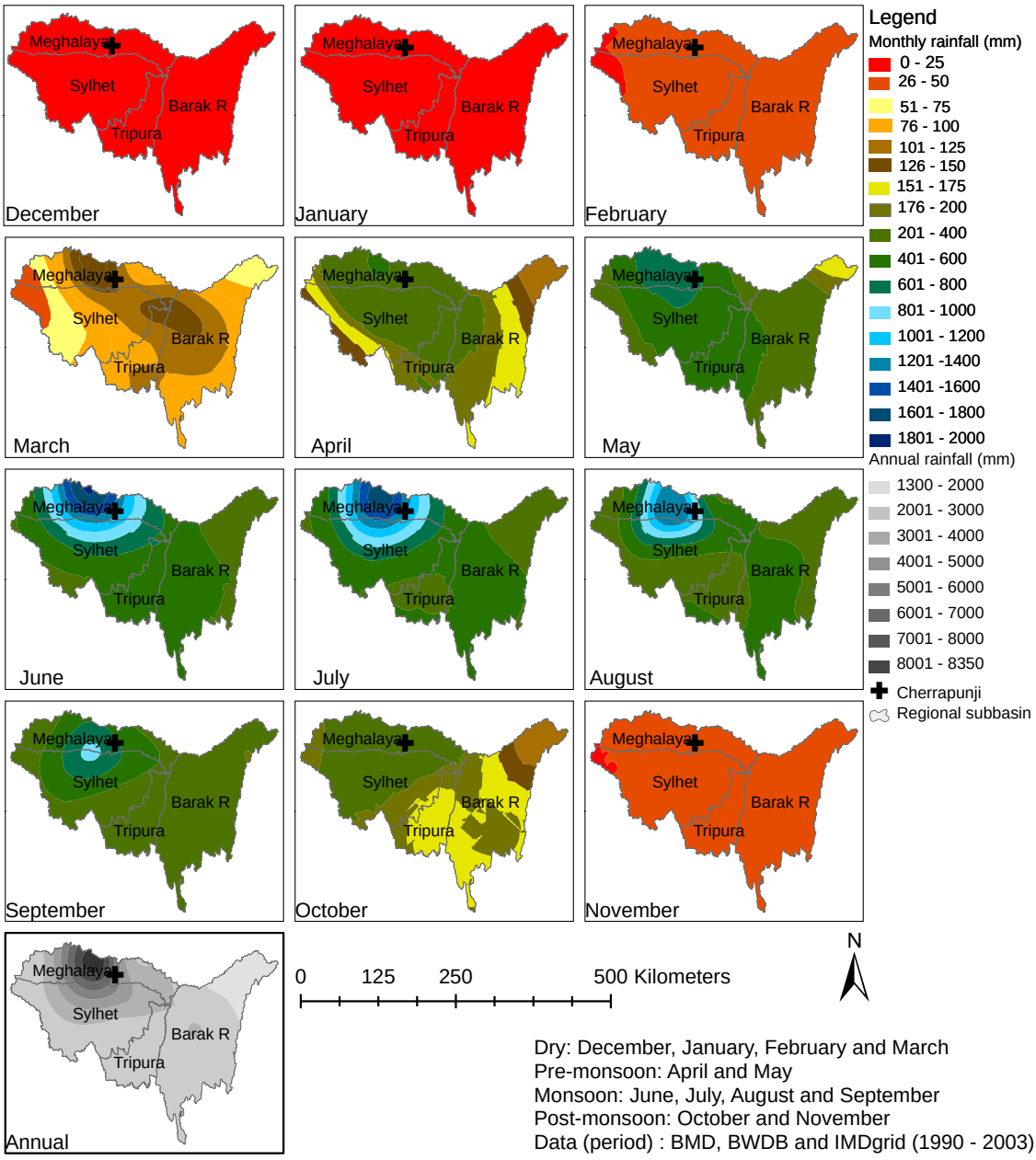

Figure 4.9. Spatial distribution of mean monthly and annual rainfall (mm) in the UMRB. These maps were generated from the rainfall of 28 stations/grids (BMD, BWDB and IMDgrid) during the period of 1990–2003. The ordinary Kriging geostatistical interpolation method was used while generating those maps. In most cases, the rainfall data followed the Gaussian distribution.

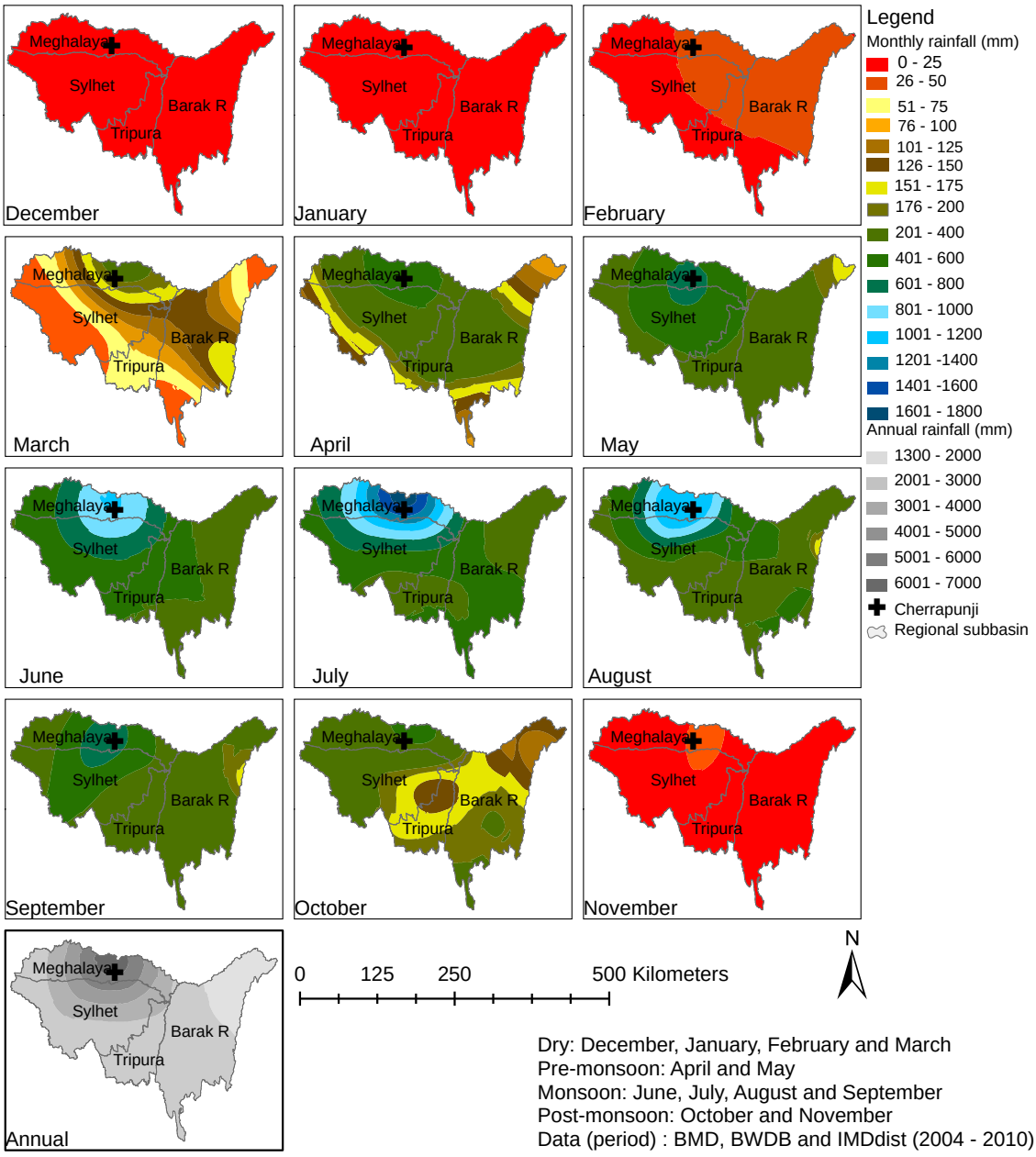

Figure 4.10. As same as Figure 4.9 but the period (2004–2010) and rainfall sources (BMD, BWDB and IMDgrid).

4.2.5.2. Temperature

The necessary temperature data were obtained from the BMD weather stations, IMDgrid and CRU TS 3.20 (Harris et al., 2014) grid points lying in and around the boundary of the UMRB (see Figure 4.7). The temporal resolution of temperature data is daily for the first two sources and monthly for the latter. Since the spatial resolution of IMDgrid temperature stations are relatively coarse (1°), a combined use of IMDgrid and CRU data is expected to reduce any uncertainties arising

from spatial variability of temperature. The Climate Research Unit (CRU), University of East Anglia produces gridded temperature time series (hereafter CRU data) from the observed data recorded at thousands of stations across the world. The spatial resolution of the temperature grid is 0.5°. Figure 4.11 depicts boxplot statistics (median, maximum and minimum) of monthly temperature for the four regional subbasins. These statistical properties are generated from the monthly data from 1990–2010. The summer monsoon (June–September) experiences not only highest temperatures (24 to 29 °C) in all the regional subbasins but also the smallest fluctuations. The Barak River and Meghalaya basins are comparatively cooler than the remaining two. The monthly temperature starts to fall in October with the lowest temperature occurring in January (15 °C in Barak River and Meghalaya basins). The period of increasing temperature between February and May, coincides with the period of largest variability in temperature within the four regional subbasins.

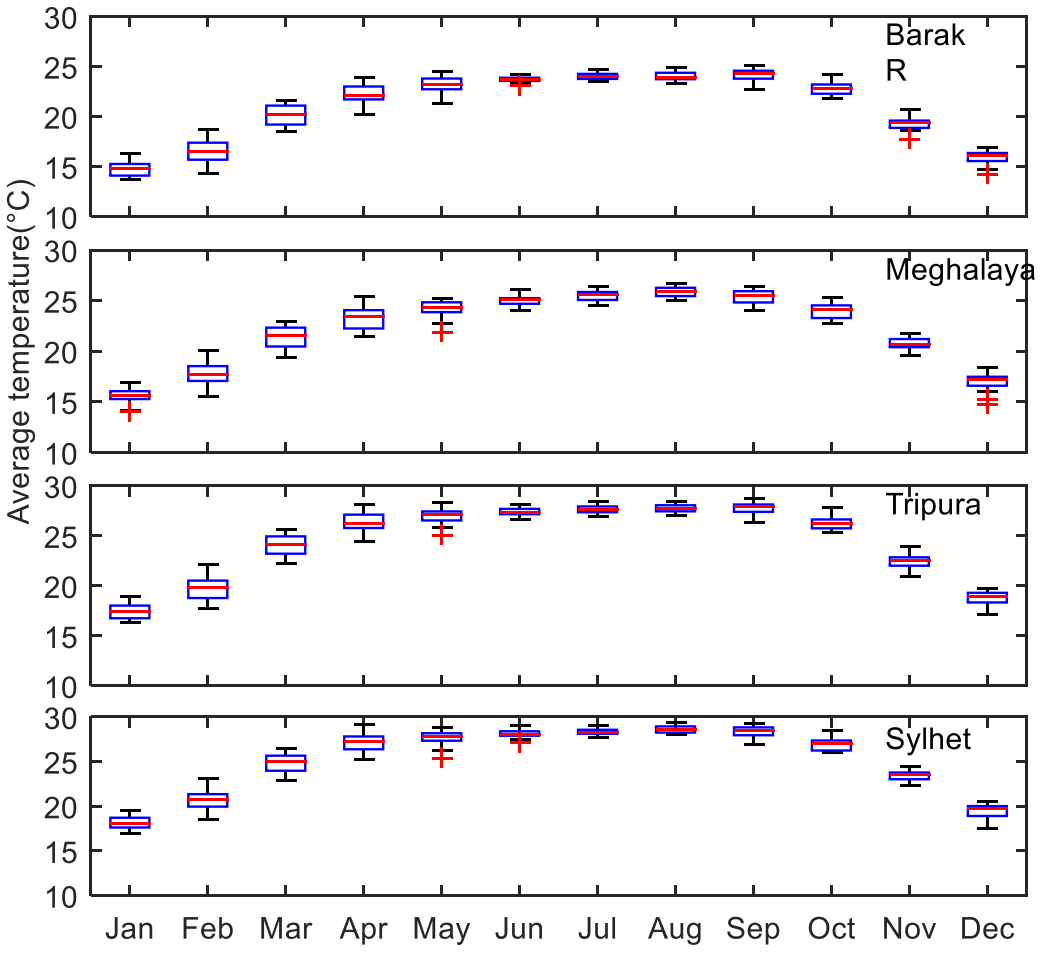

Figure 4.11. Boxplot statistics of monthly average temperature in the four regional subbasins.

Because daily observed time series of humidity, wind speed, and solar radiation were unavailable, SWAT's built-in weather generator "WXGEN" (Sharpley and Williams, 1990) was used to produce these climate data using long-term monthly climate statistics (mean, standard deviation, number of wet days) that were estimated from the CRU and FAO CLIMWAT 2.0 databases. The three climatic time series are essential for the P-M ET method (Equation 3.6) employed in this study. Although the Hargreaves method requires only temperature information, using this approach could not produce as satisfactory calibration results for the UMRB as was found for the P-M method. Since streamflows and flash flooding in the UMRB is mainly driven by rainfall, it is expected that errors arising from using statistically generated P-M ET forcing will introduce little additional uncertainty in modelling results.

4.2.6. River flows

Historical river flow data are frequently used to calibrate catchment models (Ivanov et al., 2004; Lai et al., 2013; Narasimhan et al., 2010; Nishat and Rahman, 2009; Rahman et al., 2014; Thompson et al., 2014b; Xie and Cui, 2011). The most reasons behind the use of river discharge for model calibration and validation are: (i) a catchment's integrated response to any changes is easily observable in the flow regime at its outlet and at locations within the river system and (ii) historical flow records at catchment's outlet are easily available. In the present study, daily historical river flow data from 15 gauging stations within the Sylhet Basin were collected from the Bangladesh Water Development Board (BWDB). Most of the gauging stations are installed on transboundary rivers near the border between Bangladesh and India (Figure 4.12). Discharge data at the upper Indian basins could not be obtained from the Indian authority.

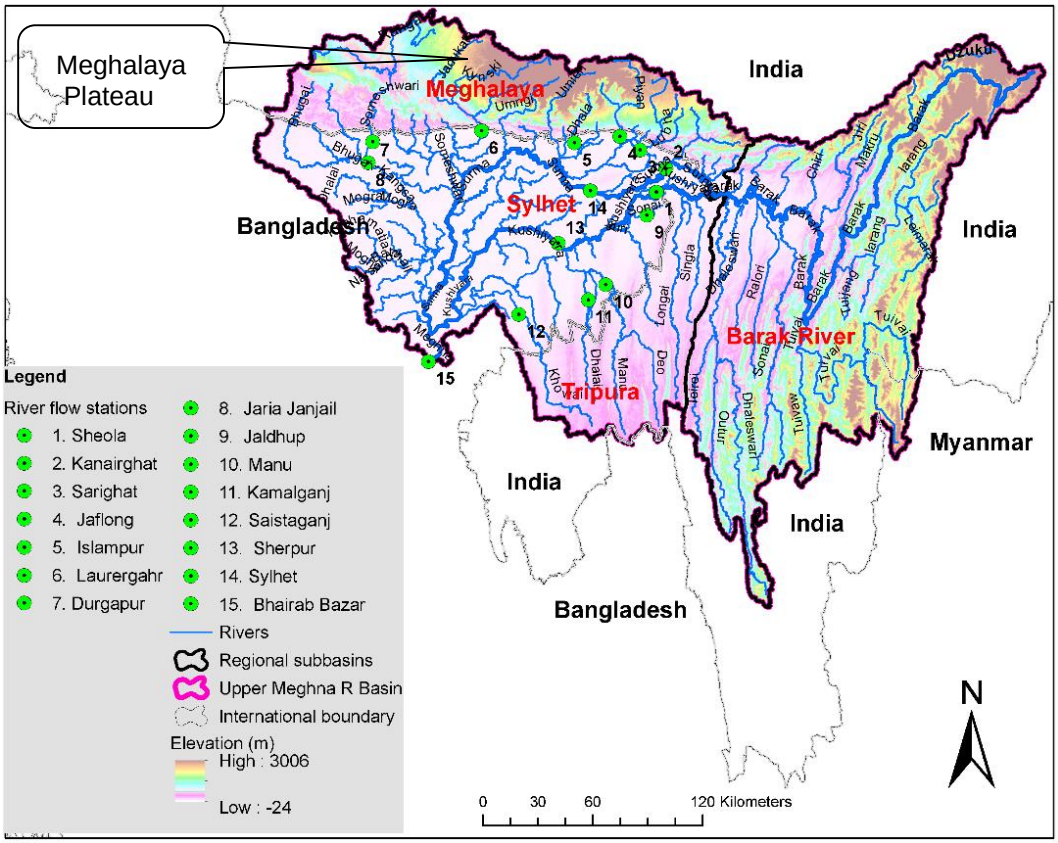

Figure 4.12. Location of discharge gauging stations in the UMRB.

The BWDB generates river flow data at each gauging station using daily observed river water stage as input to previously developed rating curves which were developed based on directly measured weekly or fortnightly flow data. However, the frequency at which these rating curves are updated is unknown. Therefore, a considerable amount of uncertainty and potential errors may impact these flow data as many alluvial rivers in the UMRB are subjected to sedimentation and human interference. Although the common duration of collected flow data is 1990–2010 almost all stations contain many missing data (Figure 4.13 and Figure 4.14). Among the 15 gauging stations, Jaflong, Islampur, Laurergahr, Durgapur, JariaJanjail, Jaldhup and the basin's lowest station Bhairab Bazar, the outlet of the UMRB, have the largest amount of missing data. The greatest drawback of discharge data from the Bhairab Bazar gauging station is the very limited data that are available in the dry season (December–March). According to the boxplot statistics as represented in Figure 4.15, the gauging stations draining the wettest and most variable rainfall catchments of Meghalaya (Sarighat, Jaflong, Islampur, Laurergahr, and Durgapur) show many outliers in each month. Similarly, the

Manu, Kamalganj, and Saistaganj stations that drain basin's driest catchments in the Tripura region also contain large outliers for all months. Moreover, outliers for the Sheola station during monsoonal months (June–September) may be inherited from the flows of upstream stations Manu and Kamalganj. The existence of substantial outliers in each month of the year indicates that a high temporal variation among daily flows for each month.

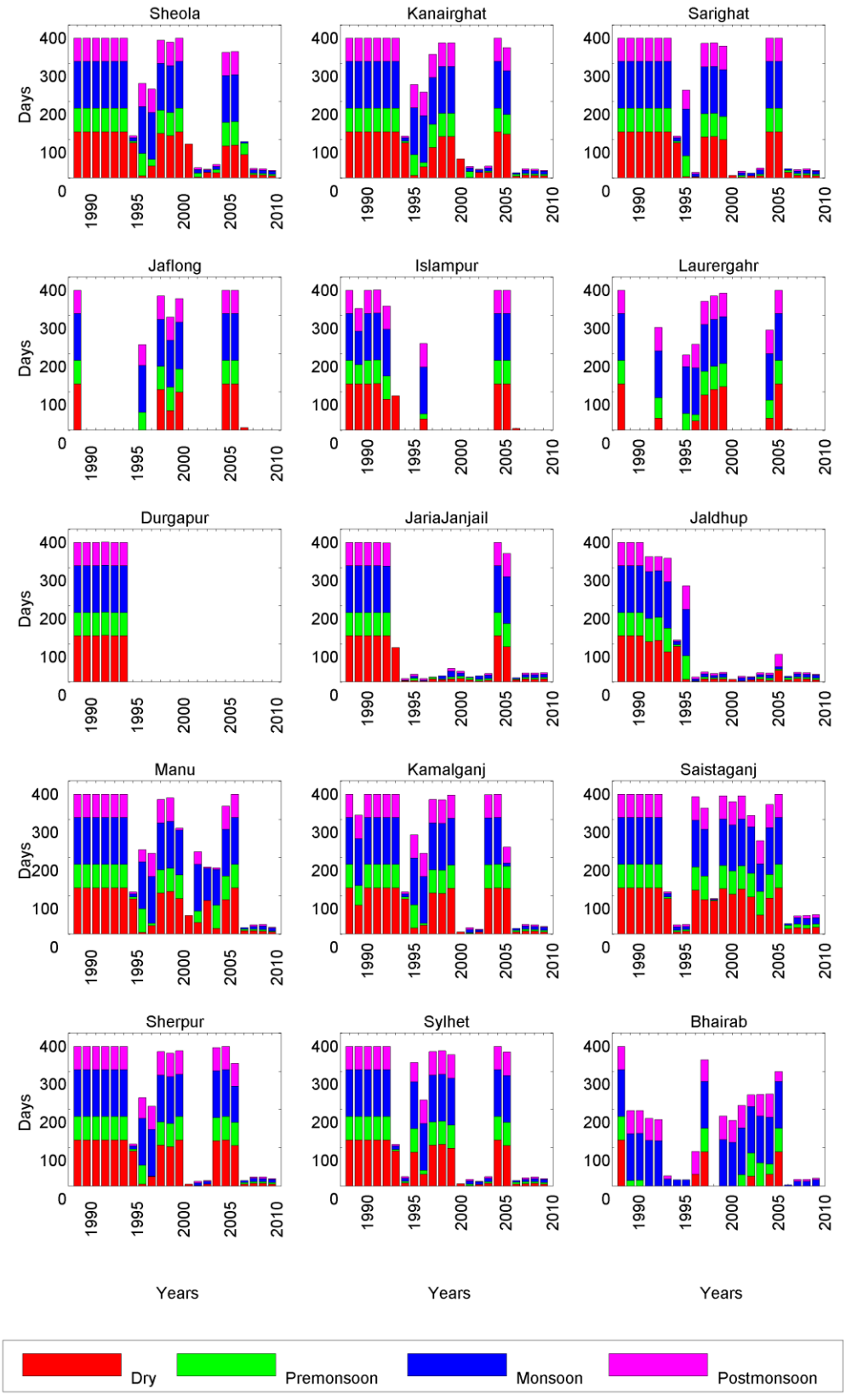

Figure 4.13. Number of daily observed river flow data records in a year where each colored stack indicates a specific season. Height of extreme left bar in each diagram indicates the **ideal** condition i.e. a year with no missing data must be seen alike to the ideal one. The height of each seasonal stack is given in number of days. Dry season (Red)= 121 or 122 (if leaf year) days, Pre-monsoon season (Green)=61 days, Monsoon season (Blue)=122 days, and post-monsoon season (magenta)=61 days.

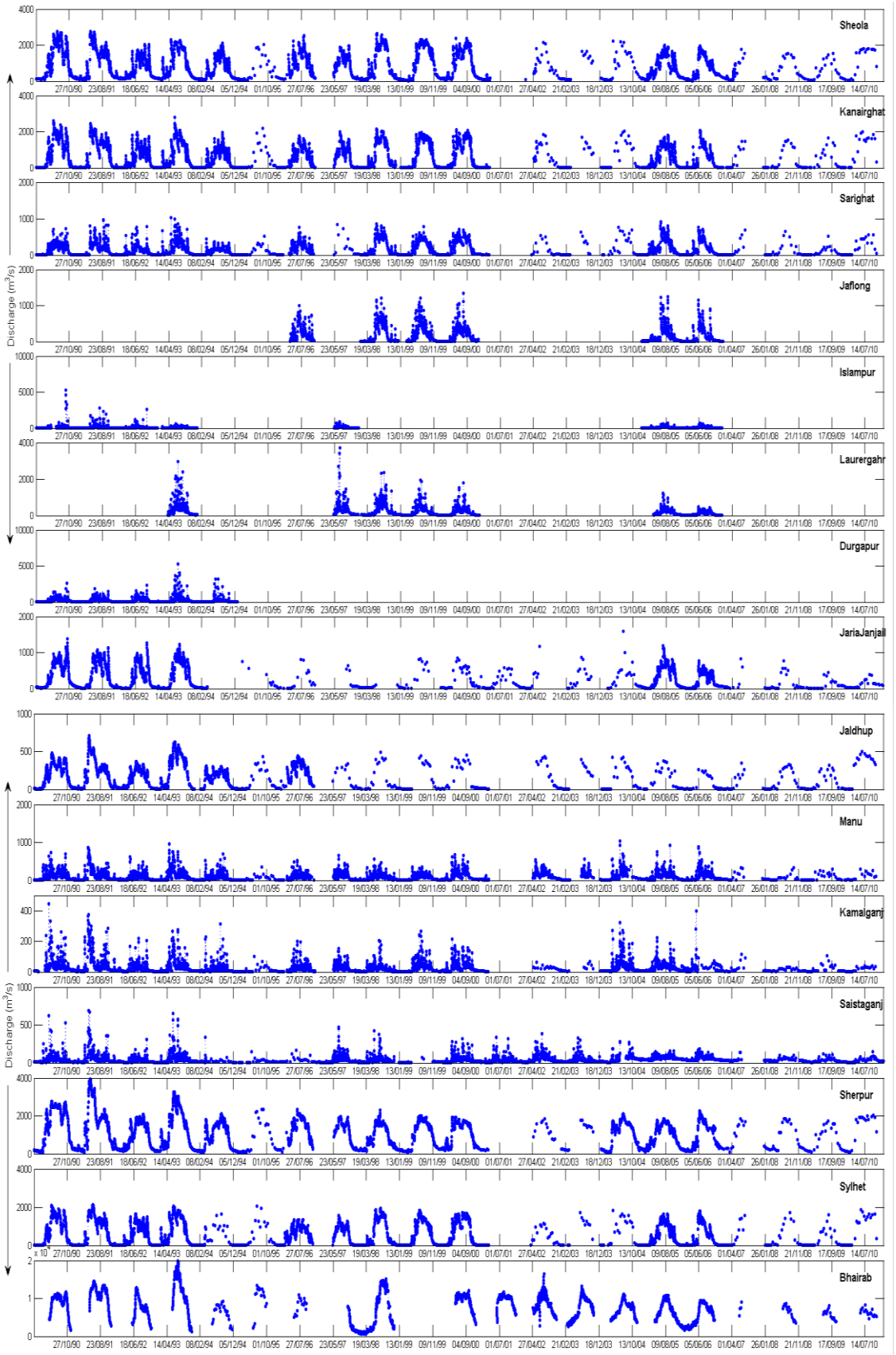

Figure 4.14. Daily observed discharge data recorded at each of the 15 gauging stations during the period of 1990–2010.

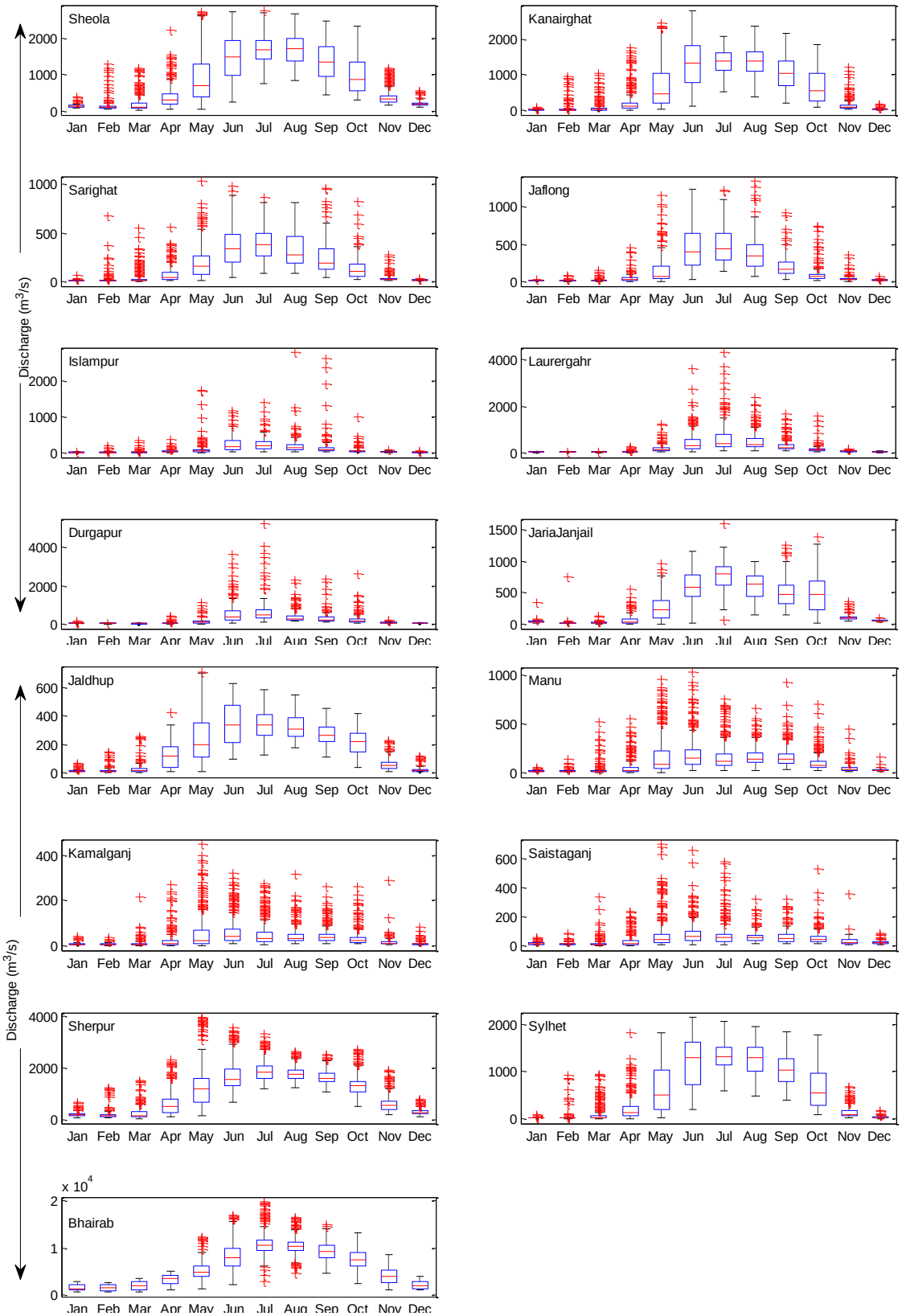

Figure 4.15. Boxplot statistics of daily flows in each month for the period of 1990–2010.

4.3. Summary

This chapter has provided a detailed account of the physio-graphic and hydro-meteorological data of the UMRB. The topography of the three Indian regional basins is extremely hilly whereas the lower Sylhet Basin is a deltaic floodplain with numerous depressional wetlands and dense river networks. Such a physio-graphic configuration will complicate the water dynamics towards basin's downstream end due to increased interactions among hydrological processes. This complication is further increased by high spatial and temporal variability of basin's rainfall.

FAO's HWSD soil data has only six distinct soil types for the entire basin. Seemingly this generalized soil data might mask some influential soil types, which can be a potential source of uncertainty in catchment modelling. The GLC land cover data were originally derived from the imageries taken during the period 1981–1994. This may be another source of uncertainty if land use pattern changes markedly after that period. Previous studies documented that population pressure in this region is accelerating deforestation and shifting cultivation, locally called Jhum cultivation, on hill slopes (Dabral et al., 2008; Forest Survey of India, 2011; Hossain, 2011).

Although a decent river network was prepared in combination of SRTM DEM data, Google Earth imagery and CEGIS provided river network for the Sylhet Basin, there were no measured cross section profiles for any of the river reaches. Instead a uniform cross section for each river reach is delineated from the DEM data. A number of river gauging stations (Jaflong, Islampur, Laurergahr, Durgapur, JariaJanjail, and Jaldhup) lack a considerable amount of missing data whereas the station Bhairab at the outlet of the basin lacks dry season flow records for 17 years of the entire period of 21 years.

Chapter 5
Development of an enhanced wetland module for SWAT

5.1. Introduction

Since the lower floodplain of the UMRB contains many riparian wetlands, a thorough investigation was undertaken to evaluate the extent to which the current SWAT is able to simulate interactions between wetlands, rivers and shallow aquifers. Section 5.2 discusses the important roles of wetlands within the catchment hydrology. It also reviews existing modelling approaches for wetlands. Sections 5.3 and 5.4 respectively describe the formulation of wetland modelling in SWAT and SWATrw (SWAT for riparian wetland), a revised version of SWAT with an enhanced wetland module. A case study is presented which compares both models' performance in simulating a relatively data rich haor wetland system (Sections 5.5 and 5.6).

5.2. A review on wetland's hydrology and its modelling

Wetlands are widely recognised as important habitats for a wide range of plants and animals as well as providing benefits to people through numerous hydrological, biological and chemical functions (Bengtson and Padmanabhan, 1999; Frohn et al., 2012; Hattermann et al., 2008, 2006; Junk et al., 2013; Kadlec and Wallace, 2009; Kulawardhana et al., 2007). Of these functions, those related to the hydrological processes taking place within wetlands are amongst the most frequently and intensively studied (Bullock and Acreman, 2003; Heimann and Krempa, 2011; Lindsay et al., 2004; Mendoza-Sanchez et al., 2013; Phan et al., 2011; Thompson, 2004; Walton et al., 1996; Wu and Johnston, 2008). Hydrological characteristics exert a dominant role in determining the ecological conditions within a wetland whilst the presence of wetlands within a river catchment impacts downstream flow regimes (Bullock and Acreman, 2003; Golden et al., 2014; Heimann and Krempa, 2011; Karim et al., 2012; Krause et al., 2007; Lindsay et al., 2004; Singh, 2010; Walton et al., 1996; M. Wang et al., 2010; Wu and Johnston, 2008) as well as influencing groundwater systems (Fan

and Miguez-Macho, 2011; Golden et al., 2014; Kazezyılmaz-Alhan et al., 2007; Mansell et al., 2000; Min et al., 2010; Restrepo et al., 1998; Thompson et al., 2004). At the catchment-scale, wetlands are commonly thought of as potentially providing a buffer storage which can retain runoff during wet periods and in turn attenuate peak flows further downstream (Craft and Casey, 2000; Hattermann et al., 2008; Heimann and Krempa, 2011; Kulawardhana et al., 2007; Smith et al., 1995). However, this supposed “flow reduction” ability is not equally applicable to all wetlands and is influenced by factors that include the location of wetlands within a catchment, their geometry and storage capacity, antecedent storage and the nature and degree of hydraulic connectivity with adjacent water bodies such as rivers and underlying aquifers. For example, a geographically isolated wetland (GIW) which is completely surrounded by upland areas to form a depressional landscape (Golden et al., 2014) can have strong interactions with the underlying groundwater systems depending on the hydraulic properties of the underlying substrate (Fan and Miguez-Macho, 2011; Golden et al., 2014; Hollis and Thompson, 1998; Pyzoha et al., 2008; Restrepo et al., 1998). However, if such a wetland is poorly connected with local river systems, it will have negligible influences on downstream stream flows compared to riparian wetlands which are in close hydraulic contact with river channels (Ogawa and Male, 1986; Sun et al., 2004). As a result of this interaction with other water bodies riparian wetlands generally exhibit more complex hydrological behaviour than GIWs with, for example, inflows from rivers and runoff from upland areas occurring more rapidly than groundwater exchanges (Walton et al., 1996).

A number of studies have investigated the differential influences of riparian and GIW wetlands upon surface and groundwater systems. Ogawa and Male (1986) used hydrological simulation of three catchments in eastern Massachusetts, USA to demonstrate enhanced floodwater storage associated with wetland size. During wet periods, which might be associated with individual storm event or a prolonged wet season, a surficial hydraulic connection can be established between a riparian wetland and an adjacent river as a result of higher water levels (Karim et al., 2012; Thompson et al., 2004). Such a connection can significantly alter the nature of downstream stream flows; a positive hydraulic gradient towards the river causes a fraction of stream flow to be intercepted by the wetland that, in turn, attenuates downstream stream flows. Conversely, a negative gradient will

accentuate downstream river flows as water moves from the wetland to the river. In some cases control structures such as levees, sluice gates and weirs can limit such wetland-river interactions despite a sufficient hydraulic gradient existing between them (Junk et al., 2013).

A wetland can recharge or receive water from an aquifer following the same hydraulic gradient principle (Kadlec and Wallace, 2009; Mansell et al., 2000; Min et al., 2010; Pyzoha et al., 2008; Restrepo et al., 1998; Singh, 2010). In upland areas wetlands predominantly recharge aquifers since groundwater level (GWL) is less frequently above wetland water levels (Min et al., 2010; Singh, 2010). On the other hand, riparian/floodplain wetlands can receive a significant amount of groundwater as well as contributing water to aquifers depending upon the relative water levels of the two which may change throughout the year (Singh, 2010). Rates of exchange are also influenced by factors that include the hydraulic properties of the aquifer and any wetland bed material as well as the size, shape and depth of the wetland.

The hydrological/hydraulic interactions between wetlands, other water bodies and aquifers can potentially be assessed through in-situ monitoring programmes. This approach is particularly valuable in relatively small sites where interactions among hydrological processes are relatively tractable over small spatial scales (e.g. Clilverd et al., 2013). However, instrumenting a much larger catchment which might contain many wetlands is frequently impractical (Kite and Droogers, 2000; Krasnostein and Oldham, 2004). Hydrological/hydraulic modelling provides an alternative approach that can be employed in large wetlands and for catchment-wide studies of the influence of wetlands on hydrological processes. Recognising their importance in catchment hydrology, wetland processes are either directly incorporated in, or have been indirectly modelled by, many catchment models including SWAT (Arnold et al., 1993), SWIM (Hattermann et al., 2008; Krysanova et al., 2005), WATFLOOD (Kouwen, 2013, 1988), MIKE SHE (DHI, 2009b), MODFLOW (McDonald and Harbaugh, 1988; Restrepo et al., 1998), WETSIM (Poiani and Johnson, 1993), Wetlands Dynamic Water Budget Model (Walton et al., 1996), Bucket Model (Mendoza-Sanchez et al., 2013), WETLANDS (Mansell et al., 2000), WETSAND (Kazezyılmaz-Alhan et al., 2007),

WETFLOW (Feng and Molz, 1997), FLATWOODS (Sun et al., 1998) and SLURP (Kite, 2001).

Regardless of model type (e.g. conceptual lumped approaches versus physics-based distributed model codes), a wetland is commonly considered to be a depressional type landscape feature with an outflow determined by its temporally varying water storage (Arnold et al., 1993; Kadlec and Wallace, 2009; Kazezyılmaz-Alhan et al., 2007; Kouwen, 2013; Krasnostein and Oldham, 2004; Neitsch et al., 2011; Powell et al., 2008; Walton et al., 1996; Wen et al., 2013). In many fully distributed catchment models, where the model domain is discretised into a number of grids that are used to represent spatial variability in model parameters, modelling of depressional (GIW) wetlands can be difficult (Thompson et al., 2004). Golden et al. (2014) suggested that in such cases model grid size could be as large as a wetland's maximum areal extent. This approach is, however, problematical for catchments that contain many wetlands of varying size. Although the adoption of a finer model grid resolution might enable the representation of such a catchment's wetlands, it will impose progressively larger computational costs as the grid size is reduced (Karim et al., 2012; Tucker et al., 2001). An alternative method that avoids this problem, and which is employed in some models, is to represent wetlands within a separate conceptual model (Kazezyılmaz-Alhan et al., 2007; Mansell et al., 2000; Singh, 2010; Wen et al., 2013). In this case, the different hydrological components such as overland flow, interflow, groundwater flow and channel flow in the surrounding uplands are firstly simulated by a catchment model. These are then used to simulate hydrological exchanges to a conceptual wetland model. Unlike fully-distributed models, semi-distributed models (e.g. SWAT, GSFLOW, WATFLOOD, SLURP) need not strictly preserve the spatial location of each constituent grid. Instead, homogeneous grids are grouped into a single Hydrologic Response Unit (HRU) or Grouped Response Unit (GRU) (Arnold et al., 2010; Kouwen, 2013). Therefore, grids lying within a series of wetlands within a defined area such as a sub-catchment can be assigned to a single wetland HRU/GRU (Arnold et al., 2010; Bingeman et al., 2006; Feng et al., 2012; Golden et al., 2014; Hattermann et al., 2008; Jing and Chen, 2011; Kouwen, 2013; Markstrom et al., 2008). This modelling technique not only reduces computational cost but also addresses some of the spatial conformity problems that can impact fully-distributed models.

In contrast to GIWs, the representation of riparian wetlands in a distributed model can be simplified by assuming they are a part of the river or floodplain system (Wen et al., 2013). Riparian wetlands that are traversed by main rivers can be termed on-channel wetlands whilst off-channel wetlands are those that are bypassed by the main rivers. An on-channel wetland can be modelled as a component reach or storage node within the modelled river system (Jaber and Shukla, 2012, 2005; Martinez-Martinez et al., 2014; Wen et al., 2013). Alternatively modelling of an off-channel wetland, which exists in a floodplain, can be simulated as a depressional wetland linked to the river by a connecting channel.

Many modelling approaches for representing the hydrological influences of wetlands rely on volume-area-depth relationships which are in turn controlled by wetland geometry (Hayashi and van der Kamp, 2000; Nilsson et al., 2008). Improperly specified wetland geometry will affect simulated hydrological processes and water level regimes (Baker et al., 2006; Mansell et al., 2000). As described above, within fully-distributed catchment models representation of wetland geometry relies on the models' grid size and the vertical accuracy of available digital elevation data. For semi-distributed or conceptual lumped models, wetland geometry is usually expressed by empirical power equations describing the relationships between volume, area, and depth. This approach is employed in a number of catchment or wetland hydrological models including SWAT, WETSIM and WETLANDSCAPE (Johnson et al., 2010). Empirical wetland morphometric equations can be easily embedded in catchment models and used flexibly for representing wetlands of variable geometry by calibrating their scale and shape parameters. For example, Wang et al. (2008) demonstrated the utility of such empirical wetland formulae in the representation of multiple depression wetlands in the State of Minnesota, USA as a single "Hydrologic Equivalent Wetland" (HEW). Where the precise spatial distribution of wetlands is less important than their hydrological impacts on the catchment water balance, the HEW concept can reduce computational cost of distributed models.

Hydrological interactions between wetlands and their surrounding environment can be broadly divided into four domains: wetland-atmosphere, wetland-upland,

wetland-groundwater and wetland-river. Within each domain, multiple interactions can occur through different hydrological processes (Golden et al., 2014). Depending upon the model platform and how it represents these processes, interactions may be simulated as unidirectional or bidirectional (Krause et al., 2007). For example, in MODFLOW, the direction and mass exchange rate between groundwater and surface water (wetland or river) are determined from a hydraulic gradient based leakage equation (Krause et al., 2007; Restrepo et al., 1998). This exchange can occur bidirectionally depending upon relative water levels. In contrast, SWAT's wetland-groundwater interaction is only represented as downward seepage. Golden et al. (2014) presented an excellent review of the usability and limitations of some frequently used catchment models in emulating wetland-groundwater interactions. To avoid complexity, many models assume that the residual of the wetland water balance provides an estimate of wetland-groundwater interaction (Chen and Zhao, 2011; Kouwen, 2013; Krasnostein and Oldham, 2004). Other models adopt a simplified Darcy's leakage formula to quantify mass exchange rates between wetlands and groundwater systems (Arnold et al., 1993; Kazezyılmaz-Alhan et al., 2007; Mendoza-Sanchez et al., 2013; Restrepo et al., 1998; Sophocleous, 2002; Walton et al., 1996; Wilsnack et al., 2001). In this leakage formula, flow is generally assumed to occur vertically through the wetted interface separating wetland and aquifer. However, when the water table is very close to the wetland bed, wetland-groundwater interaction will be dominated by horizontal flow (Bouwer, 2002). In such situations, the Dupuit-Forchheimer horizontal groundwater flow equation may be more appropriate (Min et al., 2010; Sun et al., 1998).

In representing wetland-river interactions involving GIWs, many models assume that the wetland can discharge into a river but cannot receive overbank flows from the river. In such models, the volume of water (or water level elevation) in a wetland and its corresponding threshold value (predominantly controlled by outlet elevation) are the prime determinants of wetland outflow (Feng et al., 2012; Hammer and Kadlec, 1986; Johnson et al., 2010; Kadlec and Wallace, 2009; Powell et al., 2008; Voldseth et al., 2007; Wen et al., 2013; Zhang and Mitsch, 2005). However, in regions characterised by widespread riparian wetlands that are hydraulically connected with an adjacent river, wetland-river interaction is

likely to be bidirectional. Therefore, such interactions should be quantified according to hydraulic principles involving the relative water level elevations in the river and the wetland as well as the properties of the connection between the two (Kouwen, 2013; Liu et al., 2008; Min et al., 2010; Nyarko, 2007; Restrepo et al., 1998). In the WATFLOOD model, for instance, riparian wetland-river interaction is modelled using the principle of Dupuit-Forchheimer lateral/radial groundwater flow (Kouwen, 2013). Since exchange between a riparian wetland and a river can occur over the surface and/or through the subsurface, Restrepo et al. (1998) incorporated an equivalent transmissivity expression, obtained for surficial wetland vegetation and the subsurface soil system, into the Darcy flow equation of the MODFLOW model.

The ability of SWAT to reproduce the hydrology of GIWs has been demonstrated (Javaheri and Babbar-sebens, 2014; Martinez-Martinez et al., 2014; Wang et al., 2008; Wu and Johnston, 2008) but the capability of the model in emulating riparian wetland-river interactions has been relatively under-studied. Liu et al. (2008) did, however, replace the original hydrological routing algorithm in SWAT's wetland module with a more robust hydraulic routing algorithm. They also incorporated lateral subsurface wetland-river interactions. This modification improved simulation performance of flow and sediment discharges in a Canadian river basin that included significant coverage of riparian wetlands.

Despite the utility of this enhanced SWAT wetland algorithm for simulating riparian wetland-river interactions, several shortcomings remain. Firstly, although the direction of wetland-river exchange is determined from the relative hydraulic head, the lateral surface exchange rate is still based on the hydrological routing (i.e. volume basis) of the original SWAT model. Secondly, the proposed wetland volume-area-depth relationship was site specific rather than taking a generalised form that would enable its wider applicability. Thirdly, the hydraulic head independency on downward seepage means that wetland-groundwater exchange in the current SWAT model does not represent bidirectional wetland-groundwater interaction. These issues are likely to impact SWAT performance in catchments with many riparian wetlands in which wetland-groundwater-river interactions exert a strong influence upon hydrological functioning. Therefore, the existing wetland module in SWAT (Section 5.3) has been redefined with an

enhanced module (Section 5.4) that can better simulate hydraulic interactions between rivers, riparian wetlands and aquifers.

5.3. Wetland simulation in the current SWAT model

To model a wetland's hydrological and non-hydrological processes, SWAT incorporates a simple conceptual wetland module. If there are any wetlands in the modelled basin, then the SWAT subbasins in which they are located must first be identified. The wetland area within each subbasin area must be specified. This information can be obtained from digital map data, land use data, topographic maps, or remotely sensed imagery (Baker et al., 2006; Dwivedi et al., 1999; Frohn et al., 2012; Maxa and Bolstad, 2009; Murphy et al., 2007; Rahman et al., 2014). In principle, SWAT allows only one wetland within each subbasin (Figure 5.1). However, if a subbasin contains more than one wetland, a "Hydrologic Equivalent Wetland" (HEW) can be employed (see Section 5.2) with its area specified as the total area of all the wetlands within the subbasin. Like HRUs, wetlands have no real spatial location within a subbasin. Since the total area of a subbasin is apportioned among its constituent HRUs, all wetland attributes that affect mass balance, for instance, water surface area and volume, are also proportionally distributed among the HRUs.

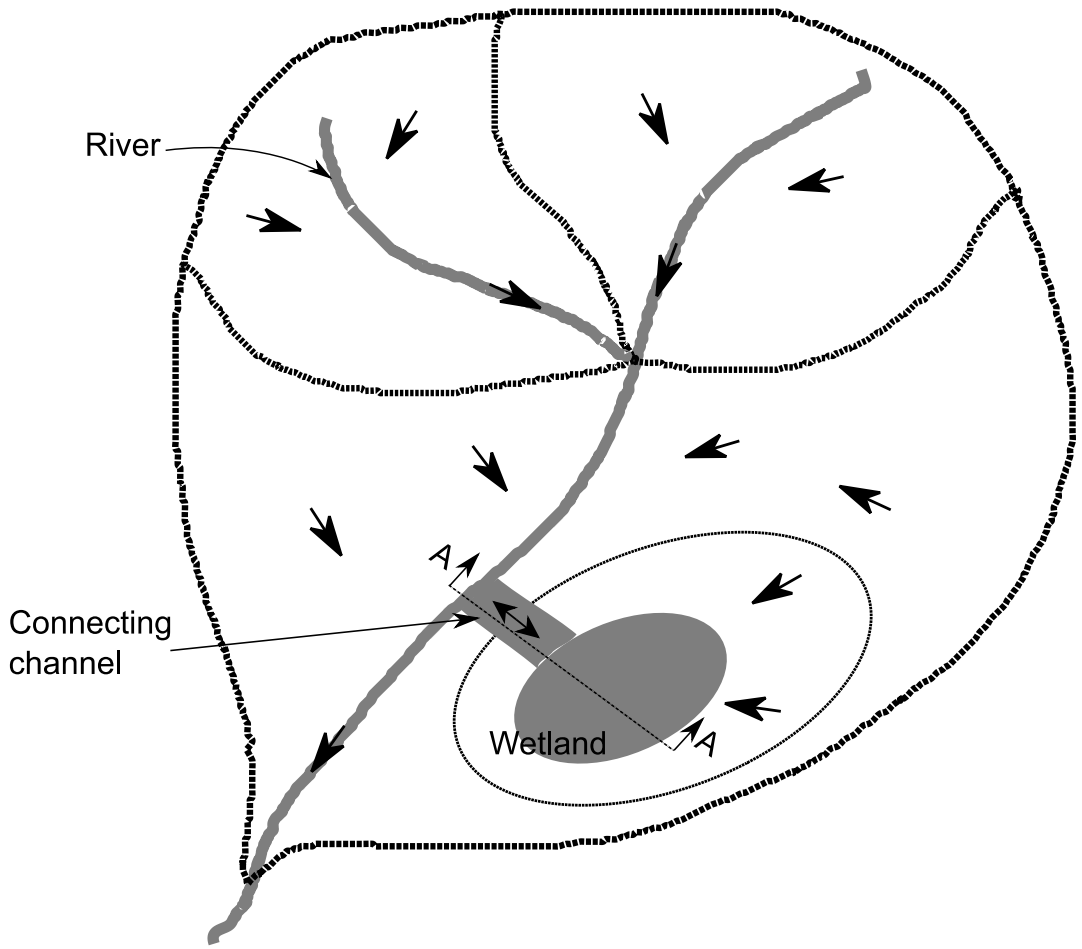

Figure 5.1. Graphical representation of a wetland and sub-basin in the SWAT model. The black dotted lines indicate drainage boundaries of them and arrow heads indicate direction of overland flow or channel flow. Grey color represents the extent of water surface in rivers, connecting channels and wetlands.

Figure 5.2 summarises the hydrological interactions involving a wetland in the original SWAT wetland module (as well as the revised wetland module developed in the current study which is discussed in Section 5.4). Unless otherwise stated all equations presented in this paper are for HRU-scale computations although different schematic depictions are drawn at sub-basin scale. The water mass balance equation in SWAT's original wetland module can be written as:

$$S_{wet}^{i} = S_{wet}^{i-1} + (P + Q_{sur} + Q_{lat})_{wet,in} - (E + Q_{ch\ \&\ wet} + Q_{wet\ \&\ aq})_{wet,out} \quad 5.1$$

where S indicates water storage; P and E are precipitation and evaporation, respectively and $Q_{wet\ \&\ aq}$ is the wetland-aquifer exchange which, as discussed above, is unidirectional such that only seepage from the wetland to groundwater is represented. Q_{sur} and Q_{lat} are surface runoff and lateral subsurface or interflow at the HRU-scale, respectively generated from the surrounding uplands where the area of these uplands is the difference between total wetland catchment area (upland catchment plus wetland water surface area) and wetland i.e. the wetland water surface area. $Q_{ch\ \&\ wet}$ is the discharge of water from the wetland to the river (as discussed above, the original wetland module does not represent flows in the opposite direction). The subscripts $wet, in, \&\ out$ indicate wetland, inflows and outflow respectively. The superscript i is time step and any absence of this time step notation should be read for current time step. Dimension of each element of the water balance is L^3.

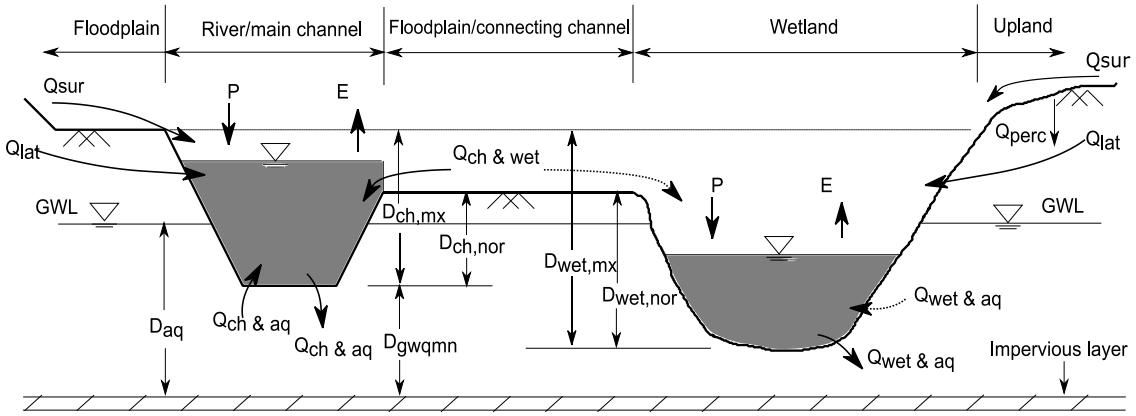

Figure 5.2. An example of hydrological interaction, along section A-A (Figure 5.1), between a river, riparian wetland and groundwater. This interaction is drawn from SWAT's concept. The extent of wetland shown with the double headed arrow line means the extent at maximum wetland capacity. P= precipitation, E= evaporation, Q_{perc} = percolation, Q_{sur} = surface runoff, Q_{lat} = lateral/inter flow, $Q_{ch\ \&\ aq}$ = exchange between river/main channel and aquifer, $Q_{ch\ \&\ wet}$ = exchange between the river/main channel and wetland, $Q_{wet\ \&\ aq}$ = exchange between the wetland and aquifer either over the floodplain or through the connecting channel, GWL = groundwater level, D_{aq} = height of groundwater level above the aquifer's impervious layer, D_{gwqmn} = height of river's bottom above the aquifer's impervious layer, $D_{ch,mx}$ = maximum channel's depth, $D_{ch,nor}$ = channel's depth from the normal level which is the elevation of river bank at connecting channel, $D_{wet,mx}$ = maximum wetland's depth and $D_{wet,nor}$ = normal depth of wetland. Processes drawn with the dotted lines ($Q_{ch\ \&\ wet}$ and $Q_{wet\ \&\ aq}$) are not currently modelled in SWAT but in the SWATrw (SWAT for riparian wetland) model developed in this research.

Since the wetland water surface area varies with time due to the net effect of incoming and outgoing fluxes, incoming surface runoff and interflow into a wetland are updated at each time step according to equation 5.2:

$$(Q_{sur} + Q_{lat})_{wet,in} = (Q_{sur} + Q_{lat})_{hru} * (A_{hru} * wet\_fr - A_{wet}) \quad 5.2$$

where the subscript hru indicates HRU (hydrologic response unit), A_{hru} is the area of an HRU (L^2), wet_fr is the fraction of subbasin area draining into the subbasin-scale wetland (i.e. the wetland's catchment area), A_{wet} is the wetland's water surface area (L^2) at HRU-scale and other symbols are previously defined. SWAT first estimates surface runoff and interflow without considering any wetland in an HRU. Subsequently the equivalent amount of water, which would have been produced from the HRU area occupied by the HRU-scale wetland (i.e. fraction of total wetland area in an HRU) had it not existed, is deducted from the flows generated across the total HRU area. This is an excellent feature of the SWAT model for a region like that considered in the present study area where wetlands are used for seasonal rice cultivation (see Section 1.3.1) during the dry season. As the flood recedes, the extent of wetlands continuously changes with rice cultivation; thereby, local hydrological processes are also be impacted.

The stored volume of water in a wetland is used as an input to an empirical exponential equation in order to calculate the corresponding wetland water surface area:

$$A_{wet} = \beta . S_{wet}^{\alpha} \quad 5.3$$

$$\alpha = \frac{\log_{10}(A_{wet,mx}) - \log_{10}(A_{wet,nor})}{\log_{10}(S_{wet,mx}) - \log_{10}(S_{wet,nor})} \quad 5.4$$

$$\beta = \frac{A_{wet,mx}}{S_{wet,mx}^{\alpha}} \quad 5.5$$

where the coefficients β and α are referred to as the scale factor and shape factor, respectively. $A_{wet,mx}$ and $A_{wet,nor}$ are the wetland water surface areas at maximum and normal capacities of the wetland, respectively. Similarly, $S_{wet,mx}$ and $S_{wet,nor}$ indicate wetland water volumes at maximum and normal capacities, respectively. The normal wetland capacity is a threshold volume that must be exceeded before the wetland discharges to the river within its subbasin. For example, in a weir controlled wetland, the normal capacity might be the volume of water that corresponds to the water level reaching the weir crest level. Note that while estimating scale and shape factors (equations 5.4 and 5.5 respectively), SWAT uses all necessary wetland inputs for subbasin-scale wetland although these same factors are subsequently used for all HRU-scale wetlands in the subbasin. Discharge or surface outflow ($Q_{ch\ \&\ wet}$) from the wetland to the river during a given time step is determined by:

$$Q_{ch\ \&\ wet} = \begin{cases} 0 & if \quad S_{wet} \leq S_{wet,nor} \\ \dfrac{S_{wet} - S_{wet,nor}}{10} & if \quad S_{wet,nor} < S_{wet} \leq S_{wet,mx} \\ S_{wet} - S_{wet,mx} & if \quad S_{wet} > S_{wet,mx} \end{cases} \qquad 5.6$$

The unidirectional wetland-groundwater interaction ($Q_{wet\ \&\ aq}$) i.e. downward seepage from the wetland is estimated from:

$$Q_{wet\ \&\ aq} = K_{sat}.A_{wet} \qquad 5.7$$

where K_{sat} is the saturated hydraulic conductivity of the wetland bed (LT^{-1}). The seepage from equation 5.7 is routed to the aquifer through an imaginary vadose zone with an exponential decay function (equation 5.8) that gives the wetland's final contribution to aquifer recharge:

$$Q^{i}_{rchrg,aq} = (1 - \delta_{gw}).Q_{wet\ \&\ aq} + \delta_{gw}.Q^{i-1}_{rchrg,aq} \qquad 5.8$$

where, $Q^{i}_{rchrg,aq}$ and $Q^{i-1}_{rchrg,aq}$ are the recharge from the wetland (L) to the aquifer at times i and $i-1$, respectively and δ_{gw} is the groundwater delay coefficient.

Percolation from the deepest soil layer in the uplands and other seepages (e.g. from rivers and ponds) are also added to $Q_{wet\ \&\ aq}$ to provide the total groundwater recharge from the catchment. Since wetland-river and wetland-groundwater interactions are the focus of the current study, other wetland processes, for example evaporation, are not elaborated here.

5.4. Wetland simulation in the SWATrw model

Whilst the wetland module of the current version of SWAT does enable some representation of the hydrological interactions between wetlands and other hydrological components of a river basin, there are, as discussed above, a number of issues that could still be addressed. The following section details the approaches employed in SWATrw (SWAT for riparian wetland) model that has been developed in the current study to improve the representation of the hydrological processes and properties of wetlands.

5.4.1. Wetland volume-area-depth relationship

The empirical equation used in the current SWAT model to represent wetland geometry (equation 5.3) does not explicitly relate the depth of water within a wetland with the other two morphometric properties, wetland area and volume. This presents problems in situations where accurate simulation of the wetland water depth is essential, for example in representing hydraulic interactions between wetlands and other water bodies (e.g. rivers and aquifers). Another drawback is the difficulty of establishing appropriate scale and shape parameters. SWAT requires two sets (normal and maximum) of known values for wetland water surface area and volume for inclusion in equation 5.4. Estimates of actual wetland water volume are much less frequently available than wetland water surface area. Consequentially, normal and maximum wetland volumes may be established through calibration. This increases uncertainty in the model's simulation of wetland hydrological functioning. Uncertainty could be reduced by expressing wetland water volume as a function of both wetland water surface area and depth because observed values of these two variables are in many cases more readily available. Wetland water surface area can be measured using various techniques including ground survey, aerial photography (Harvey and Hill,

2001), and remotely sensed data (e.g. land use, soil and elevation data) (Baker et al., 2006; Kulawardhana et al., 2007; Lindsay and Creed, 2005; Maxa and Bolstad, 2009; Murphy et al., 2007; Townsend and Walsh, 2001). Wetland water depth at specific locations can be monitored periodically using a range of instrumentation from simple staff gauges to automatic water level recorders. By assuming that wetland side slope is the same as that of floodplain, Liu et al. (2008) showed that equation 5.3 can be related to wetland water depth (D_{wet}) as shown in equation 5.9. Nonetheless, this assumption of consistent wetland slope narrows their model's wider applicability particularly in shallow but extensive low-relief wetland systems. Moreover, the compatibility of their wetland model to different wetlands was not reported.

$$D_{wet} = \beta^{-1}.S_{wet}^{1-\alpha} \qquad 5.9$$

In order to overcome these limitations, a more robust, generalised and flexible wetland geometric formula was incorporated into the SWATrw model. This formula was developed by Hayashi and van der Kamp (2000) who tested it for a range of depressional wetlands with non-unique shapes. For the sake of simplicity, their volume-area-depth model is, hereafter, referred to as the H-K wetland morphometry model. The mathematical form of the model as incorporated in SWATrw is shown in equations 5.10 and 5.11:

$$A_{wet} = b.\left(\frac{D_{wet}}{D_{wet,0}}\right)^{2/p} \qquad 5.10$$

$$S_{wet} = \left(\frac{b}{1 + \frac{2}{p}}\right).\frac{D_{wet}^{(1+\frac{2}{p})}}{D_{wet,0}^{\frac{2}{p}}} \qquad 5.11$$

where b and p are the scale and shape parameters of the model, respectively and $D_{wet,0}$ indicates unit wetland depth. Only the shape parameter has to be calibrated as the scale parameter is calculated from the user specified maximum values of wetland water surface area and depth. Increasing the value of p

indicates a more cylindrical shaped wetland. One distinguishing feature of the H-K wetland morphometry model is that with only one set of b and p values the model can satisfactorily represent the average geometry of a natural depressional wetland having heterogeneous side slopes (Hayashi and van der Kamp, 2000).

5.4.2. Wetland-river interaction

In this study wetlands are assumed to be on the floodplain of a river but not directly next to the river (see Figure 5.1 and Figure 5.2) in accordance with the riparian off-channel wetlands (see Section 5.2) that SWATrw is designed to represent. The wetland water level at its maximum capacity is assumed to be the river's highest bank level (i.e. the bed elevation of the intermediate floodplain between the river and the wetland). If a subbasin contains more than one wetland, then initially one approximate HEW can be generated by summing maximum water surface areas of each wetland and by averaging the maximum wetland water depths. Nonetheless, a larger variation among wetlands' shape restricts the usability of such a technique.

A riparian wetland can exchange water with the adjacent river according to three processes: (i) overbank flow across the floodplain during periods of high water level, (ii) flow through a connecting channel, if any exists, between the river and wetland, and (iii) lateral subsurface flow (not considered in this study; see the next paragraph). Although SWAT assumes that the maximum depth of a river within a subbasin is uniform throughout the river length, this is, in reality, rare. In lowland areas which contain many riparian wetlands the banks of flood-prone rivers are frequently altered by the construction of embankments and dykes that are designed to reduce the incidence of overbank flows and hence flooding (Clilverd et al., 2013; Gopal, 2013; Junk et al., 2013). High stage river flows can often breach these dykes at vulnerable sections, for example, at the lowest point of the main riverbank where a connecting channel from a riparian wetland joins the river. To model this wetland-river interaction within SWATrw, a connecting channel rather than a floodplain (Figure 5.1 and Figure 5.2) is conceptualised at the vulnerable part of the river bank(s). The cross section of a connecting channel is assumed to be rectangular and its width and depth are some fractions of main

channel length and maximum depth, respectively and can be established through calibration. When a favourable hydraulic connection is established between a wetland and a river (see below), mass exchange between them occurs through the connecting channel. The connecting channel has no retention capacity itself but offers resistance to flow due to aquatic vegetation that is common in floodplain/wetland environments. Unlike SWAT, SWATrw divides a subbasin-scale river that is connected to a wetland into reach segments whose lengths are proportional to the HRU fractions in the sub-basin containing the wetland (Figure 5.3). As a result there is the same number of river reaches as HRUs in a subbasin. Similarly, the width of a subbasin-scale connecting channel is also proportioned based on HRU relative extent, and each pair of HRU and river reach sections is associated with the respective downscaled connecting channel. In this way, the largest sized HRU is paired with the longest river reach and thus the widest connecting channel.

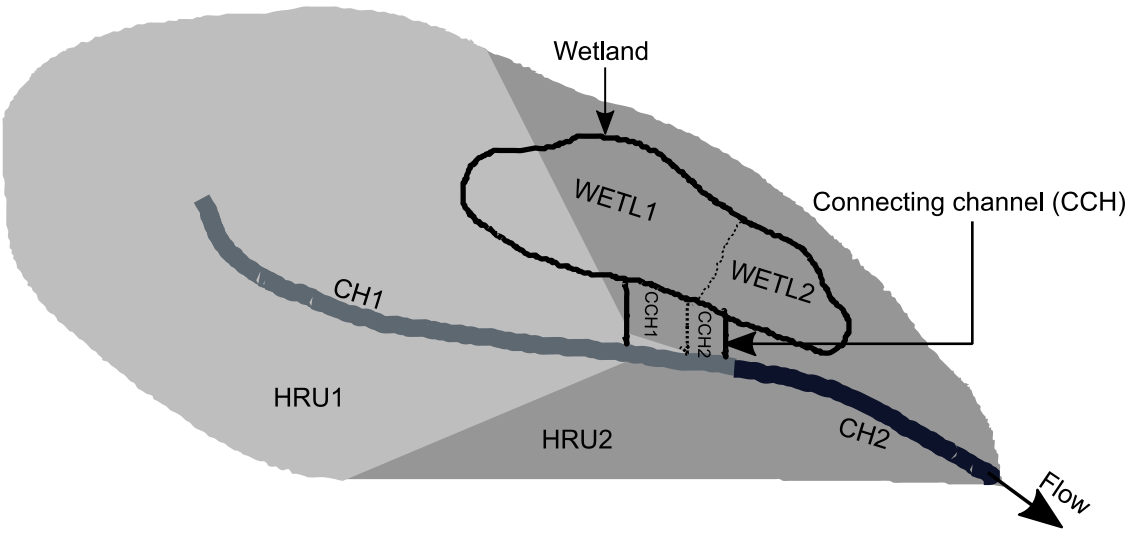

Figure 5.3. A hypothetical representation of how SWATrw apportions wetland, main channel and connecting channel among HRUs in a subbasin. The illustrated subbasin has two HRUs (shaded light and dark grey colour) assuming that the area of HRU1 (A_{HRU1}) is larger than that of HRU2 (A_{HRU2}). Therefore, the existence wetland, main channel and associated connecting channel are also disintegrated in such a way so that each of their respective properties (area of wetland, A_{WETL}; width of connecting channel, W_{CCH}; and length of main channel, L_{CH}) has a ratio (A_{WETL1}: A_{WETL2}, W_{CCH1}: W_{CCH1} and L_{CH1}: L_{CH2}) of equalled to A_{HRU1}:A_{HRU2}. During model computation a HRU in a subbasin is paired with other disintegrated features (wetland, connecting channel and main channel) based on their size of respective properties.

In SWATrw, wetland-river interaction is assumed to occur only as surface water i.e. direct lateral subsurface interaction is not considered. It is assumed that any phreatic or seepage line evolving from a wetland or river will terminate at the intermediate aquifer between them before reaching the downstream river or wetland. This is likely for any of the following reasons or their combinations: permeability of the soil is low, the difference between surface water and groundwater levels is small, and the distance between a wetland and river is large. Hydraulic principles are used to quantify wetland-river interactions. Firstly, the model needs to fix a datum level against which other elevations such as water levels are referenced. Since the horizontal plane of a wetland water surface at its maximum capacity is assumed to be level with the floodplain (or the highest river bank elevation), a datum of zero elevation is set to either the bed of the river or the wetland depending on which is deeper. Unlike SWAT, the normal threshold depth or normal storage capacity of a wetland is defined by the bed elevation of the connecting channel. The product of a parameter "fraction of maximum river depth at normal level" (CCH_DFR) and maximum river depth ($D_{ch,mx}$) gives the connecting channel's bed height from the river bed, thus the connecting channel's bed is referenced to the datum (bed of wetland or river). When both wetland and river water levels fall below the normal level (i.e. the bed of the connecting channel), exchange ceases. When there is a hydraulic head difference between a wetland and a river, and at least one of the water levels is above the normal level, the specific exchange flow rate (flow rate per unit water area) is calculated based on the wetland surface flow equation developed by Kadlec and Wallace (2009):

$$q_{ch\,\&\,wet} = c.d^m.s_f^n \qquad 5.12$$

where $q_{ch\,\&\,wet}$, d and s_f represent specific exchange flow rate (LT^{-1}), depth of flow (L), and friction slope, respectively. The terms c, m, and n are the conveyance coefficient, depth exponent and slope exponent, respectively. Equation 5.12 is based on the Manning's channel flow formula ($if\ c = \frac{1}{N},\ m =$

$\frac{2}{3}, n = \frac{1}{2}$) which was originally developed for turbulent flow. However, evidence from different field experiments shows that surface flow over a wetland is most likely laminar or transitional (Hammer and Kadlec, 1986; Kadlec and Wallace, 2009). When applied to a wetland, the value of d in equation 5.12 is the mean overland flow depth. However, in this case, the value of d is the depth of flow at the midpoint of the connecting channel and is estimated from Bernoull's energy equation. With reference to Figure 5.2, since river water level is above both the normal level (i.e. the bottom of the connecting channel) and wetland water level, a flow occurs from the river to the wetland due to the available driving hydraulic head. Flow would be reversed if water levels in the river and the wetland were exchanged. For the example in Figure 5.2, the driving hydraulic head is the elevation difference of the river water level and the normal level. Alternatively, if the wetland water level was above the bed of the connecting channel (but still below the river level) the driving hydraulic head would be the difference between the river and wetland water levels. The same principles are applied when wetland water levels are higher than river levels and the direction of exchange is reversed. After simplification of Bernoulli's energy equation, the equation takes the form:

$$d + \frac{1}{2g}\left(c.s_f^n\right)^2 d^{2m} + \left(s_f.\frac{l}{2}\right) - d_{dh} = 0 \qquad 5.13$$

where l is the length of the connecting channel (L), d_{dh} is the driving hydraulic head (L), and other symbols are previously described. For the given values of c, m, n and S_f, the above equation is numerically solved with the Newton-Rapson method.

After calculating the average depth of flow through the connecting channel, the maximum volume of water that can be exchanged between a wetland and a river during an individual time step is estimated as follows:

$$Q_{ch\ \&\ wet} = (\ q_{ch\ \&\ wet}\ .d.w)\Delta t \qquad 5.14$$

where w is the width of the connecting channel (L) and Δt is the time step (T). Multiplying total river length by the calibration value of CCH_LFR (fraction of the river length overflowed at normal elevation) gives the value of w. According to hydraulic principles, flow between two hydraulically connected water reservoirs (here the wetland and river) can continue until their water levels reach the same elevation (or until, in this instance, the water level of the loosing reservoir reaches the bed of the connecting channel as discussed above). Therefore, if the water volume estimated by equation 5.14 is greater than the intake capacity of a receptor reservoir, the actual transferred water volume is re-calculated by reducing the duration of flow time (initially flow time is equal to the model time step) so that water levels reach an equilibrium state. Intake capacity is the volume of water in a receptor reservoir at equilibrium water level less its initial water volume. The necessary mathematical calculations and procedures used in SWATrw to estimate transferable water volume between a wetland and a river are described below. The same procedure is followed for both directions of exchange (i.e. river to wetland and wetland to river).

For the example illustrated in Figure 5.2, since the river is in hydraulic connection with the riparian wetland and the water level of the river is higher than that of the wetland, there is clearly a potential discharge into the wetland. For the exchange of a specific volume of water from the river to the wetland, water depths in the loosing river at the end of each time step can be estimated as:

Change in water volume

$$S_{ch}^{t1} - S_{ch}^{t2} = q_{ch\,\&\,wet} \,.\, \Delta t \qquad 5.15$$

$$\left\{W_{bot,ch} \,.\, D_{ch}^{t1} + z.\left(D_{ch}^{t1}\right)^2\right\} L_{ch} - \left\{W_{bot,ch}.\, D_{ch}^{t2} + z.\left(D_{ch}^{t2}\right)^2\right\} L_{ch} = q_{ch\,\&\,wet} \,.\, \Delta t \qquad 5.16$$

$$D_{ch}^{t2} = \frac{-W_{bot,ch} \pm \sqrt{\left(W_{bot,ch}\right)^2 - 4\,.\,z.\left[\frac{\left(q_{ch\,\&\,wet} \,.\, \Delta t\right)}{L_{ch}} - \left\{W_{bot,ch} \,.\, D_{ch}^{t1} + z.\left(D_{ch}^{t1}\right)^2\right\}\right]}}{2.\,z} \qquad 5.17$$

where, S_{ch}^{t1} and S_{ch}^{t2} are the water volumes of the river at time $t1$ and $t2$, D_{ch}^{t1} and D_{ch}^{t2} are the water depths of the river at time $t1$ and $t2$ and $W_{bot,ch}$, L_{ch}, and z are the bottom width, length and side slope of the river (trapezoidal shape), respectively. For the gaining wetland, water levels at the end of each time step can be estimated as:

Change in water volume

$$S_{wet}^{t2} - S_{wet}^{t1} = q_{ch\,\&\,wet} \,.\, \Delta t \qquad 5.18$$

and the combination of equations 5.11 and 5.18 gives:

$$D_{wet}^{t2} = \left[\frac{S_{wet}^{t1} + q_{ch\,\&\,wet} \,.\, \Delta t}{\left(\frac{b}{b + \frac{2}{p}} \right)} \times D_{wet,0}^{\frac{2}{p}} \right]^{\left(\frac{1}{(1+\frac{2}{p})} \right)} \qquad 5.19$$

where S_{wet}^{t1} and S_{wet}^{t2} are the water volumes of the wetland at time $t1$ and $t2$ and D_{wet}^{t2} is the water depth in the wetland at time $t2$. For the following constraints (equations 5.20, 5.21 and 5.22), equations 5.17 and 5.19 are solved iteratively by changing the value of Δt. The iteration process starts from the maximum value of Δt (i.e. the time step of the model) and is continued with smaller time steps until a satisfactory solution is achieved. Since the time step in the present modelling study is daily (see below), the maximum number of iterations is set to 142 and the process operates in the chronological order of equation 5.23.

$$\frac{(q_{ch\,\&\,wet} \,.\, \Delta t)}{L_{ch}} \leq \left\{ W_{bot,ch} \,.\, D_{ch}^{t1} + z.(D_{ch}^{t1})^2 \right\} \qquad 5.20$$

$$D_{ch}^{t2} \geq 0 \; and \; D_{wet}^{t2} \geq 0 \qquad 5.21$$

$$\left(E_{ch,bed} + D_{ch}^{t2}\right) \geq \left(E_{wet,bed} + D_{wet}^{t2}\right) \quad 5.22$$

$$\left.\begin{array}{l} \Delta t_1, \Delta t_1, \Delta t_1 \ldots\ldots\ldots\ldots \Delta t_{22}, \Delta t_{23}, \Delta t_{24} = 24,23,22, \ldots\ldots\ldots 3,2,1 \ \ (\mathrm{hr}) \\ \Delta t_{25}, \Delta t_{26}, \Delta t_{27} \ldots\ldots\ldots\ldots \Delta t_{81}, \Delta t_{82}, \Delta t_{83} = 59,58,57, \ldots\ldots\ldots 3,2,1 \ \ (\mathrm{min}) \\ \Delta t_{84}, \Delta t_{85}, \Delta t_{86} \ldots\ldots\ldots\ldots \Delta t_{140}, \Delta t_{141}, \Delta t_{142} = 59,58,57, \ldots\ldots\ldots 3,2,1 \ \ (sec) \end{array}\right\} \quad 5.23$$

$E_{ch,bed}$ and $E_{wet,bed}$ are the elevations of the river and wetland beds, respectively. Once a solution is attained, the final transferable water volume is re-calculated using equation 5.14 for the resultant time step (Δt). Thereafter, storages of water in the wetland and river are updated accordingly. A resulting smaller time step than the model's time step (1 day or 24 hours) indicates that the receiving water body (i.e. the wetland in the example in Figure 5.2) will reach a hydraulic equilibrium state with its delivering waterbody (the river in the example) in less than a whole day. Such a phenomenon can occur where riparian wetlands are rapidly flooded due to a sudden increase in river discharge (Nishat and Rahman, 2009). Finally, if wetland water exceeds its maximum level, which may happen due to heavy rainfall on the wetland catchment, all water excess to the wetland maximum capacity will be transferred to the river on the same day as adopted in SWAT. This water, in turn, can be seen on the floodplain if the river exceeds its maximum capacity.

5.4.3. Wetland-groundwater interaction

Application of the current wetland module within SWAT is problematical in situations where bidirectional wetland-groundwater interactions are a common phenomenon. This includes floodplain areas where the groundwater level is very close to the ground surface and fluctuates throughout the hydrological year. As indicated in equation 5.7, whilst SWAT simulates the seepage of water from a wetland to the underlying aquifer, water from the aquifer does not discharge into the wetland. Moreover, the amount of seepage from a wetland is only controlled by the hydraulic conductivity of the wetland bed material. The role of hydraulic head is completely neglected which is contradictory to the well known Darcy's flow formula. Although a number of past studies have demonstrated SWAT's abilities in modelling the downward wetland-aquifer interaction of North American

prairie wetlands where groundwater level seldom crosses the wetland bed level (Wang et al., 2008; Wang et al., 2010), its application is not recommended for bidirectional interactions between a wetland and an aquifer (Golden et al., 2014; Sun et al., 2004). This is addressed in SWATrw through the incorporation of a Darcy's flow law based wetland-groundwater interaction algorithm. Initially the elevations of the aquifer bed ($E_{aq,bed}$) and groundwater surface (E_{aq}) are calculated using equations 5.24 and 5.25:

$$E_{aq,bed} = E_{ch,bed} - D_{gwqmn} \quad 5.24$$

$$E_{aq} = \begin{cases} E_{aq,bed} + D_{aq} & if\ D_{aq} \leq \left(E_{wet,bed} - E_{aq,bed}\right) \\ E_{aq,bed} + D_{aq} + \left[\dfrac{\left(\dfrac{b}{b + \dfrac{2}{p}}\right).\dfrac{D_{wet,aq}^{\left(1+\frac{2}{p}\right)}}{D_{wet,0}^{\frac{2}{p}}}}{A_{hru} - b.\left(\dfrac{D_{wet,aq}}{D_{wet,0}}\right)^{\frac{2}{p}}}\right] & if\ D_{aq} > \left(E_{wet,bed} - E_{aq,bed}\right) \\ where, D_{wet,aq} = D_{aq} - \left(E_{wet,bed} - E_{aq,bed}\right) \end{cases} \quad 5.25$$

In Figure 5.2, D_{gwqmn} is demonstrated as of height of channel bed from the aquifer bed which can be determined by dividing the given threshold aquifer water depth to initiate baseflow by the aquifer specific yield. The elevation of the channel bed ($E_{ch,bed}$) has already been estimated in Section 5.4.2. D_{aq} is the height of groundwater level above the aquifer bed uniformly distributed across the HRU area. The expression within the square brackets of equation 5.25 returns an additional groundwater depth to be superimposed over the original SWAT simulated GWL uniformly distributed across the HRU. This is estimated by dividing the water volume that would have been contained in a wetland at GWL had the wetland been filled with the aquifer material, by HRU area less the wetland surface area at GWL. The reason of this arrangement is that SWAT currently assumes that the areal extent of an HRU-scale aquifer, with uniform depth, is the same as that of the HRU. This would underestimate the actual GWL

of a shallow aquifer when the GWL rises above the wetland bed (see Figure 5.2) because the volume occupied by a depressional wetland is not a part of the aquifer. The total amount of water in an aquifer during a time step is divided by aquifer specific yield (S_y) to obtain the equivalent depth of groundwater in the aquifer (D_{gwqmn} & D_{aq}). Once the elevation of GWL is calculated, SWATrw simulates wetland-groundwater interaction using the following assumptions: (i) if the GWL is below the wetland bed seepage water is routed through a vadose zone to obtain net recharge from the wetland, and (ii) if the GWL is at or above the wetland bed wetland-groundwater interaction is instantaneous i.e. any seepage from the wetland or groundwater flow to the wetland will not be lagged by a time factor. The following equations represent the mathematical formulations of the wetland-groundwater interactions:

$$Q_{wet\,\&\,aq} = \begin{cases} K_{sat}.\dfrac{E_{wet} - E_{wet,bed}}{wet_{th}}.A_{wet} & if\ E_{aq} < E_{wet,bed} \\ K_{sat}.\dfrac{E_{wet} - E_{aq}}{wet_{th}}.A_{wet} & if\ E_{aq} \le E_{wet}\ \ and\ E_{aq} \ge E_{wet,bed} \\ K_{sat}.\dfrac{E_{aq} - E_{wet}}{wet_{th}}.A_{wet,aq} & if\ E_{aq} > E_{wet}\ and\ E_{aq} \ge E_{wet,bed} \end{cases} \quad 5.26$$

$$Q^{i}_{rchrg,aq} = \begin{cases} (1 - \delta_{gw}).Q_{wet\,\&\,aq} + \delta_{gw}.Q^{i-1}_{rchrg,aq} & if\ E_{aq} < E_{wet,bed} \\ Q_{wet\,\&\,aq} + \delta_{gw}.Q^{i-1}_{rchrg,aq} & if\ E_{aq} \le E_{wet}\ \ and\ E_{aq} \ge E_{wet,bed} \end{cases} \quad 5.27$$

where E_{wet}, $A_{wet,aq}$, and wet_{th} represent wetland water level elevation, wetland water surface area at GWL elevation (i.e. when the wetland water depth is $D_{wet,aq}$), the thickness of the wetland bottom (commonly known as hyporheic zone), respectively and other symbols are previously described. After estimating $Q_{wet\,\&\,aq}$, the mass balance in both wetland and aquifer is updated.

5.5. SWAT and SWATrw modelling of the Barak-Kushiyara River Basin

Both SWAT and SWATrw were employed on the Barak-Kushyiara River Basin which lies within the UMRB (Figure 5.4). The physiographic and hydro-meteorologic characteristics of the basin have been discussed in Section 1.3.1

and Chapter 4. The main reason for selecting the Barak-Kushyiara River Basin is that the Hakaluki haor, an ecologically important wetland, exists in the lower floodplain of the basin (see Figure 5.4). Moreover, while data scarcity is a major hurdle for wetland research in Bangladesh's hoar region, the availability of morphometric characteristics of the Hakaluki haor, together with hydrological time series data (stream flows, river stage and groundwater level) from around the wetland, enables the use of this particular wetland and the Barak-Kushiyara River Basin as a case study in the development of the models. The Hakaluki haor is traversed by the Juri River, a tributary of the Kushiyara River that it joins at the Fenchuganj gauging station. The Sonai River is the main tributary of the Juri River. Their junction is at the north end of the Hakaluki haor. During the monsoon season, higher water stage in the Kushiyara River can cause water to flow back into the Juri River and as a result the Hakaluki haor wetland can receive large amount of water from the Kushiyara at this time.

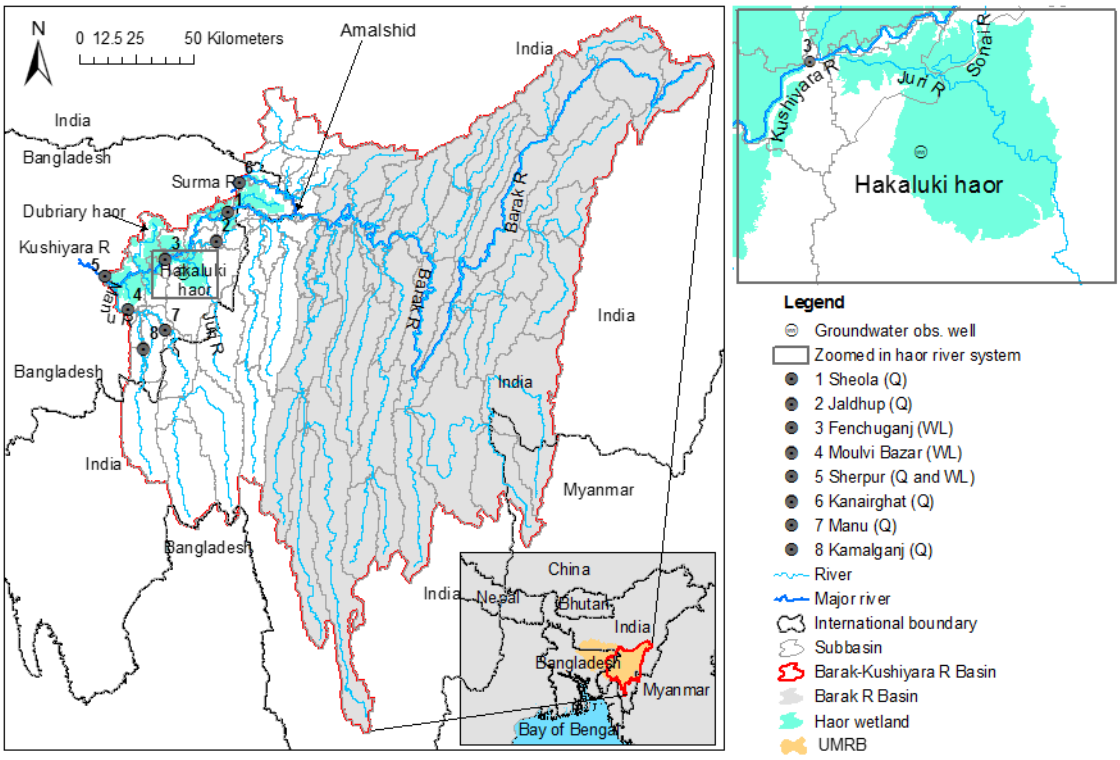

Figure 5.4. The geographical location of the Barak-Kushiyara River Basin and haor wetlands therein. The areal extent of wetlands indicates their maximum water surface areas. Hakaluki haor, which is central of the research, is shown in zoom-in view. Under river gauging stations, "Q" and "WL" indicate respectively discharge and water level or stage.

Because both models do not preserve the spatial geometric configuration of a wetland within a subbasin, they require some geometric properties (e.g. maximum wetland area and depth) of the wetland in order to establish its volume-area-depth relationship. The study area lacks any measured morphometric properties of wetlands except for a volume-area-depth relationship curve provided by Choudhury and Nishat (2005) for the catchment of the Hakaluki haor (Figure 5.5). This morphometric curve was originally developed from the Water Development Map of 1963 (BWDB and FPCO, 1993). For the Hakaluki haor, the area corresponding to depths of 4.29 m and below is considered as the maximum wetland water surface area (13889 ha) based on the wetland areal map obtained from the Center for the Environmental and Geographic Information Services (CEGIS), Bangladesh. The required maximum wetland water surface area of other wetlands within each subbasin was derived using the same areal map and the corresponding maximum wetland water depth was approximated based on the available documentary information (Oka et al., 2013; Uddin et al., 2012), the DEM data and Google Earth. To retrieve the required depth from Google Earth, the map (KML file) of the maximum surface area for each wetland was overlaid on Google Earth followed by manual identification of the lowest and highest elevations within each wetland. In general, the mean water depth of the haor wetlands within the basin varied from 1 m in the dry season to 6 m during the monsoon season.

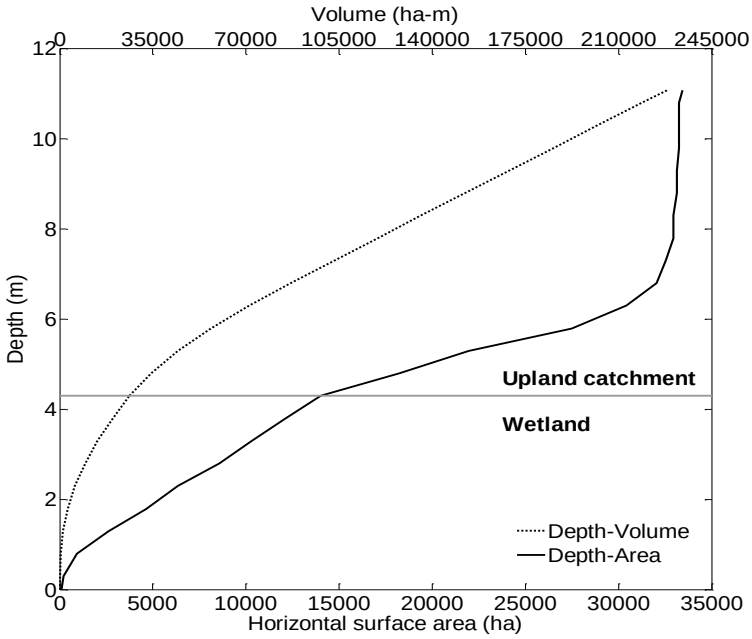

Figure 5.5. The measured volume-area-depth relationship curves of the Hakaluki haor catchment after Choudhury and Nishat, 2005.

5.5.1. Simulation of the Hakaluki haor's morphometric curve

An assessment of the ability of the wetland geometric models in SWAT and SWATrw (i.e. the H-K wetland geometric model) to represent the measured morphometric characteristics of the Hakaluki haor was undertaken by simulating the wetland morphometric properties using a spreadsheet programme. First, the wetland shape parameter 'p' in the SWATrw model (see equations 5.10 and 5.11) was calibrated by iteratively changing its value until the simulated volume-depth and volume-area curves matched the observed counterparts as closely as possible. The observed wetland volumes were the only input variable to the calibrated model; however, this input was replaced by simulated wetland water storage in catchment-scale hydrological modelling. While calibrating 'p' the two required values of wetland area and depth at its maximum capacity were set to 13889 ha and 4.29 m, respectively. Similarly, the shape parameter (see equation 5.4) of the SWAT wetland module was calculated using two sets of known values of wetland volume and area, which were 21143 ha-m, 13889 ha and 2883 ha-m, 3841 ha, respectively at wetland's maximum and normal water levels. All the values but the maximum wetland area (13889 ha) were obtained from the previously developed wetland volume-area-depth relationship curve by SWATrw for maximum and normal wetland water depths of 4.29 and 2.1 m, respectively. Once the shape and scale parameters of both wetland models were determined, volume-area-depth curves were generated using measured volumes as input to the calibrated models. Finally, the generated volume-area and volume-depth curves simulated by both models were compared to the corresponding observed curves.

5.5.2. Model setup

The model building procedure can be described in four sequential steps: catchment delineation, HRU definition, setting up management operations (e.g., tillage, plantation, irrigation, and fertilization of cultivated crops), and finally calibration and validation. Catchment delineation generates the basin boundary that is then discretised into the constituent subbasins. Delineation was performed

using the pre-defined river network (Section 4.2.4) that, as described in Section 3.2.1, forces SWAT to generate a more realistic river network and hence associated subbasins. Like many other contemporary catchment models, SWAT does not explicitly model flows of distributary channel or connecting channel rather a “Transfer” function can be used to manually proportionate the flow of an upstream main channel between its descendent distributaries. In order to make a dendritic river network, therefore, all distributary channels within the lower flat part of the basin were removed. Through an iterative process, a threshold value of 3000 ha for minimum area for which a river reach is generated using the DEM was found to give a good approximation of the actual river network. The final model had a total of 116 subbasins that were manually inter-connected based on the river network (Figure 5.4).

Each subbasin was further discretised into HRUs using threshold values of 10, 20, and 35% for land use, soil, and slope, respectively. As described in Section 3.2.2, firstly, the area of a subbasin is portioned according to the percentage of individual land use coverage but excluding those that fall below the land use threshold value. Secondly and similarly, the area of each unique land use unit within a subbasin is further fragmented into unique land use and soil pairs based on the soil threshold value. Finally, the area of each unique land use and soil unit is further discretised based on the threshold value of soil slope to generate the HRUs of the subbasin. In general, a large spatial variation of each property (land use, soil and slope) demands a smaller threshold value and thus many HRUs. Although the GLC (see Section 4.2.2) land use classification does not contain rural villages, 5% of the rice land use area was assumed to be rural settlements since most of South Asia’s rice dominated agricultural land is dotted with scattered rural villages. These rural villages contain homesteads, perennial trees, and road networks. Therefore, when defining HRUs, a rice land HRU was further divided into two smaller HRUs in which 95% of the area of the parent HRU was classified as rice and the remaining 5% as rural village.

Having versatile options for management operation of different land uses is one of the distinguishing features of the SWAT model. Because rice cultivation dominates the lower flat area of the basin, it is important to adequately represent the operation schedule for rice cultivation. Usually two major rice varieties are

grown in the study area, Boro and Aman. Boro rice, a high yielding variety, is the dominant crop that is grown during the period of December/January–April, sometimes extending to early May. On the other hand, Aman rice is cultivated in comparatively high agricultural lands, which are less prone to inundation during monsoonal and post-monsoonal rainfall in the period of August to early December. A buffer time period of 20–30 days is allowed between harvesting of Aman rice and planting of the next Boro rice crops. Fertilizers are applied according to the prescribed doses (Table 5.1) by Bangladesh Rice Research Institute (BRRI). Commonly three types of fertilizers are applied to rice crops namely urea (Nitrogen), TSP (Triple Super Phosphate) and MOP (Muriate of Potash). Urea is applied in three different split doses whereas TSP and MOP are applied during planting time of each rice variety.

Table 5.1. Doses of applied fertilizer in rice crops of the UMRB

Rice variety	Growing period	Urea (kg ha^{-1})			TSP (kg ha^{-1})	MOP (kg ha^{-1})
		1st split	2nd split	3rd split		
Boro	01 Jan – 10 May	66.66 (01 Jan)	66.66 (01 Feb)	66.66 (01 Mar)	90 (01 Jan)	163 (01 Jan)
Aman	01 Aug – 10 Dec	54.33 (01 Aug)	54.33 (01 Sep)	54.33 (01 Oct)	60 (01 Aug)	104 (01 Aug)

Dry season Boro rice is a high water demanding rice variety. Due to low rainfall in the growing season, crop water demand is to meet by irrigation if needed. Inadequate available water in surface storages such as rivers and haors creates tremendous pressure on groundwater for irrigation. In this study, the rice crop is irrigated based on the threshold value of soil water stress, which is the deficit soil water content below field capacity. When the water content of rice growing field falls below the threshold value then the model will apply water to the respective rice HRUs until its water content reaches field capacity. If the amount of available water in user assigned sources (e.g. river, groundwater, and reservoir) is less than the rice demand water, then the applied irrigated water will not be sufficient to recharge soil water content up to field capacity.

The models were manually calibrated for the period of 1990–2003 against observed monthly discharge (see Section 4.2.6) and daily water stage data

recorded at the six different river gauging stations (Figure 5.4). Apart from using these observed data, expert knowledge of this author on the local hydrology was utilised while calibrating the model parameters. The validation period for the models was 2004–2010. In order to reduce any uncertainties associated with initial conditions, the model was additionally run for the three preceding years (warm-up period) before both the calibration and validation periods. The models respectively used IMDgrid and IMDdist rainfall data during calibration and validation periods for the Indian part of the basin. Since the models were run using a daily time step, monthly IMDdist rainfall and CRU temperature data were disaggregated to a daily resolution using the stochastic Monthly to Daily Weather Converter (MODAWEC) developed by Liu et al. (2009). This disaggregation uses the specified number of wet days in a month to distribute monthly totals through each month. Similarly daily temperature (maximum and minimum) was generated based on the standard deviation of temperature for a specific month in a year. Historical daily groundwater level data from an observation well (Figure 5.4) within the Hakaluki haor were also acquired from BWDB for the period of 1990–2010. These groundwater data were not used for model calibration rather as an ancillary data to check the models' capability in simulating local groundwater.

Since the ultimate goal of this study is to compare the simulation capabilities of the SWAT and SWATrw models, with a specific focus on wetland-river-aquifer interactions, the calibration and validation procedures were kept alike. Firstly the SWATrw model was calibrated, and then subsequently SWAT was run using the values of common parameters derived from SWATrw calibration. Calibration was started from the extreme upstream gauging stations (Sheola and Kanairghat; see Figure 5.4) followed by succeeding stations. Simulated flows in the Barak River at Amalshid and in the Kushiyara River at Fenchuganj are proportioned between their downstream distributaries using *transfer* function of the models. Table 5.2 lists the values of all calibrated parameters. The simulated river water depth was found to be very sensitive to the CH_N2 parameter (Manning's roughness coefficient for a river). Therefore, the value of CH_N2 calibrated against monthly discharge was further fine-tuned using daily river stage data from the Fenchuganj, Moulvi Bazar and Sherpur gauging stations which had comparatively fewer missing data in their records. Once a satisfactory result was attained, the consistency of model performance was validated using the period 2004–2010.

Table 5.2. Calibrated parameters governing hydrological processes in the Barak-Kushiyara River Basin*

Models	Parameters	Description (unit)	Default values	Calibrated values
SWAT & SWATrw	Basin level			
	SURLAG[a]	Surface runoff lag coefficient (day)	4.00	0.10
	HRU level			
	CN2[a]	Curve number	70 - 92	55 - 81
	ESCO[a]	Soil evaporation compensation factor	0.95	0.50 - 0.95
	EPCO[a]	Plant uptake compensation factor	1.00	0.30 - 1.00
	GW_DELAY[a]	Groundwater delay (day)	31	10 - 45
	ALPHA_BF[a]	Baseflow factor (day)	0.048	0.01 - 0.7
	SHALLST	Initial depth of water in shallow aquifer (mm)	0.50	0.50 - 1520.00
	GWQMN	Threshold depth of water in shallow aquifer for baseflow (mm)	0.00	0.00 - 1480.00
	REVAPMN	Threshold depth of water in shallow aquifer for revap (mm)	1.00	0.00 - 2000.00
	RCHRG_DP[a]	Fraction of soil percolated water to deep aquifer	0.05	0.0 - 0.80
	GW_SPYLD	Specific yield of shallow aquifer	0.003	0.003 - 0.02
	Subbasin level			
	CH_N2	Manning's roughness coefficient for a river	0.014	0.014 – 0.017
	TRANS_AMT	Fraction to distribute a main channel flow between two downstream tributaries	-	0.1 – 0.7
	WET_FR	Fraction of sub-basin area drained into a wetland	-	0.82 - 1.00
	WET_MXSA[b]	Maximum wetland water surface area (ha)	-	372 - 14869
	WETEVCOEF[a]	Wetland evaporation coefficient	-	0.0.70
	WET_K[a]	Hydraulic conductivity of wetland bottom (mm/hr)	-	0.30 - 8.00
SWAT	WET_VOL	Initial volume of water in wetlands (ha-m)	-	22 - 894
	WET_MXVOL	Maximum wetland water volume (ha-m)	-	419 - 29748
	WET_NSA	Normal wetland water surface area (ha)	-	108 - 11764
	WET_NVOL	Normal wetland water volume (ha-m)	-	58 - 22264
SWATrw	WET_D	Initial wetland water depth (m)	-	1.00
	WET_DMX[b]	Maximum wetland water depth (m)	-	3.00 - 8.00
	WET_P[a]	Wetland shape factor	-	0.9 - 1.5
	WET_TH[b]	Thickness of wetland bottom (m)	-	1.00
	CCH_M[b]	Depth exponent in connecting channel flow equation	-	2.00
	CCH_N[b]	Slope exponent in connecting channel flow equation	-	1.00
	CCH_SF[b]	Friction slope of connecting channel	-	0.01
	CCH_DFR[a]	Fraction of main channel maximum depth at normal level	-	0.10 - 0.80
	CCH_LFR[a]	Fraction of main channel length to be overflowed at normal level	-	0.10 - 0.90
	CCH_C	Conveyance coefficient of connecting channel (m^{-1} s^{-1})	-	667.00

*parameters are grouped based on models (SWAT and SWATrw) and spatial scales (Basin, subbasin and HRU). Parameters within the cap of "SWAT & SWATrw" mean both the models use these parameters. Basin level parameter indicates all HRUs in the basin use the same value of that parameter. Under subbasin level, the value of each volumetric, areal and CCH_LFR wetland parameters is apportioned among HRUs according to their respective areal extents in the subbasin; values of other subbasin level parameters are unique for all HRUs in the subbasin.

[a]These parameters are used for sensitivity analysis (see Section 5.5.4).

[b]These parameters were not calibrated rather their values were taken from available data, literature and in some cases approximated based on the experience about the study area.

Values for four required volumetric and areal parameters (WET_VOL, WET_MXVOL, WET_NSA, WET_NVOL shown in Table 5.2) of SWAT were generated from the calibrated wetland morphometric curves by SWATrw using corresponding wetland water depths at maximum, normal and initial levels. The assumption behind this strategy is that wetland morphometric characteristics are well captured by the calibrated SWATrw model; therefore, a wetland property (volume or area) generated by that model for a known depth would be much better than calibrating those unknown parameters (volume and area) in SWAT. The initial wetland water volume in each wetland was defined as the equivalent volume at 1 m depth since both the calibration and validation periods started in the dry month of January.

5.5.3. Model evaluation

Two commonly used approaches were employed to evaluate the performance of the SWAT and SWATrw model : (i) visual or graphical comparison of simulated and observed values, and (ii) statistical or mathematical performance indicators (Jain and Sudheer, 2008; Krause et al., 2005). Jain and Sudheer (2008) stated that visual inspection is a subjective approach since the same model may not receive an identical rank when evaluated by different observers. On the other hand, mathematically based performance statistics are objective as the same model, for a given input set of data, will produce identical result irrespective of the number of runs or who runs the model. Many statistical formulas have been developed to evaluate catchment model performance. Each approach has its own merits and demerits. Rather than merely choosing an evaluation criterion, a modeller should carefully investigate the strength and weakness of that indicator in context of the experimental catchment. Krause et al. (2005) argued that even an experienced modeller may face difficulties in selecting appropriate performance indicators as well as in interpreting the modelled results. They critically evaluated some popularly used model performance indicators and modified them to minimize their limitations. Fitting a model with multiple evaluation criteria reduces a model's uncertainty and helps to interpret the model response realistically (Jain and Sudheer, 2008; Moriasi et al., 2007). The following performance indicators were employed.

Nash-Sutcliffe efficiency (NSE)

The NSE indicator (equation 5.28), developed by Nash & Sutcliffe (1970), is one of the most widely used statistical evaluation criteria in hydrological simulating studies (Schaefli and Gupta, 2007):

$$NSE = 1 - \frac{\sum_{i=1}^{n}(O_i - P_i)^2}{\sum_{i=1}^{n}(O_i - \bar{O})^2} \qquad 5.28$$

O_i and P_i respectively indicate observed and simulated discharge at time step i, $\bar{O}$ is the mean observed discharge for the entire time period, and n is the number of total data records. The value of NSE represents how much of the variance in observed data is captured by the model. As can be seen from the equation, the range of NSE can be 1 to - ∞ where a value of 1 indicates perfect simulation. A NSE value of ≤0.0 indicates that the mean of observed values is better predictive value than simulated ones. Despite being used widely, some serious limitations of NSE were identified in previous research (Jain and Sudheer, 2008; Krause et al., 2005; Legates and McCabe Jr, 1999; Schaefli and Gupta, 2007). Krause et al. (2005) argued that because of squaring the difference between observed and simulated values, NSE overestimates the influence of peak flows and underestimates that of low flows. Using such a model where seasonality in discharge time series data is strong would mislead the model. The authors suggested a modified NSE (NSE_m) to reduce the disadvantage of the original NSE (see equation 5.28).

$$NSE_m = 1 - \frac{\sum_{i=1}^{n}|O_i - P_i|^j}{\sum_{i=1}^{n}|O_i - \bar{O}|^j} \quad j \in N \qquad 5.29$$

Here, j is equal to 1. Replacing the original j value of 2 in NSE with 1 reduces its tending demerits of over- and underestimation. Moreover, this modified NSE is more sensitive to simulated values because of decreased normalized factor i.e. denominator in the right term of equation 5.29.

Coefficient of determination (R^2)

The coefficient of determination, shown in equation 5.30, indicates the strength of the linear association between observed and simulated data. Maximum value of R^2 is 1.00 which implies that the model is perfectly capable to explain the dispersion in observed values whereas a value 0.00 implies no linear relation between observed and predicted values.

$$R^2 = \left(\frac{\sum_{i=1}^{n}(O_i - \bar{O})(P_i - \bar{P})}{\sqrt{\sum_{i=1}^{n}(O_i - \bar{O})^2}\sqrt{\sum_{i=1}^{n}(P_i - \bar{P})^2}} \right)^2 \quad 5.30$$

In equation 5.30, $\bar{P}$ indicates the average of model predicted values. In an explanatory analysis, Krause et al. (2005) showed that, unless taking the effect of slope of the regression line, use of only R^2 can result in misinterpretation of the modeled results because a systematically over- and underestimated model may produce value of R^2 close to 1.00. For this reason, the authors modified equation 5.30 in the form of equation 5.31:

$$R_m^2 = \begin{cases} |b|.R^2 & if\ b \le 1 \\ |b|^{-1}.R^2 & if\ b > 1 \end{cases} \quad 5.31$$

where R_m^2 is the modified coefficient of determination, and b is the slope of regression line.

Percent bias (PBIAS)

PBIAS indicates the average tendency of over- or under-prediction by a model. It is calculated using equation 5.32. A value of 0.0 means perfect model simulation where negative value indicates overestimation and vice-versa. Probably the most useful application of the PBIAS family indicators is in water mass balance error studies (ASCE, 1993; Moriasi et al., 2007).

$$PBIAS = \left[\frac{\sum_{i=1}^{n}(O_i - P_i)}{\sum_{i=1}^{n} O_i} \right] \times 100 \quad 5.32$$

Refined index of agreement (d_r)

Willmott (1981) developed the "index of agreement" often denoted by "d" as shown by equation 5.33. Like other squared error based performance indicators, d suffers from two serious limitations, firstly, oversensitivity to larger error (Krause et al.,2005; Willmott et al. 2012), and secondly, difficulty of model interpretation if a value of d is other than perfect i.e. 1.0 (Willmott et al., 2012). Willmott et al. (2012) redefined the index of agreement in order to minimize these limitations. The modified "d" is named the "refined index of agreement (d_r)" by Willmott et al. (2012) and expressed as equation 5.34. The interpretation of a modeled results with d_r is straightforward because "It indicates the sum of the magnitudes of the differences between the model-predicted and observed deviations about the observed mean relative to the sum of the magnitudes of the perfect-model (P_i = O_i, for all *i*) and observed deviations about the observed mean". Values of d_r range between 1 to -1 where a positive unity value indicates a perfect simulation.

$$d = 1 - \frac{\sum_{i=1}^{n}(O_i - P_i)^2}{\sum_{i=1}^{n}(|P_i - \bar{O}| + |O_i - \bar{O}|)^2} \quad 5.33$$

$$d_r = \begin{cases} 1 - \dfrac{\sum_{i=1}^{n}|O_i - P_i|}{2 * \sum_{i=1}^{n}|O_i - \bar{O}|} & if \sum_{i=1}^{n}|O_i - P_i| \leq 2 * \sum_{i=1}^{n}|O_i - \bar{O}| \\ \dfrac{2 * \sum_{i=1}^{n}|O_i - \bar{O}|}{\sum_{i=1}^{n}|O_i - P_i|} - 1 & if \sum_{i=1}^{n}|O_i - P_i| > 2 * \sum_{i=1}^{n}|O_i - \bar{O}| \end{cases} \quad 5.34$$

Ratio of root mean square error to the standard deviation of observed data (RSR)

Taking into account the recommendations of past studies (Legates and McCabe Jr, 1999; Singh, Knapp and Demissie, 2004), Moriasi et al. (2007) proposed the RSR performance index, as depicted in equation 5.35. A value of 0 indicates a perfect model simulation while poorer performance is indicated as the value of RSE increases.

$$RSR = \frac{\sqrt{\sum_{i=1}^{n}(O_i - P_i)^2}}{\sqrt{\sum_{i=1}^{n}(O_i - \bar{O})^2}} \quad 5.35$$

The evaluation metrics discussed here are the most widely used indicators in hydrological modelling though many other formulas exist (see Reusser et al. (2009) who list 48 different performance indicators). As discussed above, each indicator has its own merits and demerits, and also numerical range. Therefore, developing a common framework with all the indices is problematic and probably inappropriate. A model might be identified as satisfactory with respect to a specific metric but another metric might classify that model as unsatisfactory. Reviewing a large number of hydrological model based studies conducted for real world applications, Moriasi et al. (2007) recommended a generalized framework to grade model's performance based on NSE, $PBIAS$, and RSR (see Table 5.3). In this study, their recommended framework was used while grading (very good, good, satisfactory, and unsatisfactory) the performance of UMRB-SWAT model.

Table 5.3. Recommended model performance indicators by Moriasi et al. (2007)

Performance rating	NSE	RSR	PBIAS (%)		
			Streamflow	Sediment	N, P
Very good	0.75<NSE≤ 1.00	0.00<RSR≤ 0.50	PBIAS<±10	PBIAS<±15	PBIAS<±25
Good	0.65<NSE≤ 0.75	0.50<RSR≤0.60	±10≤PBIAS<±15	±15≤PBIAS<±30	±25≤PBIAS<±40
Satisfactory	0.50<NSE≤ 0.65	0.60<RSR≤ 0.70	±15≤PBIAS<±25	±30≤PBIAS<±55	±40≤PBIAS<±70
Unsatisfactory	NSE≤ 0.50	RSR>0.70	PBIAS≥±25	PBIAS≥±55	PBIAS≥±70

5.5.4. Sensitivity analysis of model parameters

A sensitivity analysis with the TEDPAS (Temporal dynamics of parameter sensitivity (Reusser et al., 2011)) method was conducted to investigate how the newly incorporated wetland parameters influence on streamflows and wetland water storages (or water balance). TEDPAS estimates sensitivity of each parameter at each time step based on the FAST (Fourier Amplitude Sensitivity Test (Cukier et al., 1975, 1973)) global sensitivity analysis approach. The main feature of TEDPAS is that the time series of parameter sensitivities generated during a simulation period help to identify dominant hydrological processes and

their duration of existence (Guse et al., 2014; Reusser and Zehe, 2011). The sensitivity for a particular parameter at a time step is estimated based on the first-order partial variance approach (Reusser et al., 2011). In this study TEDPAS was employed for the two subbasins respectively containing Hakaluki haor and Dubriary haor (Figure 5.4) for the calibration period. Table 5.4 gives the major distinguishing characteristics of the two subbasins related to wetland modelling. Streamflows of the first subbasin are influenced by its upstream subbasins generated flows whereas this is not the case for the second subbasin. This is the reason to take these two haors for sensitivity analysis despite there was no measured volume-area-depth relationship curve for the Dubriary haor.

Table 5.4. Major distinguishing characteristics of the two subbasins containing Hakaluki and Dubriary haor wetlands

Characteristics	Hakaluki haor subbasin	Dubriary haor subbasin
Area of sub-basin (ha)	79200	24200
Streamflows influenced by inflows from upstream subbasins	Yes	No
Wetland drainage area (ha)	78408 ha (99% of the sub-basin)	23232 ha (96% of the sub-basin)
Maximum wetland water surface area (ha)	13889 (18% of the sub-basin)	13882 (57% of the sub-basin)
Maximum wetland water depth (m)	4.29	5.00
Hydraulic conductivity of wetland bottom (mm/hr)	0.1	1.0
Maximum main channel depth (m)	2.42	1.17

Unlike conventional practices where sensitivity analysis precedes model calibration, we followed the reverse practice. This intention was not to identify sensitive model parameters but rather to see how the parameters of already carefully manually calibrated model influence on target hydrological components (streamflows and wetland water balance). To do so, parameter ranges were chosen around the corresponding calibrated parameter value. For the total 12 parameters (see Table 5.2) that are thought to have a major influence on streamflows and wetland water balance, TEDPAS produced 579 parameter sets (i.e. 579 model runs at each time step of the simulation period).

5.6. Results and discussion

5.6.1. Simulated morphometric properties of the Hakaluki haor wetland

The calibrated values of the two paired morphometric parameters (shape and scale) are 0.65 and 22.54 for SWAT and 1.1 and 983 for SWATrw. Figure 5.6 shows the volume-area and volume-depth relationships from both models and those derived from the observed morphometric data for the Hakaluki haor. Both the models produce identical volume-area curves (Figure 5.6a) that closely match (R^2 = 0.99 and slope of the observed vs simulated line = 1.1) the observed until the wetland volume reaches 14200 ha-m. Subsequently for a given volume the wetland areas are consistently overestimated so that the models are unable to represent the natural morphometric properties of the Hakaluki haor catchment. This is because the geometry of the upland catchment differs markedly from that of wetland (Figure 5.5). While exploring the reason for the two models' identical volume-area curves, it was found that the values of the wetland's shape and scale factors become the same if SWATrw's wetland formulas (equations 5.10 and 5.11) are rearranged to the form of SWAT's wetland volume-area relationship (equation 5.3). This is intuitively because the wetland volumes and areas at maximum and normal levels required by SWAT originated from the SWATrw generated wetland morphometric curve (see Section 5.5.2). This argument is further justified for other wetlands in the basin.

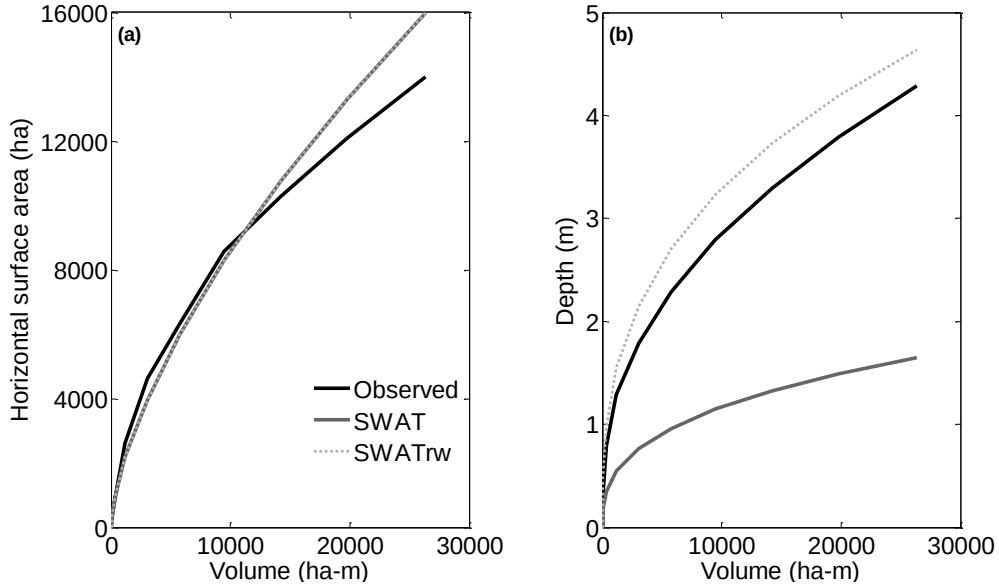

Figure 5.6. Comparison of wetland morphometric properties simulated by SWAT and SWATrw for the Hakaluki haor wetland. Wetland depths in SWAT are calculated from equation 5.9 as proposed by Liu et al., 2008.

Unlike the volume-area relationship, the volume-depth relationships from the two different models vary markedly and exhibit different abilities in emulating the observed relationship for the Hakaluki haor (Figure 5.6b). The relationship for the SWATrw model provides a good approximation to the observed (R^2 = 0.99 and slope of the observed vs simulated line = 1.1). Depths are slightly overestimated by on average 15% across the full range of volumes. On the other hand, SWAT consistently underestimates (R^2 = 0.99 and slope of the observed vs simulated line = 0.38) the actual wetland depths by on average 58%. Since for a given volume both models simulate exactly the same surface area, a shallower wetland simulated by SWAT for that volume must be more cylindrical (i.e. higher side slope) than that of SWATrw. As discussed in Section 5.4.1, Equation 5.9, which was proposed by Liu et al. (2008) for SWAT, assumes an equal side slope of 1/4 for both a riparian wetland and an associated floodplain. The DEM data used in this study (Figure 4.3) suggest that the average side slope of the Hakaluki haor wetland is 2%, much smaller than SWAT's representation of the wetland (25%). The large differences in the wetland morphometric relationships, and the considerable underestimation of depth by SWAT, demonstrate the potential difficulties in applying SWAT where depth-dependent hydraulic simulations of wetland interactions with rivers and aquifers are required.

5.6.2. Calibrated parameters

A total of 30 parameters were selected for calibration (Table 5.2). Of these parameters, the first 16 are common to both the models. The next four are limited to SWAT and the last 10 to SWATrw. A precise interpretation of calibrated parameters within a conceptual model is not possible because different combinations of values of the same parameters may produce an almost identical simulation as explained by the equifinality concept (Beven and Freer, 2001). However, the relative influence of 12 selected parameters (Table 5.2) on hydrological processes, derived from TEDPAS analysis, are discussed later. The value of the only basin level calibrated parameter, SURLAG, was found to be 0.1. This relatively low value compared to the default 4.0 indicates that surface runoff generated within a subbasin moves at a moderate rate towards its river system. A catchment with flat topography and/or higher resistance to overland flow generally responds relatively slowly at the outlet to the generated overland flow in the catchment. Although the lag time of surface runoff for steep sloped headwater catchments would be expected to be smaller, the lower flat topographic properties of the extensive lowland parts of the basin leads to the smaller value of SURLAG. It seems stream flows at all gauging stations that are in the lower floodplains of the basin are predominantly characterised by the lower floodplain flow dynamics. For example, a steep hydrograph produced at the foothill of an upper subbasin is likely to be diffused in the lower floodplain.

The curve number for the moderate antecedent moisture condition (CN2) plays a major role in separating rainfall that reaches the ground into infiltrated water and surface runoff. Table 5.2 shows the initial calibrated values and the model automatically updates CN2 based on simulated daily soil moisture. The soil evaporation compensation factor (ESCO) enables the model to meet evapotranspiration demands from the deeper soil layer if necessary. The calibrated values of ESCO varied between 0.5 for forested hilly HRUs to the default value of 0.95 for rice dominated floodplain HRUs that are characterised by much wetter soils. Another calibrated soil or unsaturated zone parameter is the plant uptake compensation factor (EPCO) which controls how much of the plant water demand (transpiration) that is not satisfied by the upper soil layer is drawn from the underlying soil layer. The calibrated values of EPCO for HRUs

dominated by forest and tea land covers were higher (0.6–1.00) compared to rice dominated HRUs (a consistent 0.3). An explanation could be associated with the soil profile and plant root properties. For the entire basin, a 2-layered 1000 mm soil profile was used with the top and bottom layers having specified depths of 300 mm and 700 mm, respectively. A reasonable assumption is that the root depths of mature forest trees and tea shrubs will extend below the depth of the top layer, which allows plants to satisfy their water demand from the lower soil layer. However, the root depth of rice generally varies between 0–300 mm (Sharma et al., 1994; Uddin et al., 2009) so that the contribution of water from the deeper soil layer to transpiration is negligible unless water stress occurs. In any one year, the simulated rice experienced water stress for no more than 15% of the total growing period suggesting that transpiration from deeper layers was limited.

Seven calibration parameters (GW_DELAY to GW_SPYLD in Table 5.2) are associated with the groundwater simulation. Although SWAT does not directly use any observed data beyond the soil profile, a prior knowledge of the aquifer properties within a river basin may assist the calibration process by appropriately parameterizing the groundwater model. For the wetlands dominant lower part of the basin, calibrated values of SHALLST, GWQMN and GW_SPYLD were 1300 mm H_2O, 1280 mm H_2O and 0.02, respectively. Calibration of these parameters benefitted from data provided by Shamsudduha (2010) who produced spatial geological properties of the local aquifers compiled from multi-source field data. These calibrated values yield an initial GWL of 1 m ((1300–1280)/(0.02*1000)) above the riverbed level. Such a low GWL eventually produces negligible base flow in the dry season (MPO, 1991; WARPO, 2000; cited in Shamsudduha, 2010). Since the simulation period starts on the first day of January in 1990 (validation) or 2004 (calibration), these calibrated parameters can be considered reasonable for the Bangladesh part of the basin. In the absence of sufficient field data, it is not possible to further explore and justify the calibrated values of the other groundwater parameters.

All of the subbasin level calibration parameters are associated with the wetland simulation except CH_N2 for the river simulation. The range of values of each parameter shown in Table 5.2 is estimated from the results of all the wetlands or

rivers in the basin. Most of the rivers in the upper hilly region took the default value (0.014) for CH_N2 where lower floodplain rivers had slightly higher values (0.015–0.017). More resistance to flow from instream vegetation could account for the larger CH_N2 for the river system in the lower floodplain. The parameter WET_MXSA was not directly calibrated but instead its values were obtained from the CEGIS wetland shape file.

The high calibrated values of WET_FR (0.82–1.00) replicates the reality of floodplains in the study area where a large proportion of local surface runoff flows towards wetlands rather than rivers. The two most important SWATrw parameters in are CCH_DFR and CCH_LFR because they exert the largest influence upon the quantity of transferable water during wetland-river interaction through the connecting channel. In general, a combination of deeper river reaches and a greater distance between river and wetland results in larger values of CCH_DFR and smaller CCH_LFR values whereas the opposite combination (a shallower river reach and a shorter distance between river and wetland) produces the opposite results. For all connecting channels, the value of the calibrated conveyance coefficient (CCH_C) was found to be 667 m^{-1} s^{-1}. Kadlec and Wallace (2009) suggested values of CCH_C for densely or sparsely vegetated wetlands of 116 and 580 m^{-1} s^{-1}, respectively. The higher CCH_C value for the connecting channels within the SWATrw model indicate relatively low resistance which reflects the channelized nature of the river-wetland exchanges in which water is relatively deep in comparison to overland flow across a wetland's surface.

5.6.3. Sensitivity of selected parameters to streamflows and wetland water balance

Figure 5.7 shows the temporal sensitivity of selected parameters to streamflows (a), wetland water volumes (b), and wetland water surface areas (c) simulated by SWATrw for the subbasin containing the Hakaluki haors (Figure 5.4). The two surface runoff parameters CN2 and SURLAG, groundwater parameter RCHRG_DP and the hydraulic conductivity of wetland (WET_K) show noticeable sensitivity (as large as 0.8) to streamflows during the three rainy seasons (pre-monsoon, monsoon and post-monsoon) or wet period (Figure 5.7a). CN2 is found to be measurably sensitive during the pre-monsoon season (April and May) when

separate storms separated by dry spells cause soils to be alternatively wetted and dried. However, its influence on streamflows gradually dampens in the subsequent monsoon (June–September) and post-monsoon (October–November) seasons when a consistently wetter soil prevails. SWATrw/SWAT daily updates the value of CN2 depending on soil water content. In the wet season soil remains almost saturated leading a less variable CN2 and thus a smaller sensitivity to streamflows. Since CN2 remains relatively less sensitive during the period of almost continuous monsoonal rainfall, modelled surface runoff can be categorized as a non-Hortonian process driven by soil saturation. The apparent sensitivity of the soil evaporation parameter ESCO at the beginning of the wet season indicates that the role of soil water content on streamflows at this time should not be neglected. In contrast to the other parameters, a more consistent and larger sensitivity of RCHRG_DP during the wet season indicates that streamflows in this sub-basin are mainly characterised by the amount of shallow aquifer recharge, thus by baseflow. On the other hand, the variance of low flows from the late wet season (November) onwards is mostly described by GW_DELAY, the travel time of percolated soil water to reach the groundwater table. All wetland parameters except WET_K demonstrate negligible influences on streamflows (sensitivity: 0 to 0.05). The sensitivity of WET_K (0.15–0.6) is visible only during the wet period and sporadic in pattern. The disappearance of WET_K sensitivity can be associated with the role of hydraulic head potential between interacting water bodies (wetland, river and aquifer). Despite a larger variation in WET_K values, its influence on streamflows can be trivial if the driving hydraulic head potential is small. Nonetheless, the variance in simulated streamflows caused by WET_K can be transmitted through surficial wetland-river interaction and/or sub-surficial wetland-aquifer-river interaction.

The above results together suggest that streamflows in the Hakaluki haor subbasin are mainly influenced by baseflow and moderately influenced by overland routed surface runoff (not wetland routed i.e. surficial exchange between the wetland and river is not prominent due to the negligible sensitivity values of CCH_LFR and CCH_DFR).

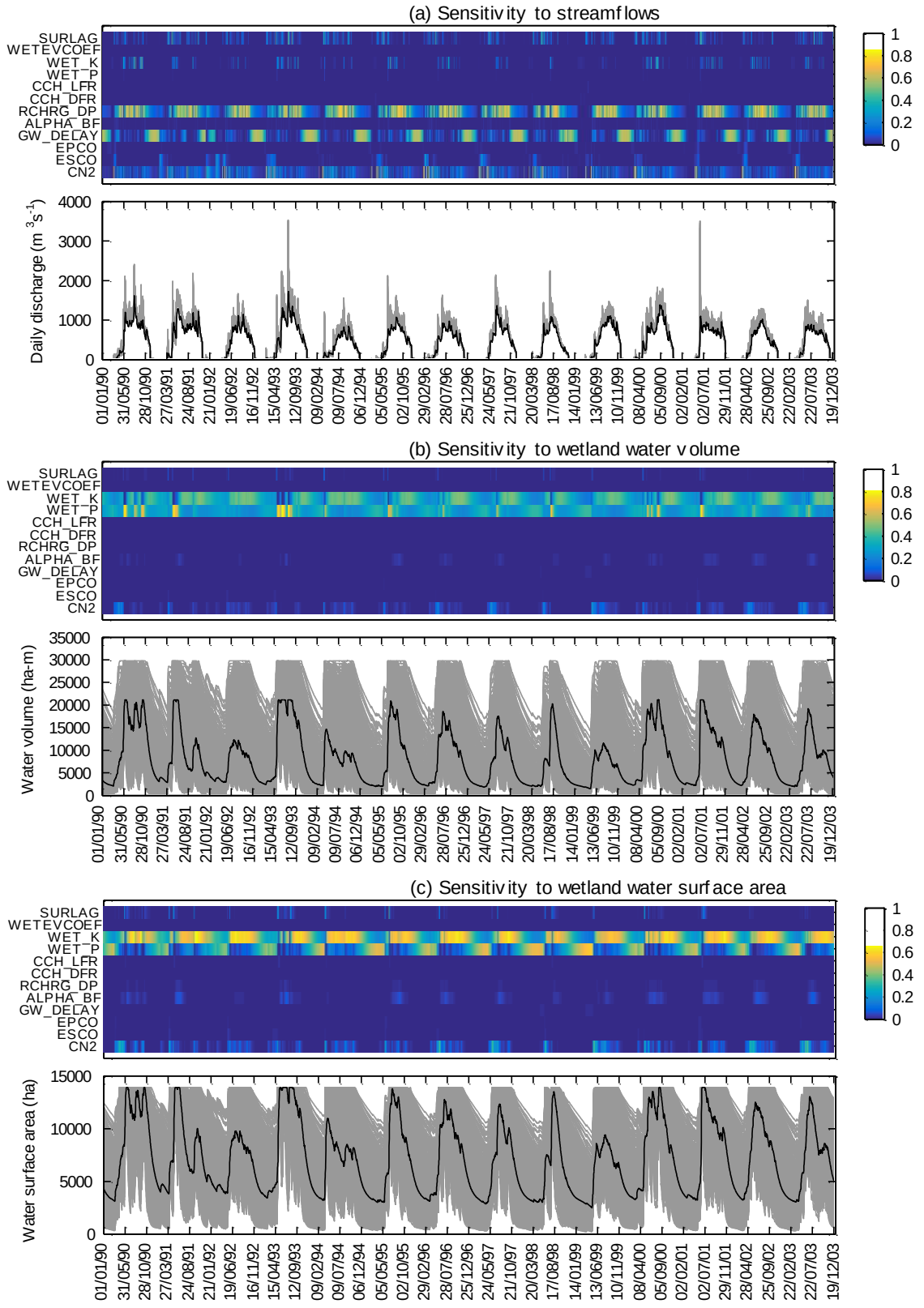

Figure 5.7. Temporal parameter sensitivity to (a) streamflows, (b) wetland water volume and (c) wetland water surface area for the Hakaluki haor subbasin. All parameters are described in Table 5.2. The line plots indicate time series of target simulated variables (streamflows, wetland water volume and surface area) for all 579 simulations during TEDPAS analysis. The black line is for the calibrated parameter set.

As shown in Figure 5.7b, wetland water balance (i.e. water volume) is almost completely controlled by the hydrological processes involved with parameters WET_K and WET_P. The surface runoff parameter CN2 shows a trace sensitivity during the onset of wet period. Although WET_P (shape factor) has no direct association with any hydrological processes (precipitation, evaporation, exchanges between wetland and rivers/aquifers), it indirectly influences those processes due to variation in wetland water surface area and depth (equation 5.10). The signal of WET_K, however, implies that interaction between the wetland and aquifer is the principal hydrological process that influences the water balance of the wetland. Since wetland water surface area and depth are the direct function of wetland water volume (see equations 5.10 and 5.11), a similar explanation for these two former wetland variables can be expected (see Figure 5.7c for wetland water surface area). However, WET_P remains almost completely insensitive to wetland water surface area during monsoonal months (Figure 5.7c) in contrast to that for water volume (Figure 5.7b). The reason is elaborated in the next paragraph.

For the Hakaluki haor subbasin, it was not possible to investigate how wetland-river interaction affects the streamflows of the subbasin because streamflows were found to be insensitive to the newly incorporated wetland parameters (WET_P, CCH_LFR and CCH_DFR). One potential reason is that the streamflows of the Hakaluki haor subbasin is strongly influenced by inflows from its upstream subbasins that do not contain any wetlands (Figure 5.4). Therefore, the variance in streamflows from the upper subbasins dominates flows in the downstream Hakaluki haor subbasin. To further investigate wetland-river interactions, the sensitivity results for the Dubriary haor subbasin (Figure 5.8) were analysed. Flows in this subbasin are not affected by any upstream inflows. Moreover, wetland water occupies a sizeable proportion of the subbasin area (57%, see Table 5.4). Like the Hakaluki haor subbasin, the availability of shallow aquifer water for baseflow explains most of the variance in streamflows of the Dubriary haor subbasin during the wet period as reflected by the large sensitivity (~0.8) of RCHRG_DP (Figure 5.8a). Baseflow gradually dominates the recessional streamflows towards the early dry season, which is mapped by the temporal pattern of GW-DELAY.

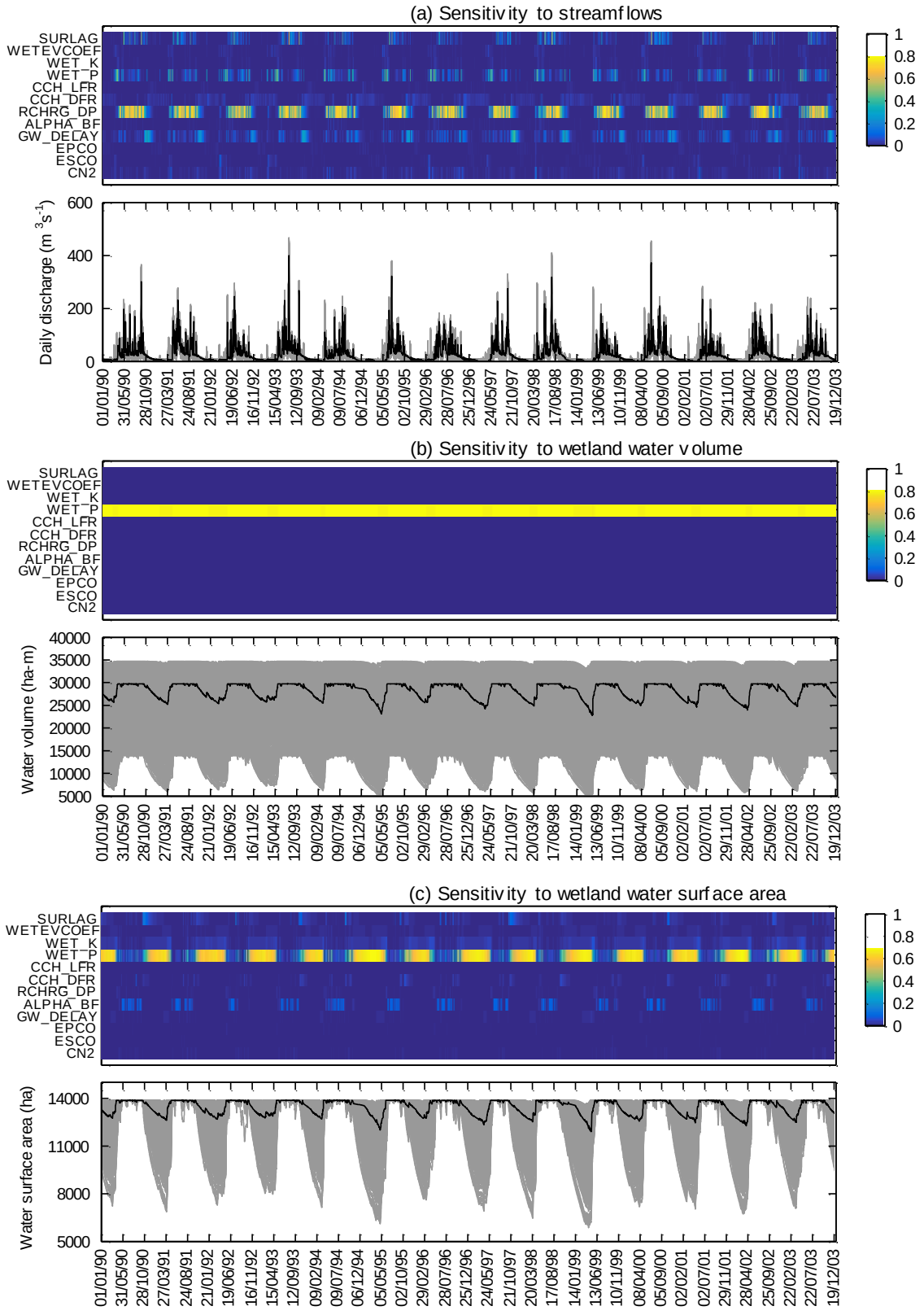

Figure 5.8. Temporal parameter sensitivity to (a) streamflows, (b) wetland water volume and (c) wetland water surface area for the Dubriary haor subbasin. All other necessary descriptions are mentioned in Figure 5.7.

The distinguishing feature of the Dubriary haor subbasin in contrast to the Hakaluki haor subbasin is the large sensitivity of WET_P and reduced sensitivity of surface runoff parameters (CN2 and SURLAG) in Figure 5.8a. This evidences a measureable wetland influence on the streamflows of the Dubriary haor subbasin. Since WET_K remains quite small (0–0.05) throughout the simulation period, it can be conjectured that streamflows are less sensitive to the variation of the wetland hydraulic conductivity. Looking at the partial parameter sensitivity (Figure 5.8a), the wetland influence on streamflows can be translated into two decomposed interactions: heavy sub-surficial (wetland-aquifer-river) weighing by RCHRG_DP and GW_DELAY, and small surficial (wetland-river) weighing by CCH-DFR (0.05–1.5). The sensitivity signal of CCH_DFR appears between the period of post-monsoon (October–November) and the next early pre-monsoon (April) and disappears in the monsoon season. This demonstrates that wetland-river interaction happens via the connecting channel during the rising and falling period of wetland water and via direct transferral of water beyond the wetland maximum level in monsoon (see Section 5.4.2). As mentioned in Section 5.4.2, this transferred water may appear in the river floodplain depending on the river's maximum capacity. In both SWAT and SWATrw, although water on a floodplain can seep to the underneath aquifer through the entire floodplain area the reverse process is restricted. Rather that seepage water can return to river through baseflow that is not a function of area through which it flows. Recently Sun et al. (2015) addressed this issue by employing Darcy's equation in the catena based discretized floodplain land units. It can be justified that the greater influence of baseflow on streamflows of the Dubriary haor subbasin is due to large aquifer recharge through the more conductive upland soils (hydraulic conductivity = 4 to 8 mm hr^{-1}) compared to the less interaction between the wetland and its underlying aquifer.

A constant yellow signal (sensitivity ~0.8) for WET_P throughout the simulation period (Figure 5.8b) suggests that the variance in wetland water volume is completely explained by the geometry of Dubriary haor wetland; hydrological processes involved with the remaining 11 parameters (sensitivity ~0) have no significant influence on wetland water balance. Although this result is partly in agreement with results for the Hakaluki haor subbasin for the dry period but totally disagreement for the wet period. From Figure 5.8c, the water surface area of the

Dubriary haor wetland remains almost static for all model runs (i.e. all parameter sets) at its maximum level (area = 13882 ha; depth = 5 m) during wet periods. However, this is not the case for wetland water volumes (Figure 5.8b) since wetland's capacity varies with its shape factor (WET_P) despite having constant surface area and depth at maximum water level. Because all vertical hydrological processes (e.g. precipitation, evaporation, wetland-aquifer interaction) in the modelled wetland occurs through its water surface area, the invariance of this area among model runs at a particular time step suggests a stable state of all these processes. For this reason, variance in simulated wetland water volumes caused by the associated process-based parameters is not seen in wet periods. Nonetheless, one might expect some variation due to groundwater parameters because (i) wetland-aquifer interaction is not only affected by water surface area but hydraulic head difference and hydraulic conductivity and (ii) groundwater parameters are found to be sensitive for streamflows. For most of the time wetland water level remains very close to both ground surface and GWL; and the given range of wetland hydraulic conductivity is very small (0.1–0.3 mm hr^{-1}). Therefore, a small water transfer rate between the wetland and aquifer is likely; the impact on the very large wetland water volume therefore negligible. The reason for GWL and wetland water level being close to ground surface in the Dubriary haor subbasin can be explained by its physiographic settings. The river bed in the Dubriary haor subbasin is much closer to the ground surface than that of Hakaluki haor subbasin (see Table 5.4). Because baseflow to river cannot lower GWL beyond the river bed, GWL can only fluctuate above the river bed unless aquifer water is lost by any other means (e.g. wetland interception). Again a wetland can intercept aquifer water only when wetland water level is below GWL. This did not happen for the Dubriary haor wetland, at least during the wet periods, because wetland water level always remains at maximum capacity i.e. ground surface level.

5.6.4. Simulated streamflows and river stages

Although the principal interest of the study was to develop a catchment model that can better simulate wetland hydrological processes therein, the developed models (SWAT and SWATrw) could not be explicitly evaluated for such processes as there were no observed time series of wetland hydroregimes (e.g. water depth and inundation extent) for the basin. At this situation, it was assumed

that calibrating the models against streamflows that are impacted by upstream wetlands could be an indirect parameterizing approach for the wetlands. As described above, the performance of the SWAT and SWATrw models in emulating streamflows and river stages during the calibration and validation periods were evaluated graphically and statistically. Performances at the two upper gauging stations (Sheola on the Kushiyara River and Kanairghat on the Surma River) are first investigated since discharges at these locations are principally controlled by the runoff from the Barak River Basin (see Figure 5.4). Because a wetland only exists upstream of Sheola and Kanairghat, the influences of floodplain wetlands on river discharges at these locations are limited. Therefore SWAT and SWATrw can be expected to yield similar results. This is demonstrated in the very similar results when shown graphically (Figure 5.9 and Figure 5.10), and the nearly identical model performance statistics for the two models at these stations (Table 5.5). For the calibration period the values of these statistics fall in the *good* category for Sheola and *very good* category for Kanairghat according to the evaluation criteria (see Table 5.3) suggested by Moriasi et al. (2007). For the validation period, the above performances are exchanged between the two stations. Although the models capture peak flows at Sheola reasonably, dry season low flows are underestimated for both calibration and validation periods (Figure 5.9). Referring to the residual subplot (Figure 5.9c), most of higher flows are within the boundary of ±20% residual lines (inner dashed lines). This indicates that simulated large monsoonal flows may fluctuate by ±20% compared to the corresponding observed flows. A thorough investigation of both daily and monthly discharge time series reveals that the models tends to overestimate observed flows of 250–1000 m^3 s^{-1} during the recession period of the hydrograph in the post-monsoon season. This is demonstrated in Figure 5.9c. At Kanairghat, both models tend to slightly underestimate large flows (Figure 5.10a) but the majority of these flows are contained within the 20% residual lines. Compared to Sheola, dry season low flows (0–250 m^3 s^-1) at Kanairghat are better represented. The dissimilarities between simulated and observed flows at both stations are partly accounted for manually apportioning Barak River flows between its two distributaries (Kushiyara and Surma Rivers) with a constant ratio of 3:2. Such a distribution might not represent the actual flow dynamics at the river bifurcation. An annual water balance study of the modelled Barak River Basin shows that actual ET varies from 515 to 593 mm which is equivalent to 20–23% of average annual rainfall (2575 mm). Jhajharia et al. (2012) found that potential evapotranspiration (PET) demands over this part of the basin are about 1100 mm $year^{-1}$ and that the highest monthly PET of 110–150 mm is in May. These values are very close to those employed in both hydrological models (1115 and 121 mm, respectively). Model results suggest that both SWAT and SWATrw are able to simulate the hydrological dynamics of the hill and forests dominated upper Barak River Basin.

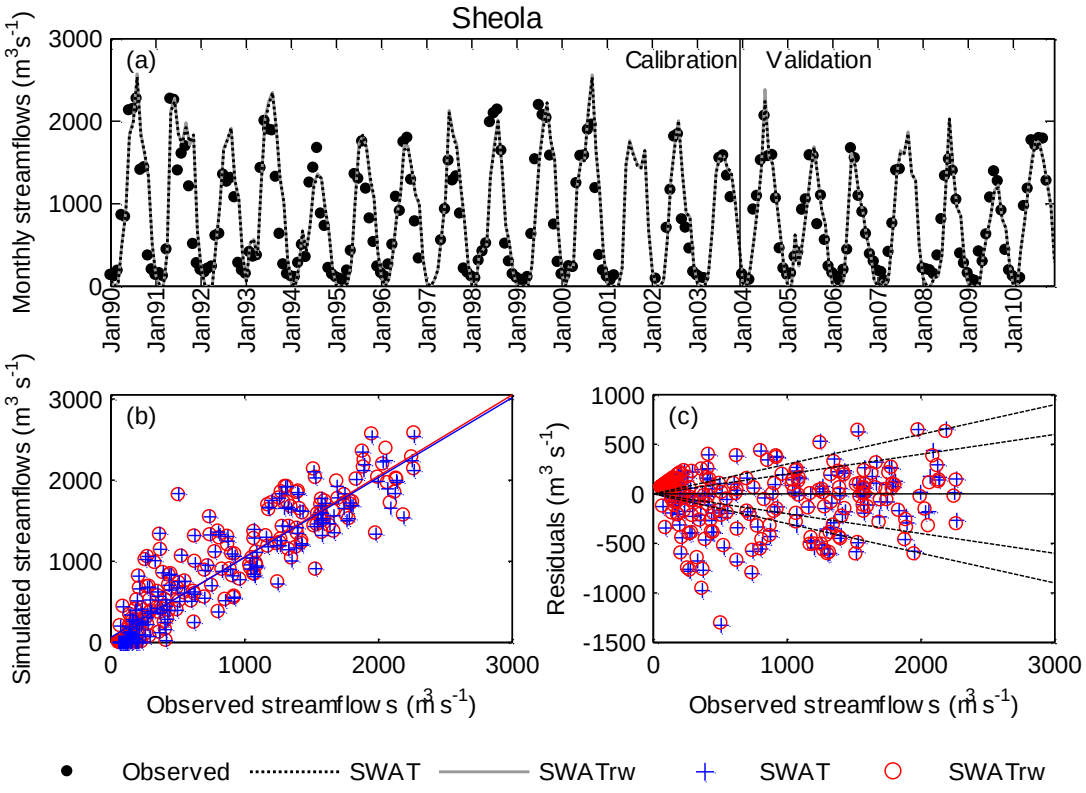

Figure 5.9. Graphical representation of SWAT and SWATrw performance in simulating mean monthly streamflows at Sheola station. In subplot (c), residuals = observed value – simulated value. The two inner inclined lines represent 20% residual boundary whereas outer pair is for 30% residual boundary.

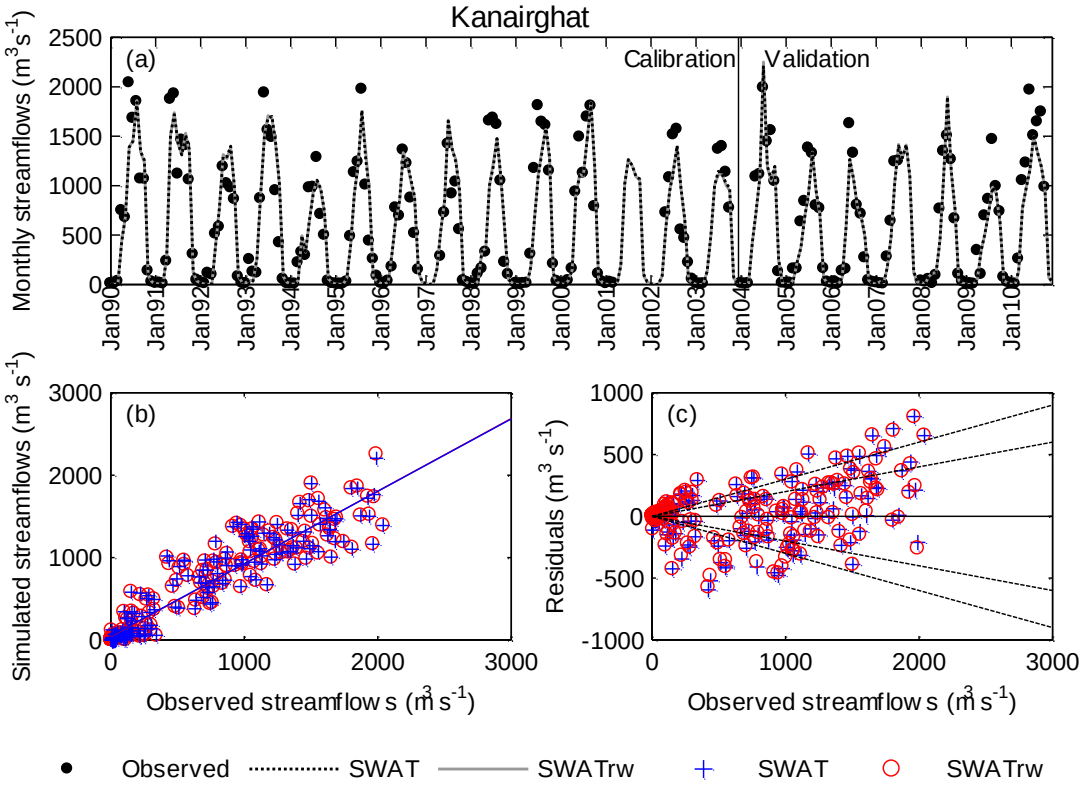

Figure 5.10. Graphical representation of SWAT and SWATrw performance in simulating mean monthly streamflows at Kanairghat station.

Table 5.5. Statistical performance metrics for simulated monthly streamflows and daily river stages/water levels during calibration (1990–2003) and validation (2004–2010) periods

Variables	Gauging stations	Period	Values of performance metrics																Remarks[a]
			NSE		NSE_m		RSR		R^2		R^2_m		PBIAS (%)		d		d_r		SWAT
			SWAT	SWATrw	SWAT	SWATrw	SWAT	SWATrw	SWAT	SWATrw	SWAT	SWATrw	SWAT	SWATrw	SWAT	SWATrw	SWAT	SWATrw	(SWATrw)
Mean monthly streamflow ($m^3 s^{-1}$)	Sheola	Calibration	0.76	0.76	0.59	0.59	0.49	0.49	0.81	0.82	0.79	0.81	-12.43	-13.06	0.94	0.94	0.80	0.80	G (G)
		Validation	0.88	0.88	0.71	0.71	0.34	0.34	0.90	0.90	0.89	0.90	6,04	5.33	0.97	0.97	0.85	0.85	VG (VG)
	Kanairghat	Calibration	0.88	0.88	0.74	0.74	0.35	0.34	0.88	0.88	0.79	0.80	0.44	0.99	0.97	0.97	0.87	0.87	VG (VG)
		Validation	0.88	0.88	0.75	0.74	0.35	0.35	0.90	0.89	0.75	0.75	12.34	12.72	0.97	0.96	0.87	0.87	G (G)
	Jaldhup	Calibration	0.72	0.71	0.56	0.55	0.53	0.54	0.87	0.87	0.50	0.49	20.45	20.88	0.89	0.89	0.78	0.78	S (S)
		Validation	0.62	0.62	0.54	0.54	0.62	0.62	0.63	0.62	0.42	0.42	6.83	7.30	0.88	0.88	0.77	0.77	S (S)
	Manu	Calibration	0.77	0.77	0.58	0.58	0.48	0.48	0.78	0.78	0.69	0.69	-5.25	-5.27	0.94	0.94	0.79	0.79	VG (VG)
		Validation	0.74	0.74	0.58	0.58	0.51	0.51	0.76	0.76	0.67	0.67	5.69	5.68	0.93	0.93	0.79	0.79	G (G)
	Kamalganj	Calibration	0.23	0.23	0.11	0.11	0.88	0.88	0.67	0.67	0.63	0.63	-48.74	-48.74	0.85	0.85	0.56	0.56	US (US)
		Validation	0.25	0.25	0.16	0.16	0.87	0.87	0.61	0.61	0.58	0.58	-20.26	-20.26	0.85	0.85	0.58	0.58	US (US)
	Sherpur	Calibration	0.72	0.69	0.54	0.52	0.53	0.55	0.86	0.87	0.75	0.73	-15.95	-18.03	0.94	0.94	0.77	0.76	S (S)
		Validation	0.75	0.71	0.59	0.56	0.50	0.54	0.90	0.90	0.71	0.69	-4.43	-6.69	0.95	0.95	0.79	0.78	VG (G)
Daily river stage (m)	Fenchuganj	Calibration	0.65	0.87	0.48	0.66	0.59	0.37	0.90	0.89	0.78	0.68	-16.17	3.08	0.93	0.96	0.74	0.83	S (G)
		Validation	0.85	0.82	0.68	0.61	0.39	0.43	0.91	0.91	0.84	0.67	-6.86	9.45	0.97	0.94	0.84	0.80	VG (VG)
	Moulvi Bazar	Calibration	0.89	0.89	0.69	0.68	0.33	0.33	0.93	0.93	0.88	0.88	-3.54	-3.55	0.97	0.97	0.84	0.84	VG (VG)
		Validation	0.87	0.87	0.72	0.72	0.35	0.35	0.89	0.89	0.88	0.88	-1.72	-1.73	0.97	0.97	0.86	0.86	VG (VG)
	Sherpur	Calibration	0.60	0.85	0.43	0.68	0.63	0.38	0.91	0.90	0.77	0.88	-16.56	-7.14	0.92	0.96	0.71	0.84	S (VG)
		Validation	0.82	0.93	0.64	0.77	0.42	0.26	0.92	0.93	0.79	0.91	-6.65	1.86	0.96	0.98	0.82	0.89	VG (VG)

[a] VG = Very Good, G= Good, S=Satisfactory and US = Unsatisfactory. These overall performance grading are based on NSE, RSR and PBIAS as suggested by Moriasi et al. (2007), see Table 5.3; however, although they did not suggest any grading criteria for river stage simulation here we have assumed their recommended criteria for streamflows are equally applicable to river stages.

For Jaldhup station on the Sonai River, both models show very similar performance (satisfactory) with consistent underestimation of peak flows (Figure 5.11a and Figure 5.11c). This underestimation can be as large as 55% for some observed peak flows. One potential reason behind this discrepancy may be the exclusion of possible monsoonal overbank flow contributions from the adjacent lower floodplain of the Barak River Basin (see Figure 5.4). The drainage divide between subbasins in the lower flat floodplain may not strictly maintain the supposed zero boundary flow conditions during these high flow periods.

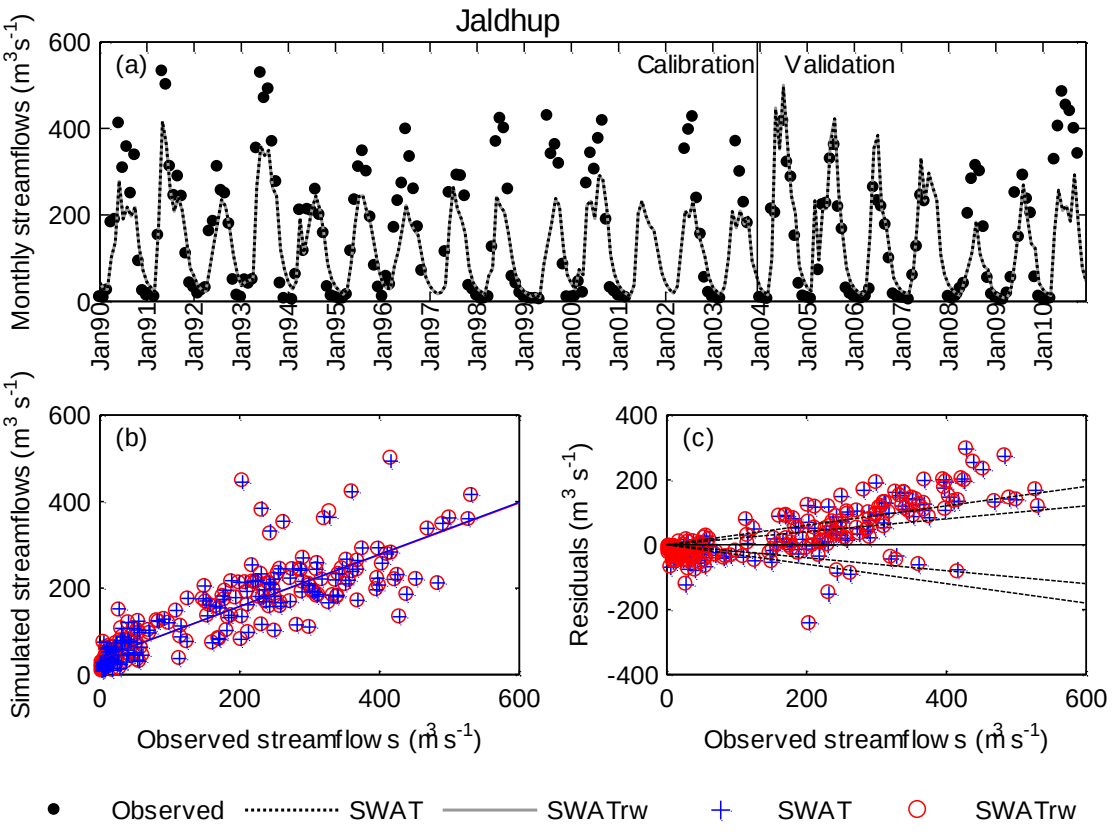

Figure 5.11. Graphical representation of SWAT and SWATrw performance in simulating mean monthly streamflows at Jaldhup station.

The two headwater catchments of the River Manu at the Manu gauging station and the River Dhalai at Kamalganj station are situated in the Tripura region of the UMRB (see Figure 4.12). For the Manu River, both models are classified as very good during the calibration and validation periods (Table 5.5). The models'

practically identical results are obviously reflecting the absence of any wetlands in the catchment of Manu. Residual analysis (Figure 5.12c) shows that the majority of flows are within the 20% uncertainty band lines. However, smaller flows in the dry season are more likely to cross the 30% uncertainty bands i.e. such an observed flow can be over- or underestimated by more than 30%.

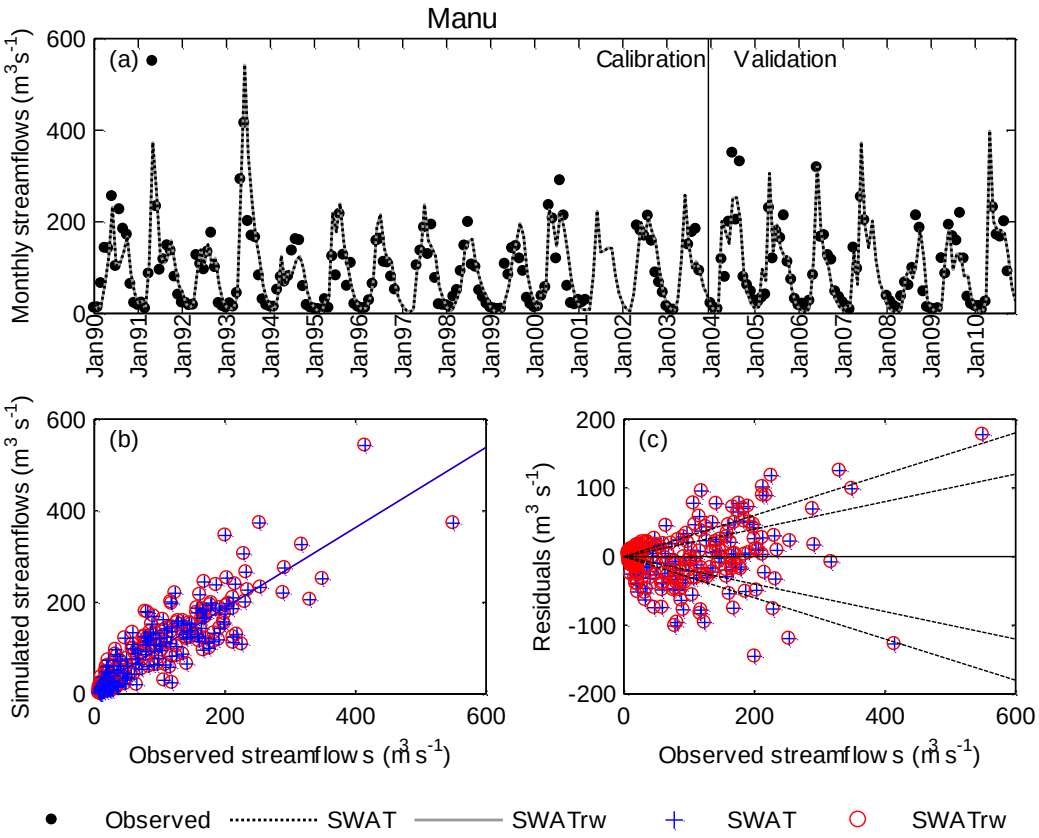

Figure 5.12. Graphical representation of SWAT and SWATrw performance in simulating mean monthly streamflows at Manu station.

Of the seven flow gauging stations in the Barak-Kushiyara River Basin, only the Kamalganj station on the River Dhalai receives an unsatisfactory (US) grade in simulating monthly flows (Table 5.5). This poor performance is mainly attributed to overestimation of observed flows as reflected in Figure 5.13 and negative PBIAS values of 20.26 to 48.74 (Table 5.5). The time series plot (Figure 5.13a) shows that this overestimation evolves from the region of peak to the recession tail of each annual hydrograph. In order to reduce shallow aquifer governed baseflow contributions to the simulated hydrographs, the calibrated models

transferred 51% of annual shallow aquifer water (1237 mm H_2O) to the underlying deep aquifer. Further reduction of baseflows, at the expense of underestimated peak flows, worsened the simulation performance of the models. River flows in these catchments are principally characterised by baseflow. Therefore, the conceptual exponential groundwater modules adopted in the models seem less reliable for the baseflow dominated Dhalai River catchment.

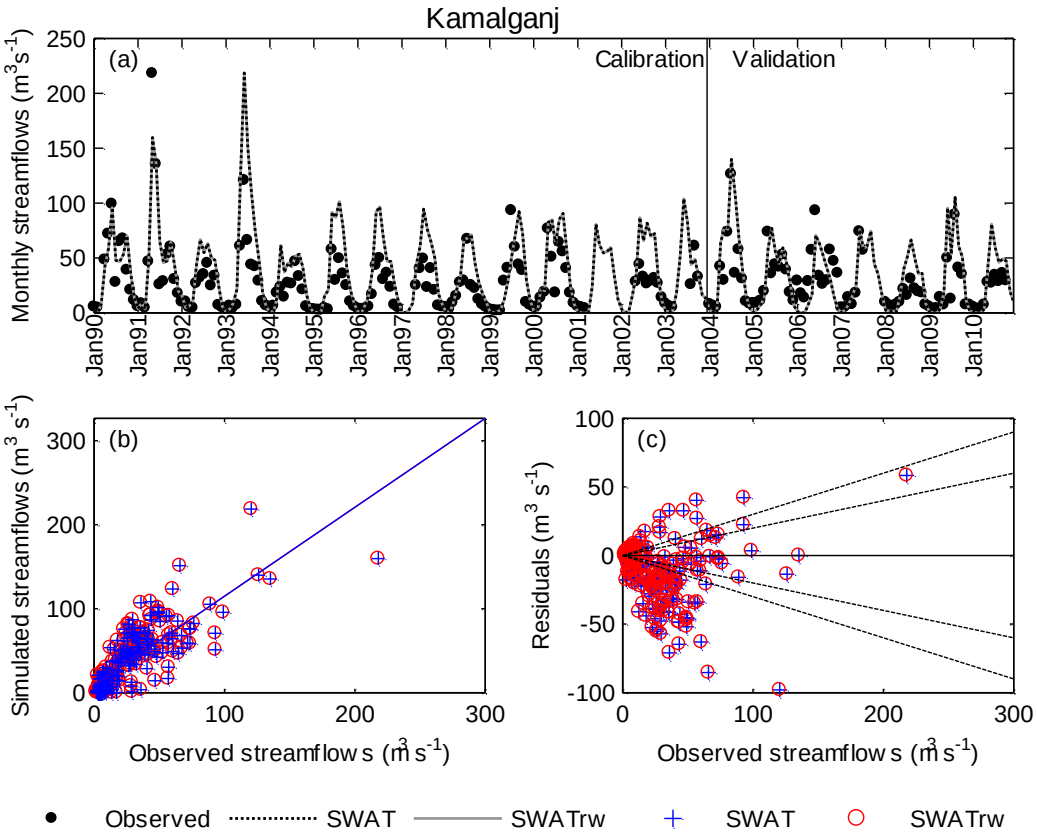

Figure 5.13. Graphical representation of SWAT and SWATrw performance in simulating mean monthly streamflows at Kamalganj station.

For Sherpur, the outlet of the Barak-Kushiyara River Basin, although both models show reasonable simulation skills in terms of all the metrics (see Table 5.5), a trend of overestimating larger flows is observed (Figure 5.14a and Figure 5.14c). Peak flows simulated by SWATrw are slightly higher (~2%) than those of the SWAT model and this is reflected in the weaker PBIAS value in Table 5.5. To investigate the reasons of flow overestimation by the models, we compared the annual hydrographs of daily flows at stations Sheola and Sherpur because streamflow characteristics at the later station is predominantly controlled by the flows at the upstream station Sheola (Figure 5.15). In some years (e.g., 1991 –

1994, 1997, 2005 - 2006), overestimated peak flows at Sherpur (red coloured line) are directly inherited from upstream station Sheola (cyan coloured line). Therefore, modelled discrepancies at Sherpur in such years can be explained by what argued for upstream Sheola. In some years (e.g., 1998, 1999, 2002, 2005), however, flow overestimation at Sherpur seems to be caused by local factors rather than inherited overestimation from upstream. For example, in 1998, although the simulated hydrograph at upstream Sheola (cyan coloured line) fits with the observed counterpart (grey coloured dots), at downstream Sherpur a noticeable overestimation is seen. Furthermore, a lower observed hydrograph at Sherpur compared to Sheola during the high flow period and subsequently almost the same hydrograph during the recession period indicates that a considerable amount of Sheola's outflows does not reach the downstream Sherpur station. This water may initially be retained in the floodplains and wetlands and later lost to the atmosphere through evaporation, to the shallow aquifer through seepage and/or to the adjacent subbasins through overbank flows. Since both models consider all major hydrological processes associated with an existing wetland, evaporation and seepage from the stagnant floodplain might be a potential cause of the lower hydrograph at Sherpur. Nonetheless, both models currently ignore such hydrological processes from a floodplain, rather the floodplain can only store water during overbank flowing period.

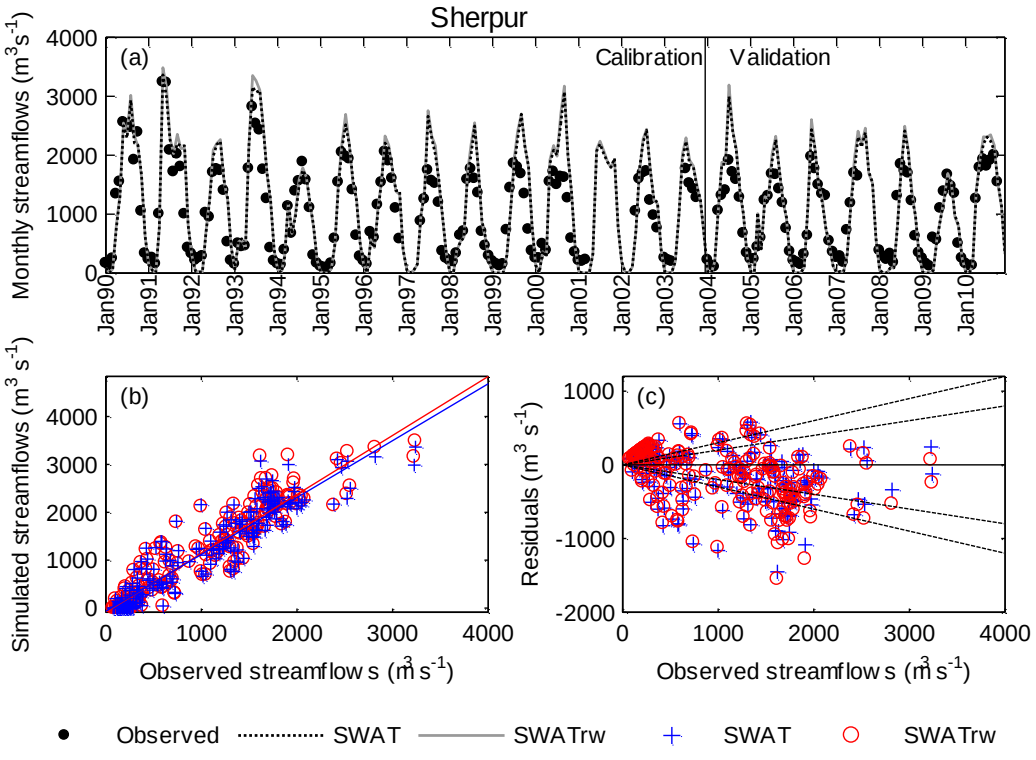

Figure 5.14. Graphical representation of SWAT and SWATrw performance in simulating mean monthly streamflows at Sherpur station.

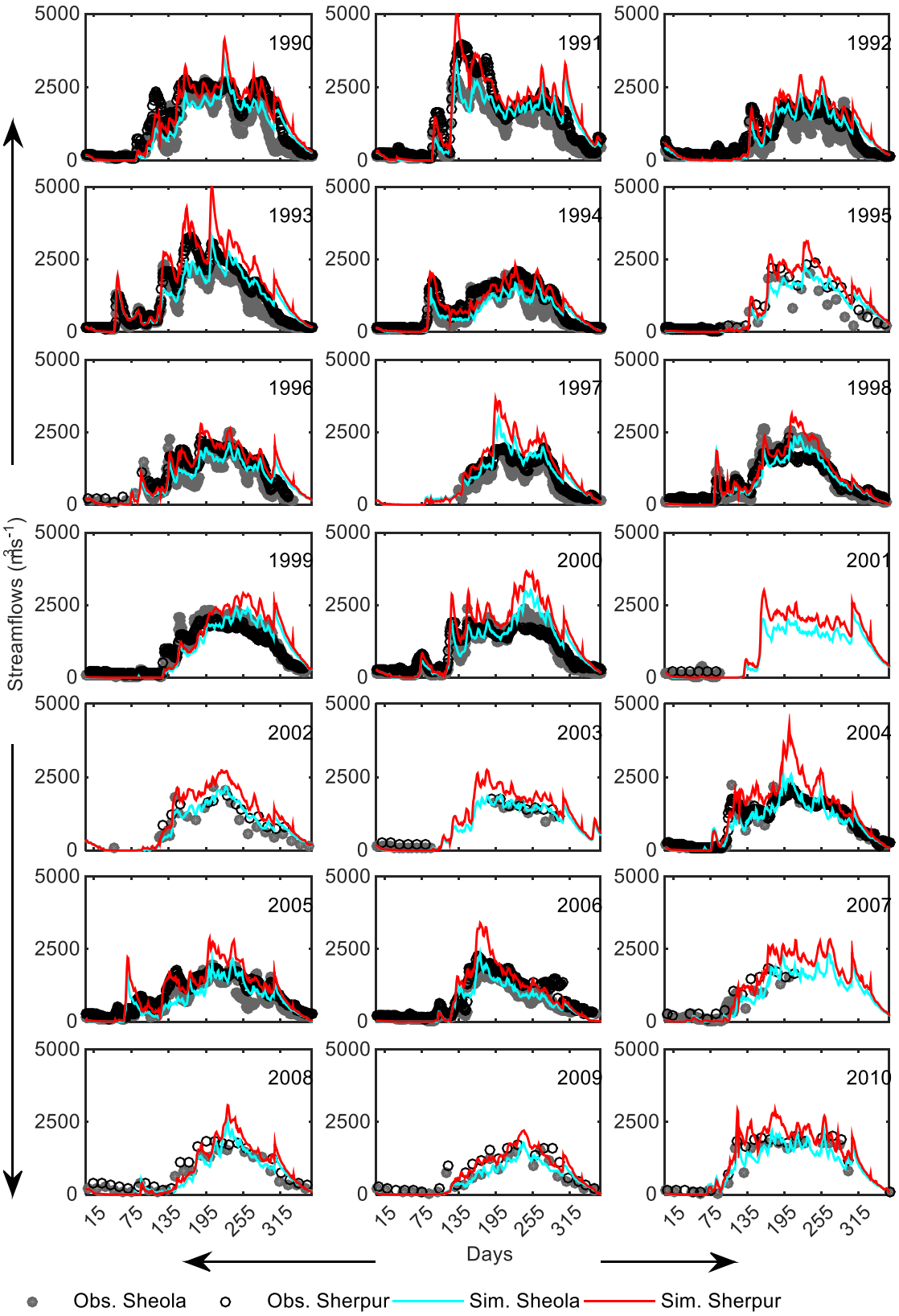

Figure 5.15. Annual hydrographs of daily observed and simulated flows at the Sheola and Sherpur gauging stations. Since SWAT and SWATrw produces almost similar hydrographs at these stations, only SWATrw simulated hydrographs are presented in this figure.

SWATrw outperforms SWAT in simulating daily river stage at Fenchuganj (Figure 5.16a) and Sherpur (Figure 5.16c). These two gauging stations are downstream of many wetland areas suggesting that the different performance of the two models is related to the different approaches used to represent wetlands within the two models. In contrast, identical simulation performance of the two models in terms of daily river levels at Moulvi Bazar (Figure 5.16b) is indicated by the evaluation metrics (Table 5.5). This gauging station is downstream of a series of subbasins that do not contain any wetlands (see Figure 5.4) and so both models respond identically.

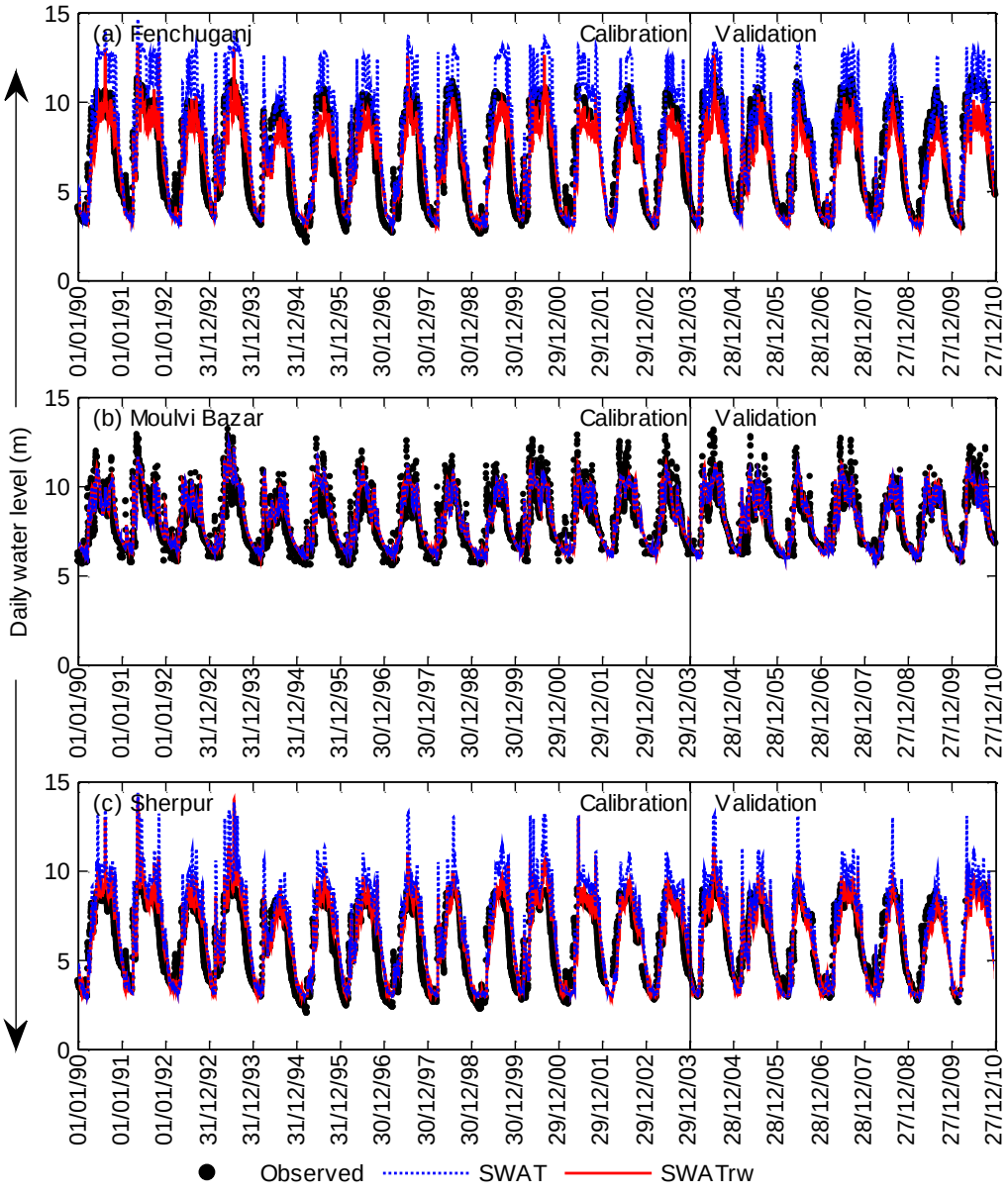

Figure 5.16. Comparison of simulated daily river stages/water levels by SWAT and SWATrw at the three designated stations: Fenchuganj, Moulvi Bazar and Sherpur.

An interesting disparity between the models is evident when their discharge and river stage simulation behaviours are simultaneously analysed for the Sherpur gauging station. Although SWATrw-generated peak flows are higher than those produced by SWAT (Figure 5.14a), the former model simulates lower river stages (Figure 5.16c), which is reflected in the reduced PBIAS values both in the calibration (-7.14%) and validation (1.86%) periods (Table 5.5). The higher outflows at Sherpur for SWATrw is associated with the higher inflows from the upstream river. This is intuitively because all upstream wetlands collectively produce more inflows at the inlet of the Sherpur river reach (the portion of Kyshiyara River that lies in the lowest subbasin) compared to SWAT. Larger inflows to the river system simulated by SWATrw should have produced higher river stages compared to those of SWAT; however, this was not seen in the Sherpur river reach. While routing flows through a river reach, inflows to the inlet of the river reach are the sum of outflows from its upstream river(s), water yield from the associated subbasin and initial (beginning of each time step) stored water in the river reach. The volume of this total inflow is used to estimate the water depth in a river reach based on the Manning's formula. Therefore, any changes in this total inflow will affect river water depths and downstream flows. An investigation of wetland-river interaction in the subbasin associated with the Sherpur station reveals that the SWATrw model transfers a daily flow of 5–40 m^3 s^{-1} from the Sherpur River reach to the connected wetland throughout the wet seasons (pre-monsoon, monsoon and post-monsoon). This reduction in total inflows to the reach compared to SWAT produces smaller river water depths, thus lower river stages. However, this reduction in total inflows negligibly affects routed downstream outflows of the river reach. The reasons are twofold: (i) the amount of daily water transferred from the river to the wetland is small (5–40 m^3 s^{-1}) compared to the increased concurrent daily river inflows (50–800 m^3 s^{-1}) from upstream rivers, and (ii) while routing inflows to the main river reach to the downstream outlet, storage within the reach is less than that represented by the storage time constants of the routing equation. However, if the amount of water transferred from a river reach to a wetland is offset due to higher storage effects of a river reach, then such a difference in simulated river stages between SWAT and SWATrw might not be seen. In general, the two models showed very little

differences in reproducing stream flows despite their dissimilar wetland-river interaction modules but SWATrw showed a better skill in simulating daily river stages compared to SWAT.

5.6.5. Comparison of wetland's hydrology simulated by SWAT and SWATrw

Comparison of SWAT and SWATrw simulations of the hydrological dynamics of haor wetlands is investigated using the Hakaluki haor wetland (see Figure 5.4) as a case study (Section 5.5). Since there are no observed hydrometric time series data for the Hakaluki haor, a very common situation for wetlands in this and similar regions, modelled results are evaluated using the average hydrological properties of the wetland in the dry and monsoon seasons. According to previous studies (CEGIS, 2012b; Choudhury and Nishat, 2005), the total water surface area of all the beels (defined in Section 1.3.1) in the Hakaluki haor is approximately 4500 ha in the dry season and the corresponding average water depth is 2 m. In the monsoon season, the maximum water surface area of the wetland can be as large as 14000 ha at a water depth of 4.30 m. Beside these average wetland observations, remotely sensed 10 day average inundated area data with 25 km of resolution for the period of 2002–2009 were obtained from the NASA's global inundated wetlands database (Schroeder et al., 2012). This database was developed under the auspices of NASA's Making Earth Science Data Records for Use in Research Environments (MEaSUREs) program. Therefore, any reference to this data, hereafter, will be denoted as MEaSUREs data. The inundated area of each grid is expressed as a fraction of the grid area (625 km^2). To determine the total inundated area within a subbasin, the following steps were followed: (i) MEaSUREs grids that completely or partially fall within a subbasin were identified, (ii) the area shared by each grid with the subbasin was estimated i.e. a grid completely being in the subbasin shares all of its total area, (iii) each grid's shared area was multiplied by its corresponding inundation fraction value (0 to 1) to obtain shared inundated area by each grid, and (iv) all shared inundated areas were summed to evaluate the total wetland water surface area in the subbasin. The illustrations in Figure 5.17 for the Hakaluki haor can be seen to easily understand the procedure.

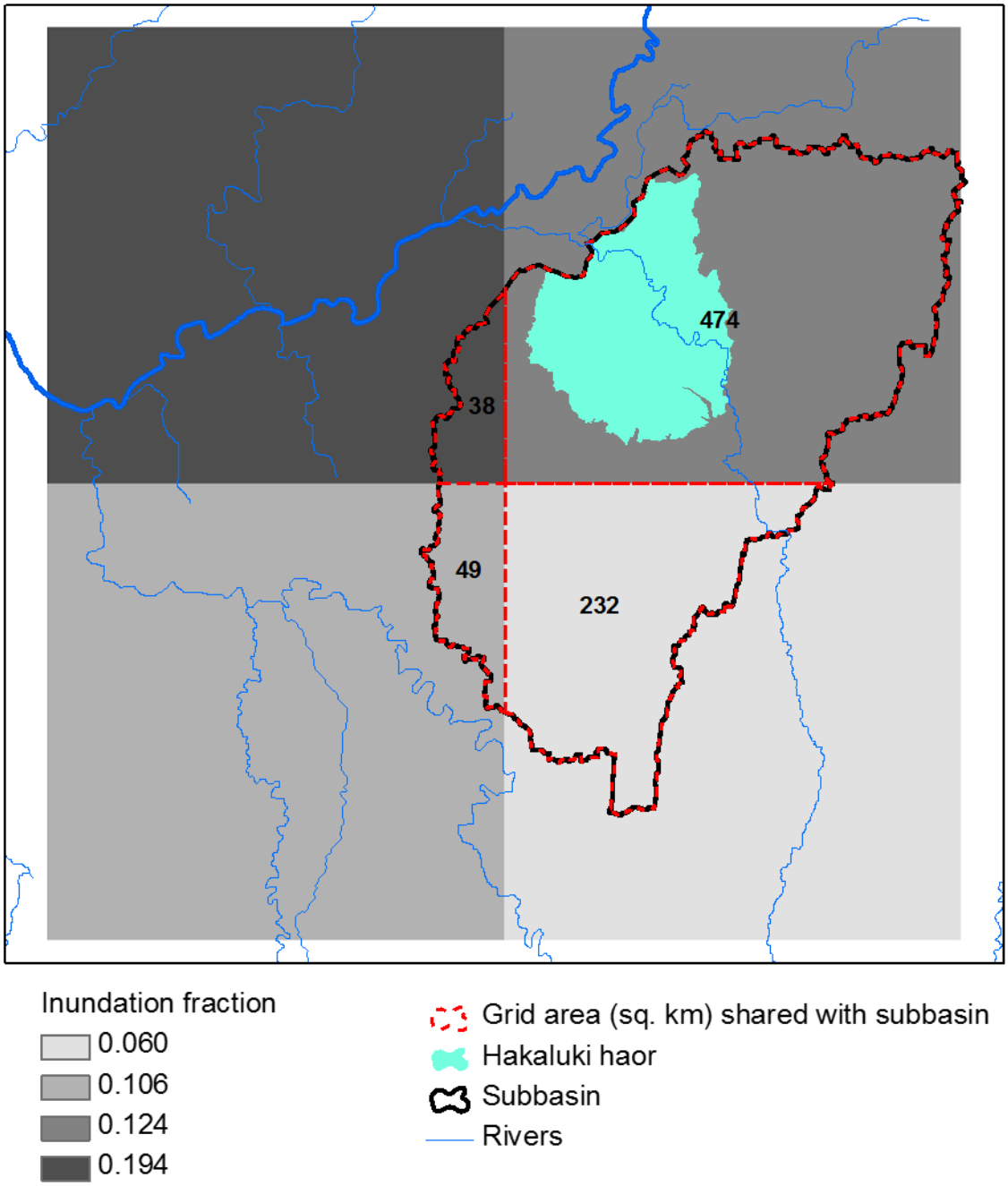

Figure 5.17. MEaSUREs inundation grids lying in the subbasin containing the Hakaluki haor. The numbers on the map represent the corresponding grid area (km^2) shared with the subbasin. This area is multiplied by the corresponding inundation fraction to obtain the respective shared inundated area for each grid.

Figure 5.18 shows the simulated daily time series of water storage, surface area and depth for the Hakaluki haor wetland. In contrast to SWAT, SWATrw results more closely agree with the reported hydrological behaviour of the wetland

(CEGIS, 2012b; Choudhury and Nishat, 2005)). Through the 21 years of the simulation period, the mean value of annual maximum wetland water surface areas modelled by SWATrw was 12464 ha. The wetland flooded eight times to its maximum capacity (13890 ha) during the monsoon seasons (June–September) in seven simulation years (1990, 1991, 1993, 2000, 2001, 2004 and 2006) (Figure 5.18b). This modelled monsoonal maximal water extent is very close to the reported value (14000 ha) of Hakaluki haor wetland. In the dry season (December–March) the SWATrw simulated wetland water surface area shrinks to between 2497 and 4000 ha. This shrinkage range well encapsulates the reported 3525 ha of the existing wetland during dry season. However, SWAT simulated surface areas are always lower than that of SWATrw (Figure 5.18b). According to SWAT, the flooding extent of the wetland reaches a maximum 10000 ha in 1993 and 2001; and the wetland remains almost empty of water during the second half (February and March) of the dry season in all years. These simulated results differ considerably from those reported by Choudhury and Nishat (2005).

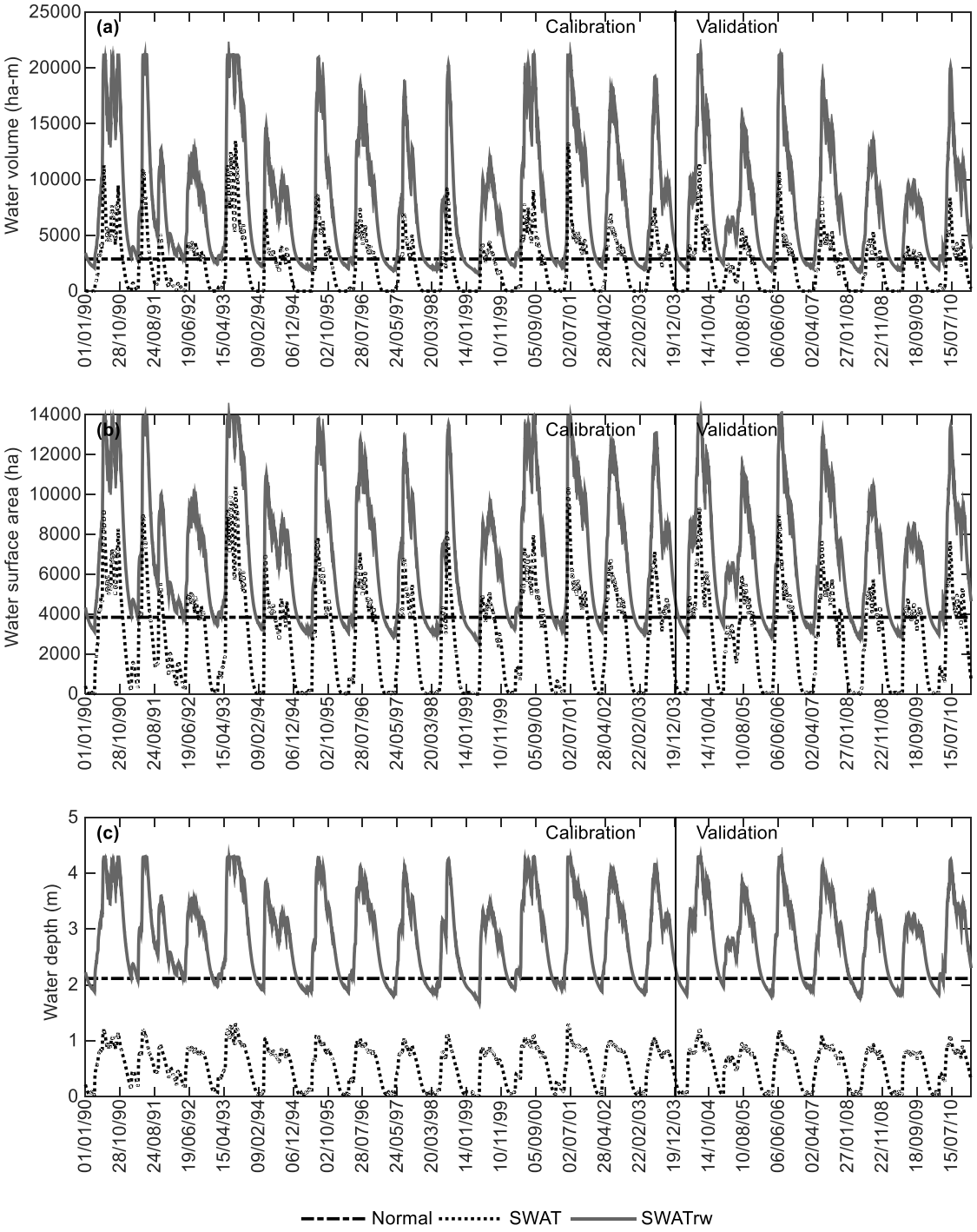

Figure 5.18. Comparison of SWAT and SWATrw simulated time series of different hydrometric properties (e.g., storage, area and depth) for the Hakaluki haor wetland. The “normal” horizontal line indicates the wetland hydrometric properties at the bed level of connecting channel.

A further comparison between 10-day mean simulated water areas during the period of 2002–2009 and corresponding MEaSUREs inundation areas for the

Hakaluki haor is illustrated in Figure 5.19. With respect to MEaSUREs estimations, SWAT consistently underestimates wetland water surface areas whereas SWATrw overestimates monsoonal maximal areal extents (5059–10261 ha) and this trend persists till the following dry season. For dry seasons, a greater variability in 10-day mean water extents is seen in the case of MEaSUREs data (670–7749 ha) compared to that of SWATrw (2991–7400 ha) and SWAT (14–3914 ha). In addition to graphical representation, the goodness of fit between simulated and MEaSUREs 10-day mean wetland water extents was measured with five statistical evaluators (R^2_m, d_r, NSE, RSR and PBIAS). SWATrw shows a closer fit to MEaSUREs in terms of all the five metrics compared to that of SWAT (Table 5.6). The tabulated PBIAS values indicate that the degree of SWAT's average underestimation is about twice the degree of SWATrw's average overestimation.

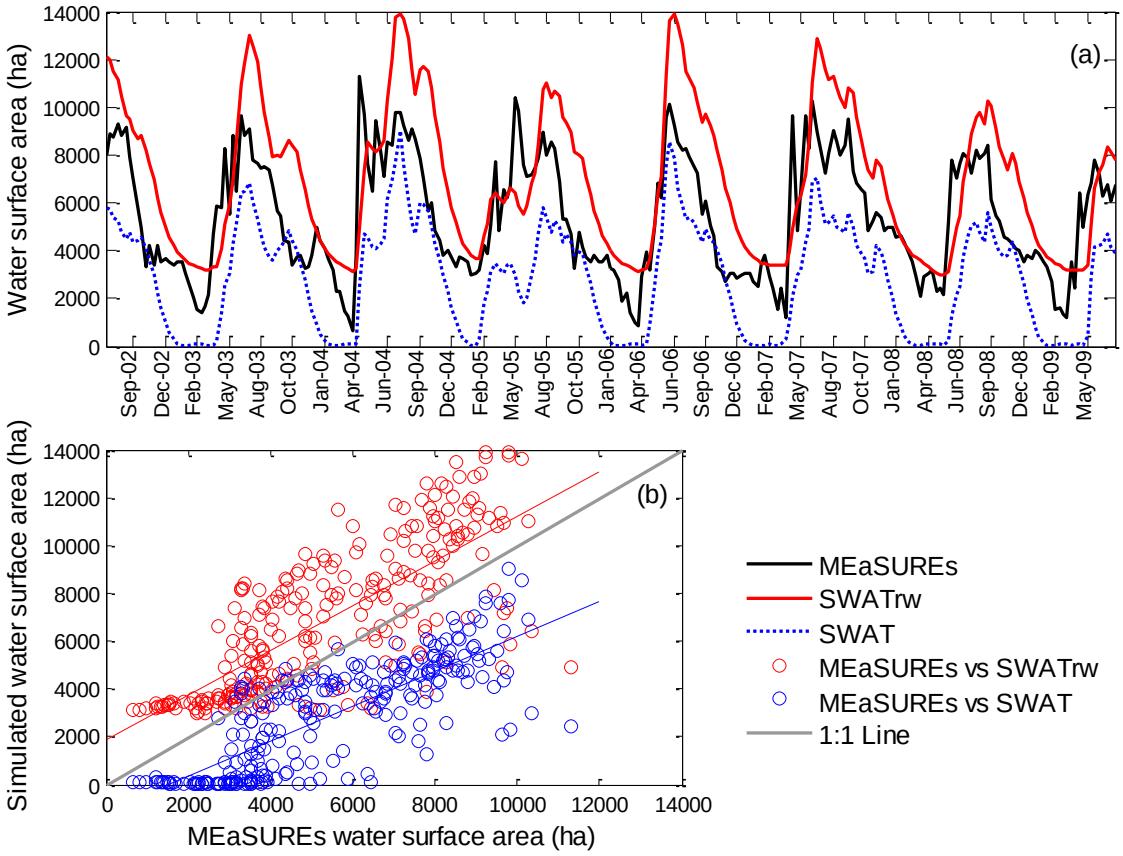

Figure 5.19. Comparison of simulated (SWAT and SWATrw) and MEaSUREs time series of 10-day average water surface areas for the Hakaluki haor wetland.

Table 5.6. Statistical performance of the models in simulating 10-day mean wetland water extents.

Models	Values of performance metrics				
	R^2_m	d_r	NSE	RSR	PBIAS (%)
SWAT	0.46	0.48	-0.48	1.22	47.89
SWATrw	0.54	0.58	0.02	0.99	-26.21

SWAT constantly underestimates wetland water depths during the simulation period (Figure 5.18c). Simulated water depths from this model range from 0.01 m in the dry season to a maximum of 1.3 m in the monsoon season whereas the corresponding values for SWATrw are 1.7 to 4.3 m, respectively, agreeing closely the documented value of 1.55 to 4.26 m (Choudhury and Nishat, 2005).

The improved performance of SWATrw over SWAT in representing hydrological conditions within the Hakaluki haor is linked to more representative volume-area-depth relationships and the inclusion of more realistic wetland-river and wetland-groundwater interactions. The large underestimation of wetland water volume and therefore surface area and depth by SWAT signals two possible shortcomings of SWAT: (i) inadequate incoming flows to the wetland and/or (ii) excessive water loss from the wetland. These two points are elaborated in the subsequent paragraphs.

Figure 5.20a shows daily inflows to the Hakaluki haor generated by both SWAT and SWATrw for the calibration period. The daily inflow comprises upland runoff, interflow and in the case of SWATrw any exchange inflows with the river and groundwater. Results for SWATrw show sudden and short-lived increases in inflows compared to SWAT. For example, SWATrw produces about 100 $m^3 s^{-1}$ more wetland inflows compared to SWAT's 126 $m^3 s^{-1}$ (the dotted line in Figure 5.20a) on 3rd June 1990, the onset of monsoon season. Similarly, the sudden peak inflow of 137 $m^3 s^{-1}$ on 3rd May 2004 (the solid line in Figure 5.20a) is plausibly associated with a pre-monsoonal flash flood event in the wetland due to gains in river stage caused by increased river discharges from the upper subbasins (see Figure 5.4). During this flooding event the wetland expanded by 518 ha from the initial pre-flooding area of 8179 ha (Figure 5.18b). However,

SWAT is completely unable to capture this sudden wetland response to local flash flood. Instead the wetland shrinks to 4652 ha from the pre-flooding area of 4714 ha.

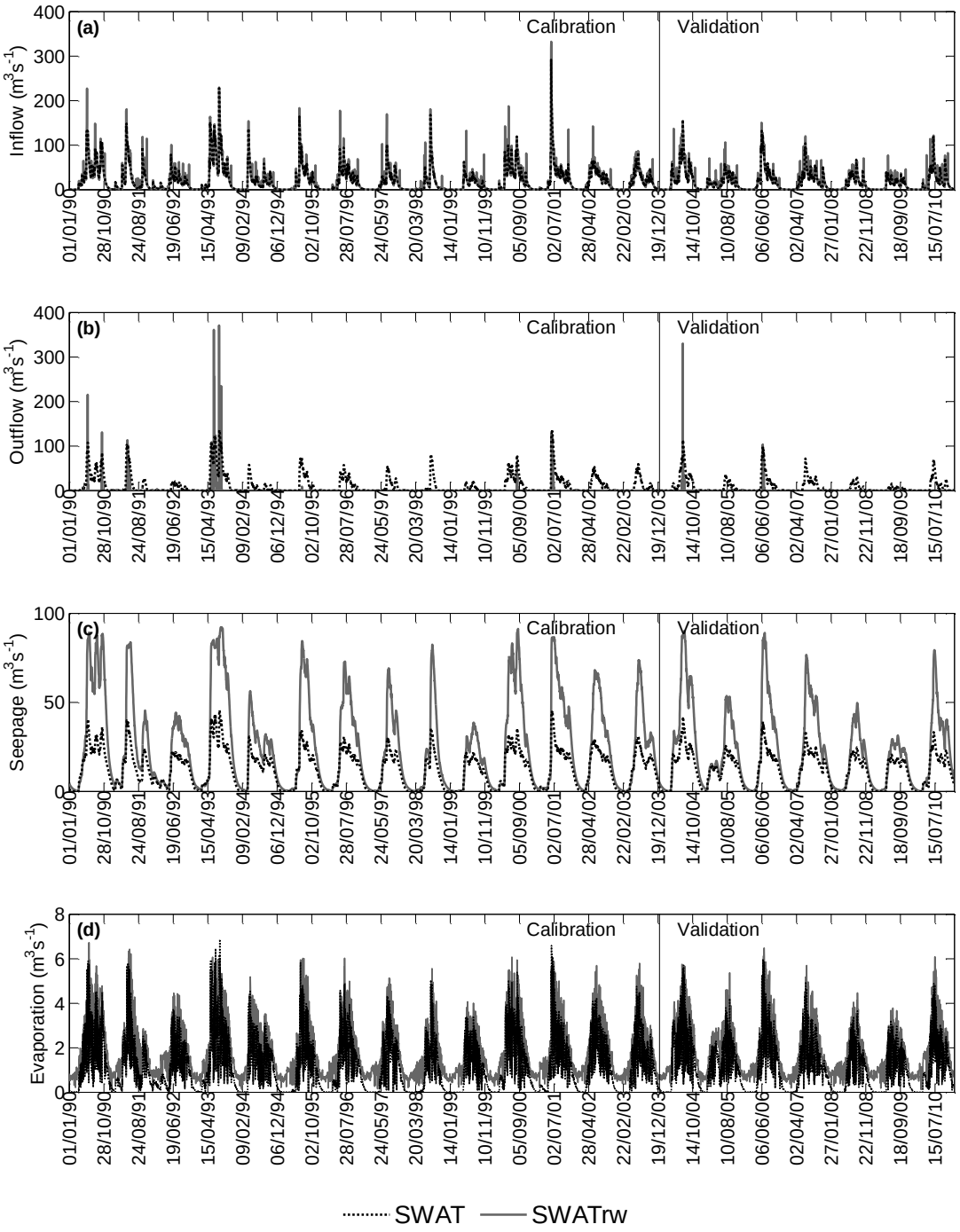

Figure 5.20. Comparison of SWAT and SWATrw simulated daily inflows to, and surface outflows (wetland spillage), seepage and evaporation from the Hakaluki haor wetland. The inflow comprises upland runoff, interflow and in the case of SWATrw any exchange inflows with the river and groundwater. The surface outflow and seepage from a wetland are destined for the adjacent river and aquifer, respectively.

Average annual mass balance analysis of the different hydrological components shows that total inflow to the wetland is 8417 ha-m (9.35%) higher in SWATrw compared to SWAT (Table 5.7). These increased inflows are mainly diverted into the wetland from the River Juri via the connecting channel which is featured in the SWATrw model.

Table 5.7. Annual average values of modelled hydrological components of the Hakaluki haor wetland

Hydrological components	SL. NO.	SWAT	SWATrw
Precipitaiton (ha-m yr^{-1})	(i)	23758	30971
Inflows (ha-m yr^{-1}) from upland, river and aquifer*	(ii)	89844	98261
Evaporation (ha-m yr^{-1})	(iii)	5306	8214
Seepage from wetland (ha-m yr^{-1})	(iv)	57699	115762
Outflows (wetland spillage) to river (ha-m yr^{-1})	(v)	50586	5224
Balance (ha-m yr^{-1}) = (i) + (ii) - (iii) - (iv) - (v)		11	32

* SWAT wetland receives only upland inflows (surface runoff and interflow) but SWATrw wetland receives all the three inflows

Analysis of SWAT's wetland morphometric formula (equation 5.3) shows that the model tends to produce less upland inflows compared to SWATrw for any specific water storage in the wetland. Equation 5.3 cannot conserve the additive principle of surface area adopted in the SWAT model. This principle entails that the total surface area of a subbasin may be fractioned into a number of spatial units (HRUs, see Section 3.2.2) but the combined area of these units must be equal to the subbasin's area. Accordingly, since a wetland is fractioned among the HRUs within a subbasin (see Section 3.2.2), the sum of any specific wetland property (e.g. wetland water volume and surface area) across all the HRUs in a subbasin must be equal to the full-scale (i.e. subbasin-scale) value of the property. For "n" number of HRUs within a subbasin, equation 5.36 can be derived from equation 5.3 based on the areal conservation principle:

$$\frac{A^*_{wet}}{A_{wet}} = \left(\frac{S_{wet,1}}{S_{wet}}\right)^{\alpha} + \left(\frac{S_{wet,2}}{S_{wet}}\right)^{\alpha} + \left(\frac{S_{wet,3}}{S_{wet}}\right)^{\alpha} + \cdots\cdots\cdots + \left(\frac{S_{wet,n}}{S_{wet}}\right)^{\alpha} \quad 5.36$$

$$S_{wet} = S_{wet,1} + S_{wet,2} + S_{wet,3} + \cdots\cdots\cdots + S_{wet,n} \quad 5.37$$

where A^*_{wet} indicates the subbasin-scale total wetland water surface area estimated by summing HRU-scale fractioned wetland areas which is estimated from equation 5.3 for known wetland water storage (S) in each HRU. SWAT applies the value of the scale factor β (see Equation 5.3) derived from subbasin-scale wetland properties (the user specified wetland water volume and surface area at maximum and normal levels) to each of the smaller HRU-scale wetland units in the subbasin. Depending on the nature of the shape factor α in equation 5.28, the following relationships can be established:

$$A^*_{wet} = A_{wet} \ \ if \ \alpha = 1 \quad 5.38$$

$$A^*_{wet} > A_{wet} \ \ if \ \alpha < 1 \quad 5.39$$

$$A^*_{wet} < A_{wet} \ \ if \ \alpha > 1 \quad 5.40$$

Therefore unless the value of shape factor (α) is unity (equation 5.38), the wetland algorithm used in SWAT will overestimate the wetland water surface area for a shape factor value of less than unity (equation 5.39) and underestimate the areas if the shape factor is larger than unity (equation 5.40). In the current SWAT model the maximum value of the shape factor is 0.9 and for the Hakaluki haor the estimated shape factor was found to be 0.65. Consequently, for a given volume of water stored in a wetland, the surface area estimated by SWAT would be unrealistically high and exceed that estimated by SWATrw, which does not suffer from this limitation. An overestimated wetland water surface area reduces its upland catchment area and thus upland inflows are also reduced (see equation 5.2). On the other hand, the three vertical hydrological processes (precipitation, evaporation and seepage) that are quantified based on wetland water surface area, are likely to be overestimated by the SWAT model. However, these overestimating (precipitation, evaporation and seepage) and underestimating (upland inflows) phenomena associated with SWAT are not apparent in results

for the Hakaluki haor wetland (Table 5.7, Figure 5.20c and Figure 5.20d) when compared with the results from SWATrw. The reason is that SWATrw consistently simulates larger volumes of water (Figure 5.18a), thus larger water surface area (Figure 5.18b), compared to SWAT throughout the entire simulation period.

According to Figure 5.20b, the Hakaluki haor wetland simulated by SWAT starts to spill at some time between the end of the pre-monsoon season (last fortnight of May) and the onset of monsoon season (June). The resultant hydrographs from this spilling wetland cease at the end of post-monsoon season (November) and generally look like a typical free-flow river hydrograph. The outflow during the wetland spilling period ranges between 0.5 and 136 $m^3 s^{-1}$. On the other hand, wetland outflows from the SWATrw model happens in the monsoon or early post-monsoon season of years 1990, 1991, 1993, 2000, 2001, 2004 and 2006. The outflow hydrographs are very flashy with dramatic, rapid increases which differs from those projected by SWAT. Peak outflows can be up to 372 $m^3 s^{-1}$. On average SWAT produces annual outflows which are 9.60 times larger than those (5224 ha-m yr^{-1}) simulated by SWATrw (Table 5.7). In SWAT, the wetland water level is above the normal volume level (threshold value required to initiate wetland spills) during the monsoon and post-season season (Figure 5.18a) and so continuously discharges to the river. Within SWATrw, although the wetland water level did exceed the normal level for a considerable period in most years (Figure 5.18c), flows to the river were restricted. This was because for most of the time the hydraulic head gradient between river and wetland was such that water was simulated as entering rather than leaving the wetland.

As discussed in Section 5.4.3, SWAT adopts a very simple GW model where any recharge from the upper soil profile of an HRU is homogeneously accommodated in the underlying aquifer reservoir. In addition, since HRUs within a subbasin are isolated from each other they do not exchange mass. Therefore, simulated horizontal GWLs (groundwater level) are just an approximation of reality where natural GWL follows a curvilinear phreatic line while interacting with wetlands and rivers. Figure 5.21 shows simulated GWLs from both SWAT and SWATrw for the largest HRU (Area = 30448 ha; land use: Rice; soil: Cambisols, slope: 0 to 2%) in the subbasin containing the Hakaluki haor. This HRU contains the properties

of the areas around the groundwater observation well in the haor (see Figure 5.4). Observed GWL data from this well that are referenced with respect to the wetland bed are also shown. The groundwater observation well is approximately 5 km away from the deepest point of the wetland and the elevation of ground surface at the well site is 7 m above the wetland's deepest point. The two models produce very similar GWL results although they are slightly higher (0.03–0.16 m) for SWATrw. Clearly and expectedly, HRU averaged GWLs do not reflect the actual fluctuations (difference between highest and lowest GWLs in a year) of daily GWLs in a year which range from 0.64 m (Highest GWL_h = 5.93, Lowest GWL_l = 5.93) in 1995 to 3.2 m (Highest GWL_h = 6.48, Lowest GWL_l = 3.2) in 1990. On the other hand, SWAT produces the lowest annual GWL fluctuation of 0.10 m (Highest GWL_h = 1.91, Lowest GWL_l = 1.81) in 1992 and the highest fluctuation of 0.51 m (Highest GWL_h = 2.08, Lowest GWL_l = 1.57) in 2010. SWATrw produces similar results but GWLs are slightly elevated. Moreover, neither of the models can capture the declining trend in observed GWLs. One of the potential reasons of these limitations may be that both models assume that any change in aquifer water level due to recharge or discharge during a time step is uniform throughout the entire areal extent (equalled to HRU area) of the aquifer. This approach ignores the influence of local factors surrounding an observation well on GWLs. Where GW flow is dominated by its horizontal component frictional head loss can be an important factor in GWL fluctuations. For the present study, the fluctuations in observed GWLs might be affected by local groundwater drawdowns originated after shallow tube well (STW) operations during the dry season. Neither of the models (SWAT and SWATrw) is able to replicate such local drawdown effects on GWLs.

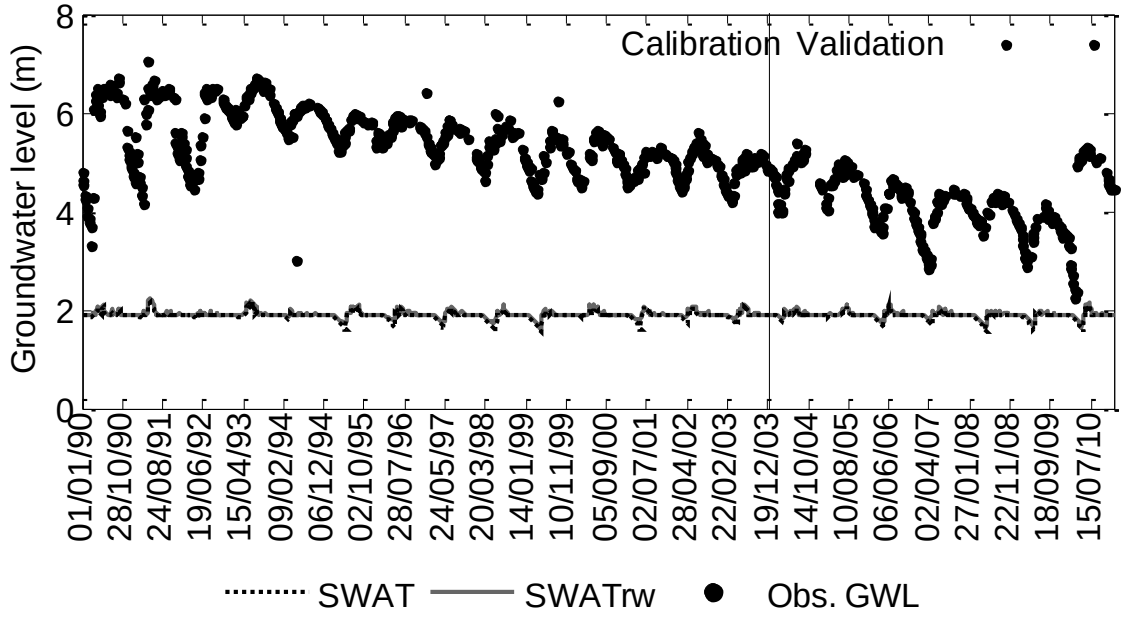

Figure 5.21. Comparison of simulated groundwater levels (GWL) for the dominant HRU (Land use: Rice; soil: Cambisols, slope: 0 to 2%) and observed GWLs. GWL is referenced from the wetland bottom i.e. wetland bottom is set to zero datum and observed GWLs is obtained from an observation well about five km apart from the deepest wetland bottom. The “normal” horizontal line indicates the wetland hydrometric properties at the bed level of connecting channel.

Since the falling wetland water levels (Figure 5.18c) after the monsoonal peaks gradually approach an equilibrium condition with the lower aquifer water levels (Figure 5.21) until the beginning of the next pre-monsoon season, the SWATrw model always retains some water in the wetland due to a slower downward seepage rate. The slight decline in wetland water level (Figure 5.18c) during the dry season is controlled by evaporation (mean rate = 6.91 ha-m day^{-1} or 0.8 $m^3 s^{-1}$) and seepage (mean rate = 34.5 ha-m day^{-1} or 4.0 $m^3 s^{-1}$). However, the dry conditions (i.e. absence of water) within the wetland between December and until the return of rainfall in the next pre-monsoon season (April–May) that are simulated by SWAT lead to the elimination of evaporation and seepage at this time. Despite reproducing almost similar GWL, SWAT was not able to simulate the actual hydrological characteristics of the wetland since it completely ignores the principles of hydraulics for modelling wetland-groundwater interaction. The hydraulic gradient independent groundwater scheme of SWAT allows a wetland

to seep water at a constant rate until it is empty. In the case of the Hakaluki haor, this results in the complete drying out of the wetland that is not experienced in reality and which SWATrw avoids by preventing unrealistic wetland water loss through seepage.

Annual analysis of hydrological components shows that the SWATrw-simulated Hakaluki haor annually receives 8417 ha-m more water as inflow that mainly comes from direct additional precipitation falling on the larger wetland and from the over flowing river (Table 5.7). The ratios of three average annual wetland outflows (evaporation, seepage and spilling) are 1:11:10 and 2:22:1 for SWAT and SWATrw respectively. This finding demonstrates a considerable change in the distribution of the wetland seepage and spilling between the two models. Therefore, this study suggests using the more skilled SWATrw in estimating wetland water dynamics, particularly those that are highly interactive with rivers and shallow aquifers, would drastically reduce the model uncertainties involved with SWAT when it comes the applications in which riparian wetlands are important hydrological components of river basins.

5.7. Summary

The SWATrw model addresses two crucial issues in modelling water dynamics of depressional riparian wetlands with SWAT: (i) the unrealistic representation of real world wetland morphometric (volume-area-depth) relationships and (ii) the unidirectional interaction of wetlands with rivers and groundwater/aquifers. The SWATrw model replaces SWAT's wetland morphometric algorithm with the more robust and tested H-K wetland geometric formula. Wetland-river and wetland-groundwater interactions are re-structured based on the principles of hydraulics without violating the mass conservation law. Therefore, the SWATrw model is more physics-based concerning the representation of the direction of wetland interactions with other water bodies (rivers and aquifers) and in the quantification of these interactions. The case study of the Barak-Kushiyara River Basin shows that SWATrw model is more skilful in representing different hydrological processes occurring within haor wetlands and thus wetland-river-aquifer

interactions compared to SWAT. Therefore, this improved version SWATrw was employed for the remaining part of the UMRB which is detailed in Chapter 6.

Chapter 6

Development of a SWATrw model for the wider UMRB

6.1. Introduction

It has been demonstrated that the SWATrw model provides superior simulation performance for the haor wetlands in the Barak-Kushiyara River Basin (Chapter 5). The model, as opposed to the model developed using the original SWAT, was therefore employed for the rest of the UMRB (Figure 6.1). The discussion of the significance of the calibrated parameters for the Barak-Kushiyara River Basin (see Section 5.6.2) is equally applicable for the rest of the UMRB.

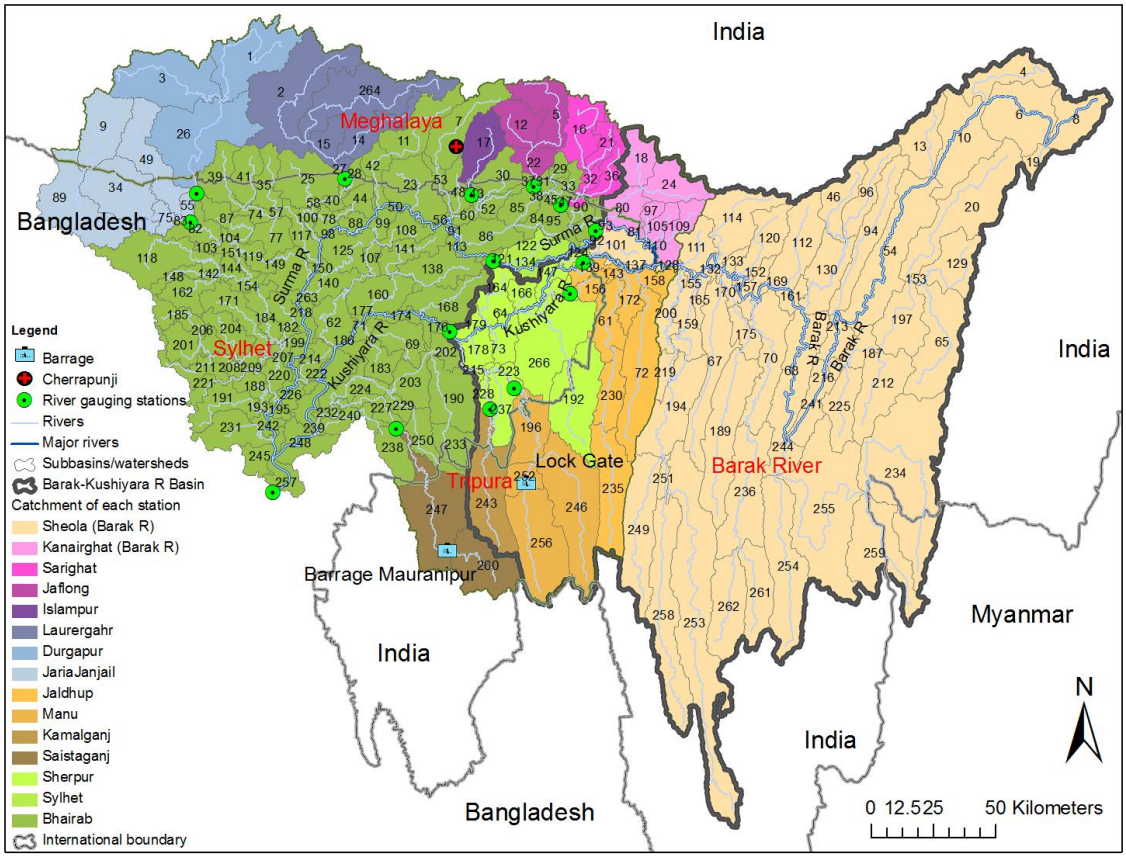

Figure 6.1. Rivers and subbasins of the UMRB after delineation. The catchment area drained by each of 15 gauging stations is portrayed with a unique colour. While illustrating this map, for a downstream station, its catchment area excludes the catchment areas of any existing upstream stations. This is because just to better show the areal extent of a catchment drained by a particular station, although in modelling the catchment area of a downstream station means the sum of all its upstream catchments.

The building process of the model was as same as discussed in Section 5.5.2 for the Barak-Kushiyara River Basin. Basin delineation discretizes the whole UMRB into 267 subbasins (Figure 6.1) and 1237 HRUs for the same threshold values of land use, soil and slope described in Section 5.5.2. There were total 119 subbasins that contain haor wetlands; therefore, required inputs for each wetland were prepared according to the process previously detailed (see Section 5.5.2). Although the two upstream dams (Figure 6.1), Lock Gate across the River Manu and Mauranipur Barrage across the River Khowai, are present in the basin, they are not modelled due to lack of dam operation details (e.g., opening and closing time, release rate).

Table 6.1 shows the values of calibrated parameters for the UMRB less the Barak-Kushiyara River Basin since its calibrated parameters have already been provided in Table 5.2 and discussed in Section 5.6.2. The values of the calibrated parameters for the nine catchments of their corresponding stations (Sarighat, Jaflong, Islampur, Laurergahr, Durgapur, JariaJanjail, Saistaganj, Sylhet and Bhairab) are clustered into five catchment groups depending on catchment topography and rainfall (see Table 6.1). For instance, catchments drained by Sarighat, Jaflong and Islampur are very steep sloped and fall in the rainiest zone of the basin. Unlike other catchments, heavy rainfall (annual rainfall range 4800–8500 mm) receiving steep sloped catchments (e.g. Sarighat, Jaflong, Islampur, Laurergahr and Durgapur) in the Meghalaya region were assigned larger CN2 values in order to match observed flows by generating enough surface runoff at their gauging stations.

Table 6.1. Calibrated parameters governing hydrological processes in the UMRB excluding the previously calibrated Barak-Kushiyara River Basin (Table 5.2)

Parameters (Unit)	Default values	Calibrated values				
		Sarighat, Jaflong and Islampur	Laurergahr	Durgapur and JariaJanjail	Saistaganj	Sylhet and Bhairab
HRU level						
CN2	70-92	75 - 95	75 - 80	47 - 92	55 - 71	65 - 81
ESCO	0.95	0.95	0.00	0.95	0.95	0.95
EPCO	1.00	0.1 – 1.0	1.0	1.0	1.0	0.0 – 1.0
GW_DELAY (day)	31	31	1	31	61	31
ALPHA_BF (day)	0.048	0.01 - 0.7	0.048 - 0.70	0.048 - 0.70	0.01-0.011	0.01-0.7
SHALLST (mm)	0.50	0.5 - 1520	0.05 - 1520	0.05-1520	0.0-0.5	1500-1520
GWQMN (mm)	0.00	0.0-1480	1000	0.0-1480	0.0	1480
REVAPMN (mm)	1.00	1.0-2000	1-1000	1.0-1000	1.0	1000-2000
RCHRG_DP	0.05	0.0-0.05	0.5	0.0	0.4-0.7	0.0-0.1
GW_SPYLD	0.003	0.003-0.02	0.003-0.02	0.003-0.02	0.003	0.003-0.02
Subbasin level						
CH_N2	0.014	0.014	0.014	0.01	0.014	0.06-0.014
TRANS_AMT				0.4		
WET_FR	-	-	-	-	-	0.81-1.00
WET_MXSA (ha)	-	-	-	-	-	5-29509
WET_DXM (m)	-	-	-	-	-	3-5
WET_D (m)	-	-	-	-	-	1
WET_P	-	-	-	-	-	0.9-1.20
WET_TH (m)	-	-	-	-	-	1.0
CCH_M	-	-	-	-	-	
CCH_N	-	-	-	-	-	
CCH_SF	-	-	-	-	-	
CCH_DFR	-	-	-	-	-	0.5-0.8
CCH_LFR	-	-	-	-	-	0.1
CCH_C (m^{-1} s^{-1})	-	-	-	-	-	
WETEVCOEF	-	-	-	-	-	0.7
WET_K (mm/hr)	-	-	-	-	-	0.3-8
Basin level						
SURLAG	4.0	0.1	0.1	0.1	0.1	0.1

6.2. Streamflow simulation performances of SWATrw for the wider UMRB

The model's performance in reproducing monthly flows at the nine gauging stations beyond the Barak-Kushiyara River Basin (Figure 6.1) are discussed here (performance at the remaining six stations within the Barak-Kushiyara River Basin were discussed in Section 5.6.4). For the calibration period, the model captures the monthly flows at Sarighat station on the River Sari-Gowain as indicated by the reasonable values of the statistical indicators (Table 6.2) as well as by graphical representation (Figure 6.2a). For the validation period, on the

other hand, the model's consistent under-prediction of observed flows (PBIAS = 51.22%) in all but dry season months leads to unsatisfactory results. The greater residuals for higher observed flows in Figure 6.2c are from the validation period (red colored circles). Underestimated flows at Sarighat during the validation period are likely due to unrealistically low rainfall in its catchment that comprises five subbasins (subbasins 16, 21, 32, 36 and 47 inFigure 6.2). All these subbasins receive rainfalls from the pJaintaH station (see Figure 4.7), a station from the IMDdist database, whose mean annual rainfall is 4166 mm. In contrast, the average annual rainfall for these subbasins is 5283 mm during the calibration period when the model uses IMDgrid rainfall. Therefore, a substantial potential shortfall in input rainfall during the validation period is thought to be the prime cause of model's underestimated flows. Investigation of daily streamflow time series reveals that the model commonly underestimates spontaneous peak observed flows but overestimates the flows during recession period of the hydrographs (Figure 6.2).

Table 6.2. Statistical performance metrics for SWATrw simulated monthly streamflows during calibration (1990–2003) and validation (2004–2010) periods for the nine stations below the Barak-Kushiyara River Basin

Variables	Gauging stations	Period	Values of performance indicators								Remarks[2]
			NSE	NSE_m	RSR	R^2	R^2_m	PBIAS (%)	d	d_r	
Mean monthly streamflow ($m^3 s^{-1}$)	Sarighat	Calibration	0.84	0.70	0.40	0.85	0.80	6.60	0.96	0.85	VG
		Validation	0.33	0.39	0.82	0.61	0.26	51.22	0.75	0.69	US
	Jaflong	Calibration	0.89	0.73	0.32	0.90	0.83	2.68	0.97	0.86	VG
		Validation	0.90	0.74	0.31	0.91	0.80	7.51	0.97	0.87	VG
	Islampur	Calibration	0.75	0.66	0.50	0.77	0.52	13.12	0.92	0.83	G
		Validation	0.61	0.43	0.62	0.84	0.51	42.15	0.86	0.72	US
	Laurergahr	Calibration	0.61	0.48	0.62	0.70	0.66	-5.80	0.91	0.74	S
		Validation	0.90	0.71	0.32	0.91	0.83	9.03	0.97	0.85	VG
	Durgapur	Calibration	0.83	0.64	0.41	0.86	0.64	12.38	0.95	0.82	G
		Validation	-	-	-	-	-	-	-	-	-
	JariaJanjail	Calibration	0.77	0.67	0.48	0.82	0.82	-9.30	0.95	0.84	VG
		Validation	0.54	0.44	0.68	0.71	0.69	-31.59	0.90	0.72	US
	Saistaganj	Calibration	0.43	0.16	0.76	0.60	0.42	-37.88	0.83	0.58	US
		Validation	0.05	0.09	0.98	0.43	0.32	17.84	0.77	0.55	US
	Sylhet	Calibration	0.85	0.70	0.39	0.89	0.85	-11.03	0.97	0.85	G
		Validation	0.90	0.78	0.31	0.90	0.83	1.91	0.97	0.89	VG
	Bhairab	Calibration	0.70	0.45	0.55	0.83	0.76	15.97	0.93	0.73	S
		Validation	0.14	0.05	0.93	0.71	0.53	5.85	0.86	0.53	US

[2] VG=Very Good, G=Good, S=satisfactory, and US=Unsatisfactory

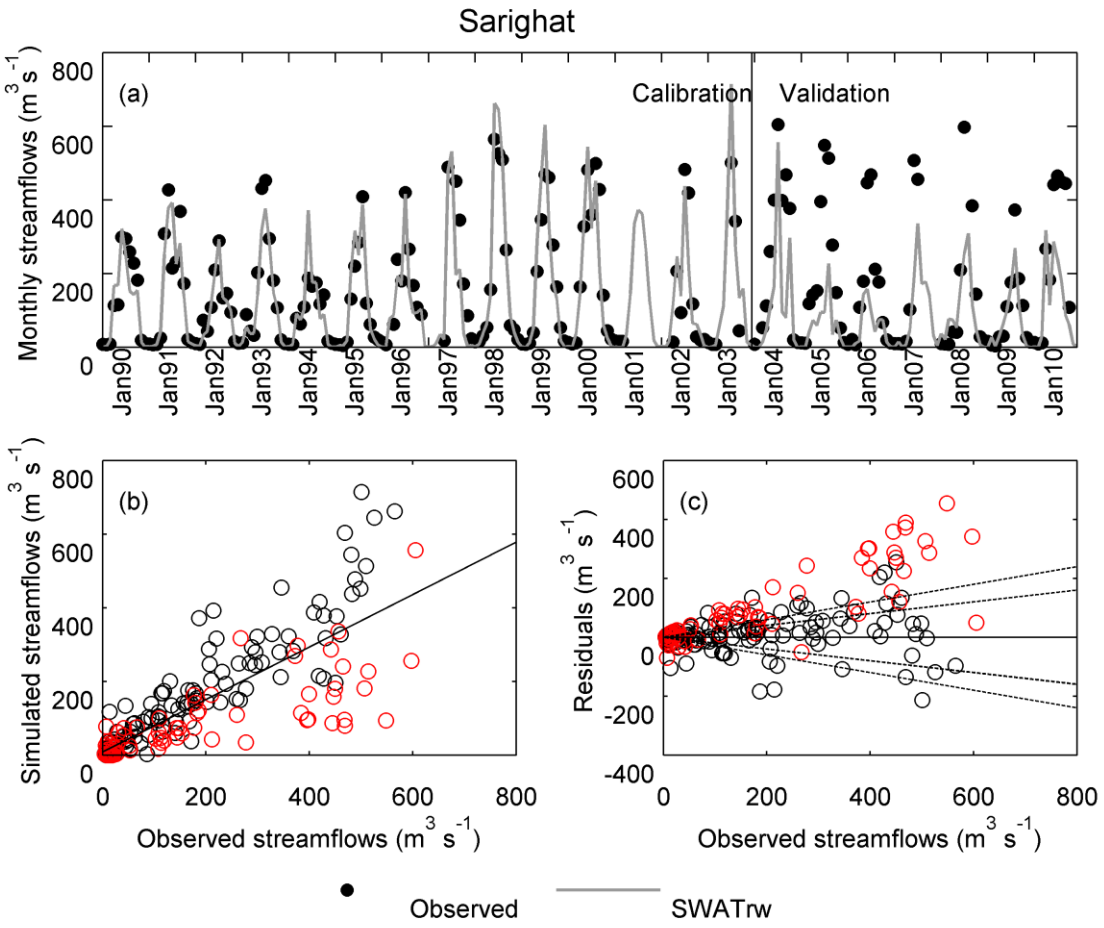

Figure 6.2. Graphical comparison of observed and SWATrw simulated mean monthly streamflows at Sarighat on the Sari-Gowain River. The black and red circles in subplots b and c are respectively for the calibration and validation periods.

The model shows an excellent simulation ability at Jaflong on the Piyan River although observed discharge records are limited both in the calibration and validation periods (Figure 6.3 and Table 6.2). Although a good fit is achieved during the calibration period at the Islampur station on the River Dhala (Figure 6.4), unsatisfactory results are obtained for the validation period (Table 6.2). Poor performance at this station is possibly also due to unrealistic input rainfall data. The mean annual rainfall of the Dhala River catchment at Islampur (subbasin number 17 in Figure 6.1) is 8327 mm during calibration and 7133 mm during the validation period. The catchment receives rainfall from the pIMDgrid4(t) gauging

station (see Figure 4.7) that is 30 km away from Cherrapunji. Since this catchment is very close (<10 km) to Cherrapunji, the rainiest place on the Earth (rainfall ~11,500 mm yr^{-1}), using a very accurate and high spatio-temporal resolution rainfall data may improve the model's performance.

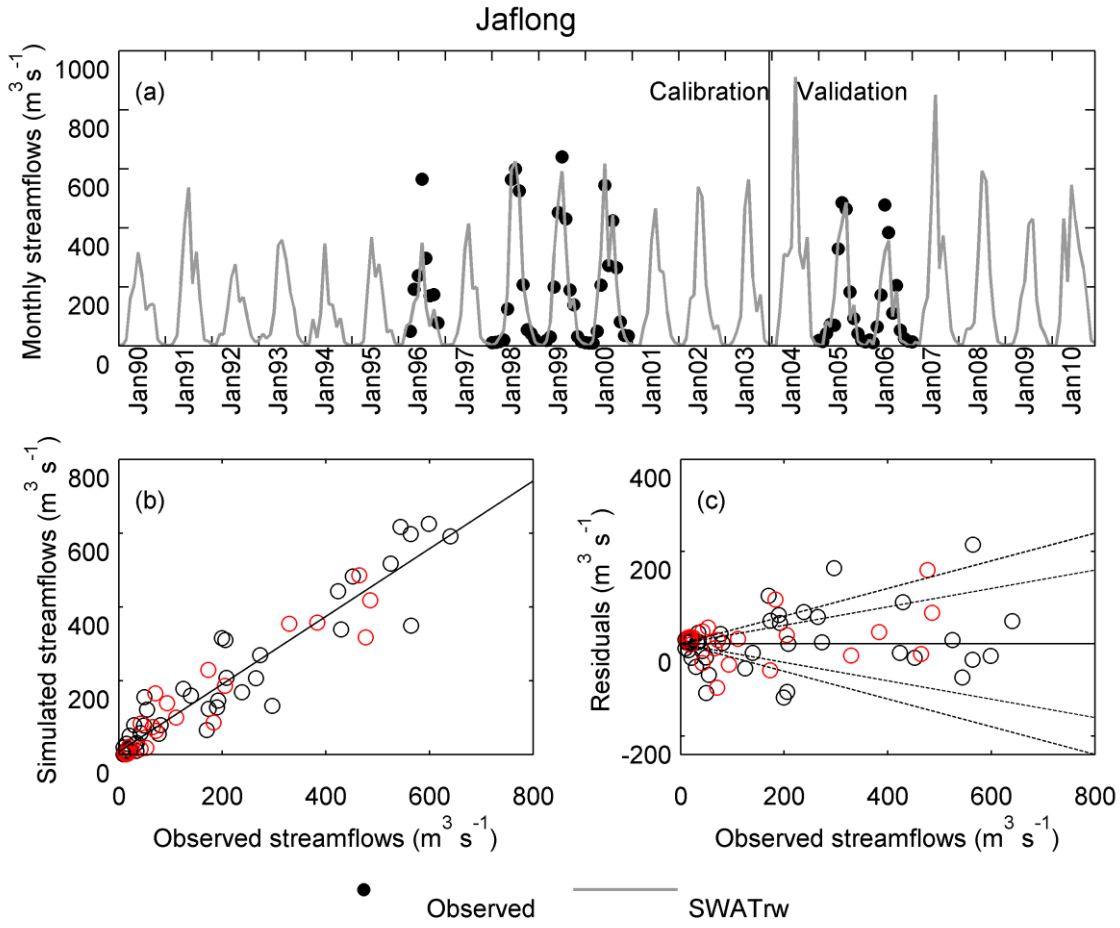

Figure 6.3. Graphical comparison of observed and SWATrw simulated mean monthly streamflows at Jaflong. The black and red circles in Figure 6.3b and Figure 6.3c are respectively for the calibration and validation periods.

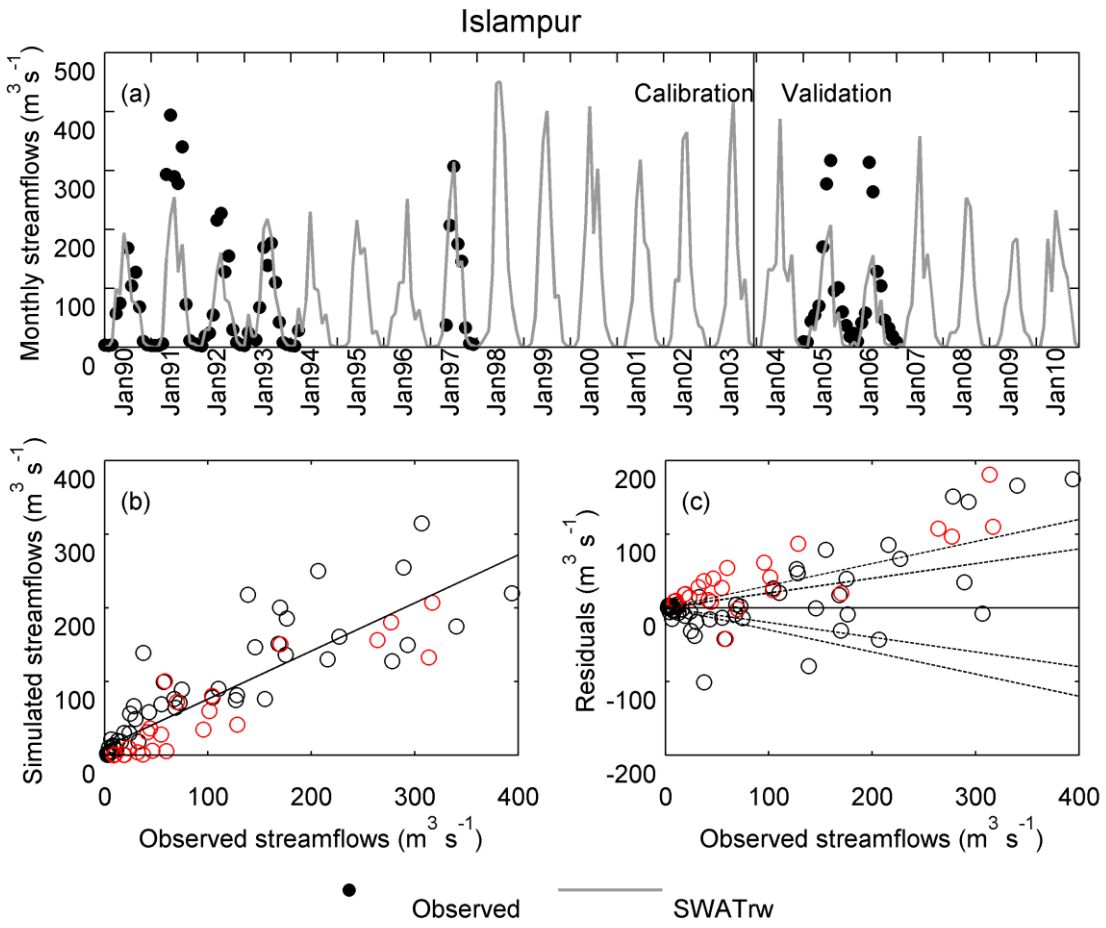

Figure 6.4. Graphical comparison of observed and SWATrw simulated mean monthly streamflows at Islampur on the river Dhala. The black and red circles in Figure 6.4b and Figure 6.4c are respectively for the calibration and validation periods.

Mass balance analysis of the three steep sloped catchments (Sarighat, Jaflong and Islampur) reveals that about 74–92% of annual rainfall (4166–8327 mm) can be converted into total water yield (sum of surface runoff, lateral flow, base flow/groundwater flow). This high water yield potential of the catchments lying in the basin's rainiest zone will have a considerable influence on the flooding process in the downstream Sylhet Basin.

The model showed 'satisfactory' and 'very good' performances in simulating monthly streamflows of Jadukata River at the Laurergahr gauging station for both the calibration and validation periods, respectively (see Table 6.2 and Figure 6.5).

In common with other steep sloped catchments in the Meghalaya Basin, the Laurergahr catchment responds to rainfall very rapidly, although such rapid responses cannot be seen in the time series plot of monthly average discharge due to levelling out of fluctuations in the time series of the original simulated daily flow data. The present simulation performance was achieved by transferring 50% of the annual shallow aquifer water (1483–1600 mm) to the underlying deep aquifer system of the model. Water entering the deep aquifer system of the model does not have any influence on the hydrological cycle unless that water is pumped back to the land surface. Without depleting the shallow aquifer in this way, the model constantly overestimated observed flows throughout the simulation period. There are two possible reasons why the calibrated model required this large removal of water from the surface water system (i) higher input rainfall compared to the real situation, and (ii) the aquifers of the catchment poorly interact with the river system, instead having stronger interactions with outer boundary aquifers and/rivers; therefore, despite huge recharge (24–30% of annual rainfall) to the aquifer no direct response in surface flow is evident. The weaker performance in the calibration period can be linked to the higher rainfall (~1700 mm per year) compared to the validation period. The catchment converts 83% of mean annual rainfall (6556 mm) to water yield (SURQ:GWQ:LATQ = 5:1:1) for the calibration period; the corresponding value of water yield (SURQ:GWQ:LATQ = 3:1:1) for the validation period is 77% of mean annual rainfall (4862 mm).

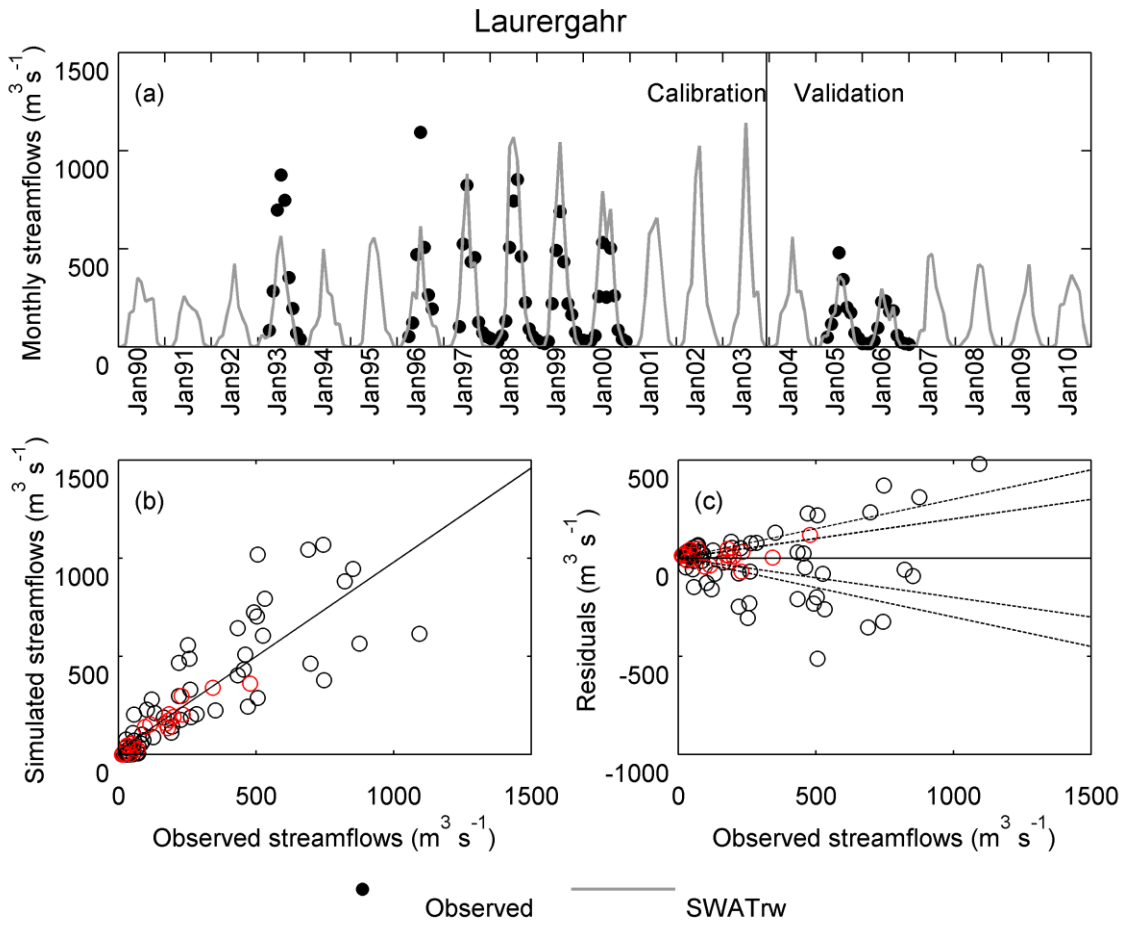

Figure 6.5. Graphical comparison of observed and SWATrw simulated mean monthly streamflows at Laurergahr on the river Jadukata. The black and red circles in Figure 6.5b and Figure 6.5c are respectively for the calibration and validation periods.

At the Durgapur gauging station, there was no observed discharge record for the River Someshwari for the validation period. For the calibration period the model showed 'good' performance (Table 6.2). Overall underestimation of observed flows, as reflected by positive PBIAS (12.38%), can be attributed to the model's inability to capture some of highest peak flows (Figure 6.6a and Figure 6.6c). One potential source of uncertainty with the model results may arise from the way distributaries are represented. The Someshwari River branches into two upstream of the Durgapur station. In the model, the river in subbasin-55 (Figure 6.1) represents the parent Someshwari River and that in subbsin-87 represent the distributary of the river. While calibrating the model, therefore, a value of 0.4

for the TRANS_AM parameter (see Table 6.1) was found to provide the best agreement with observed flows at Durgapur. This implies that 40% of Someshwari river's flow is diverted into its downstream distributary and remaining 60% follows through the Durgapur station on the main river. This diversion was allowed during the high flow period of April–October. This fixed flow proportion, which is required within the model, does not enable changes in the distribution of flows according to discharge magnitude.

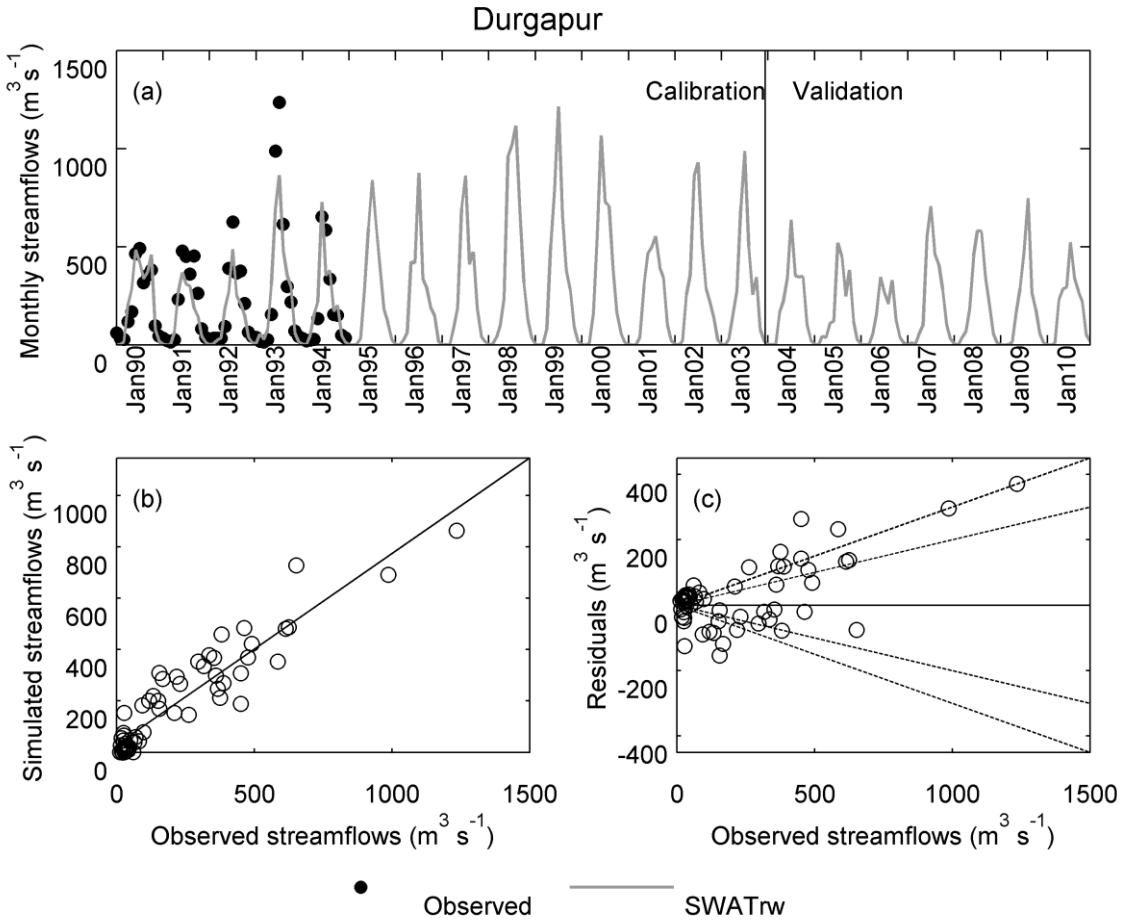

Figure 6.6. Graphical comparison of observed and SWATrw simulated mean monthly streamflows at Durgapur on the river Someshwari.

The model's performance was graded as 'very good' and 'unsatisfactory' in simulating flows of Boghai-Kangsa River system at the JariaJanjail gauging station during the calibration and validation periods, respectively (Table 6.2). Most of residual flows in the calibration period fall in the 20% residual boundary

and their distribution seems random i.e. they do not follow any specific trend. Such conditions affirm the reliability of the model. Moreover, about half of the JariaJanjail catchment area (i.e. total area drained through the JariaJanjail station) is occupied by the upstream catchment of Durgapur. For this reason, simulation behavior of the model at JariaJanjail can be partly explained by the previous discussion of the results for the Durgapur station. Nonetheless, the model overestimates the observed flows in the last three years (2008–2010) of the validation period (Figure 6.7a) which is responsible for model's overall poor performance during validation.

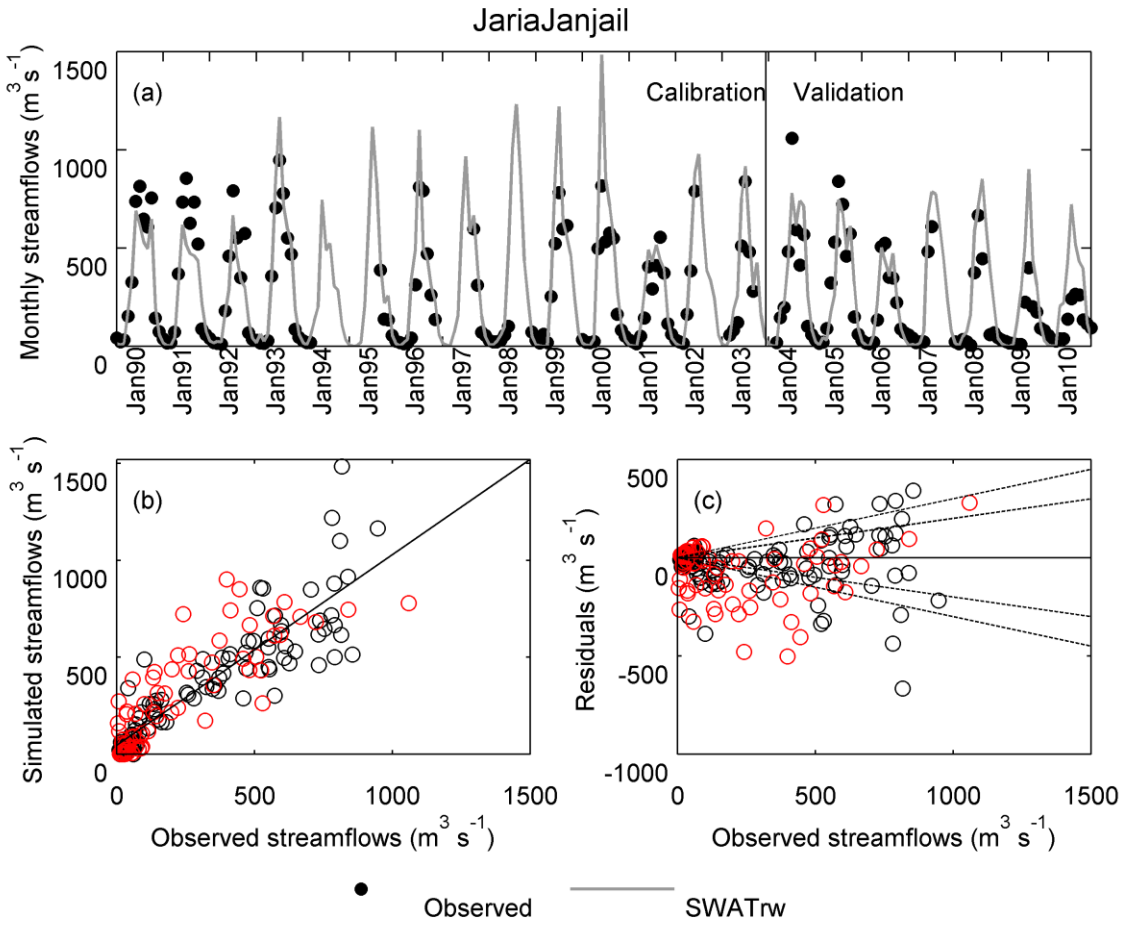

Figure 6.7. Graphical comparison of observed and SWATrw simulated mean monthly streamflows at JariaJanjail on the river Boghai-Kangsa. The black and red circles in Figure 6.7b and Figure 6.7c are respectively for the calibration and validation periods.

Like Kamalganj (see Section 5.6.4), the model produces unsatisfactory results for the Saistaganj station for both calibration (NSE = 0.43, RSR = 0.76, PBIAS = -37.88%) and validation (NSE = 0.05, RSR = 0.98, PBIAS = 17.84%) periods. The poor performance originates from over- and under-estimated observed flows during the calibration and validation periods, respectively. This is evident both in PBIAS values and in Figure 6.8. As argued for Kamalganj, the majority of discrepancies between modelled and observed flows are seen during the recession period of the annual hydrograph (Figure 6.8). The model respectively transfers 67% and 54% of mean annual rainfalls to the upper shallow aquifer system in the calibration (2654 mm) and validation (2079 mm) periods. Subsequently 54% of annual shallow aquifer water (1781 mm for calibration and 1130 mm for validation) is transferred to the deep aquifer system. As discussed for Laurergahr, no water in the deep aquifer system is used for consumptive purpose (e.g. pumping for irrigation) and is effectively removed from subsequent hydrological processes (e.g. groundwater flow between neighbouring subbasins). Therefore, such a modelled deep aquifer is represented as having unlimited water storage capacity which is contradictory to reality. Ignoring the effects of the upstream Mauranipur Barrage (Figure 6.1) on the catchment's hydrology might partly be responsible for the model's unrealistic water balance. This barrage controls 36% (area) of the catchment's hydrology. This is a drought prone area (Datta, 2010) and the barrage is used to store runoff for local consumptive uses (irrigation, house hold etc). Moreover, in the absence of information, no consumptive uses are modelled throughout the catchment. If consumptive use of catchment water had been modelled, the performance of the model might have been improved further.

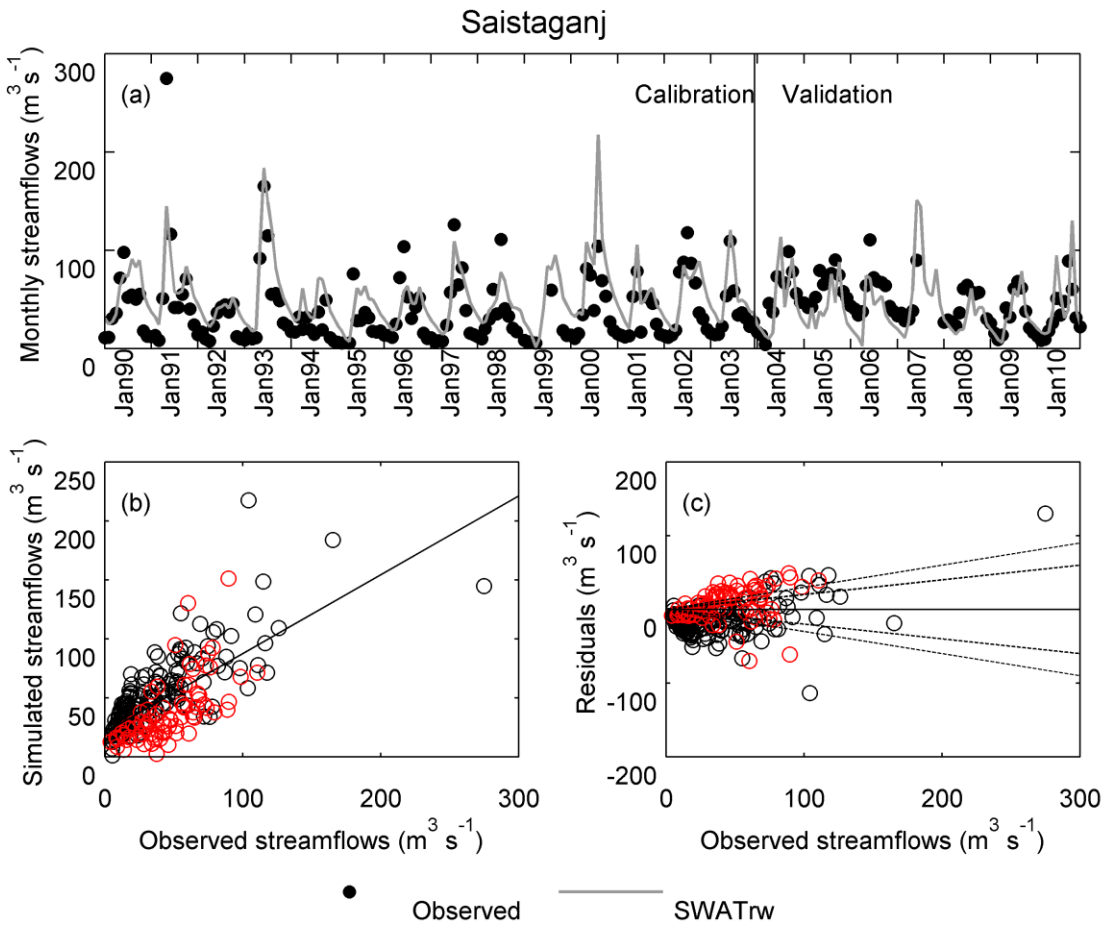

Figure 6.8. Graphical comparison of observed and SWATrw simulated mean monthly streamflows at Saistaganj on the river Khowai. The black and red circles in Figure 6.8b and Figure 6.8c are respectively for the calibration and validation periods.

Flows of the Surma River at the Sylhet gauging station are similar to those simulated for the upstream station at Kanairghat (see Section 5.6.4). Therefore, the discussion of model performance at Kanairghat similarly applies to Sylhet. The model shows reasonable skills in terms of all statistical metrics (Table 6.2). The good agreement between modelled streamflows and observation is also demonstrated in Figure 6.9.

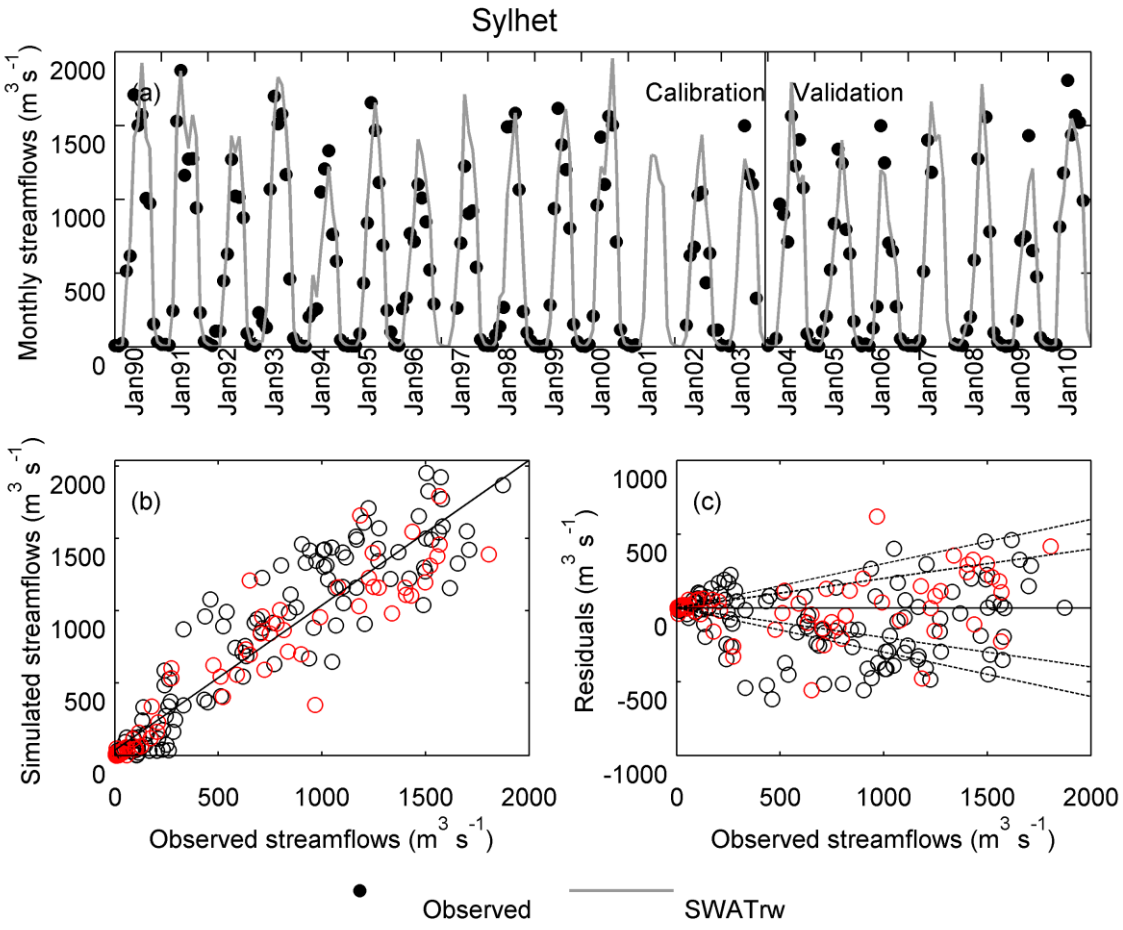

Figure 6.9. Graphical comparison of observed and SWATrw simulated mean monthly streamflows at Sylhet on the river Surma. The black and red circles in Figure 6.9b and Figure 6.9c are respectively for the calibration and validation periods.

Bhairab Bazar gauging station on the River Meghna is the lowest outlet of the UMRB (Figure 6.1). According to the criteria of Moriasi et al. (2007), the model falls in the satisfactory (S) and unsatisfactory (US) categories respectively for the calibration and validation periods (Table 6.2). In both periods, an overall tendency to underestimate observed flows is seen (Figure 6.10c), which is also reflected in positive PBIAS values of 15.97% for calibration and 5.85% for validation (Table 6.2). The time series plot of simulated and observed flows (Figure 6.10a) shows that monsoonal peak flows are often underestimated (e.g. in years 1990–1994, 2001, 2005–2006) whereas flows during the recession tail of the annual hydrographs from late monsoon to dry season months are consistently

underestimated. In the dry season (December–March), the simulated Meghna River completely dries out. However, the available observed dry season records in 1998 and 2006 indicates that the discharge using this period was between 1600 and 3864 $m^3 s^{-1}$.

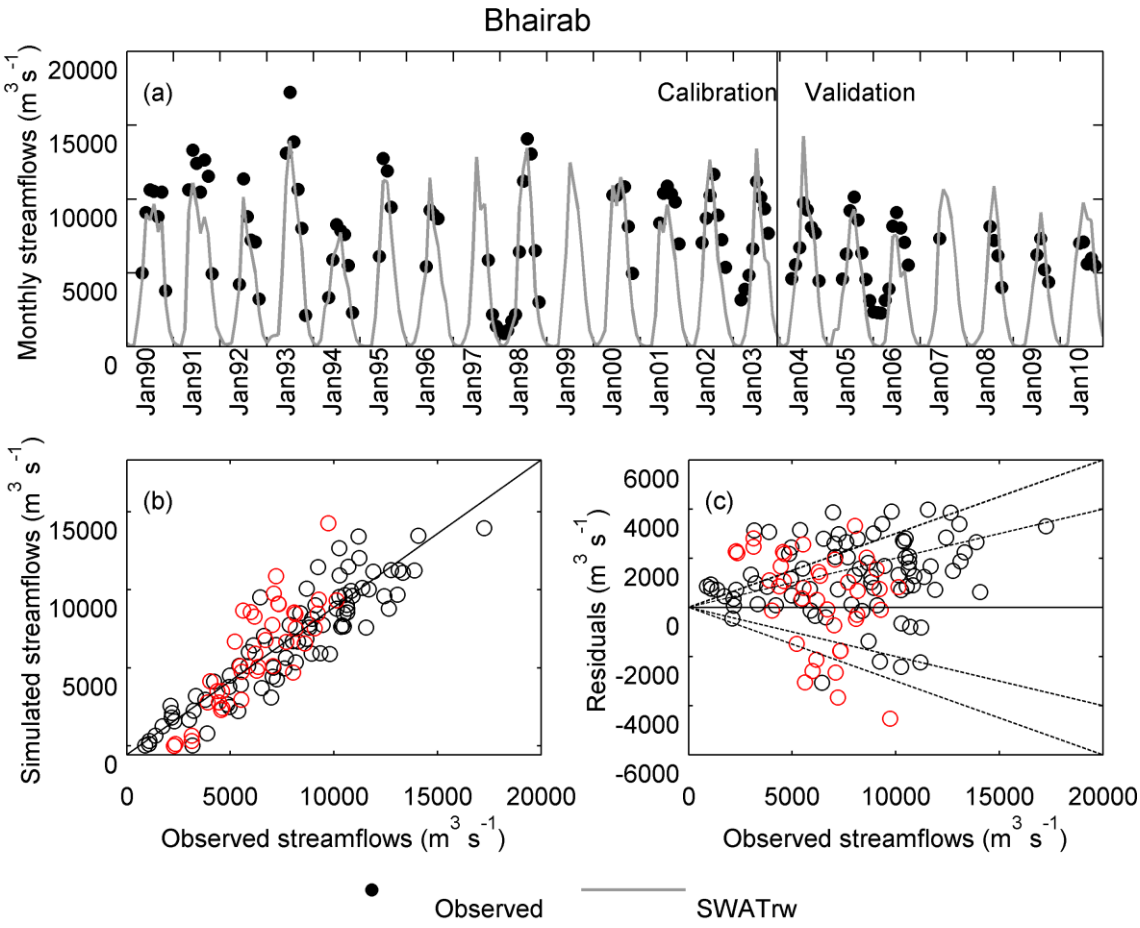

Figure 6.10. Graphical comparison of observed and SWATrw simulated mean monthly streamflows at Bhairab Bazar on the river Meghna. The black and red circles in Figure 6.10b and Figure 6.10c are respectively for the calibration and validation periods.

To investigate this limitation of the model, the daily discharges of the Meghna River at Bhairab were simultaneously compared with those from three large upper catchments; the Barak River, Meghalaya and Tripura (Figure 1.3 and Figure 6.11). Of these three catchments, runoff generated from the wettest Meghalaya catchment predominantly shape the hydrograph of the basin's outflows at

Bhairab (Figure 6.11). Therefore, an unrealistic model for the Meghalaya catchment would greatly impact the model's simulation skill at the basin outflows. As discussed previously for the Laurergahr catchment (2493 km^2) in the larger Meghalaya catchment, on average about 764 mm (calibration) and 814 mm (validation) of shallow aquifer water had to be transferred to the deep aquifer. It is suspected that the aquifer in the Laurergahr catchment is not absolutely confined within the catchment boundary (as assumed within the model setup), rather the aquifer may be connected to the aquifers/surface water bodies (wetlands, rivers) in the lower Sylhet catchment. The water within the deep aquifer of the upper Laurergahr catchment would therefore appear in the hydrological system of the lower catchment, a process that could not be represented within the model. Adding such large volume of water (764 mm×2493 km^2–814 mm×2493 km^2) to the hydrology of the lower Sylhet catchment would significantly increase the flows (surface and/or baseflow) of Meghna River at Bhairab. This zero boundary flow assumption between subbasin level aquifers in SWATrw (also in SWAT) may be even more unrealistic for topographic plain areas such as the lower Sylhet catchment of the UMRB.

In order to preserve the high density of the river networks in the flat Sylhet catchment, as many subbasins as the number of rivers were manually delineated. However, the number of delineated subbasins might have been lowered if the more topographically uniform adjacent subbasins were amalgamated although this would impact how well the actual river network is represented. These assumed isolated aquifers (zero boundary flow) underlying the subbasins of the flat Sylhet catchment are unlikely to accurately represent the continuous shallow aquifer spread across the catchment as previously explained for the Laurergahr catchment. In such a situation, incorporating a more robust physics-based distributed groundwater model is recommended although this is not possible in the current version of SWATrw / SWAT.

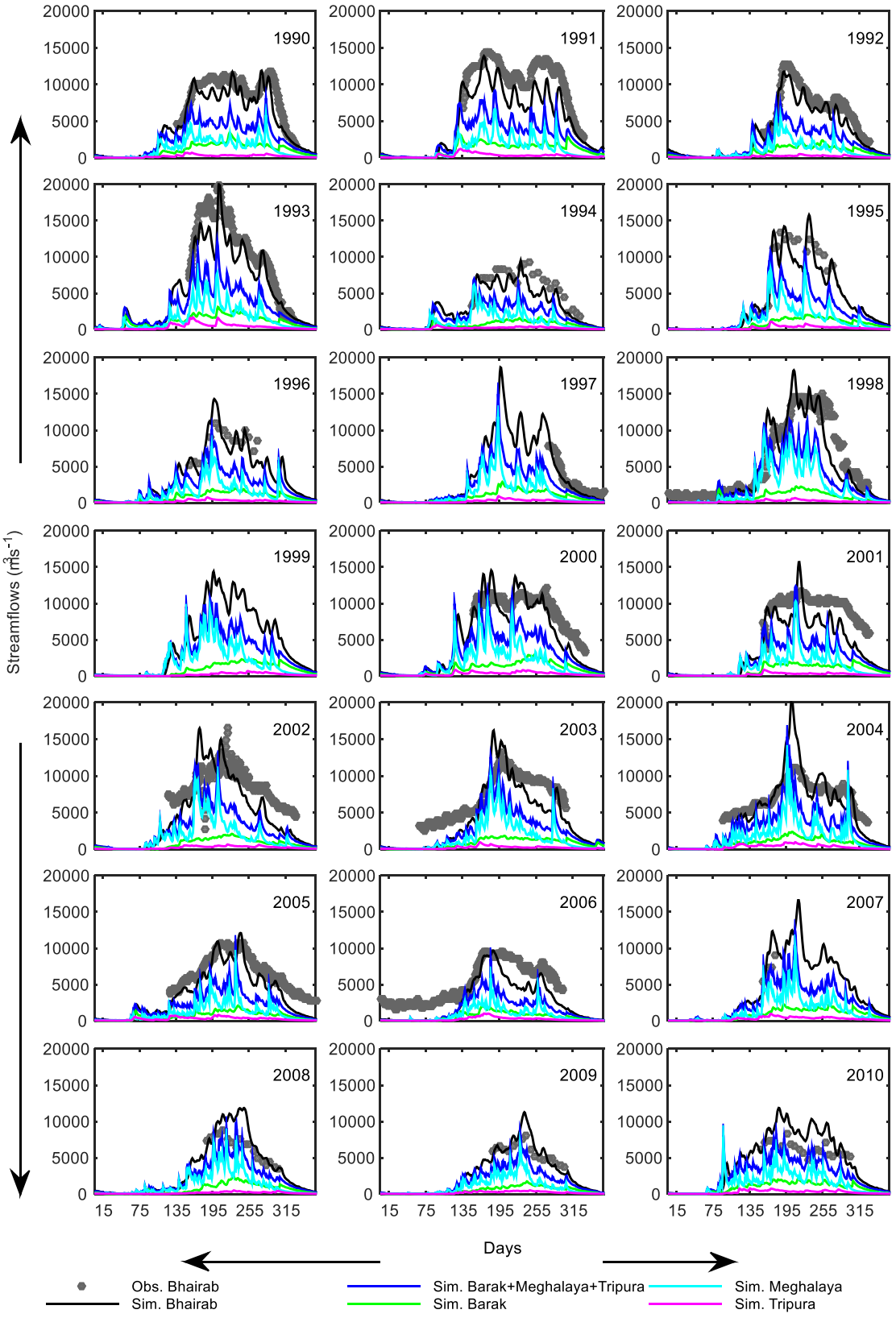

Figure 6.11. Comparison of daily discharges at Bhairab (the outlet of UMRB) on the Meghna River with those of from three large catchments Barak, Meghalaya and Tripura (see Figure 1.3). For each of the last two catchments, daily discharge is calculated by summing simulated daily outflows of all transboundary rivers entering the lower Sylhet catchment in Bangladesh. Similarly, the total hydrograph of the three upper catchments (blue coloured) is derived by summing their individual hydrograph ordinates for a particular day. The difference between the hydrographs of UMRB (black line) and of the combined three large catchments (blue line) is the potential runoff generated from the lower regional Sylhet catchment.

Another possible reason for the underestimated discharge at Bhairab may be associated with the BWDB developed rating curve of the Meghna River at Bhairab. The observed discharge data provided by the BWDB are not directly measured values rather they are generated from the rating curve model previously developed by the BWDB. Since 'river stage' is the only input variable to the BWDB rating curve model, any other unseen and/or ignored factors might limit the quality of rating curve generated flows. Uncertainties in rating curve generated flows may be induced due to altered channel geometry, unsteady flow, changing channel's roughness (for example due to vegetation growth) and backwater effects (Clilverd et al., 2013; Di Baldassarre and Montanari, 2009; Hidayat et al., 2011). Since the flow regime of the Meghna River at Bhairab is reportedly impacted by backwater originating from the downstream confluence of Padma and Meghna rivers at Chandpur (Chowdhury and Salehin, 1997; Chowdhury and Ward, 2004) (see Figure 1.3), the BWDB rating curve might be overestimating actual river flows as a result of the higher river stages resulting from these effects.

6.3. Summary

Streamflow simulation performance of the SWATrw model for the nine gauging stations below the Barak-Kushiyara River Basin of the UMRB has been demonstrated in this chapter. For the calibration period, the model shows satisfactory or better performance, on the recommended statistical scale (see Table 5.3), at all gauging stations except Saistaganj in Tripura region. For the validation period, however, the model produces unsatisfactory results at Sarighat, Islampur and JariaJanjail stations that drain some part of the Meghalaya region, and at Bhairab that is the outlet of the UMRB. The poor performance for the first three stations is plausibly due to unrealistic low rainfall in the Meghalaya region as being provided by IMDdist weather grids for the validation period. The tendency of underestimating streamflows at Bhairab is linked to the current inability of both models (SWATrw and SWAT) to transfer groundwater between adjacent subbasin-level aquifers. Moreover, any unrealistic low flows from the

upper Meghalaya region contributes to this underestimation. Perhaps this shortcoming downgrades the model's performance at Bhairab from satisfactory for the calibration period to unsatisfactory for the validation period when the aforementioned three gauging stations at the foothill of Meghalaya showed underestimated flows.

Chapter 7
Climate change impact assessment for water regimes of river-wetland systems in the UMRB

7.1. Introduction

Climate change is now an established truth (Strzepek et al., 2011; World Bank, 2013). The world is already 0.85 °C warmer than the pre-industrial period (1880) and temperature is projected to rise by a further 1.8 °C by the end of the 21st century compared to the period 1986–2005 if the current climbing trend of greenhouse gas emission rate can be stabilized (IPCC, 2013). The potential consequences of climate change on hydrological processes and associated sectors (e.g. water resources, agriculture, ecology and human livelihoods) have been extensively documented in previous studies conducted across the world (Brown et al., 2015; Dai et al., 2009; Palmer et al., 2008; Schneider et al., 2013; Strzepek et al., 2011; Tang and Lettenmaier, 2012). Precipitation, evapotranspiration and runoff/streamflow are the three most widely studied hydrological processes that have been investigating in responses to a warmer world. In general, these processes define the land's water balance, expressed as net change in water storage (surface and subsurface) within the domain of interest (e.g. catchment) (Khandu et al., 2016).

Currently 60% of global mean precipitation returns to the atmosphere through evapotranspiration (ET) and some research shows that this will increase to 80% by the end of the 21st Century (Pan et al., 2015). In another study, Murray et al. (2012) showed that all of the world's 12 largest river basins would generate more runoff from per unit precipitation (i.e. runoff ratio) for a 2 °C warmer world compared to the period 1961–1990. Their study, which used a dynamic global vegetation model, showed that a warmer environment decreases vegetation coverage and transpiration due to water stress in the soil system which reduces overall ET. Apportioning of precipitation fallen over an area between ET and runoff relies upon the spatial characteristics of the landscape (land use,

topography, geology), climatic variables and anthropogenic activities. Since the variability of and complexity in interactions among state variables increase with expansion in spatial scale (e.g. basin or global scale), contrasting results of ET and runoff generated from per unit precipitation are likely e.g. those reported by Pan et al. (2015) and Murray et al. (2012). Whereas annual runoff sensitivity to temperature (change in runoff per unit change in temperature) in the catchments of arid regions is projected to be negative, it is positive for the catchments in southern Asia due to dominant role of more intense extreme rainfalls over the predicted accelerated evapotranspiration (Arnell, 2003; Tang and Lettenmaier, 2012). Failing to adequately account for the influence of landscape characteristics on hydrological processes may lead to misleading quantifications of the predicted regional/local water resources in the face of climate change. For instance, the presence of wetlands in a catchment can accelerate ET by providing expanded water surface areas and limiting soil water stress (Ambrose and Sterling, 2014; Wu et al., 2016).

A climate change induced accelerated hydrological cycle is likely to modify water regimes of wetlands and in turn impacts their numerous functions and services as well their productivity (Carolina and Jackson, 2011; Greenberg et al., 2015; Montroull et al., 2013). Since the inception of Ramsar Convention (1971), a pioneering initiative for world's wetlands conservation, much research has concentrated on the investigation of anthropogenic impacts on wetlands. In recent years a number of studies conducted on a variety of wetlands around the world have focused on the detrimental consequences of climate change on wetlands (Acreman et al., 2009; Carolina and Jackson, 2011; Greenberg et al., 2015; Singh et al., 2010; Thompson et al., 2015). It has been suggested that North American GIWs which are mainly sustained by precipitation and groundwater will undergo a shallower and shorter hydroregime due to increased water loss through accelerated ET (Greenberg et al., 2015; Johnson et al., 2010; Nungesser et al., 2015; Pitchford et al., 2012). Consequently, a number of wetland species (both animal and plant) was identified as being at risk of extinction in the future (Greenberg et al., 2015; Nungesser et al., 2015; Pitchford et al., 2012). The same consequence is projected for the Elmley Marshes in southeast England (Thompson et al., 2009). For some European wetlands,

Carolina and Jackson (2011) showed that decreased precipitation might lower aquifer recharge by up to 35% by the end of the 21st Century. As a result, wetlands which rely on groundwater influxes will be less frequently hydraulically connected with declining aquifers. Peatland wetlands that contain a considerable amount of organic carbon, for example the north American Everglades, can become a potential source of greenhouse gases through oxidization of stored carbon if they become dry (Malone et al., 2013). In contrast to GIWs, the hydrological response of riparian wetlands to climate change is thought to be more complex and uncertain. This is because the hydrodynamics of riparian wetlands not only are defined by the processes those involved in GIWs, but can be potentially influenced by flow characteristics of adjacent rivers and floodplains (Karim et al., 2016, 2015; Mohamed and Savenije, 2014; Popescu et al., 2015). An altered climate might substantially shift the current wetland-river connectivity in terms of timing, duration and frequency of connections (Karim et al., 2016, 2015). From a study on the Sudd wetland, South Sudan, Mohamed and Savenije (2014) found that changes in the wetland inundation over the 20th century were strongly related to the climate change in the ~1000 km upstream Lake Victoria that links the downstream wetland via the White Nile River.

Like other riparian wetlands within the floodplains of South Asia (e.g. the Mekong delta), existing anthropogenic pressures on the numerous wetlands in the Upper Meghna River Basin (UMRB) which are being used for agriculture (rice cultivation and aquaculture; see Section 1.3.1) is likely to be further exacerbated by future climate change. Many studies have found that the area will experience higher temperatures and heavier extreme rainfall in the 21st Century compared to the 20th Century (Chadwick et al., 2015; Dash et al., 2012; Donat et al., 2016; Li et al., 2016; Masood et al., 2015; Naidu et al., 2009; Tang et al., 2016). The temperature may increase by 0.7–3.8 °C whilst the annual mean precipitation may increase by 0.09–0.47 mm day^{-1}.

Although the projected climate of the UMRB is likely to shift to a new state that is even beyond the natural variability of the current climate (Chadwick et al., 2015), its implications on the haor wetlands have not been assessed. Improved understanding of future water regime shifts in the river-wetland system of the

UMRB that could result from climate change is essential. An important associated question is whether the changing climate will lessen or exacerbate the current flooding risk of haor wetlands. Therefore, this chapter describes the approaches taken for preparing future climate scenario data in order to drive the SWATrw model developed for the UMRB. Simulated responses in the water regimes are analysed to facilitate future plans for haor water management in the UMRB.

7.2. Preparing future climate time series

Global Climate Models or General Circulation Models (GCMs) are state-of-the-art tools to simulate the dynamics of the Earth's atmosphere (Chadwick et al., 2015; IPCC, 2013). Many GCMs have been developed by different climate modelling groups across the world. The World Climate Research Programme (WCRP), through the Coupled Model Intercomparison Project (CMIP), coordinates with these modelling groups in order to bring multi-model results to a common platform (Reclamation, 2013). The fifth phase of the CMIP (CMIP5) excels the preceding phases (e.g. CMIP3) by incorporating not only more GCMs but also more skillful models that can take into account the influence of land cover on climate system (Taylor et al., 2012). Moreover, Earth System Models (ESM) in the CMIP5 considers the contribution of Earth's biogeochemical processes to global greenhouse concentration.

Because existing GCMs are not structurally unique, their simulated climate outputs are reported to have considerable disagreements across time and space (Chang and Jung, 2010; Lutz et al., 2016). The competence of GCMs for an area is usually evaluated based on the measured historical observations. From such an attempt for the Indian summer monsoon rainfall (which accounts for, on average, 80% of annual rainfall), Menon et al., (2013) found that only 10 out of 20 CMIP5 GCMs simulated historical mean monsoonal rainfall within two times of the standard deviation range (0.7 mm day^{-1}) of observed values. Since the UMRB lies in the most intensive summer rainfall zone of this region, four of the best performing GCMs from Menon et al., (2013) was selected for this study (Table 7.1). These GCMs are in the closest agreement with observed mean summer rainfall (7.1 mm day^{-1}) and have been developed by different developers

(i.e. if there were more than one GCMs from a single developer then only the best performing was selected). For future projections, the RCP4.5 (Representative Concentration Pathway that can produce 4.5 W m^{-2} radiative forcing by the end of 21st Century) scenario was selected. The world policy makers and climate modelers together have recognized this as the most optimistic scenario if various plans undertaken to combat the current greenhouse gas emission rate could be properly implemented (IPCC, 2013).

Table 7.1. Selected CMIP5 GCMs used in this study

CMIP5 GCMs	Developers	Spatial resolution (km)
CCSM4	National Center for Atmospheric Research, USA	188×192
GFDL-CM3	NOAA Geophysical Fluid Dynamics Laboratory	144×90
MIROC-ESM	Japan Agency for Marine-Earth Science and Technology, Atmosphere and Ocean Research Institute (The University of Tokyo), and National Institute for Environmental Studies	128×64
NorESM1-M	Meteorological Research Institute Norwegian Climate Centre	144×96

Although the GCMs participating in CMIP5 have finer spatial resolution than those of the earlier CMIP3, the size of their computational grids is still not small enough to capture the variability of local climate, in particular precipitation (Bao et al., 2015; Reclamation, 2013; Werner and Cannon, 2016). Therefore, raw GCM data are, before employing them in any impact studies, downscaled to the desired spatio-temporal resolution. A number of downscaling methods have been developed, see for example Trzaska and Schnarr (2014) and Werner and Cannon (2016) for a detailed description. The NASA Earth Exchange Global Daily Downscaled Projections (NEX-GDDP) (https://nex.nasa.gov/nex/projects/1356/) is one of few initiatives to downscale CMIP5 GCM data for the entire world and to make them freely available for using in scientific research. For the selected four GCMs (see Table 7.1), daily time series of historical (1981–2000) and future

(2021–2040 and 2061–2080) climate data (precipitation and temperature) that are bias corrected and downscaled to 0.25° (~27 km) grids were collected from the NEX-GDDP repository.

A quality check was undertaken by comparing the historical NEX-GDDP data (hereafter referred to as raw GCM) with the observed data available within the study area for the same period. To do so, time series of all GCM grids that lie within the area represented by a weather station/grid (see Figure 7.1a) were spatially averaged. It was found that the raw GCM data have considerable bias. For example, the mean annual rainfall anomalies (deviation from observed values) involved in raw GCMs vary from -2750 mm yr^{-1} (underprediction) to 750 mm yr^{-1} (overprediction) across the UMRB with a dominant underprediction (Figure 7.1b-e). However, the spatial pattern of anomalies for all GCMs is almost the same. The evidence of biases in already bias corrected raw GCM data may be due to the difference in referenced data sources used for bias correction. NEX-GDDP used some globally available gridded referenced climate data that are derived from either satellite sensed information (e.g. TRMM, GPCP) or the available ground station data (e.g. NCEP-NCAR reanalysis, CRU TS2.0). Previous studies have found that most of these data are unable to capture the variability and volume, mainly underestimated, of orographic rainfall in the UMRB region (Immerzeel, 2008; Moffitt et al., 2011; Nishat and Rahman, 2009; Rahman et al., 2012). Therefore, this study hypothesised that a further bias correction of raw GCM data with reference to reliable and representative ground observation data from relatively dense stations will increase the credibility of future modelled results.

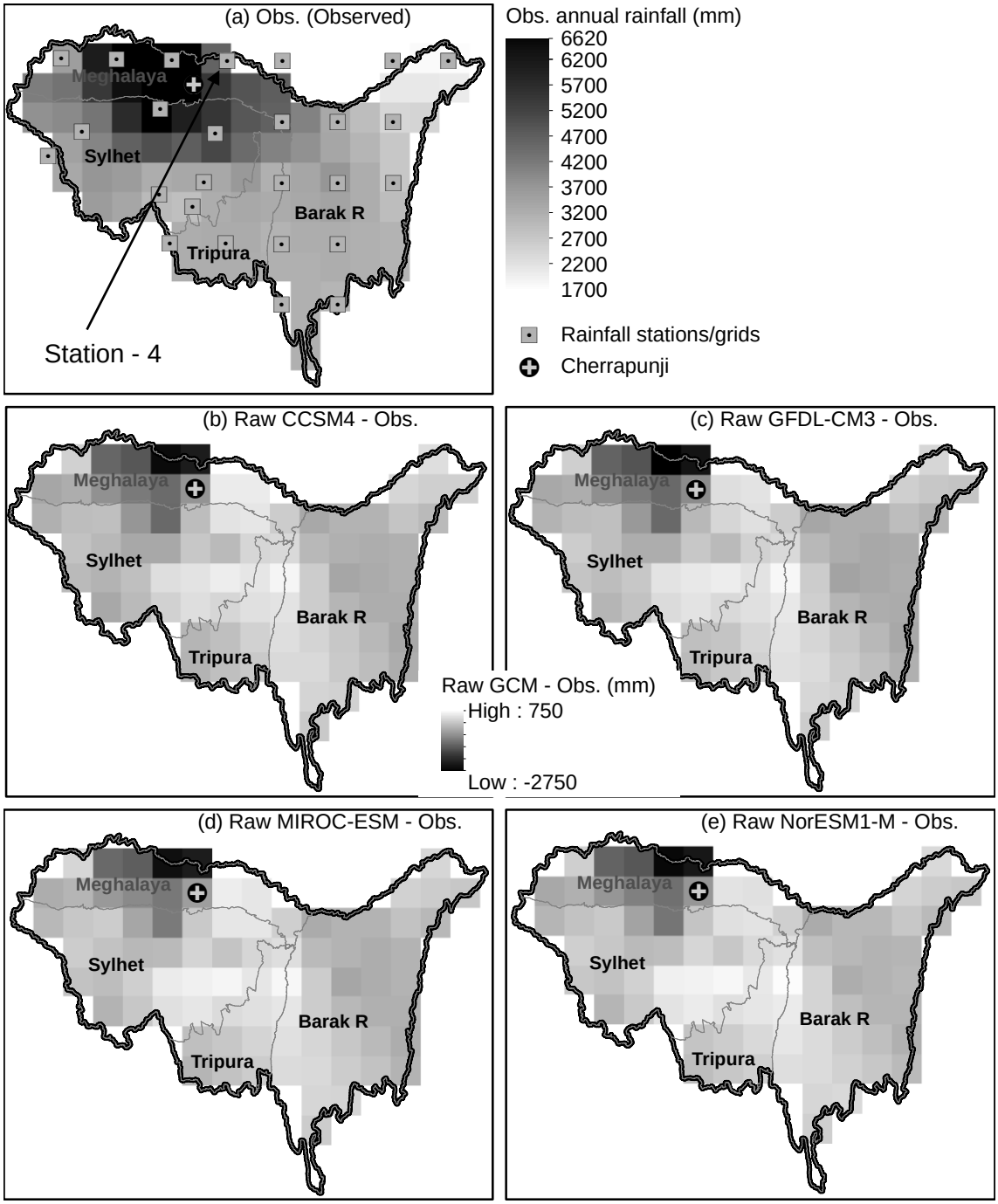

Figure 7.1. Anomalies between raw GCM and observed mean annual rainfall for the baseline period (1981–2000). Subplots (b) through (e) are derived by subtracting gridded observed mean annual rainfall from the corresponding value of respective raw GCMs. The deterministic Inverse Distance Weighted (IDW) spatial interpolation method was used to produce the gridded map in subplot (a) from observed mean annual rainfalls of 26 point stations in the UMRB (see also Figure 4.7).

7.2.1. Bias correction of raw GCM data

A Quantile Mapping (QM) bias correction method was applied to remove biases in the raw GCM data. This method overcomes the limitations of the widely used delta change method wherein bias-corrected values can only conserve the mean of observed data but not the variance (Hwang and Graham, 2014; Ines and Hansen, 2006; Leander and Buishand, 2007). In principle, any statistical bias correction method first establishes a relationship between measured and raw GCM data for a reference (or baseline) period. Assuming this relationship will persist in any future time period, later biases from the future raw GCM data are removed with that relationship.

The QM approach followed in this study can be described with five sequential steps (i) discretising the whole area (here the UMRB) into homogeneous climate zones (HCZ), (ii) producing representative observed and modelled (raw GCM) time series of climate variables for each climate zone, (iii) clustering values into twelve calendar months, (iv) constructing cumulative distribution functions (CDF) for the time series of observed and modelled values, and (v) estimating bias or correction factor (CF) at specific quantiles. These steps are illustrated in Figure 7.2. Since biases in GCM outputs are estimated with respect to observed counterparts, first the area represented by each observed station (termed a HCZ) is identified. However, the approach used herein differs from commonly used practices where a HCZ is a grid (~250 km) of raw GCM data containing observed stations. Because the NEX-GDDP raw GCM data are already spatially downscaled to finer grids (88 grid cells in UMRB) in contrast to fewer ground climate stations (26) in the basin, the opposite approach was followed. This is particularly advantageous for the SWAT/SWATrw model where each subbasin is linked with a single climate station ensuring a spatial invariant climate across the subbasin. For the present study, the subbasins represented by each climate station were first identified to form a HCZ and later the GCM grids lying on that HCZ were then indentified. Spatial averaging of daily raw GCM data for each HCZ accomplished the second step. Thirdly, observed and modelled daily time series

of climate variables for each HCZ were clustered into 12 calendar months for both the reference (1981–2000) and future/projected (2021–2040 and 2061–2080) periods. Fourthly, separate empirical cumulative distribution functions (eCDF) were developed from the daily climate time series of each calendar month for observed and raw GCM data. Since increasing extreme events in climate variables (especially for rainfall) cannot often be well fitted to a theoretical probability distribution. The eCDF approach was used for the highly variable climate of the UMRB. This approach has been used elsewhere (Hwang and Graham, 2014; Rashid et al., 2015). Note that any reference to CDF hereafter refers to eCDF unless otherwise stated. At the final step, signed biases (or CFs) in reference (or historical) raw GCM data (raw-GCM-ref) are quantified by taking the difference between quantiles of observed (obs-ref) and raw GCM data at specific CDF points. In principle, the CDF of bias free raw-GCM-ref data should perfectly match the corresponding observed CDF. Later the CFs obtained for the reference period are used as additive factor to correct future raw GCM data (raw-GCM-fur).

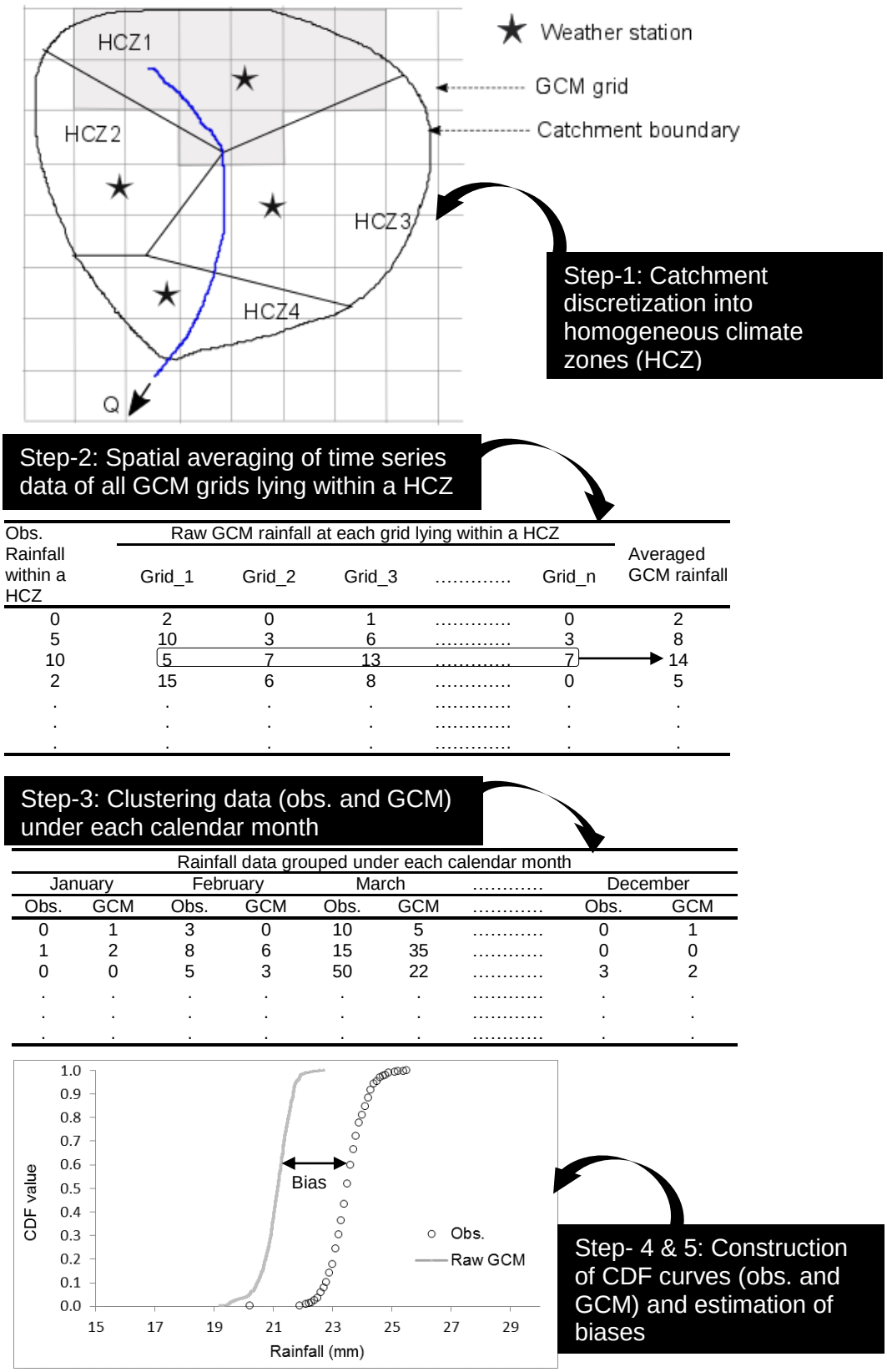

Figure 7.2. Steps for estimating bias correction factors by the adopted quantile mapping method.

The final step of the QM method as discussed above is graphically exemplified in Figure 7.3 by generating the necessary curves from a theoretical CDF (e.g. a normal distribution curve) rather than eCDF, for the sake of simplicity. One notable limitation of QM methods is their inability to adjust the frequency of dry days because a common CDF value between Obs-ref and raw-GCM-ref curves at their lowest points (i.e. dry days) is hardly ever found (Rashid et al., 2015; Sulis et al., 2012). This study addresses this issue by considering two conditions: underestimated (Figure 7.3a) and overestimated (Figure 7.3b) dry days in the raw-GCM-ref data. Procedurally the value of cumulative probability density (CPD) or CDF corresponding to a rainfall amount in a wet day of the raw-GCM-ref data is first determined (point A in Figure 7.3). B is the corresponding point on the observed CDF curve leading to a negative (Figure 7.3a) or positive (Figure 7.3b) bias of AB relative to raw-GCM-ref rainfall (A). The aforementioned strategy of correcting wet days is valid for any CDF value greater than the lowest common CDF (lcCDF) value between Obs-ref and raw-GCM-ref (equation 7.1), point E in Figure 7.3. The next step is to adjust the dry days in the raw-GCM-ref data. In the case of underestimated dry days (Figure 7.3a), any raw rainfall equal to or less than the threshold value (F) corresponding to the lcCDF are converted to dry days so as to match the number of dry days in Obs-ref data. To adjust dry day overestimation (Figure 7.3b), the dry day error fraction (equation 7.2) is estimated from:

$$lcCDF = max\left(CDF_{Obs-ref,0},\ CDF_{raw-\mathrm{GCM}-ref,0}\right) \quad 7.1$$

$$ddef = \left(CDF_{Obs-ref,0} - lcCDF\right)/lcCDF \quad 7.2$$

where, $ddef$ is the dry day error fraction, $CDF_{Obs-ref,0}$ is the CDF value of observed climate variable (rainfall in the example) corresponding to the lowest value in the time series (zero rainfall in the example) and $CDF_{raw-\mathrm{GCM}-ref,0}$ has the same meaning as $CDF_{Obs-ref,0}$ but for raw-GCM-ref data. The absolute value of $ddef$ is an estimation of what percentage of dry days in raw-GCM-ref is to be converted to wet days. The rainfall range of those wet days lies between above

zero and a threshold corresponding to the lcCDF of Obs-ref data (point F in Figure 7.3b). While adjusting these dry days in the time series of raw-GCM-ref, a random value from the space between 0 and the threshold rainfall is generated from a pre-defined distribution. This distribution assumes that the probability of a random value being '0' is $[1 - abs(ddef)]$ and for all non-zero values (i.e. wet days) within the threshold, the probability is identical i.e. uniform distribution.

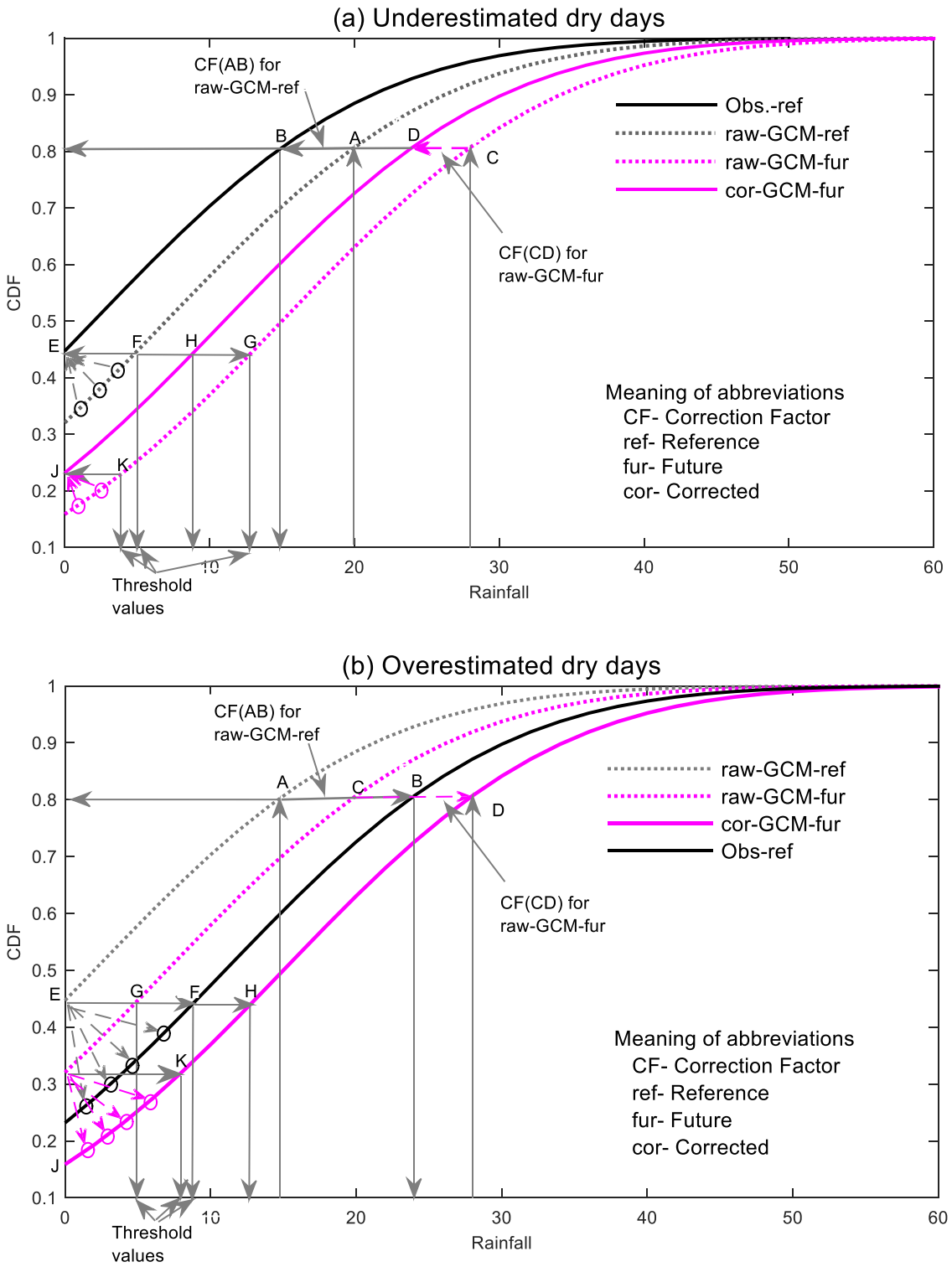

Figure 7.3. Graphical representation of the Quantile Mapping (QM) bias correction method. The value of cumulative probability density or CDF at '0' rainfall indicates the dry day frequency of each curve i.e. the percentage of dry days in the respective time series.

In order to correct future raw GCM data (i.e. raw-GCM-fur), first dry day frequency is fixed. Assuming the mismatch in the dry day frequency of raw-GCM-ref data as represented by $ddef$ will persist in the future, the dry day CDF value of raw-GCM-fur data is adjusted accordingly. To do so, the dry day frequency of raw-GCM-fur data is either increased to or lowered to the corrected J point (Figure 7.3) by respectively adding or subtracting the product of $ddef$ and the future raw CDF at zero rainfall (i.e. $CDF_{raw-\mathrm{GCM-fur},0}$). Now any raw-GCM-fur values greater than the lowest common CDF (lcCDF) among Obs-ref, raw-GCM-ref and cor-GCM-fur (i.e. J point, also see Equation 7.3) are adjusted by adding previously estimated signed CF (i.e. correction factor) corresponding to the CDF of the raw-GCM-fur value. In Figure 7.3, for example, the lcCDF is still at the E point since point J (i.e. corrected dry day CDF in the future GCM data) is still below the former point. The remaining uncorrected raw-GCM-fur values lying at or below the lcCDF are corrected by randomly choosing a value from the data space JH having a distribution such that the probability of a value to be zero (i.e. dry day) is $[1 - abs(ddef)]$. Here, $ddef$ is estimated following the equation 7.4.

$$lcCDF = max\left(CDF_{Obs-ref,0},\ CDF_{raw-\mathrm{GCM}-ref,0}\ ,\ CDF_{cor-\mathrm{GCM}-fur,0}\right) \quad 7.3$$

$$ddef = \left(CDF_{cor-\mathrm{GCM}-fur,0} - lcCDF\right)/lcCDF \quad 7.4$$

The same procedure was applied to correct raw temperature data except the dry day frequency of a calendar month should be read as the coldest day frequency.

7.3. Driving the calibrated SWATrw model with processed future climate data

In order to compare hydrological responses of the basin to the projected future climate with those of baseline, the calibrated SWATrw model was driven with the climate time series data (rainfall and temperature) for the baseline (1981–2000) and two future time slices (2021–2040 and 2061–2080). The remaining climate data (wind speed, humidity and solar radiation) required by the SWATrw model were generated by the weather WXGEN generator. The four GCMs and two time

slices required eight model runs for simulating future hydrological responses. For the historical time period, the NEX-GDDP climate data are available for up to 2005 whereas the training period (calibration and validation) of the SWATrw model was 1990–2010 (Section 5.5.2). Therefore, the time slice 1981–2000 was selected as a baseline period that leads 45% of the baseline period to fall outside the training period. In general practice, a baseline period is contained within training period for which model parameters are evaluated against some statistical criteria (Thompson et al., 2015, 2014a; Zhu et al., 2016). Since exact overlapping of baseline and training periods is conditioned by the availability of data, this conventional practice often cannot be followed, as is the case for the present study.

7.4. Results and discussion

7.4.1. Projected changes in rainfall and temperature of the UMRB

Before presenting the projected future climate of the UMRB, evidence is provided to demonstrate how the adopted QM bias correction approach improves the quality of raw GCM data. This is done using results obtained from the CCSM4 model, as an example, for climate station 4 (Figure 7.1a). For the two situations (over- and under-predicted dry days) as discussed in Section 7.2.1, daily rainfall data for the calendar months August and November are respectively illustrated in Figure 7.4a and Figure 7.4b. From both figures, it is evident that daily rainfall does not follow a typical normal distribution pattern unlike the case for temperature (Figure 7.4c). Arguably the reason can be linked to the chaotic nature of the regional rainfall not only across space but across time, even over short periods such as a calendar month. This finding supports the use of the empirical CDF based QM bias correction methods over the alternatives based on a parametric CDF. The adopted QM approach fits the raw-GCM-ref rainfall (unfilled circle) to the observed values (filled black circle) well during the reference period (Figure 7.4a and Figure 7.4b). In particular, both over- (inset in Figure 7.4a) and under-estimated (inset in Figure 7.4b) dry days in the raw-GCM-ref data are

exactly matched to the respective observed CDF points corresponding to zero rainfall. Moreover, the trend of dry day frequency shift from the reference period to the future period in the raw GCM data is included in the corrected GCM data. For example, in the inset of Figure 7.4a the raw rainfall data (raw-GCM-ref and raw-GCM-fur) indicate more dry days in future compared to the reference period (difference of dry day CDF = 0.255–0.224 = 0.031). Because the adopted QM approach takes into account this trend while correcting the raw rainfall data, the trend appears in the corrected rainfall data (cor-GCM-ref, light blue coloured + marker). This ability of the QM approach is also clearly seen in the case of underpredicting dry days (Figure 7.4b).

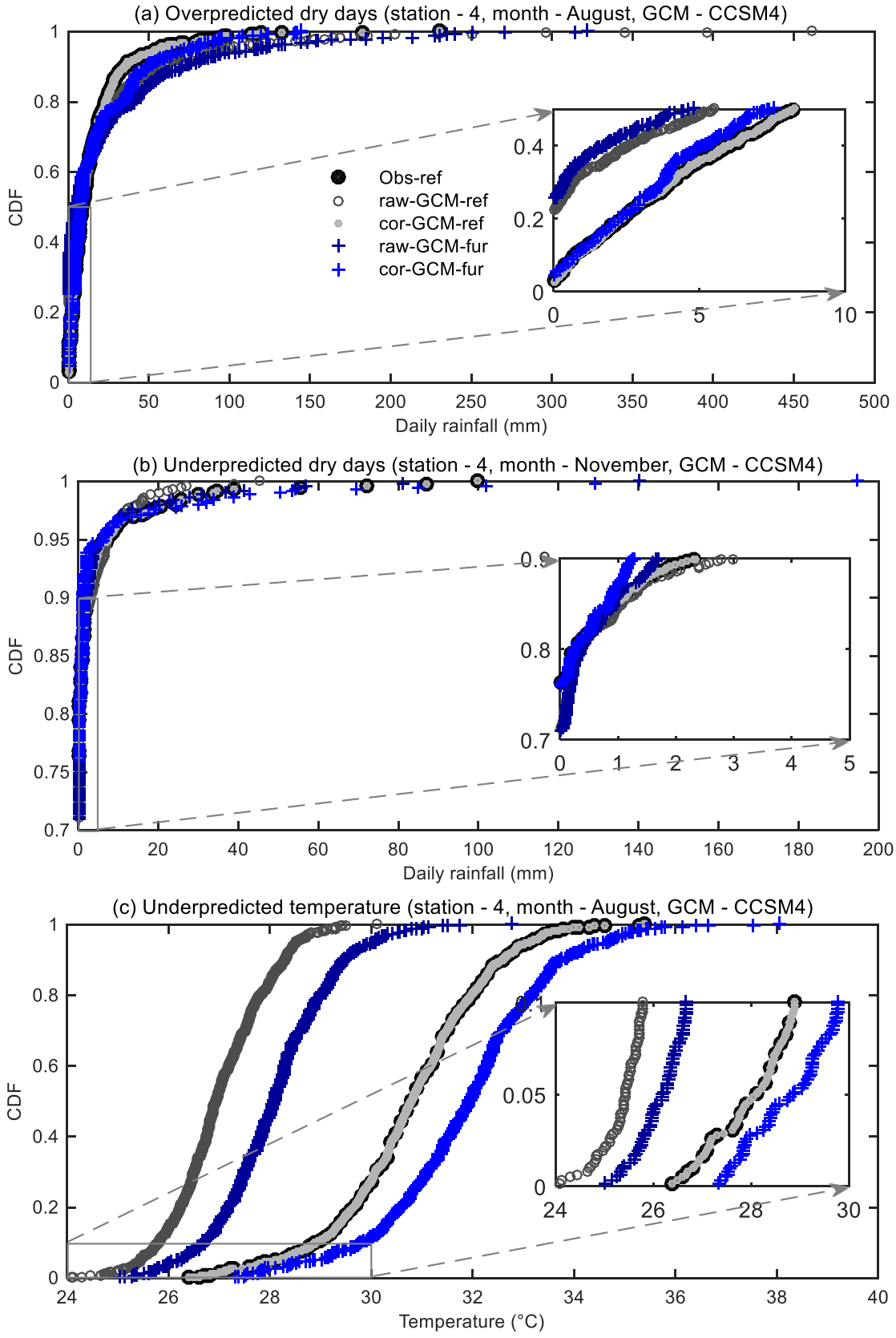

Figure 7.4. Comparison of raw and QM bias corrected daily rainfall and temperature for a calendar month. Subplots a and b respectively are for the cases of over- and under-predicted dry days (or CDF) in reference period (1980–2000) whereas c for temperature. The inset in each subplot shows the zoomed in view of the rectangle-demarcated part.

Figure 7.5, produced from bias corrected rainfalls, presents the changes in mean annual rainfall over the basin. Rather than showing individual GCM's, the ensemble minimum, mean and maximum rainfalls for each grid were used when generating the Figure 7.5. Such an arrangement is useful to show the range of uncertainties involved in using the different GCMs. A number of previous studies argue for using ensemble mean climate in impact analysis studies so as to reduce the uncertainties from the structural differences in GCM's (Carolina and Jackson, 2011; Gain et al., 2011; Trzaska and Schnarr, 2014). Most of the UMRB receives increased annual rainfall in the two projected periods 2021–2040 (subplots b, c, d) and 2061–2080 (subplots e, f, g). The exception is the ensemble minimum (Figure 7.5b and Figure 7.5e) where most of the basin receives decreased rainfall (by 1–100 mm) in 2021–2040, and for 2061–2080 this drying extent reduces to only a part of the area straddling the Sylhet–Tripura border. In the relatively near future (2021–2040), rainfall is projected to increase by up to 350 mm for the ensemble maximum (Figure 7.5d) or 150 mm for the ensemble mean around Cherrapunji (Figure 7.5c). The three lower basins (Meghalaya, Sylhet and Tripura) occupying 60.1% of the UMRB are wetter than the Barak Basin. This increasing trend of rainfall will persist in the more distant future period (2061–2080) with larger increases (annual increases of up to 2500 mm). The Sylhet Basin experiences the highest relative changes in annual rainfall. This can be understood by comparing the baseline rainfall map (Figure 7.5a) with the absolute change maps (Figure 7.5b-g).

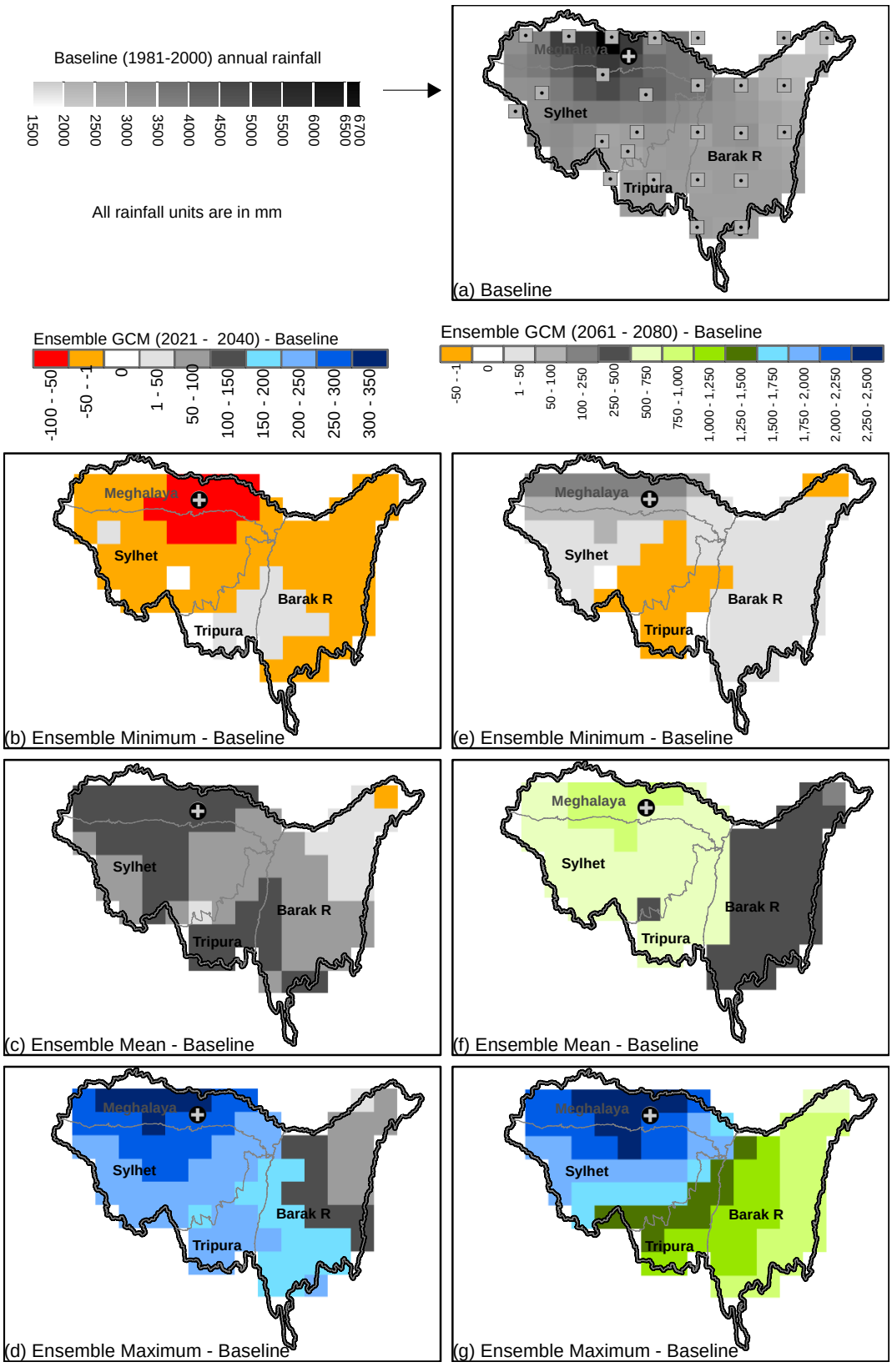

Figure 7.5. Changes in bias-corrected mean annual rainfall during the two projected periods (2021–2040: subplots b, c, d in left panel and 2061–2080: subplots e, f, g in right panel) with respect to baseline observed rainfall (1981–2000: subplot a) in the UMRB. Daily bias corrected rainfall in the time series of the 4 GCMs are used to derive the ensemble minimum, mean and maximum daily time series from which the above gridded ensemble annual rainfall statistics are generated. Any grid cell having a rainfall change within -1 to 1 mm is assumed to be zero change (white colour).

Monthly analysis of ensemble mean rainfall (Figure 7.6) reveals some noticeable inherent changes in the rainfall pattern that could not be explored from the annual analysis. Rainfall in all monsoonal months (June–September) including pre-monsoonal May increases throughout the basin by a maximum of 20%. A dramatic change appears in the two months between the dry and pre-monsoon seasons (March and April). Whereas rainfall in the pre-monsoonal April decreases (maximum change -20%) across the basin, the dry season month of March becomes wetter by an amount of up to 40% near Cherrapunji in Meghalaya. However, some lower parts of the Sylhet and Tripura basins show drier conditions in March. The whole basin's rainfall decreases by between 10% and 50% during the post-monsoon season (October–November).

The directional pattern of mean monthly rainfall changes for the far future period remains almost the same as the near future period with the exception of November during which the basin becomes up to 40% wetter compared to the baseline (Figure 7.7) whilst this month was projected to be drier for the near future (Figure 7.6). The near future increasing rainfall trend for the five rainiest months (May–September) continues for the far future period when these months become wetter still.

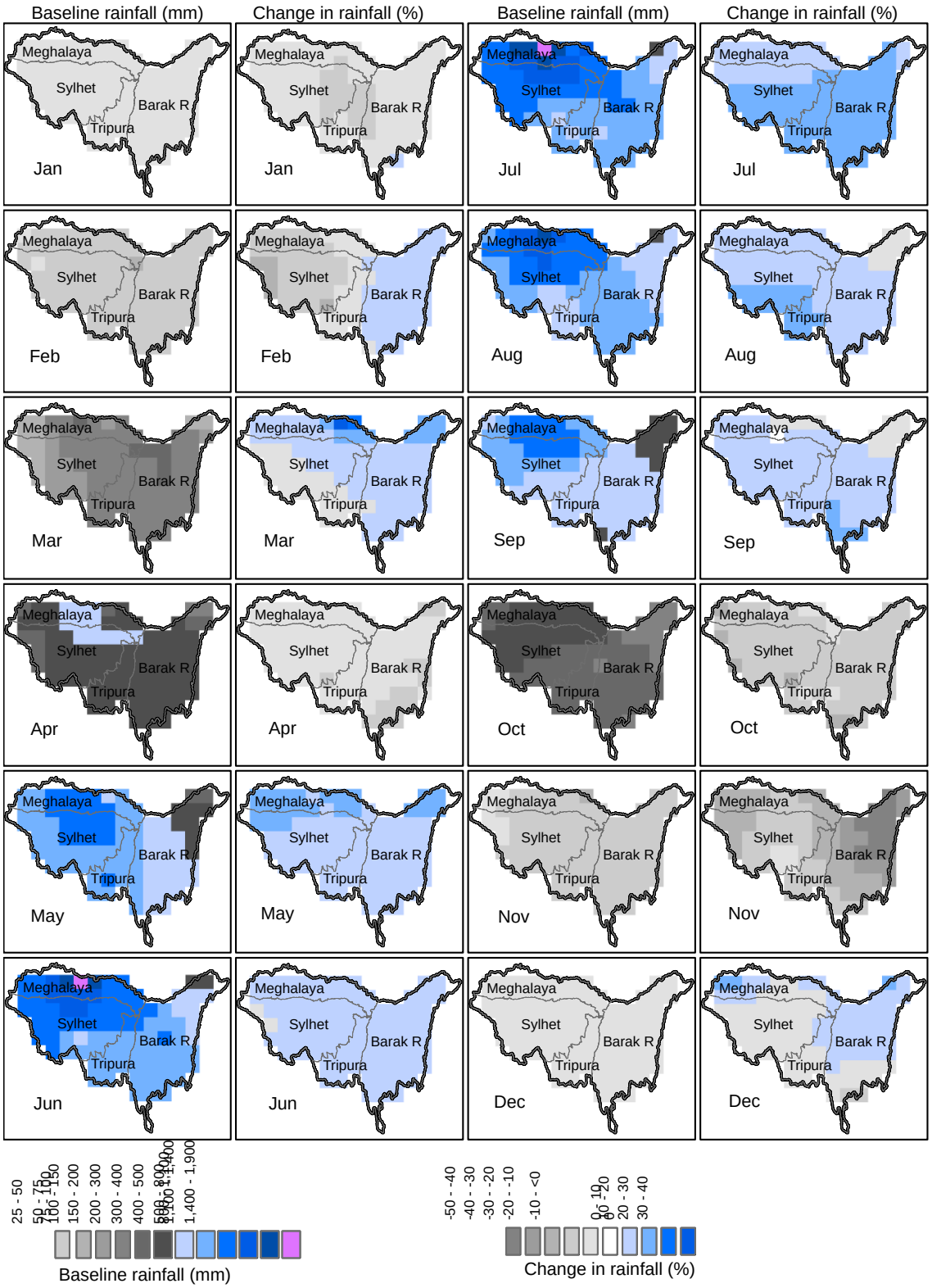

Figure 7.6. Changes in bias-corrected ensemble mean monthly rainfall during the projected period of 2021–2040. The minimum value of any range in the legends should be read as greater than that value.

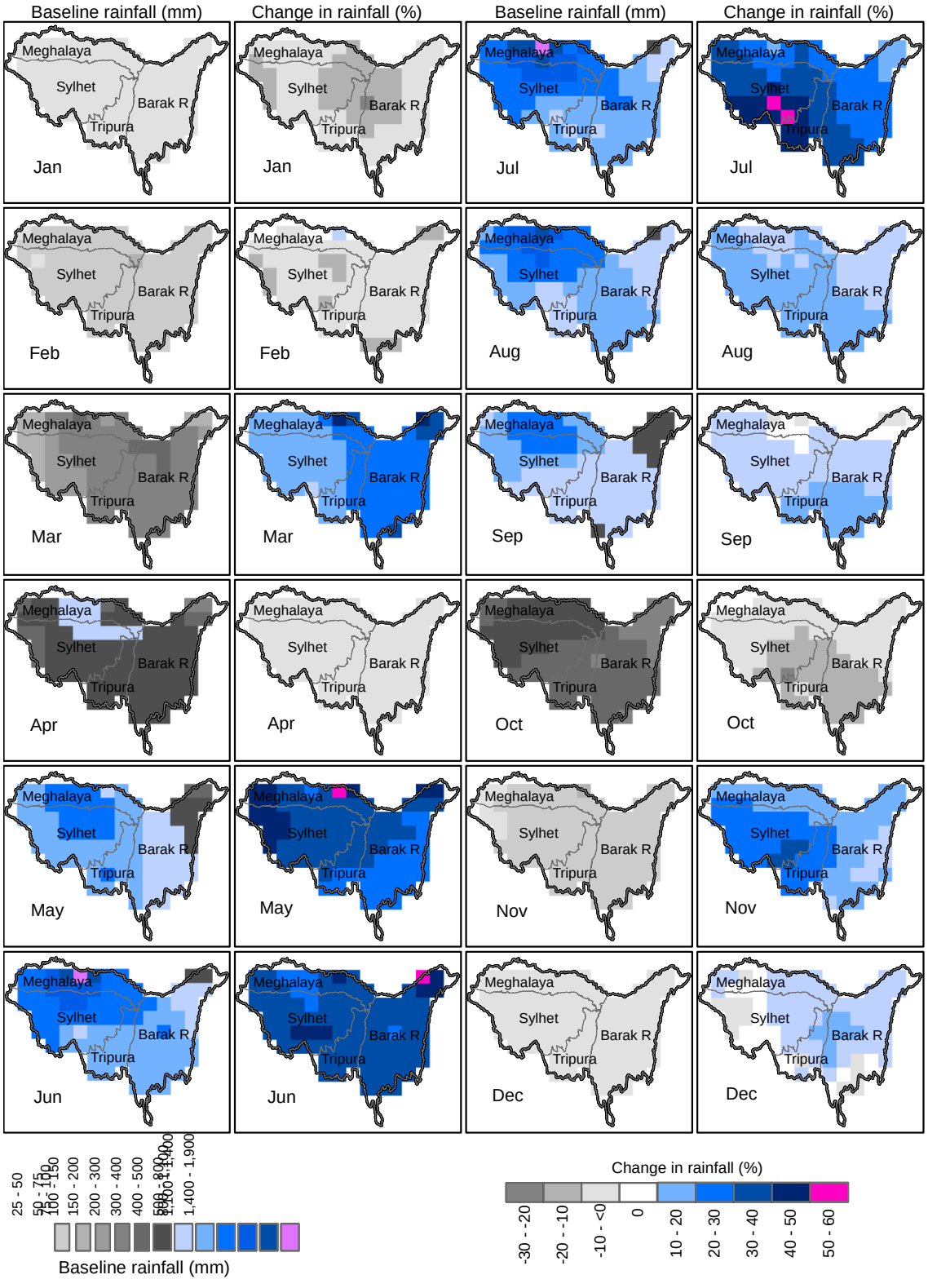

Figure 7.7. Changes in bias-corrected ensemble mean monthly rainfall during the projected period of 2061–2080. The minimum value of any range in the legends should be read as greater than that value.

A consistent rise of mean monthly temperature compared to the baseline is projected for both future periods at all 10 temperature meteorological stations (Figure 7.8). The magnitude of these changes ranges from 1.00 to 1.68 °C for the 2021–2040 period and 1.68–2.72 °C for 2061–2080. The dry season months see not only the largest increase in temperature but also greater spatial variability. This variability is reduced in the far future period (Figure 7.8c).

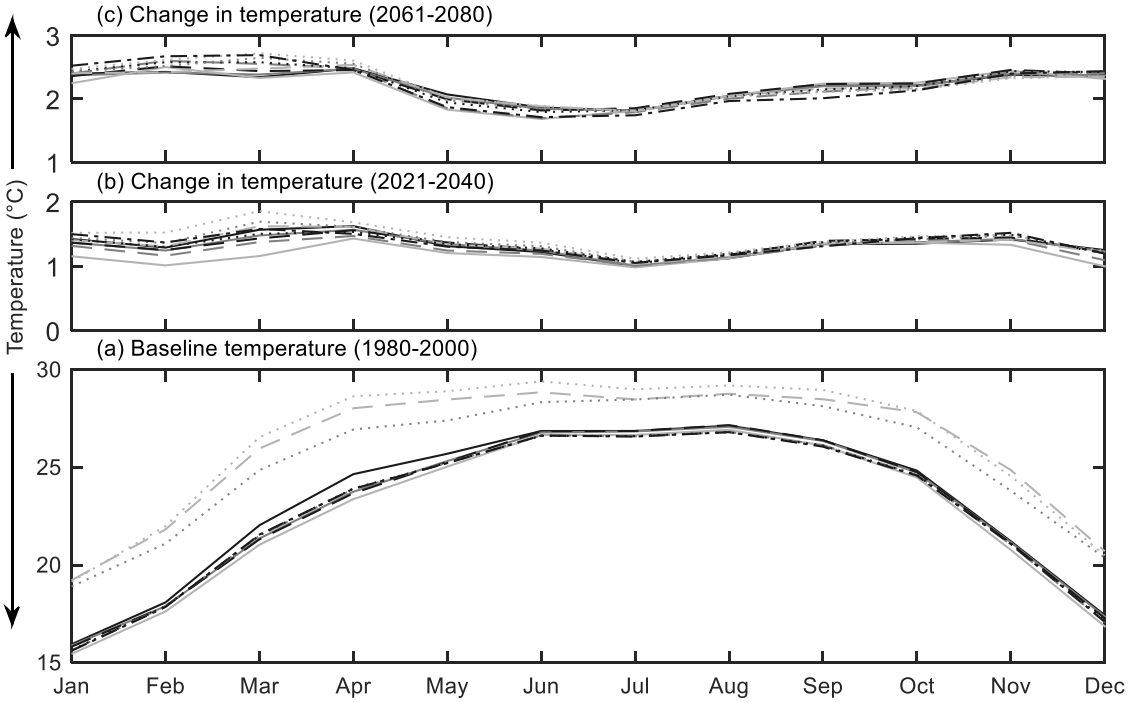

Figure 7.8. Changes in bias-corrected ensemble mean monthly temperature during the projected periods of 2021–2040 (b) and 2061–2080 (c). Each line represents a temperature station of the ten shown in Figure 4.7.

7.4.2. Projected streamflow responses to climate change

In order to investigate the impacts of the projected climate on the basin's river flow, the entire basin is divided into six regional subbasins defined by selected gauging stations as shown in Figure 7.9. These subbasins are formed by aggregating closer subbasins drained by the 15 gauging stations used in model calibration and validation (Figure 6.1) in order to better interpret projected results

for the four major constituting basins (Barak, Meghalaya, Tripura and Sylhet). The gauging stations which a subbasin drain through can be identified by their names labelled next to the subbasin legend. The Meghalaya basin is divided into three subbasins so as to better understand the hydrological responses to its highly spatially variable rainfall.

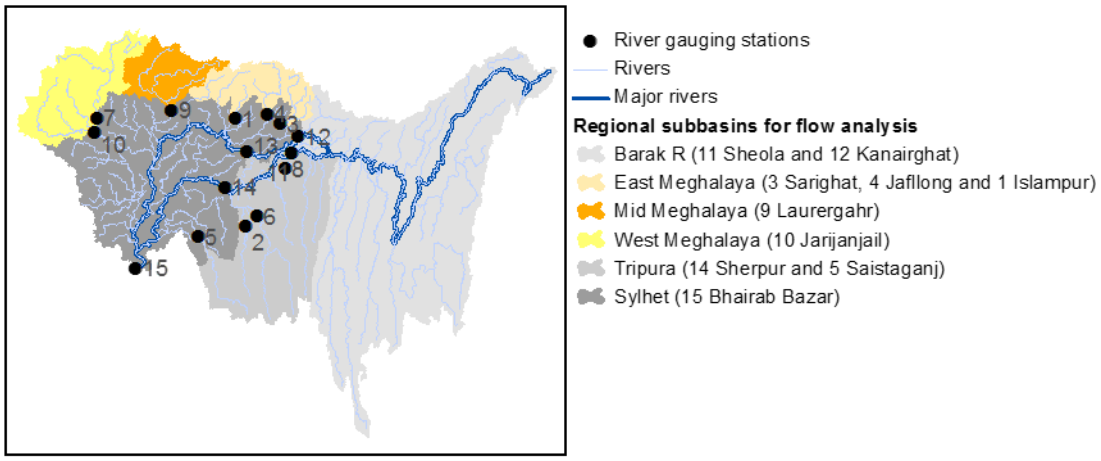

Figure 7.9. Six regional subbasins of the UMRB used to analyse climate change impacts on streamflows at their outlets.

Projected streamflow results are discussed sequentially for the Barak, East Meghalaya, Mid Meghalaya, West Meghalaya, Tripura and Sylhet subbasins. Figure 7.10 demonstrates the streamflow responses to climate change at the outlet of the Barak River subbasin. The change is demonstrated by illustrating flow duration curves (FDC) and Decomposed Monthly Flow Frequency (DMFF) of streamflows at the outlet of the subbasin for the baseline (1981–2000) and projected period 2021–2040 (near future). For each GCM, its corresponding FDC (Figure 7.10a) is computed from the daily streamflow time series simulated for a time period. There are two types of ensemble mean FDC in the figure: (i) ensemble mean (TS) FDC – the one (magenta coloured) that is generated from the time series (TS) of daily ensemble mean flows and (ii) ensemble mean FDC - the one (dark magenta coloured) that is generated by averaging flows of the four GCM FDCs at specific exceedance probabilities. The comparative utilities of the both approaches are exemplified in the next paragraph. DMFF represents frequency of a flow or flow range (or band) in the entire daily time series of a given dataset (e.g. baseline) appearing in a calendar month. Therefore, the DMFF

signature of a particular flow value or range in a calendar month weighs the extent of its contribution to forming the associated FDC generated from the whole time series. Such a framework is useful to interpret a FDC with more inherent information. Aternatively, for example, any flow value on an ensemble mean (TS) FDC accompanying with the corresponding DMFF can be easily characterized with respect to the frequency with which each value occurs in each months.

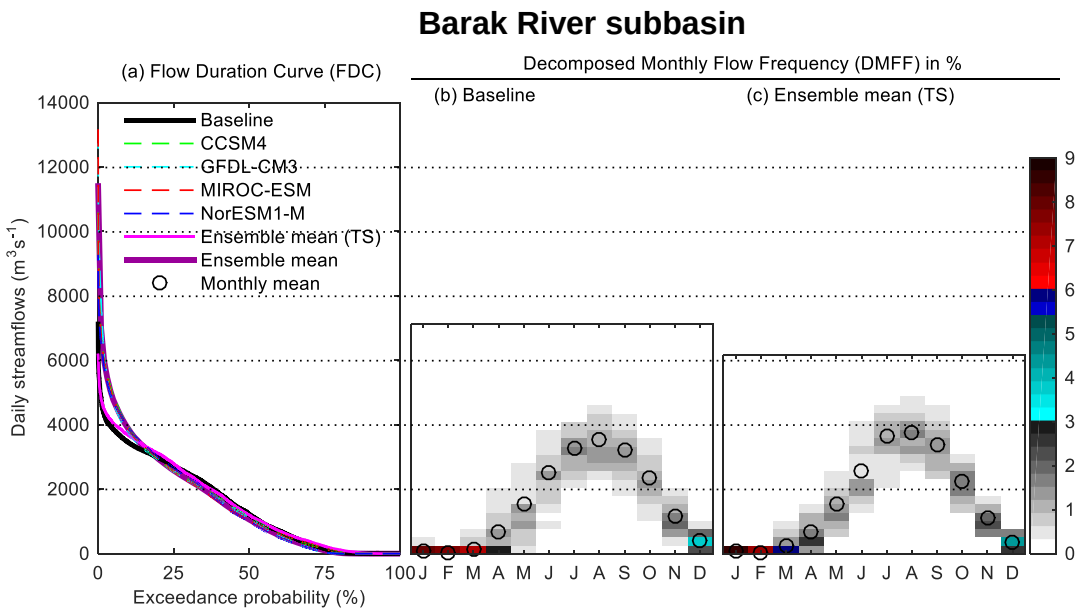

Figure 7.10. Flow duration curves (FDC) and Decomposed Monthly Flow Frequencies (DMFF) of streamflows at the outlets of Barak River subbasin for the baseline (1981–2000) and the projected 2021–2040 period. A flow interval of 250 $m^3 s^{-1}$, the height of each constituting block, is used while generating the DMFFs. This interval is chosen in such a way so that a demonstrable hydrograph-shaped DMFF curve is produced. A smaller interval value will produce smaller DMFF, thus may not be easily differentiable in the colour map produced from the entire time series. For example, since the frequency of highest extreme values is very small, the corresponding DMFF value approaches zero (white color in subplots b – c). On the other hand, a larger interval will lump most flows, thus the complete variation of discharges within a calendar month may not be revealed.

For the Barak River Basin (Figure 7.10a), the flow duration curves (FDCs) of the four GCMs' driven streamflow time series are very close to each other except at the extreme high flow (flow corresponding to exceedance probability <= 1%). This implies that the prediction of extreme high flows is not as reliable as that for other flows due to uncertainties originated from the GCMs' structures. For example, the simulated highest flows for the four GCMs can vary within the range of 9276–13312 $m^3 s^{-1}$ which implies that the baseline highest flow (7129 $m^3 s^{-1}$) is likely to be increasing (30–87%) in the near future period. Similar uncertainty is predicted for the other five subbasins in the basin. The discussion of streamflow response to climate change for the basin hereafter is limited to the ensemble mean scenario (magenta and dark magenta coloured FDCs in Figure 7.10a). According to the ensemble mean (TS) FDC (magenta coloured), no significant change in the Barak's outflow of up to 2800 $m^3 s^{-1}$ (which represents 75% of the time i.e. 25% exceedance probability) is indicated in Figure 7.10a. Streamflows with an exceedance probability of less than 25% are slightly larger for 2021–2040 compared to the baseline. The above changing pattern is also evident in the ensemble mean FDC (dark magenta coloured) but with greater upward shifts of higher baseline flows. This is further elucidated by tabulating flows at the three exceedance probability (exP) values of 95%, 50% and 5% (see Table 7.2). In absolute term, low flows corresponding to exP of 95% are slightly larger (2.014 $m^3 s^{-1}$) in the ensemble mean (TS) FDC compared to the ensemble mean FDC whereas high flows (exP = 5%) are remarkably smaller (730 $m^3 s^{-1}$, Table 7.2). Investigating the time series of daily flows simulated for each GCM's climate forcings it was found that the four GCMs show a considerable disagreement in daily simulated flows [coefficient of variation (CV): 2–173%]. This variation is large for dry season low flows and small for wet season high flows; however, in terms of flow range on a day, the GCMs show greater disagreement for high flows compared to low flows. Thererfore, averaging out of GCMs' driven daily flows to yield the corresponding ensemble mean daily flow produces a smoother time series compared to individual GCM's driven time series. In the present case, this leads to smaller high flows and larger low flows in enesmble mean (TS) FDCs compared to ensemble mean FDC (see Figure 7.10a and Table 7.2, for example). Qi et al. (2017) found similar consequences for multi-model ensemble mean temperature. Note that although both ensemble approaches can differ in their

estimated percentiles of a given dataset, they produce identical mean values of the dataset. Climate change studies conventionally compute long-term statistics of a variable for individual GCMs prior to producing the corresponding ensemble statistics. For example, the ensemble mean FDCs (i.e. dark magenta coloured lines) demonstrated in this study are constructed based on the conventional approach. On the other hand, the ensemble mean time series approach also used in this study, albeit not frequently practised, has an advantage over the conventional approach where temporal positions of data points are to be investigated. This has been discussed previously by acknowledging the combined utility of ensemble mean (TS) FDCs and the associated DMMFs.

Table 7.2. Baseline and future projected streamflows at the three exceedance probabilities (95%, 50% and 5%) as computed for FDCs.

Periods	Regional subbasins	FDC	Streamflows ($m^3 s^{-1}$) at different exceedance probabilities (exP)		
			exP =95%	exP =50%	exP =5%
2021-2040	Barak	Baseline	0.001	1221	3866
		Ensemble mean (TS)	2.052	1202	4057
		Ensemble mean	0.038	1060	4787
	East Meghalaya	Baseline	36.000	230	1994
		Ensemble mean (TS)	44.000	286	1748
		Ensemble mean	33.000	212	2067
	Mid Meghalaya	Baseline	0.000	64	678
		Ensemble mean (TS)	0.000	79	553
		Ensemble mean	0.000	53	640
	West Meghalaya	Baseline	0.001	176	939
		Ensemble mean (TS)	2.000	188	929
		Ensemble mean	0.000	149	1076
	Tripura	Baseline	21.000	1116	3044
		Ensemble mean (TS)	30.000	1151	3175
		Ensemble mean	19.000	966	3865
	Sylhet	Baseline	7.000	2510	11767
		Ensemble mean (TS)	27.000	2555	12097
		Ensemble mean	1.000	2181	14336
2061-2080	Barak	Ensemble mean (TS)	2.141	1370	4827
		Ensemble mean	0.001	1314	5411
	East Meghalaya	Ensemble mean (TS)	47.000	316	2000
		Ensemble mean	35.000	238	2275
	Mid Meghalaya	Ensemble mean (TS)	0.000	87	637
		Ensemble mean	0.000	62	738
	West Meghalaya	Ensemble mean (TS)	3.088	222	1142
		Ensemble mean	0.001	179	1297
	Tripura	Ensemble mean (TS)	35.000	1347	3895
		Ensemble mean	22.000	1175	4392
	Sylhet	Ensemble mean (TS)	38.000	2900	14652
		Ensemble mean	0.450	2655	16277

The future projected increased flows occur mainly in the monsoonal months June–September (Figure 7.10b and Figure 7.10c) which is also discernible from the monthly means (2–10% positive change, see Table 7.3). Mean flows in both post-monsoonal months (October and November) decrease slightly (5–6%, Table 7.3) and the range of baseline flows in these months reduces for the 2021–2040 period (Figure 7.10b and Figure 7.10c). Although the dry season December and January months experience more frequent low flows compared to the baseline (0.5% higher DMFF value), the two subsequent dry months (February and March) are less prone to dryness either due to decreased frequency of lean flows and/or increased flows in the near future period. Such inherent information cannot often be retrieved from only monthly mean statistics, an approach for summarizing scenario changes that is commonly practised.

Table 7.3. Projected relative changes* in mean monthly streamflows at the outlet of the six regional subbasins.

Periods	Regional subbasin		Jan	Feb	Mar	Apr	May	Jun	Jul	Aug	Sep	Oct	Nov	Dec
2021 - 2040	Barak	Baseline ($m^{-3}s^{-1}$)	74	32	149	628	1478	2440	3177	3393	3090	2287	1118	401
		Changes (%)	-25	-2	45	1	-1	2	10	7	5	-5	-6	-10
	East Meghalaya	Baseline ($m^{-3}s^{-1}$)	63	58	107	255	553	1233	1535	1073	713	427	176	103
		Changes (%)	-3	-8	19	-4	12	0	3	6	-1	-7	-2	-9
	Mid Meghalaya	Baseline ($m^{-3}s^{-1}$)	1	5	18	68	193	378	468	349	237	126	26	4
		Changes (%)	24	-45	7	-3	12	1	4	11	5	-16	-1	-58
	West Meghalaya	Baseline ($m^{-3}s^{-1}$)	14	8	15	60	270	602	783	620	534	391	176	60
		Changes (%)	-13	-33	29	14	18	2	5	12	9	-14	-6	-19
	Tripura	Baseline ($m^{-3}s^{-1}$)	115	65	170	537	1360	1995	2428	2592	2341	1732	1307	487
		Changes (%)	-12	-3	44	1	-4	0	12	7	7	-5	-4	-8
	Sylhet	Baseline ($m^{-3}s^{-1}$)	234	83	198	1063	3465	7027	9987	9448	7999	5503	2392	873
		Changes (%)	-15	-17	51	5	3	0	7	9	7	-9	-2	-11
2061 - 2080	Barak	Changes (%)	-9	-33	142	5	25	42	37	22	11	2	5	2
	East Meghalaya	Changes (%)	1	-1	33	-3	32	22	17	13	1	-1	10	-3
	Mid Meghalaya	Changes (%)	-46	-20	32	-4	32	28	25	21	6	-7	19	-41
	West Meghalaya	Changes (%)	8	0	82	11	51	40	38	34	17	-1	12	1
	Tripura	Changes (%)	3	-12	141	4	25	42	42	24	13	2	7	5
	Sylhet	Changes (%)	-2	-15	155	7	29	38	37	27	12	0	9	2

*Change in streamflow = (projected flow – baseline flow)/ baseline flow; orange coloured cells highlight decreased monthly flows (i.e. negative change) in the future periods.

Projected ensemble mean (TS) FDCs for the three Meghalaya subbasins show a somewhat similar pattern (Figure 7.11). High flows corresponding to exceedance probability of 8% (6% for West Meghalaya) or below decrease (maximum 46% for the East Meghalaya) in 2021–2040 compared to the baseline period. Again, as previously explained for the Barak River Basin, baseline high

flows are projected to be increasing in the near future period according to the ensemble mean FDCs (Figure 7.11). Beyond this exceedance probability, outflows of the subbasins slightly increase in the future period. With the exception of the most extreme high flows (exceedance probability ~0) and low flows (0–250 m^3 s^{-1} for East Meghalaya and 0–100 m^3 s^{-1} for Mid and West Meghalaya), the incident frequency of intermediate streamflows increases relatively at a faster rate during the projected future period (i.e. change in exceedance probability for per unit change in streamflow in the projected ensemble mean (TS) FDC is greater than those of the baseline FDC). This is further explored by investigating the DMFF signatures of month wise flow spectrums (Figure 7.11b and Figure 7.11c). In contrast to the baseline (Figure 7.11b), throughout May–September in the future period (Figure 7.11c) low flows within a month are either increasing or their frequency of occurrence is decreasing whereas intermediate flows occur more frequently as weighed by greater DMFF values. Such a change moves the mean monthly values to the regions of highest DMFF value (i.e. mode of flows) unlike the baseline where mean monthly flows are defined by less frequent high flows particularly in June–August. Any water resources management plans that are to be formulated based on mean flows will be more durable and optimal if the location of highest DMFF is taken into account. The reason is that the highest DMFF represents the mode of flow for a particular month. The closer the mean and DMFF values, the higher possibility the mean will be less defined by the extreme values.

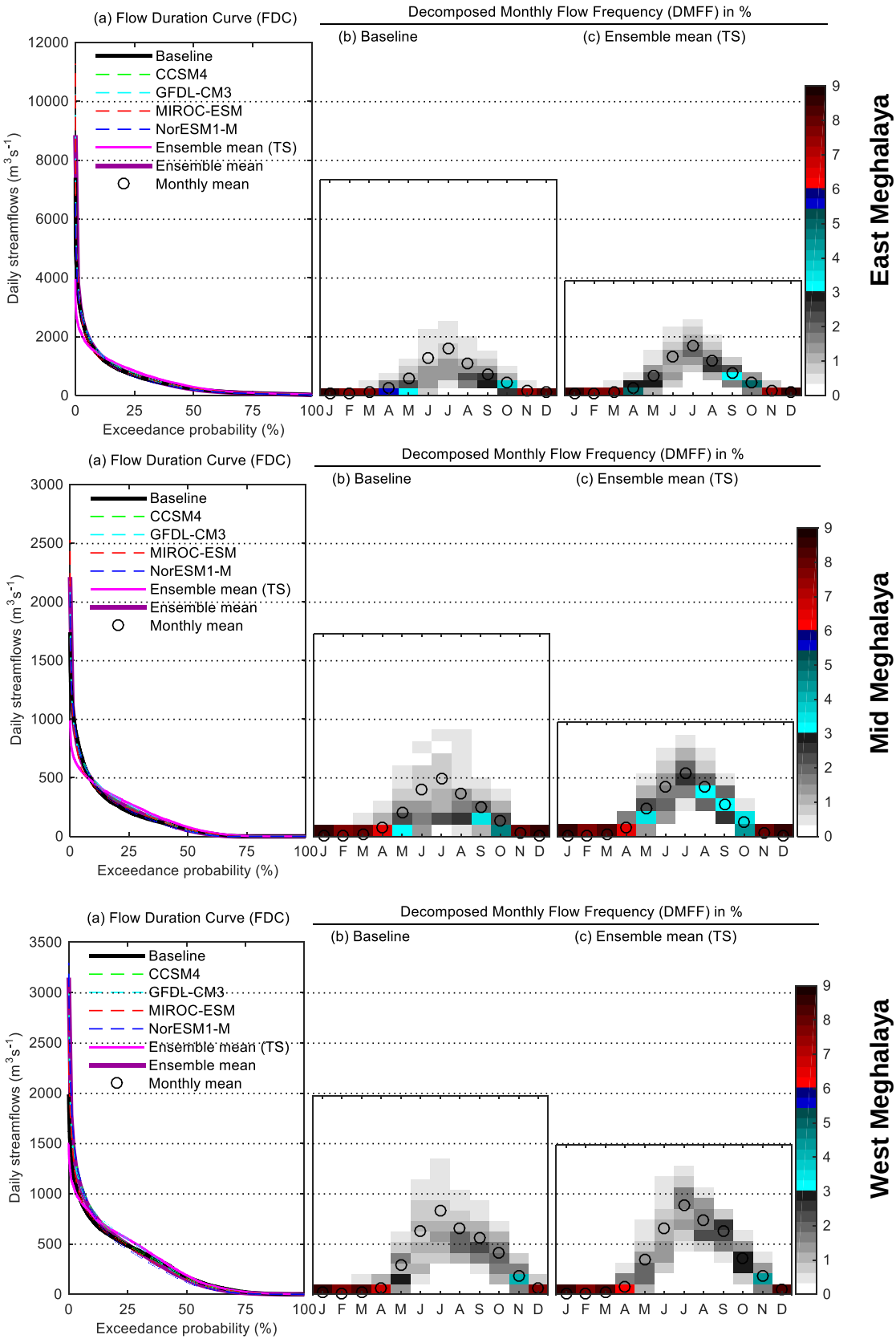

Figure 7.11. Flow duration curve (FDC) and Decomposed Monthly Flow Frequency (DMFF) of streamflows at the outlets of three subbasins for the baseline (1981–2000) and projected 2021–2040 periods. In DMFF subplots (b-c), the values of flow interval are respectively 250 and 100 $m^3 s^{-1}$ for the former one and the latter two subbasins.

The future projected lower flows in the four monsoonal months (June–September) can be as large as three times the corresponding values in the baseline period. For example, the baseline low flows (≤ 250 $m^3 s^{-1}$) in July rise to 750 $m^3 s^{-1}$ in the future period for the East Meghalaya (see Figure 7.11b). Mean monthly flows in May–September can increase by 1–18% compared to the baseline (Table 7.3). In April and October, the decrease in mean monthly flows (Table 7.3) are due to reductions in the extreme high flows (Figure 7.11c). The consistent increase in flows from the three Meghalaya subbasins in May could worsen the degree of current flash flooding in the lower Sylhet basin during the pre-monsoon season. Mean monthly outflows from the three Meghalaya subbasins during the post-monsoon (October–November) and the following dry season months December–February decrease by a range of 1–58% whereas a consistent increase in mean flows in March is projected (Table 7.3).

Since outflows from the Tripura Basin are predominantly characterized by flows from the upper Barak Basin, the projected patterns of outflow changes over the baseline indicated in ensemble mean (TS) FDCs (Figure 7.12a) and DMFF (Figure 7.12b-c) are nearly equivalent to those for the Barak (see also Table 7.3). The baseline extreme high flows (highest 20000 $m^3 s^{-1}$) at the outlet (Bhairab gauging station) of the Sylhet Basin (i.e. the outlet of the UMRB) are projected to drop by 3000–5000 $m^3 s^{-1}$ during the 2021–2040 period whereas a more frequent occurrence of flows within a range of 7000–12000 is projected for the future period [ensemble mean (TS) FDC, Figure 7.12a]. As can be seen from Figure 7.12c (Sylhet), this increased flow frequency happens during July–September in the future period. Low flows in these months are slightly higher compared to the baseline which explains the increase in mean monthly flows of up to 9% in 2021–2040 (Table 7.3). Baseline high flows in October–November drop by a maximum of 500 $m^3 s^{-1}$ in 2021–2040 and the mean flows of these months decrease by between 2–9% in the future period (Table 7.3). Similar decreasing future projections but with more intense magnitude are found for January and February. However, the dry season month of March will see a remarkable increase (mean: 51%) in the basin's outflow. This trend persists in April and May but much smaller magnitude (maximum 5% by mean).

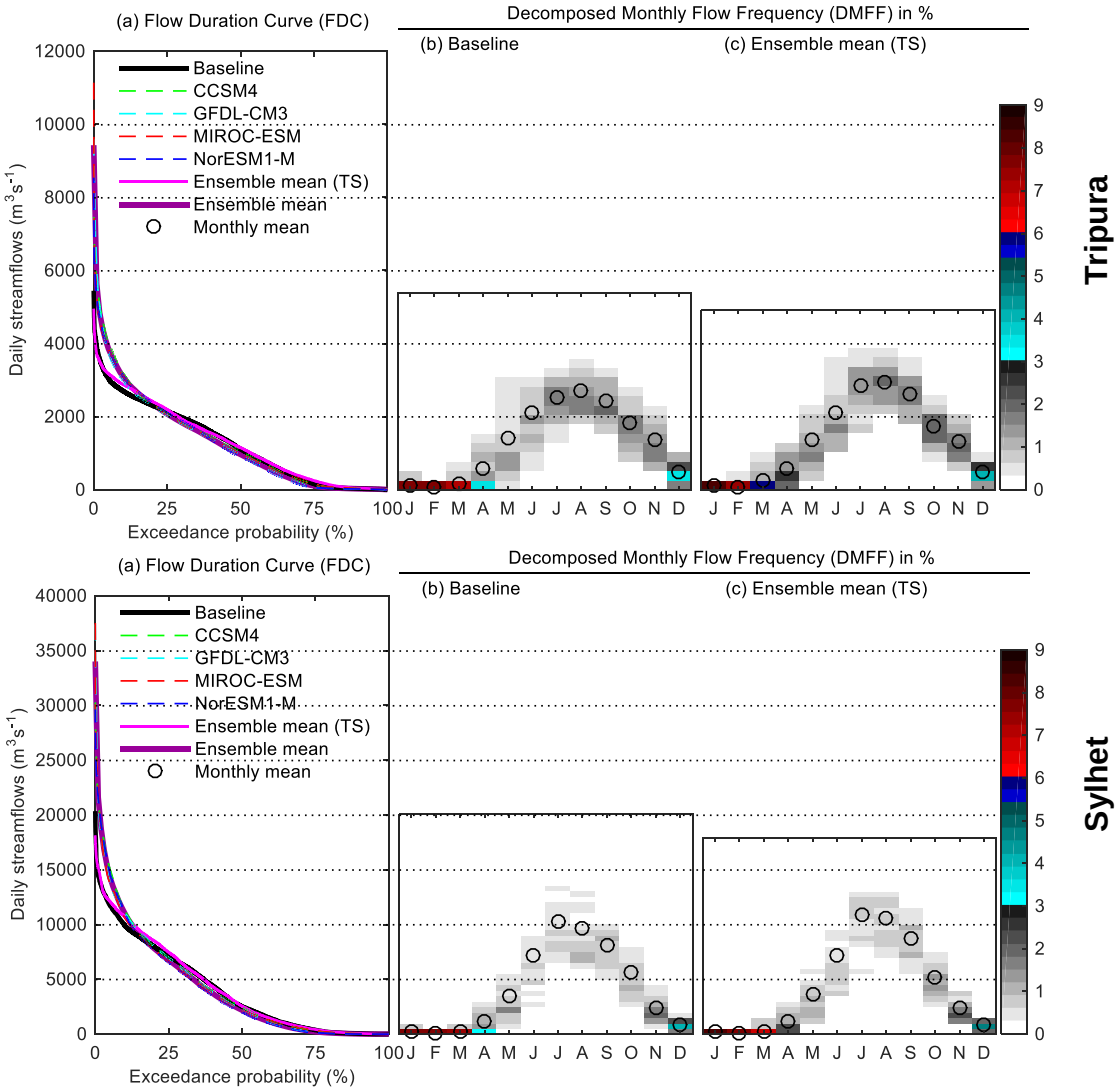

Figure 7.12. Flow duration curve (FDC) and Decomposed Monthly Flow Frequency (DMFF) of streamflows at the outlets of the Tripura and Sylhet basins for the baseline (1981–2000) and projected 2021–2040 periods. In DMFF subplots (b–c), the values of flow interval are respectively 250 and 500 $m^3 s^{-1}$ for the Tripura and Sylhet subbasins.

In general, the basin will produce more runoff during the monsoon period in 2021–2040 than it does in the baseline. Conversely, the post-monsoon and dry season months (except March) will experience reduced flows. The projected increased streamflows in March and May are a concern for the lower Sylhet basin regarding flash flooding in this area. The projection of highest flows at the outlet of all the subbasins differs both in direction and magnitude between the ensemble mean (TS) FDC and ensemble mean FDC approaches. For the former approach, the

changing direction is decreasing relative to the corresponding highest baseline flow whereas it is increasing for the latter approach.

For the far future period 2061–2080, the sign of mean monthly streamflow changes for March–September is almost same to that was found for 2021–2040 but the magnitude of changes is considerably higher for all subbasins (see Table 7.3). For example, the baseline mean flow for May at the outlet of the basin (3465 $m^3 s^{-1}$) is predicted to increase by 12% for 2021–2040 whilts for the later period it is projected to increase by 29%. However, the decreasing mean monthly flow pattern at the basin's outlet for October–December in the near future reverses in the far future period due to increased flows from the Barak and Tripura subbasins. The largest change is 7%. Another opposite result when comparing the near and far future projections is changes in extreme high outflows. Whilst projected extreme high flows are smaller in the near future compared to the baseline for all the subbasins (from 500 $m^3 s^{-1}$ for Tripura to 3500 $m^3 s^{-1}$ for East Meghalaya, see Figure 7.10 to Figure 7.12), extreme flows from the subbasins other than the Meghlaya basin rise to 1800–2350 $m^3 s^{-1}$ over baseline extremes in the far future (Figure 7.13 and Figure 7.15).

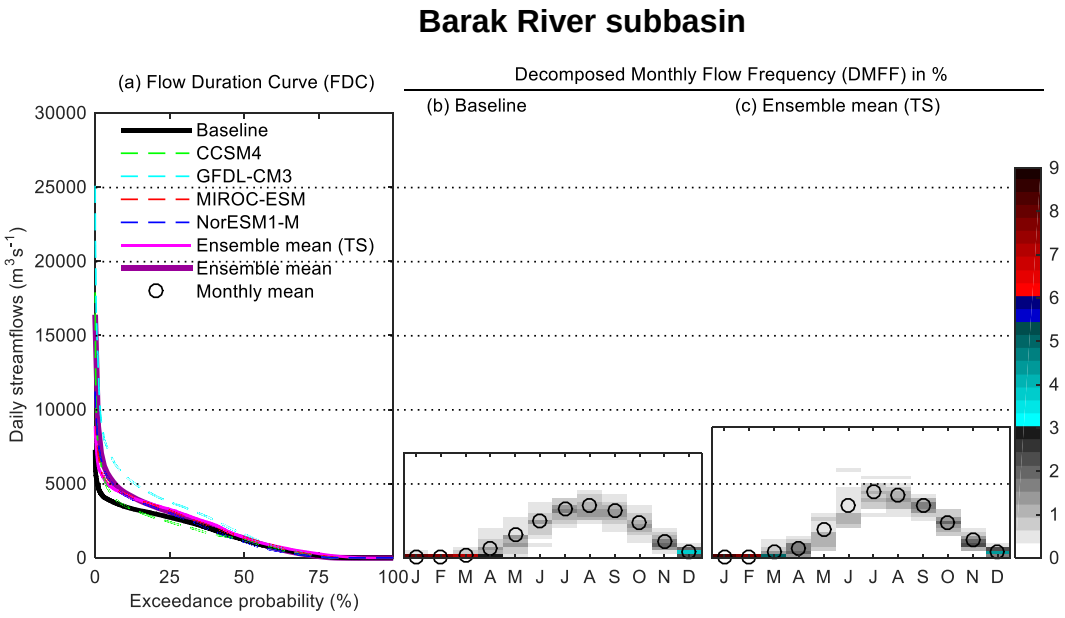

Figure 7.13. Flow duration curve (FDC) and Decomposed Monthly Flow Frequency (DMFF) of streamflows at the outlets of Barak River subbasin for the baseline (1981–2000) and projected 2061–2080 periods. A flow interval of 250 $m^3 s^{-1}$, the height of each constituting block, is used while generating the DMFFs.

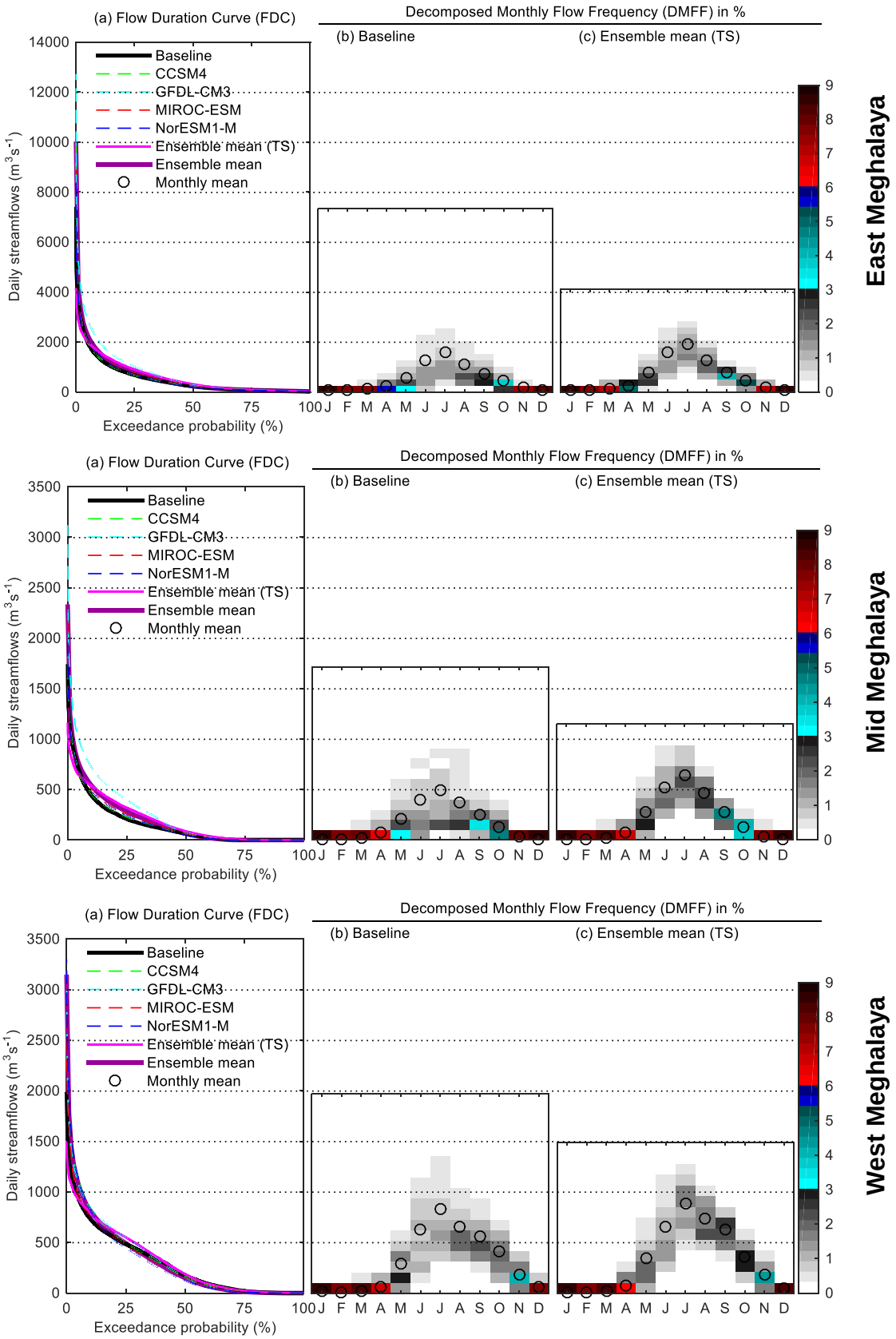

Figure 7.14. Flow duration curve (FDC) and Decomposed Monthly Flow Frequency (DMFF) of streamflows at the outlets of three subbasins in Meghalaya for the baseline (1981–-2000) and projected 2061–2080 periods. In DMFF subplots (b-c), the values of flow interval are respectively 250 and 100 m^3 s^{-1} for the former one and the latter two subbasins.

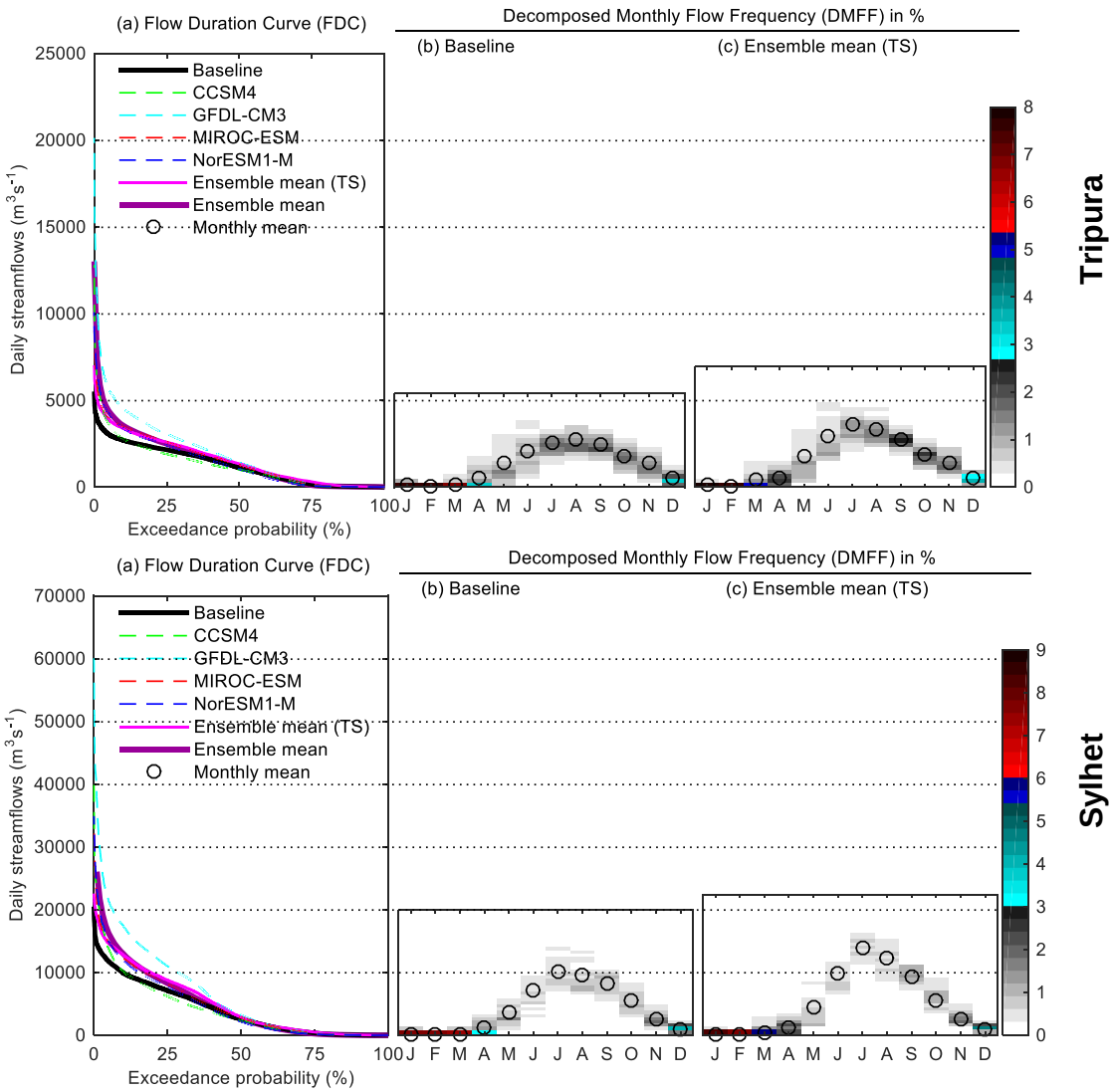

Figure 7.15. Flow duration curve (FDC) and Decomposed Monthly Flow Frequency (DMFF) of streamflows at the outlets of the Tripura and Sylhet basins for the baseline (1981–2000) and projected 2061–2080 periods. In DMFF subplots (b–c), the values of flow interval are respectively 250 and 500 m^3 s^{-1} for the Tripura and Sylhet subbasins.

7.4.3. Projected impacts on wetland hydroregimes

As discussed in Section 1.3.2 the spatial and temporal inundation extent of haor wetlands is of great importance for the lower Sylhet Basin. Therefore, this section describes the simulated changes in wetland water extent in the two projected future periods (2021–2040 and 2061–2080). Since there are 119 subbasin-level

wetlands in the area, changes in combined daily inundated area of those haors are first demonstrated (Figure 7.16). The bottom and top edges of each bar in the figure respectively define 0.05 quantile (or q0.05) and 0.95 quantile (or q0.95) of combined daily wetland inundated area for a calendar month during a simulation period (say, baseline). These two quantiles are also used to express the minimum and maximum wetland inundation extents, respectively. For the late post-monsoonal month November and dry season months December–February, the range of combined wetland inundation for a calendar month is nearly same for all GCMs. This agreement among the GCMs implies that the simulation results are less subject to GCM structural uncertainties. Similar homogeneous results among the GCMs are also found for the monsoonal months (June–September) but the NorESM1-M consistently simulates lowest q0.05. However, a great disagreement among the four GCM with respect to simulated maximum wetland inundation is evident for March–May when the next monsoon season starts to resume (Figure 7.16). This period is generally characterized with sudden heavy rainfall which often causes flash floods in the haor basin (see Section 1.3.2). The following discussion is confined to the results obtained for the ensemble mean (TS) scenario. Unlike the FDC analysis in Section 7.4.2, this section does not include any results based on the conventional ensemble mean scenario because the discussion on combined wetland inundation henceforth mainly focuses on mean monthly inundation statistics that remain identical for both the approaches.

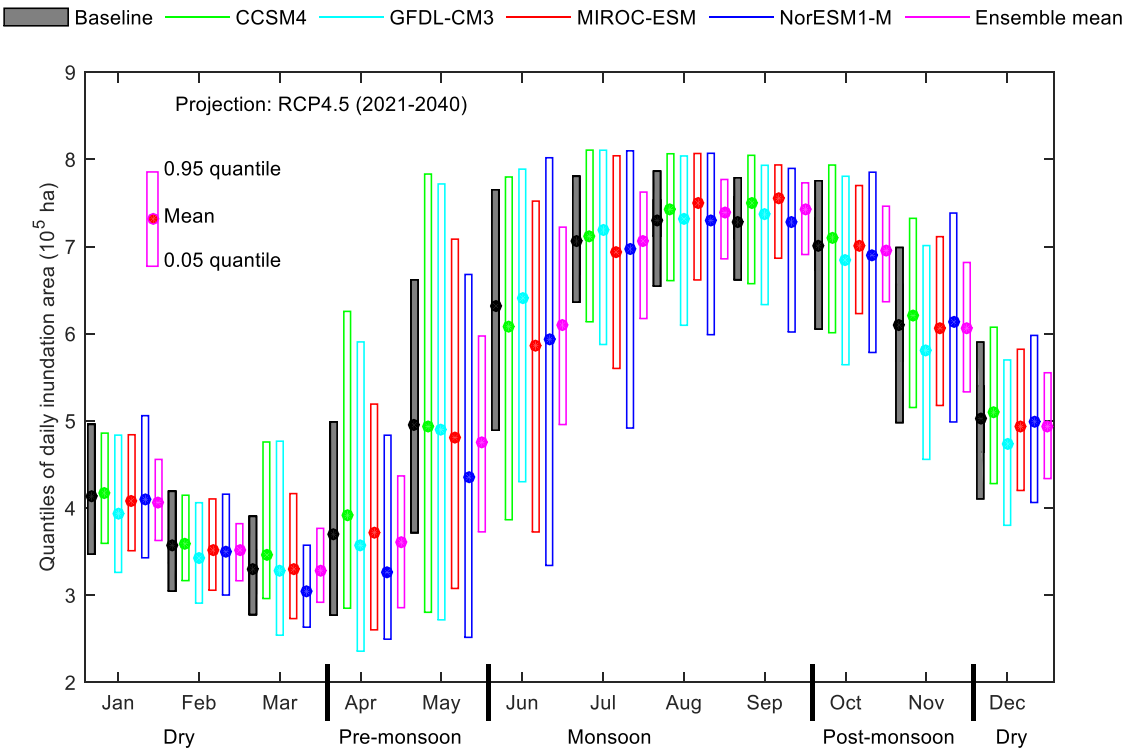

Figure 7.16. Quantiles of combined daily inundated area of all haor wetlands in the URMB for the baseline (1981– 2000) and 2021–2040 periods. Daily simulated water surface areas of all 119 subbasin-level haors are summed to obtain the corresponding combined estimates. The bottom and top edges of each bar are respectively defined by q0.05 (0.05 quantile) and q0.95 (95 quantile) estimated from all daily values in a calendar month.

With respect to the baseline period, projected monthly means of combined wetland inundation area decrease through October to June in the near future (2021–2040) by between 0.6 and 4.0% for the ensemble mean scenario (magenta coloured bar in Figure 7.16) whereas August and September experience increases in wetland inundation (1.4–2.0% compared to the baseline). There is no real change in modelled flood extent for July. Although August is the month with the highest inundated area during the baseline period (729,479 ha, 88% of total wetland catchment 829,523 ha), this shifts to September with for 2021–2040 (742,540 ha, 90% of total wetland catchment). The reduced wetland inundation in April–May for 2021–2040, as quantified by

both mean and maximum statistics, could benefit for haor agriculture. Such decreased inundation will reduce the vulnerability of Boro rice from being damaged by flash floods during harvesting time (April–May). Although this reduction in inundation extent is not notable in combined scale, this will have a great imlications for smaller individual haor-scale. This is further discussed in Section 7.4.4.

For the far future (2061–2080), the monthly mean extent of combined wetland inundation increases in all calendar months except January and February for the ensemble mean scenario (magenta coloured bar in Figure 7.17) compared to the baseline (filled black coloured bar in Figure 7.17). This increase varies from 0.4% in December to 6.50% in June. Moreover, the lowest monthly inundation extents (i.e. q0.05) simulated for 2061–2080 are consistently higher for all months compared to the baseline. With regard to the baseline, whilst the haor wetlands in the basin are predicted to become drier in April and May for 2021–2041 the projected climate of 2061–2080 turns the drier scenario into wetter scenario i.e. an expansion in wetland inundation (1.1–5.5% higher than the baseline inundation). For this reason, such a change in haor hydroregime can potentially deteriorate the current flash flood situation in the far future period and thus impact the productivity of Boro rice.

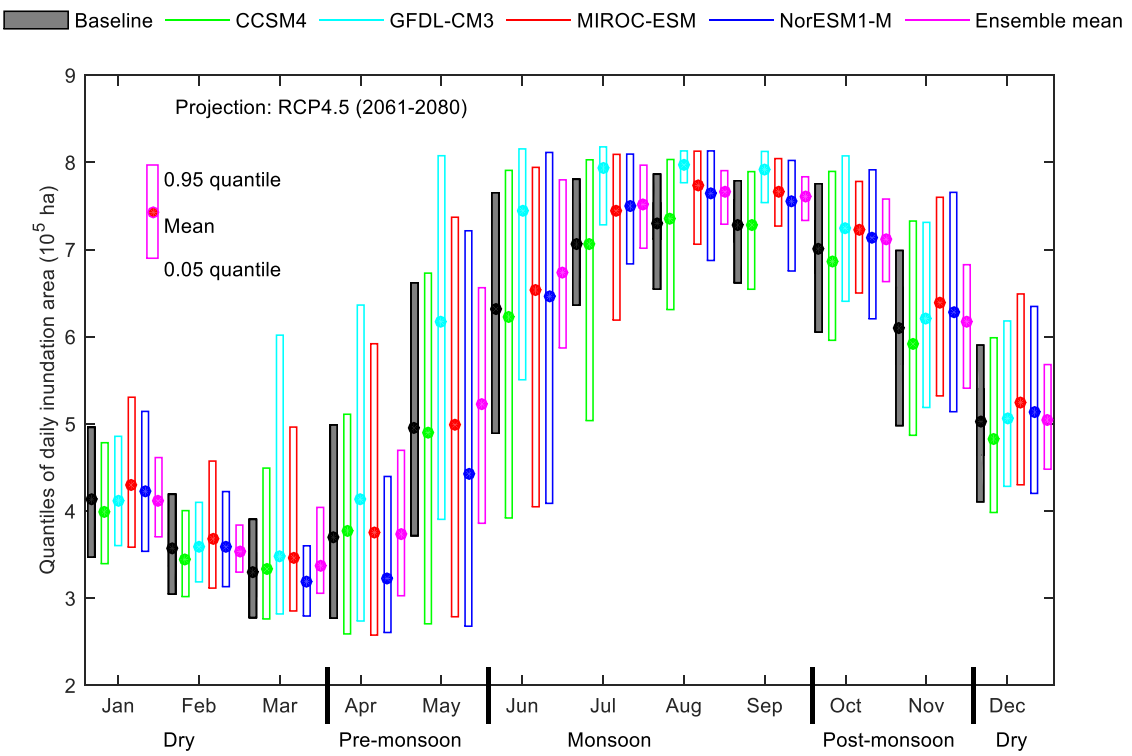

Figure 7.17. Quantiles of combined daily inundated area of all haor wetlands in the URMB for the baseline (1981–2000) and 2061–2080 periods. The explanation of the figure is as same as the Figure 7.16.

For the near future period, spatial changes in the mean monthly haor inundation represented as Inundation Fraction (InFr, the ratio of mean monthly inundated area to an individual wetland's catchment area) for 12 calendar months are mapped in Figure 7.18. These maps are generated from the results of the four GCMs' ensemble mean time series. Any reduction in wetland water area extent can be numerically seen in the corresponding loss of InFr values and vice-versa.

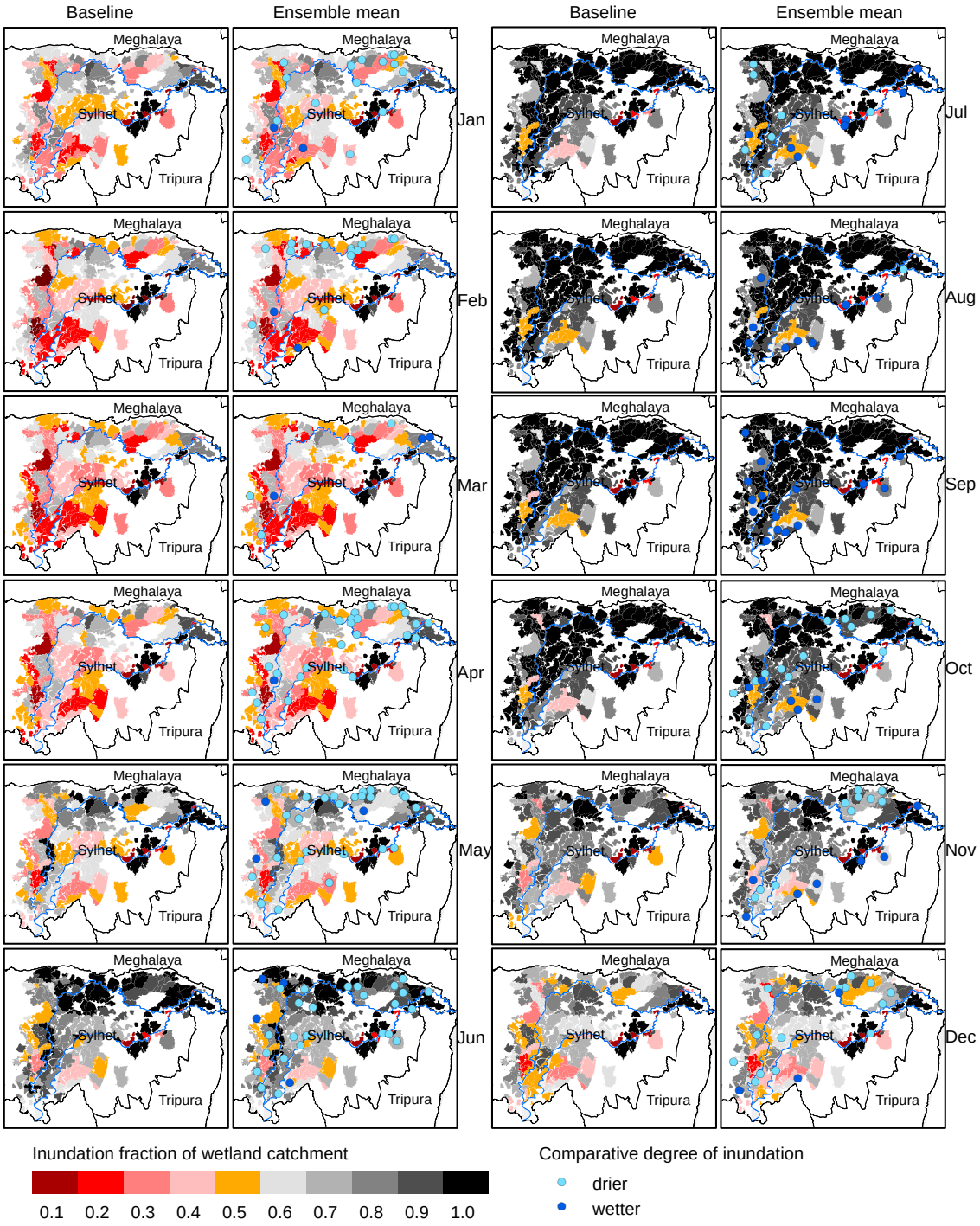

Figure 7.18. Monthly averaged inundation fraction of each individual wetland catchment (i.e. maximum area of a wetland) in the lower UMRB (or Sylhet Basin) for the baseline and the near future period (2021–2040). The circles on the ensemble mean maps are used so as to easily mark the haors where a change in inundation from the baseline period is modelled.

For the near future ensemble mean scenario, the previous evidence of shrinking total combined haors area during October–June (see Figure 7.16) is further demonstrated by the presence of a large numbers of haors in which flood extent declines (light blue circles in subplots along 2nd and 4th columns in Figure 7.18) in the basin compared to the baseline. In August and September, a number of haors, mainly lying at the downstream of Sylhet Basin, become wetter (dark blue circles) compared to the baseline. No specific spatial pattern in the change of InFr within haors is detected. However, it seems that most of the haors lying near the Meghalaya border and at the lower Sylhet Basin are vulnerable to consistent drying out during October–June whereas haors between the two major rivers (Surma and Kyshiyara) are almost unchanged in their mean monthly inundation extent.

For the far future (2061–2080) ensemble mean scenario, many haor wetlands experience an increase in inundated area during May–December in comparison to the baseline (Figure 7.19). These haors are mainly situated at the lower part of the Sylhet Basin and their extent of inundation expands by a maximum InFr value of 0.3 for the 2061–2080 period. The wetter haors in the far future period greatly outnumber those in the near future period for all months (see Figure 7.18). One potential reason for wetter conditions within haors in 2061–2080 compared to 2021–2040 is that the downstream haors may have stronger hydraulic connections with adjacent rivers in the far future since this scenario is associated with larger discharges (see Section 7.4.2). However, a number of wetlands, mainly at the border between the Meghalaya and Sylhet basins, become drier (maximum InFr value 0.1) through October–February and also in April and May for the far future period. These wetlands are relatively small in size and may have weak hydraulic connections with their adjacent rivers.

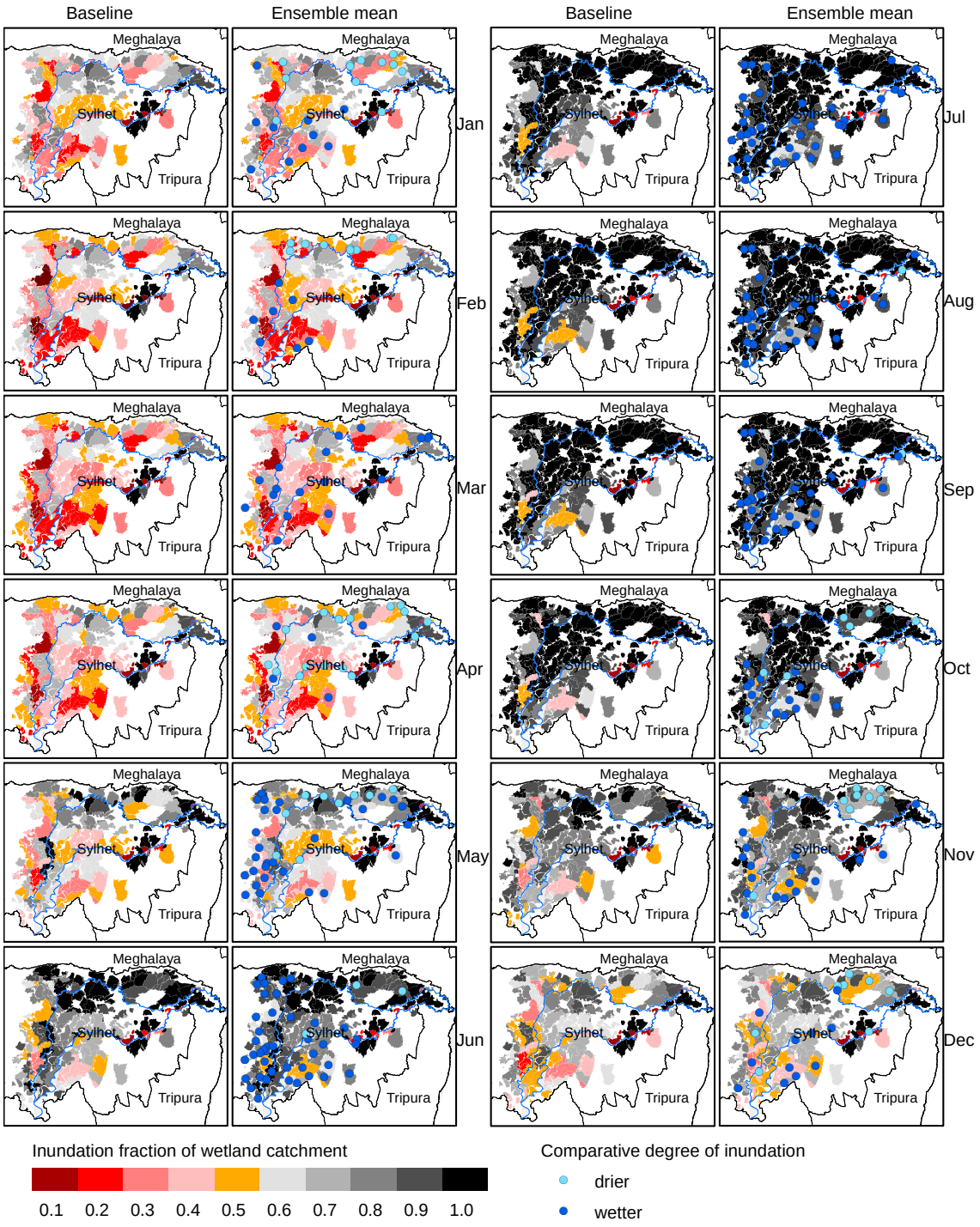

Figure 7.19. Monthly averaged inundation fraction of wetlands for the baseline and near future (2061–2080) periods. All other descriptions are as same as Figure 7.18.

7.4.4. Projected risk of flood-induced damage to Boro rice in the basin

One of the foremost objectives of the study was to assess the risks associated with the damage of Boro rice due to flash floods in the haor region during harvesting time (April or May). This is achieved by analysing a risk map (Figure 7.20) constructed from CDFs or cumulative probability curves of simulated wetland water surface areas during planting (December or January) and harvesting periods of the crop. These CDFs are constructed from simulated daily wetland water extents for corresponding calendar months. The risk zones (shaded grey colour) in Figure 7.20 indicate the exceedance probability (= 1 - CDF value) of a wetland catchment area being at risk of flooding during harvesting time. As discussed in Section 1.3.2, in common, farmers transplant Boro rice seedlings in all un-inundated haor areas during planting time. Therefore, the highest water level in a harvesting month and the lowest water level in a planting month during a period of study (e.g. 1981–2000 for baseline) are the two boundary points which account for the largest possible wetland catchment area that is exposed to flash floods during the harvesting month. This is schematically shown in Figure 7.21. Since the exceedance probability of flooding a wetland area at a particular water level is not always equal to 1.0, a risk zone in Figure 7.20 is always less than the largest or Potential Flash Flood Exposed (PFFE) area. Rationalised Flood Risk (RFR) is a metric that is defined as the ratio of risk zone area to PFFE area; therefore, the value of RFR indicates average flooding risk for per unit wetland catchment area.

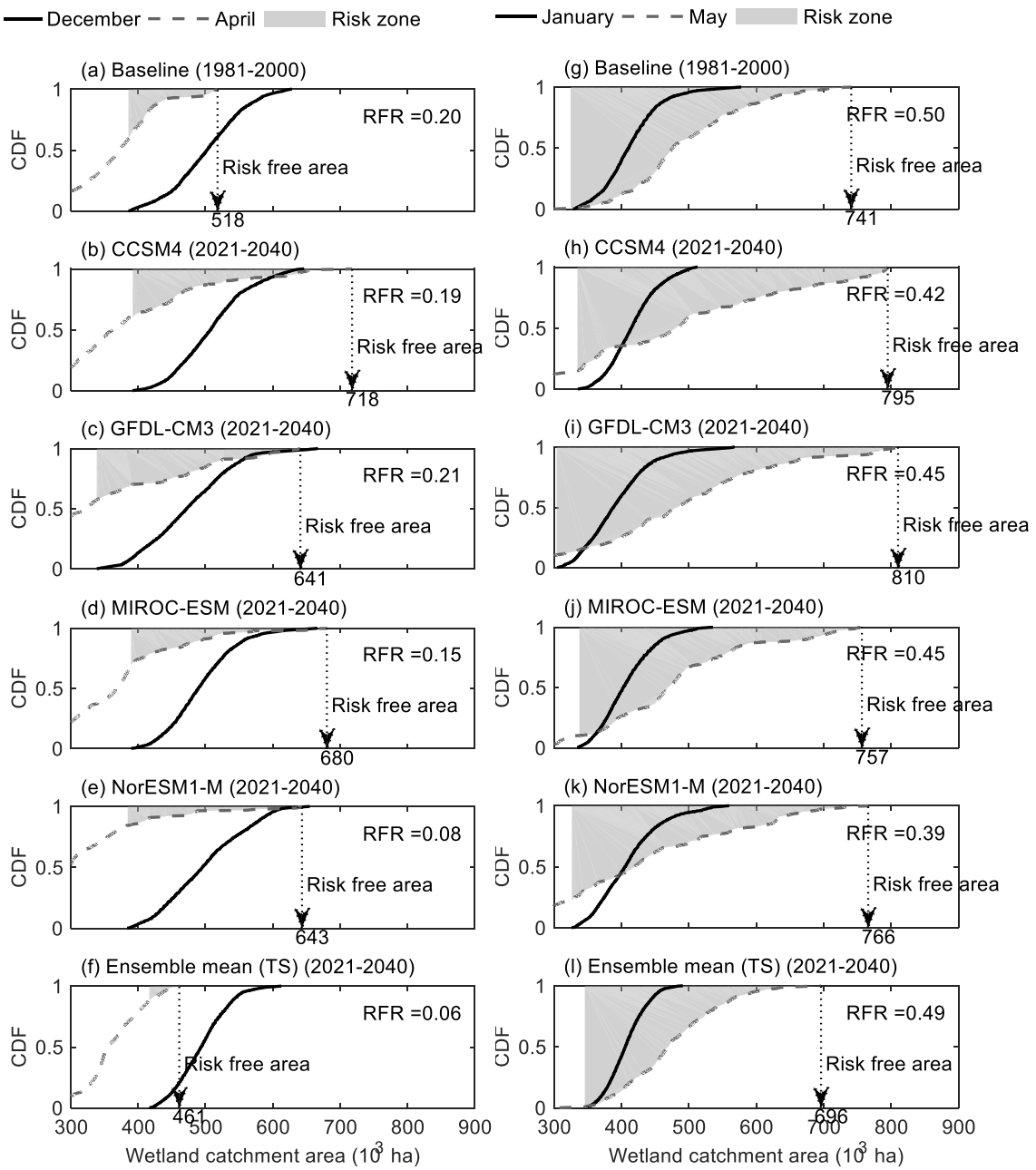

Figure 7.20. Estimated risk of Boro rice damage due to floods during harvesting time for the baseline (1981–2000) and near future period (2021–2040). For all subplots in the left panel, December (solid black CDF line) and April (dashed grey CDF line) are the planting and harvesting months, respectively while those in the right panel are for a month lag of planting (January) and harvesting (May) times. A vertical line drawn through any point on a CDF curve demarcates the interface between inundated and un-inundated areas (see subplot a). Any area beyond the highest inundation level during a harvesting month is denoted as flood or risk free area for that month.

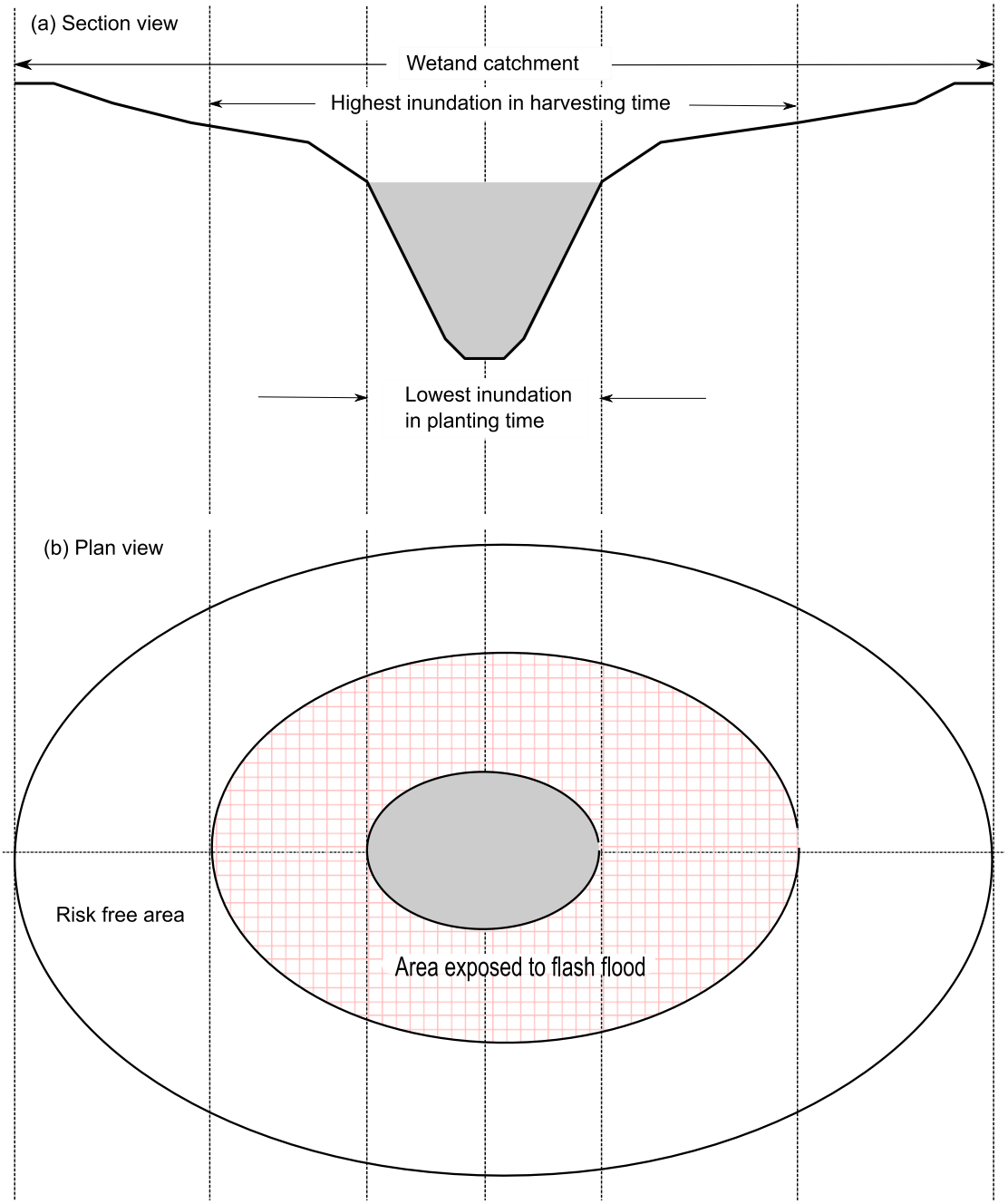

Figure 7.21. Potential wetland catchment area exposed to flash flood during harvesting time with respect to planting time. Any area above the highest inundation level is flooding risk free during harvesting time.

The current common farming practice in the haor region transplants Boro rice seedlings in December and harvests the rice in April. Assuming this traditional practice will continue in the future, projected flooding risks are compared with that of baseline period (subplots a–f in Figure 7.20). Except GFDL-CM3, the other

three GCMs (Figure 7.20b, d, e) project smaller RFR values for the near future period (2021–2040) compared to the baseline period. The decreasing RFR (ensemble mean is 0.16) signature indicates that average flooding risk of per unit wetland catchment area during the harvest month (i.e. April) is likely to decrease for the near future period. On the other hand, the baseline PFFE area of 133 ha (highest inundated area in April 518×10^3 ha minus lowest inundated area in December 385×10^3 ha, see Figure 7.20a) is consistently projected to increase to between 258×10^3 and 333×10^3 ha between the GCMs; the ensemble mean is 297×10^3 ha. This is because the projected future water regime will inundate more upland dry areas during the harvesting time whilst these areas [area between the highest inundated areas of 518×10^3 ha for the baseline period and of 671×10^3 ha (ensemble mean) for the future period] are free from any flash flooding risk under the baseline scenario. Although the PFFE area increases it does not necessarily increase the average flooding risk, as measured with RFR value, of haor wetlands because the inundation frequency of the extended upper PFFE area (i.e. risk zone area above the highest baseline inundated area of 518×10^3 ha in Figure 7.20b–e) is very small. The slight increase in flooding risk for GFDL-CM3 can be linked to exposing more area to more frequent flash floods at the lower part of the wetlands (Figure 7.20c). This happens because of the lowering of the smallest inundated area in December for the near future period which in turn releases some cultivable wetland areas that are highly vulnerable to flash flood in the harvest month.

Figure 7.20f is generated from the time series of daily ensemble mean (TS) inundated areas as described in Section 7.4.2 for streamflows. The decreasing flooding risk scaled by RFR in the near future projected period (RFR=0.06 in Figure 7.20f) is due to reduced PFFE area squeezing from both extreme inundation levels (lowest in planting time and highest in harvesting time). This RFR value is much lower than the average of RFR values estimated for each individual GCMs (Figure 7.20b–e). Whereas the two extreme levels are at 385×10^3 and 518×10^3 ha (i.e. PFFE =133×10^3 ha) during the baseline period (Figure 7.20a), the corresponding projected values are of 416×10^3 and 461×10^3 ha (i.e. PFFE =45×10^3 ha) for the 2021–2040 period (Figure 7.20f). This leads to a decrease in PFFE area of 88×10^3 ha in the future projected period that is also

reflected in a lower RFR value (Figure 7.20f). Although both ensemble mean approaches predict a decreasing average flooding risk of haor wetlands in the near future period, they contrast in their projected PFFE areas. Whereas the ensemble mean PFFE area (i.e. average of PFFE values obtained for all individual GCMs; PFFE = 297×10^3 ha) increases in the near future period, the ensemble mean (TS) PFFE area (45×10^3 ha) decreases. As discussed in Section 7.4.2, averaging of multiple GCM time series results in a smoother ensemble mean time series due to levelling out of individual GCMs' spikes. This narrows the range of the ensemble mean time series by respectively suppressing higher inundation extents and elevating lower inundation extents. In Figure 7.20f, therefore, squeezing of both boundary areas (lowest area in planting time and highest area in harvesting time) defining the PFFE area of wetlands reduces PFFE area in the near future period. Such reduction in PFFE area can be considered as a positive impact of climate change for haor agriculture. However, since the lowest inundation area increases during the planting time for 2021–2040, about 31×10^3 ha of haor area is converted to permanently inundated areas. This loss of arable land might have a negative impact for Boro rice cultivation but a positive impact for the sustenance of aquaculture.

Subplots g–l on the right panel of Figure 7.20 shows flooding risks, as expressed by RFR metric, for the delayed planting (January) and harvesting (May) of Boro rice. Although this farming practice is not generally followed in the haor region, sometimes Boro planting may be delayed by late seedlings that are not yet ready to be planted. The January–May farming practice results in a greater flooding risk, as indicated in ensemble mean RFR value of 0.43 (subplots h-k in Figure 7.20), compared to its counterpart in the December–April farming practice. This increased risk can be linked to the larger risk zone area for the delayed farming practice. The risk zone area increases in two ways (i) inundating more haor area in May than April due to increased PFFE area (see also decreasing risk free areas), and (ii) more frequent inundation of deeper haor region in May than April. This finding demonstrates that the January–May farming practice remains riskier for both the baseline and future periods compared to the normal December–April practice.

Like the case of 2021–2040, although the average flooding risk (i.e. RFR value) of haor wetlands for 2061–2080 remains below or the same as corresponding baseline risk, the highest inundation extents increase markedly thus expanding PFFE areas. The ensemble mean RFR values for the far future period are of 0.17 for the December–April farming practice (Figure 7.22b–e) and 0.43 for the January–May farming practice (Figure 7.22h–k). The reason can be linked to the increasing PFFE areas as explained for 2021–2040.

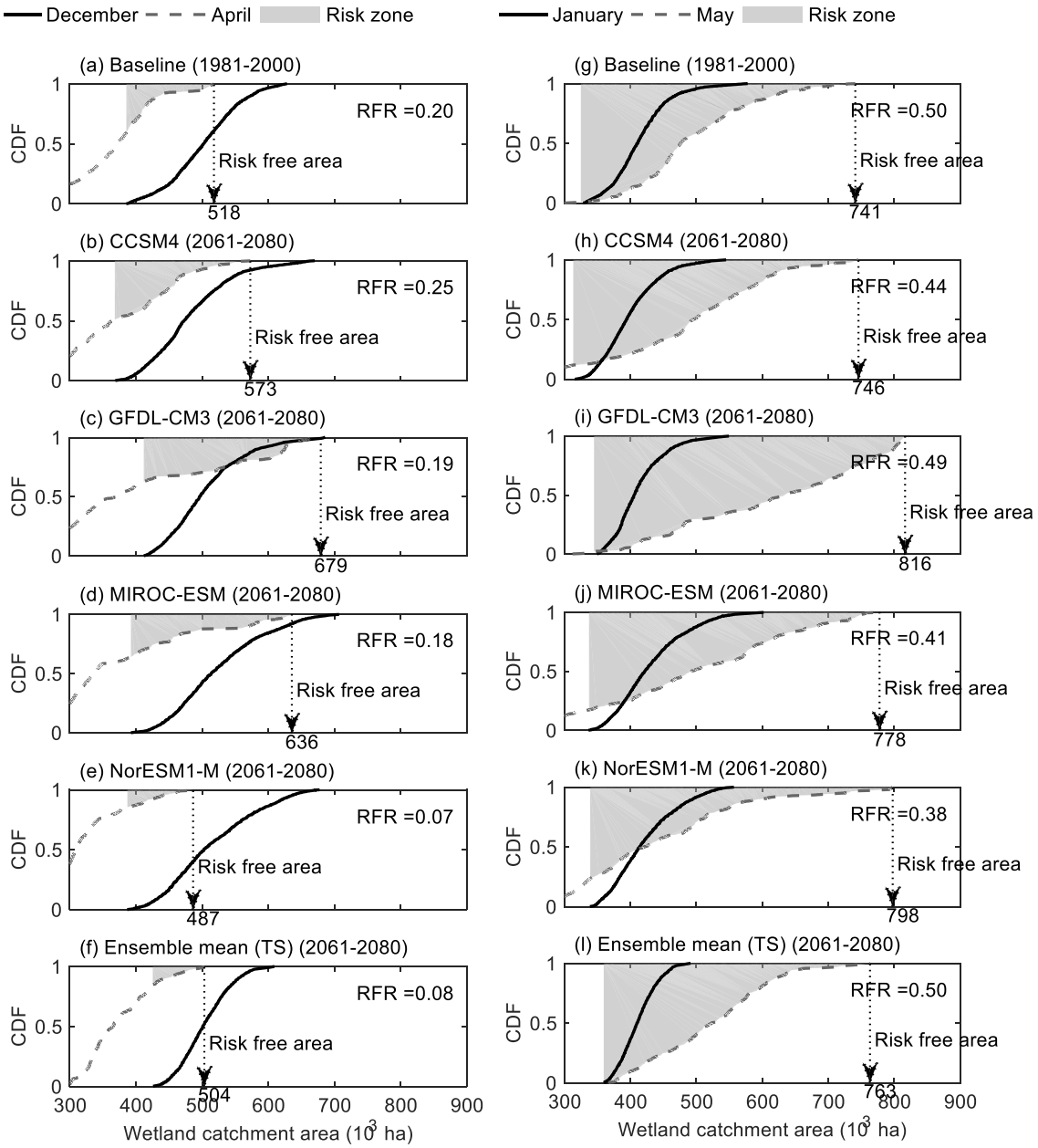

Figure 7.22. Estimated risk of Boro rice damage due to floods during harvesting time as shown in Figure 7.20 but the future projected period is 2061–2080.

7.5. Summary

The calibrated SWATrw model for the UMRB was driven with bias corrected future climate time series simulated by four GCMs that participated in the CMIP5. These GCMs are found to be comparatively more skillful over others (see Section 7.2) in representing Indian summer monsoon that dominates the climate of the UMRB. The quantile mapping bias correction method that was adopted was useful not only for removing biases from the raw GCM climate data but also for adjusting the frequency of dry days (rainfall) or coldest days (temperature). Even though the four GCMs are a good simulator of the regional monsoon, they still lead to uncertainty in simulated extreme high daily streamflows.

For the ensemble mean scenario, the SWATrw model simulated results show that streamflows of the basin will increase in the pre-monsoon and monsoon seasons for both 2021–2040 and 2061–2080 periods. However, flows from the major constituting subbasins of the UMRB decrease in the dry season months (December–March) for the near future period whereas the simulated response in December reverses for the far future period.

The mean monthly combined inundated area of haor wetlands is projected to decrease through October–June by a maximum amount of 4.0% in the near future period (2021–2040) for the ensemble mean scenario, whereas these wetlands increase by up to 2.0% in the late monsoon (August and September). However, the far future predicted climate results in an increase in the combined extent of haor wetland inundation (by a maximum of 6.5%), the number of wetlands, and duration (March–January) compared to the baseline. Although the projected average risk (i.e. RFR value) of Boro rice flooding in the haor areas decreases in both the future periods compared to the baseline period, in absolute term the projected water regime will cause the haors to be exposed to more flash floods due to frequent (measured with risk zone area) and extended (measured with PFFE area) haor inundation. For the December–April farming practice, the baseline PFFE area of 133×10^3 ha expands to 297×10^3 ha and 200×10^3 ha respectively for the near and far future periods. Nonetheless, like the baseline,

the January–May farming practice remains riskier for the two future periods compared to the December–April practice.

Chapter 8
Conclusions and recommendations

8.1. Conclusions

The three foremost aims of the research presented in this thesis were: (i) to bridge the current research gap of inadequate wetland modelling at the catchment scale by developing a hydraulic principles based wetland model that can simulate bidirectional interactions existing within wetland-river-aquifer systems, (ii) to investigate climate change impacts on the hydrological conditions within the Upper Meghna River Basin (UMRB), and (iii) to investigate flooding risk of intensively Boro rice cultivated haor wetlands in the lower Sylhet Basin of the UMRB in response to future climate change. This thesis argues that the ability of fully-distributed models to simulate depressional wetlands at the catchment scale is limited by their high demands for uniform and fine resolution DEM data. This is true particularly where simulating the water regime of individual wetlands (say, inundation extent) is of an interest. Moreover, existing catchment models (both fully- and semi-distributed) are not only inappropriate to represent wetlands geometry but also incapable of simultaneously simulating hydraulic interactions between wetland, river and aquifer systems. Semi-distributed catchment models are identified as a suitable platform to model riparian wetlands as those found in the UMRB. Therefore, the open source code distributed SWAT model, that is probably the most widely used catchment model across the world, was selected to be adapted to more accurately represent hydrological processes in operation within the study area. The following sections highlight the main findings and draw necessary conclusions.

8.1.1. Development of the SWATrw model

The development of SWATrw (SWAT for riparian wetland), an improved version of SWAT, is a fundamental contribution of this thesis to advance the present wetland modelling approach at the catchment-scale. SWATrw incorporates a

robust wetland geometric model that overcomes the flawed and unrealistic wetland shape representation within the current version of SWAT (rev627). Therefore, for a case study with the Hakaluki haor wetland within the basin, the SWATrw model was able to realistically simulate various wetland hydrological processes (precipitation, evaporation and seepage) that are greatly influenced by a wetland's water depth and surface area. Another area where SWATrw is superior to SWAT is the inclusion of bidirectional hydraulic interactions between wetlands, rivers and aquifers. This facilitates the simulation of pre-monsoonal flash floods in the haor areas that occur mainly by overflowing adjacent rivers. Since SWAT ignores the role of hydraulic pressure on water movement between hydraulically connected wetlands and aquifers, it falsely empties the Hakaluki haor of water in the dry season because of unrealistic water loss seeping through the wetland bottom. SWATrw was found to be successful in addressing this limitation and led to a more accurate simulation of the water stored in the beels of the haor during the dry season. Although both SWAT and SWATrw produced almost the same calibration results, it does not undermine the superiority of SWATrw over SWAT. Since wetlands occupy less than 3% area of the entire Barak-Kushiyara River Basin, their differentiating impacts by the models on flows at the downstream gauging stations were very small. However, it is argued that where the presence of wetlands in a catchment exerts distinguishable flow regimes (e.g. where wetlands occupy a considerable amount of a catchment area) from that if there were no wetlands in the catchment, then the better streamflow simulation by SWATrw over SWAT could be traced. This is because SWATrw has been proved more skilful to simulate wetland hydrological processes compared to SWAT. The revised SWATrw has already been reported in the international peer-reviewed literature (Rahman et al., 2016) and offers improved simulation for catchments where riparian wetlands are a major feature. This model could be used for different types of wetlands (e.g. riparian and non-riparian wetlands) existing across the world.

8.1.2. Development of a SWATrw model for the UMRB

None of the reviewed previous studies explicitly includes the role of numerous haor wetlands on the hydrology of the lower UMRB while analysing the basin's

water issues. Moreover, data limitations for the three constituting Indian basins (Barak River, Meghalaya and Tripura basins) forced the previous studies either to completely exclude those basins or to represent the basins in a lumped manner rather than distributing their hydrological behaviour. This study, for the first time, explicitly develops a distributed SWATrw model for the entire UMRB (267 subbasins and 1237 HRUs) by compiling multi-source input data (e.g. topography, land use, soil, and hydro-meteorologic). Furthermore, digitisation of the detailed river networks (total 8990 km running length and 0.14 km km^{-2} river density) for the 63,746 km^2 UMRB using DEM, different imagery and other ancillary information is another major contribution of this thesis.

In general, the model showed statistically satisfactory results in simulating river discharges (15 gauging stations) and stages (3 gauging stations) for the calibration period (1990–2003). However, under-represented Meghalaya rainfall data (i.e. IMDdist) was primarily behind the model's underestimating flows for the Meghalaya basins for the validation period (2004–2010). This study has identified one potential limitation of SWATrw (also SWAT) that the assumption of zero boundary flow condition between aquifers underneath adjacent subbasins can produce unrealistic results. For example, about 50% of shallow aquifer water had to intentionally be removed from the subbasin drained at the Laurergahr station so as to match the observed streamflows at the outlet by reducing baseflow contribution. However, later it was identified that this disappeared water might have had a potential contribution, through baseflows, to mitigate the underestimating downstream river flows during the recession period of hydrograph if there were subbasin-level aquifer connectivity in the current models.

8.1.3. Development of an improved Quantile Mapping (QM) bias correction approach for climate data

This study has improved the QM bias correction method by incorporating a new algorithm to adjust dry day frequency (coldest day for temperature) in raw GCM rainfall data to be used for local-scale studies. Whilst they are widely used, the delta factor method and less frequently used QM based approaches rarely

address the issue associated with extreme lowest quantities (i.e. dry and coldest days) in raw GCM data. This study argues that adjustment of flawed lowest extremes is essential especially when dry season hydrological responses to climate change are to be projected. The new QM approach may be a promising tool for wider applications in climate change studies.

8.1.4. Projected changes in future climate (rainfall and temperature) for the UMRB

To force the SWATrw model, future climate data were obtained from NASA's NEX-GDDP depository providing downscaled (~27 km spatial resolution) and bias corrected CMIP5 GCM data. Historical simulated climate data (1981–2000) from the four GCMs (CCSM4, GFDL-CM3, MIROC-ESM and NorESM1-M) used in the study were found to be highly biased (e.g. bias in mean annual rainfall across the basin ranges from 750 to -2750 mm yr^{-1}) in representing corresponding historical observations across the UMRB. Therefore, this study discourages direct use of NEX-GDDP GCM data, particularly in regions dominated by the Indian summer monsoon, even though the data were trained with globally available historical observations. For any local-scale study, NEX-GDDP data should be further bias corrected by training with local climate observations as undertaken with the QM method for the UMRB.

For the RCP4.5 scenario of CMIP5, climate change results were analysed using the projections from the four ensemble GCMs for the near (2021–2040) and far (2061–2080) future periods. For the ensemble mean of the four GCMs, increasing mean annual rainfall across the basin is predicted for both future periods in contrast to the baseline (1981–2000). Increases can be up to 150 mm yr^{-1} (near future) and 1000 mm yr^{-1} (far future) over the baseline rainfall. This increase is linked to increased rainfall in the late pre-monsoon (May) and the entire monsoon season (June–September). Both post-monsoonal months (October–November) are projected to experience reduced rainfall across the basin (by 10–50% of the corresponding baseline value). The basin is projected to be 1.0–1.7°C warmer than the baseline in the near future period whilst increases will be larger for far future period (1.7–2.7°C).

8.1.5. Projected future changes in streamflows and haor wetland inundation in the UMRB

The basin's river system is predicted to experience an average increase of 12% dischrage thoughout the monsoon season in the near future compared to the baseline; this might increase by up to 42% for the far future period. Whereas post-monsoon and dry season months experience lower flows for the near future period this pattern reverses for the far future period because of higher runoff from the Barak River and Tripura basins. Projected increasing flow in the two Boro crop growing months, March and May, may be a major concern for the haor agriculture by exposing crops to more flash floods.

It was found that when compared to the baseline, the combined inundation extent of all haors expands by up to 2.0% in the late monsoon (August and September) and shrinks up to 4.0% in the months of October–June for the near future period. According to the average indicator of risk, as measured by the RFR value, the commonly followed December–April (i.e. respectively planting and harvesting months) farming practice in the haor areas will be less vulnerable to damage of Boro rice by flash floods in both near and far future periods. In absolute terms, however, the baseline PFFE area of 133×10^3 ha is projected to expand by between 200×10^3 and 297×10^3 ha (ensemble mean) for the future periods. Like the baseline period, the January–May farming practice remains riskier than the December–April in the future.

8.2. Limitations and recommendations for the future research directions

One of the major limitations of the study is the lack of observed time series climate and discharge data for the three Indian basins. The IMDgrid climate data used in this study for the Indian part of the basin does appear to under-estimatee the actual rainfall pattern in Meghalaya basin. The same applies to another Indian data set IMDdist. Whereas actual mean annual rainfall at Cherrapunji, Meghalaya is >=11,500 mm (Dash et al., 2012; Dhiman, 2012; FFWC, 2011; IFAD, 2011), these data sets represent rainfall in its part of the basin as around 8350 mm.

Similarly, due to the lack of discharge data for the Indian part of the basin, the model could not be calibrated against observed flow data above the border between the downstream Sylhet and upstream three Indian basins. Although several attempts were made to collect those data, none was successful. Therefore, a major recommendation from this thesis is that collaborative research between the transboundary nations (Bangladesh and India) is required in order to better understand the regional hydrology and its responses to climate change.

The current SWAT/SWATrw model can simulate only a dendritic river system as with many other contemporary catchment models. In deltaic and flat areas where river networks are criss-crossed in pattern by many tributaries and distributaries, the application of these models is problematical. In this study, however, a number of distributaries in the Sylhet Basin are modelled with a 'transfer' function currently embedded in the models. This function can apportion a main river flow between two of its downstream distributaries using a user given ratio. There is a scope for further study of addressing this issue with more physics-based river hydraulics. In some previous studies, the above limitation was overcome by coupling SWAT with river hydraulics models e.g. SOBEK by Betrie et al. (2011b) and HEC-RAS by Javaheri and Babbar-sebens (2014). However, none of the attempts has been the integral part of SWAT nor makes those models available for wider applications.

The GLC land use data that were used in the study represent the average land use of 1981–1994 (see Section 4.2.2). Therefore, simulation results for the last 16 years of model development period (1990–2010) might contain unavoidable uncertainties if land use change in the recent two decades considerably influences the local hydrology. Some recent studies reveal that the hill slope areas of the basin are being increasingly altered with pineapple and rubber cultivation and human settlements (RRCAP, 2001; Sherwood, 2009; TEEBcase by P. Thompson and T. Balasinorwala, 2010). Such changes may significantly alter local hydrological state. According to these studies, for example, the aforesaid land use change causes sedimentation in rivers and haor wetlands of the lower UMRB. Despite the limitation of ground-based data, use of remote sensing derived vegetation maps could be useful to identify the spatio-temporal

land use changes in the basin and thus to assess consequences on the basin's hydrology.

This study used only four GCMs while projecting future climate and assessing its impacts on the hydrology of the basin. These models were handpicked from a pool of 20 GCMs studied by Menon et al. (2013) for investigating their relative skills in reproducing Indian summer monsoon. Predictions from more GCMs are suggested in order to better account for structural uncertainties involved in GCMs as used elsewhere (Ho et al., 2016; Thompson et al., 2013). With more observed climate data, specifically for the Indian part of the basin, the relative performance of currently available GCMs should be evaluated to find which GCMs are capable of reproducing historical rainfall pattern of the basin. The highly variable rainfall of the basin (see Section 4.2.5.1), both in spatial and temporal scales, is characterized by convective and orographic phenomena (see Section 1.3.1). For this reason, dynamical downscaling of GCM data can be employed to investigate whether such approach has any better skills in reproducing the basin's climate compared to the statistical QM approach. Since the former approach takes the effect of local topography into account while simulating climate data from raw GCM data, it is expected that rainfall variability can be better modelled by the approach compared to the statistical downscaling approach.

Another limitation of the present study is the lack of sufficient observed geometric and hydroperiod data of haor wetlands. Therefore, an in-situ field study can be set up for monitoring hydro-meteorological conditions within some representative haor wetlands. In addition, high resolution topographic data could be used to more accurately generate the geometry of haor wetlands. With using such data, the performance of SWATrw could be further tested and refined, if necessary.

References

Abebe, N.A., Ogden, F.L., Pradhan, N.R., 2010. Sensitivity and uncertainty analysis of the conceptual HBV rainfall–runoff model: Implications for parameter estimation. J. Hydrol. 389, 301–310. doi:10.1016/j.jhydrol.2010.06.007

Acreman, M.C., Blake, J.R., Booker, D.J., Harding, R.J., Reynard, N., Mountford, J.O., Stratford, C.J., 2009. A simple framework for evaluating regional wetland ecohydrological response to climate change with case studies from Great Britain. Ecohydrology 2, 1–17. doi:10.1002/eco

Ahmadi, S.H., Amin, S., Reza Keshavarzi, A., Mirzamostafa, N., 2006. Simulating watershed outlet sediment concentration using the ANSWERS model by applying two sediment transport capacity equations. Biosyst. Eng. 94, 615–626. doi:10.1016/j.biosystemseng.2006.04.015

Ahmed, F.H., 2014. Reducing flash floods risk for bumper Boro. News Today.

Ajami, N.K., Gupta, H., Wagener, T., Sorooshian, S., 2004. Calibration of a semi-distributed hydrologic model for streamflow estimation along a river system. J. Hydrol. 298, 112–135. doi:10.1016/j.jhydrol.2004.03.033

Akanda, A.S., 2012. South Asia's water conundrum: hydroclimatic and geopolitical asymmetry, and brewing conflicts in the Eastern Himalayas. Int. J. River Basin Manag. 10, 307–315. doi:10.1080/15715124.2012.727824

Allen, P.M., Arnold, J.G., Skipwith, W., 2008. Prediction of channel degradation rates in urbanizing watersheds. Hydrol. Sci. J. 53, 1013–1029. doi:10.1623/hysj.53.5.1013

Allison, M.A., Kuehl, S.A., Martin, T.C., Hassan, A., 1998. Importance of flood-plain sedimentation for river sediment budgets and terrigenous input to the oceans : Insights from the Brahmaputra-Jamuna River. Geology 26, 175–178. doi:10.1130/0091-7613(1998)026<0175

Alvisi, S., Bernini, A., Franchini, M., 2013. A conceptual grey rainfall-runoff model for simulation with uncertainty. J. Hydroinformatics 15, 1–20. doi:10.2166/hydro.2012.069

Ambrose, S.M., Sterling, S.M., 2014. Global patterns of annual actual evapotranspiration with land-cover type: knowledge gained from a new

observation-based database. Hydrol. Earth Syst. Sci. Discuss. 11, 12103–12135. doi:10.5194/hessd-11-12103-2014

Andersen, H.E., Kronvang, B., Larsen, S.E., Hoffmann, C.C., Jensen, T.S., Rasmussen, E.K., 2006. Climate-change impacts on hydrology and nutrients in a Danish lowland river basin. Sci. Total Environ. 365, 223–237. doi:10.1016/j.scitotenv.2006.02.036

Arnell, N.W., 2003. Effects of IPCC SRES emissions scenarios on river runoff: a global perspective. Hydrol. Earth Syst. Sci. 7, 619–641. doi:10.5194/hess-7-619-2003

Arnell, N.W., 1999. Climate change and global water resources. Glob. Environ. Chang. 9, 31–49.

Arnold, J.G., Allen, P.M., Bernhardt, G., 1993. A comprehensive surface-groundwater flow model. J. Hydrol. 142, 47–69. doi:10.1016/0022-1694(93)90004-S

Arnold, J.G., Allen, P.M., Volk, M., Williams, J.R., Bosch, D.D., 2010. Assessment of different representation of spatial variability on SWAT model performance. Trans. ASABE 53, 1433–1443.

Arnold, J.G., Gassman, P.W., White, M.J., 2010. New developments in the SWAT ecohydrology model, in: 21st Century Watershed Technology: Improving Water Quality and Environment. ASABE.

Arnold, J.G., Srinivasan, R., Muttiah, R.S., Williams, J.R., 1998. Large area hydrologic modeling and assessment part I: model development. J. Am. Water Resour. Assoc. 34, 73–89.

Arnold, J.G., Williams, J.R., Nicks, A.D., Sammons, N.B., 1990. SWRRB: A basin scale simulation model for soil and water resources management. College Station, TX.

ASCE, 1993. Criteria for evaluation of watershed models. J. Irrig. Drain. Eng. 119, 429–442.

Babel, M.S., Wahid, S.M., 2011. Hydrology, management and rising water vulnerability in the Ganges–Brahmaputra–Meghna River basin. Water Int. 36, 340–356. doi:10.1080/02508060.2011.584152

Baker, C., Lawrence, R., Montagne, C., Patten, D., 2006. Mapping wetlands and riparian areas using LANDSAT ETM+ imagery and decision-tree-based models. Wetlands 26, 465–474.

Baki, A.B.M., Bari, M.F., Haque, M.I., 2008. An analysis of upstream withdrawal scenarios using geo-spatial approach in the Surma-Kushiyara river basin. J. Civ. Eng. 36, 97–109.

Bakker, M.H.N., 2009. Transboundary river floods: examining countries, international river basins and continents. Water Policy 11, 269. doi:10.2166/wp.2009.041

Bao, J., Feng, J., Wang, Y., 2015. Dynamical downscaling simulation and future projection of precipitation over China. J. Geophys. Res. Atmos. 120, 8227–8243. doi:10.1002/2015JD023275.Received

BBS, 2011. Population & housing census 2011: prelininary results. Dhaka, Bangladesh.

Beasley, D.B., Huggins, L.F., Monke, E.., 1982. Modeling sediment yield from agricultural watersheds. J. Soil Water Conserv. 37, 113–117.

Benaman, J., Shoemaker, C.A., Haith, D.A., 2005. Calibration and validation of Soil and Water Assessment Tool on an agricultural watershed in Upstate New York. J. Hydrol. Eng. 10, 363–374.

Bengtson, M.L., Padmanabhan, G., 1999. A review of models for investigating the influence of wetlands on flooding. Fargo, ND.

Berthet, L., Andréassian, V., Perrin, C., Javelle, P., 2009. How crucial is it to account for the antecedent moisture conditions in flood forecasting ? Comparison of event-based and continuous approaches on 178 catchments. Hydrol. Earth Syst. Sci. 13, 819–831.

Betrie, G.D., Mohamed, Y.A., van Griensven, A., Srinivasan, R., 2011a. Sediment management modelling in the Blue Nile Basin using SWAT model. Hydrol. Earth Syst. Sci. 15, 807–818. doi:10.5194/hess-15-807-2011

Betrie, G.D., van Griensven, A., Mohamed, Y.A., Popescu, I., Mynett, A.E., Hummel, S., 2011b. Linking SWAT and SOBEK using Open Modeling Interface (OpenMI) for sediment transport simulation in The Blue Nile River Basin. Trans. ASABE 54, 1749–1757.

Beven, K., Freer, J., 2001. Equifinality, data assimilation, and estimation in mechanistic modeling of complex environmental systems using the GLUE methodology. J. Hydrol. 249, 11–29.

Beven, K.J., 1996. A discussion of distributed hydrological modelling, in: Abott, M.B., Refsgaard, J.C. (Eds.), Distributed Hydrological Modelling. Springer

Netherlands, pp. 255–278.

Bicknell, B.R., Imhoff, J.C., Kittle Jr., J.L., Jobes, T.H., Donigian Jr., A.S., 2001. Hydrological Simulation Program – FORTRAN, HSPF, Version 12, User's Manual. Mountain View, California.

Bingeman, A.K., Kouwen, N., Soulis, E.D., 2006. Validation of the hydrological processes in a hydrological model. J. Hydrol. Eng. 11, 451–463.

Bingner, R.L., Drive, M., Theurer, F.D., 2011. AnnAGNPS technical processes, Version 5. ed. USDA-ARS, National Sedimentation Laboratory.

Binley, A., Beven, K., 1992. Three-dimensional modelling of hillslope hydrology. Hydrol. Process. 6, 347–359.

Borah, D., Bera, M., 2003. Watershed-scale hydrologic and nonpoint-source pollution models: review of mathematical bases. Trans. ASAE 46, 1553–1566.

Bouwer, H., 2002. Artificial recharge of groundwater: Hydrogeology and engineering. Hydrogeol. J. 10, 121–142.

Brakensiek, D.L., Engleman, R.L., Rawls, W.J., 1981. Variation within texture classes of soil water parameters. Trans. ASAE 24, 335–339.

Bronstert, A., 2006. Overview of current perspective on climate change, in: Knight, D.W., Shamseldin, A.Y. (Eds.), River Basin Modelling for Flood Risk Mitigation. Taylor & Francis, pp. 59–75.

Brown, M.E., Antle, J.M., Backlund, P., Carr, E.R., Easterling, W.E., Walsh, M.K., Ammann, C., Attavanich, W., Barrett, C.B., Bellemare, M.F., Dancheck, V., Funk, C., Grace, K., Ingram, J.S.I., Jiang, H., Maletta, H., Mata, T., Murray, A., Ngugi, M., Ojima, D., O'Neill, B., Tebaldi, C., 2015. Climate change, global food security, and the U.S. food system.

Bullock, A., Acreman, M., 2003. The role of wetlands in the hydrological cycle. Hydrol. Earth Syst. Sci. 7, 358–389. doi:10.5194/hess-7-358-2003

Bulygina, N.S., Nearing, M.A., Stone, J.J., Nichols, M.H., 2007. DWEPP : a dynamic soil erosion model based on WEPP source terms 32, 998–1012. doi:10.1002/esp

BWDB, 2012. Flash Flood [WWW Document]. URL http://www.bwdb.gov.bd/index.php?option=com_content&view=article&id=177&Itemid=150

BWDB, FPCO, 1993. Manu River improvement project, FAP6, Northeast regional

water management project. Dhaka, Bangladesh.

Byomkesh, T., Nakagoshi, N., Md. Shahedur, R., 2009. State and management of wetlands in Bangladesh. Landsc. Ecol. Eng. 5, 81–90. doi:10.1007/s11355-008-0052-5

Calver, A., 2009. Water and climate : issues , examples and potential in the context of hydrological prediction. WMO Bull. 58, 197–204.

Carolina, G.A., Jackson, C.R., 2011. Potential impacts of climate change on groundwater supplies to the doñana wetland, Spain. Wetlands 31, 907–920. doi:10.1007/s13157-011-0205-4

CCC, 2009. Characterizing long-term changes of Bangladesh climate in context of agriculture and irrigation. Dhaka, Bangladesh.

CDM, 2001. Evaluation of Integrated Suface Water and Groundwater Modeling Tools. Cambridge MA, USA.

CEGIS, 2012a. Master Plan of Haor Areas (Volume II). Dhaka, Bangladesh.

CEGIS, 2012b. Master Plan of Haor Areas (Volume I). Dhaka, Bangladesh.

Chadwick, R., Good, P., Martin, G., Rowell, D.P., 2015. Large rainfall changes consistently projected over substantial areas of tropical land. Nat. Clim. Chang. 6, 177–182. doi:10.1038/nclimate2805

Chang, H., Jung, I.W., 2010. Spatial and temporal changes in runoff caused by climate change in a complex large river basin in Oregon. J. Hydrol. 388, 186–207. doi:10.1016/j.jhydrol.2010.04.040

Charrier, R., Li, Y., 2012. Assessing resolution and source effects of digital elevation models on automated floodplain delineation: A case study from the Camp Creek Watershed, Missouri. Appl. Geogr. 34, 38–46. doi:10.1016/j.apgeog.2011.10.012

Chen, H., Zhao, Y.W., 2011. Evaluating the environmental flows of China's Wolonghu wetland and land use changes using a hydrological model, a water balance model, and remote sensing. Ecol. Modell. 222, 253–260. doi:10.1016/j.ecolmodel.2009.12.020

Cheng, J., Zhang, H., Zhang, Y., Shi, Y., He, F., Qi, S., Sun, Y., 2007. Affecting factors of preferential flow in the forest of the Three Gorges area, Yangtze River. Front. For. China 2, 436–442. doi:10.1007/s11461-007-0069-1

Childs, E.C., Bybordi, M., 1969. The vertical movement water in stratified porous material: 1. Infiltration. Water Resour. Res. 5, 446–459.

doi:10.1029/WR005i002p00446

Choudhury, G.A., Nishat, A., 2005. Hydro-meteorological characteristics of Hakaluki haor. Dhaka, Bangladesh.

Chowdhury, J.U., Salehin, M., 1997. Floods and their processes, in: Proceedings of the International Seminar on Evolution of Scientific System of Flood Forecasting and Warning in the Ganges, Brahmaputra and Meghna River Basins. Bangladesh National Committee of International Commission for Irrigation and Drainage (ICID), Dhaka, Bangladesh, pp. 247–254.

Chowdhury, M.R., Ward, N., 2004. Hydro-meteorological variability in the greater Ganges-Brahmaputra-Meghna basins. Int. J. Climatol. 24, 1495–1508. doi:10.1002/joc.1076

Chu, X., Steinman, A., 2009. Event and continuous hydrologic modeling with HEC-HMS. J. Irrig. Drain. Eng. 135, 119–124. doi:10.1061/(ASCE)0733-9437(2009)135:1(119)

Clarke, R.T., 1973. A review of some mathematical models used in hydrology, with observations on their calibration and use. J. Hydrol. 19, 1–20. doi:10.1016/0022-1694(73)90089-9

Clilverd, H.M., Thompson, J.R., Heppell, C.M., Sayer, C.D., Axmacher, J.C., 2013. River-floodplain hydrology of an embanked lowland Chalk river and initial response to embankment removal. Hydrol. Sci. J. 58, 627–650.

Cohen Liechti, T., Matos, J.P., Ferràs Segura, D., Boillat, J.-L., Schleiss, A.J., 2014. Hydrological modelling of the Zambezi River Basin taking into account floodplain behaviour by a modified reservoir approach. Int. J. River Basin Manag. 12, 29–41. doi:10.1080/15715124.2014.880707

Collischonn, W., Allasia, D., Da Silva, B.C., Tucci, C.E.M., 2007. The MGB-IPH model for large-scale rainfall—runoff modelling. Hydrol. Sci. J. 52, 878–895. doi:10.1623/hysj.52.5.878

Connolly, R.D., Silburn, D.M., Ciesiolka, C.A.A., 1997. Distributed parameter hydrology model (ANSWERS) applied to a range of catchment scales using rainfall simulator data. III. Application to a spatially complex catchment. J. Hydrol. 193, 183–203. doi:10.1016/S0022-1694(96)03136-8

Cortis, C., Montaldo, N., 2013. A new ecohydrological model based on Richard equation. Procedia Environ. Sci. 19, 67–76. doi:10.1016/j.proenv.2013.06.008

Coustau, M., Bouvier, C., Borrell-Estupina, V., Jourde, H., 2012. Flood modelling with a distributed event-based parsimonious rainfall-runoff model: case of the karstic Lez river catchment. Nat. Hazards Earth Syst. Sci. 12, 1119–1133. doi:10.5194/nhess-12-1119-2012

Craft, C.B., Casey, W.P., 2000. Sediment and nutrient accumulation in floodplain and depressional freshwater wetlands of Georgia, USA. Wetlands 20, 323–332. doi:10.1672/0277-5212(2000)020[0323:SANAIF]2.0.CO;2

Cukier, R.I., Fortuin, C.M., Shuler, K.E., Petschek, A.G., Schaibly, J.H., 1973. Study of sensitivity of coupled reaction systems to uncertainties in rate coefficients. 1. Theory. J. Chem. Phys. 59, 3873–3878.

Cukier, R.I., Schaibly, J.H., Shuler, K.E., 1975. Study of the sensitivity of coupled reaction systems to uncertainties in rate coefficients. III. Analysis of the approximations. J. Chem. Phys. 63, 1140–1149. doi:10.1063/1.1680571

Cunge, J., 1969. On the subject of a flood propagation computation method (Muskingum method). J. Hydraul. Res. 7, 205–230.

da Paz, A.R., Collischonn, W., Risso, A., Mendes, C.A.B., 2008. Errors in river lengths derived from raster digital elevation models. Comput. Geosci. 34, 1584–1596. doi:10.1016/j.cageo.2007.10.009

Dabral, P.P., Baithuri, N., Pandey, A., 2008. Soil erosion assessment in a hilly catchment of North Eastern India using USLE, GIS and remote sensing. Water Resour. Manag. 22, 1783–1798. doi:10.1007/s11269-008-9253-9

Dabral, S., Cohen, M., 2001. ANSWERS-2000 Areal Non-point Source Watershed Environment Response Simulation.

Dai, A., Qian, T., Trenberth, K.E., Milliman, J.D., 2009. Changes in continental freshwater discharge from 1948 to 2004. J. Clim. 22, 2773–2792. doi:10.1175/2008JCLI2592.1

Daniel, E.B., Camp, J. V, Leboeuf, E.J., Penrod, J.R., Abkowitz, M.D., Dobbins, J.P., 2010. Watershed modeling using GIS technology: A critical review. J. Spat. Hydrol. 10, 13–28.

Dash, S.K., Sharma, N., Pattnayak, K.C., Gao, X.J., Shi, Y., 2012. Temperature and precipitation changes in the north-east India and their future projections. Glob. Planet. Change 98–99, 31–44. doi:10.1016/j.gloplacha.2012.07.006

Datta, S., 2010. Tripura faces drought spectre - Rainfall deficit, depletion of water resources hit farmers. Telegr. Calcutta, India.

Dechmi, F., Burguete, J., Skhiri, A., 2012. SWAT application in intensive irrigation systems: Model modification, calibration and validation. J. Hydrol. 470–471, 227–238. doi:10.1016/j.jhydrol.2012.08.055

Dehotin, J., Braud, I., 2008. Which spatial discretization for distributed hydrological models? Proposition of a methodology and illustration for medium to large-scale catchments. Hydrol. Earth Syst. Sci. 12, 769–796. doi:10.5194/hess-12-769-2008

Deltares, 2016. SOBEK user manual. Deltares, MH Delft, the Netherlands.

DHI, 2009a. Mike 11: A modelling system for rivers and channels, Reference Manual.

DHI, 2009b. MIKE SHE User Documentation.

Dhiman, S.C., 2012. Aquifer systems of Meghalaya. Guwahati, India.

Di Baldassarre, G., Montanari, a., 2009. Uncertainty in river discharge observations: a quantitative analysis. Hydrol. Earth Syst. Sci. Discuss. 6, 39–61. doi:10.5194/hessd-6-39-2009

Di Luzio, M., Srinivasan, R., Arnold, J.G., 2004. A GIS-coupled hydrological model system for the watershed assessment of agricultural nonpoint and point sources of pollution. Trans. GIS 8, 113–136.

Di Luzio, M., Srinivasan, R., Arnold, J.G., 2002. Integration of watershed tools and SWAT model into BASINS. J. Am. Water Resour. Assoc. 38, 1127–1141.

Dillaha, T.A., Wolfe, M.L., Shirmohammadi, A., Byne, F.W., 2014. ANSWERS-2000 [WWW Document]. URL http://ww2.bse.vt.edu/ANSWERS/Overview.php

Donald, J.R., 1992. Snowcover depletion curves and satellite snowcover estimates for snowmelt runoff modelling. University of Waterloo.

Donat, M.G., Lowry, A.L., Alexander, L. V., O'Gorman, P.A., Maher, N., 2016. More extreme precipitation in the world's dry and wet regions. Nat. Clim. Chang. 6, 508–513. doi:10.1038/nclimate2941

Douglas-Mankin, K.R., Srinivasan, R., Arnold, J.G., 2010. Soil and Water Assessment Tool (SWAT) model: Current developments and applications. Trans. ASABE 53, 1423–1431.

Dowla, F.J., Rogers, L.L., 1995. Solving problems in environmental engineering and geosciences with Artificial Neural Networks. The MIT Press, Cambridge

MA, USA.

Downer, C.W., Ogden, F.L., 2006. Gridded Surface Subsurface Hydrologic Analysis (GSSHA) User's Manual. Washington DC.

Downer, C.W., Ogden, F.L., 2004. Appropriate vertical discretization of Richards' equation for two-dimensional watershed-scale modelling. Hydrol. Process. 18, 1–22. doi:10.1002/hyp.1306

Downer, C.W., Ogden, F.L., 2003. Prediction of runoff and soil moistures at the watershed scale: Effects of model complexity and parameter assignment. Water Resour. Res. 39, 1–13. doi:10.1029/2002WR001439

Downer, C.W., Ogden, F.L., Martin, W.D., Harmon, R.S., 2002. Theory, development, and applicability of the surface water hydrologic model CASC2D. Hydrol. Process. 16, 255–275. doi:10.1002/hyp.338

Du, B., Arnold, J.G., Saleh, A., Jaynes, D.B., 2005. Development and application of SWAT to landscapes with tiles and potholes. Trans. ASAE 48, 1121–1133.

Dunne, T., Zhang, W., Aubry, B.F., 1991. Effects of rainfall, vegetation, and microtopography on infiltration and runoff. Water Resour. Res. 27, 2271–2285.

Dwivedi, R.S., Rao, B.R.M., Bhattacharya, S., 1999. Mapping wetlands of the Sundaban Delta and it's environs using ERS-1 SAR data. Int. J. Remote Sens. 20, 2235–2247.

Easton, Z.M., Fuka, D.R., Walter, M.T., Cowan, D.M., Schneiderman, E.M., Steenhuis, T.S., 2008. Re-conceptualizing the soil and water assessment tool (SWAT) model to predict runoff from variable source areas. J. Hydrol. 348, 279–291. doi:10.1016/j.jhydrol.2007.10.008

Eckhardt, K., Haverkamp, S., Fohrer, N., Frede, H.-G., 2002. SWAT-G, a version of SWAT99.2 modified for application to low mountain range catchments. Phys. Chem. Earth, Parts A/B/C 27, 641–644. doi:10.1016/S1474-7065(02)00048-7

Elbashir, S., 2011. Flood routing in natural channels using Muskingum methods. Dublin Institute of Technology (DIT).

ESB, 2004. European Commission- JRC - Institute for Environment and Sustainability, European Soil Bureau. European Soil Database (vs 2.0). Ispra, Italy.

Fairfield, J., Leymarie, P., 1991. Drainage networks from Grid Digital Elevation

Models. Water Resour. Res. 27, 709–717.

Fan, Y., Miguez-Macho, G., 2011. A simple hydrologic framework for simulating wetlands in climate and earth system models. Clim. Dyn. 37, 253–278. doi:10.1007/s00382-010-0829-8

FAO/IIASA/ISRIC/ISS-CAS/JRC, 2012. Harmonized World Soil Database (version 1.2). FAO, Rome, Italy and IIASA, Laxenburg, Austria.

FAO-Unesco, 1977. The FAO-Unesco soil map of the world. Paris, France.

Farr, T.G., Rosen, P.A., Caro, E., Crippen, R., Duren, R., Hensley, S., Kobrick, M., Paller, M., Rodriguez, E., Roth, L., Seal, D., Shaffer, S., Shimada, J., Umland, J., Werner, M., Oskin, M., Burbank, D., Alsdorf, D., 2007. The Shuttle Radar Topography Mission. Rev. Geophys. 45, 1–33. doi:10.1029/2005RG000183.1.INTRODUCTION

Feng, K., Molz, F.J., 1997. A 2-D, diffusion-based, wetland flow model. J. Hydrol. 196, 230–250. doi:10.1016/S0022-1694(96)03282-9

Feng, X.Q., Zhang, G.X., Jun Xu, Y., 2012. Simulation of hydrological processes in the Zhalong Wetland within a river basin, Northeast China. Hydrol. Earth Syst. Sci. Discuss. 9, 14035–14063. doi:10.5194/hessd-9-14035-2012

FFWC, 2011. Annual flood report 2011. Dhaka, Bangladesh.

Flanagan, D.C., Ascough II, J.C., Nicks, A.D., Nearing, M.A., Laflen, J.M., 1995. Overview of the WEPP erosion predictin model, in: USDA-Water Erosion Prediction Project (WEPP). National Soil Erosion Research Laboratory, USDA, West Lafayette.

Flanagan, D.C., Ascough II, J.C., Nieber, J.L., Misra, D., Douglas-Mankin, K.R., 2013a. Advances in soil erosion research: processes, measurement, and modeling. Trans. ASABE 56, 455–463.

Flanagan, D.C., Frankenberger, J.R., Cochrane, T.A., Renschler, C.S., Elliot, W.J., 2013b. Geospatial application of the Water Erosion Prediction Project (WEPP) model. Trans. ASABE 56, 591–601.

Flanagan, D.C., Nearing, M.A., 1995. USDA-Water Erosion Prediction Project, Hillslope profile and watershed model documentation. West Lafayette, Indiana.

Fonseca, A., Ames, D.P., Yang, P., Botelho, C., Boaventura, R., Vilar, V., 2014. Watershed model parameter estimation and uncertainty in data-limited environments. Environ. Model. Softw. 51, 84–93.

doi:10.1016/j.envsoft.2013.09.023

Forest Survey of India, 2011. India State of Forest report 2011. Dehradun.

Freeze, R.A., Harlan, R.L., 1969. Blueprint for a physically-based , digitally-simulated hydrologic response model. J. Hydrol. 9, 237–258.

Frohn, R.C., D'Amico, E., Lane, C., Autrey, B., Rhodus, J., Liu, H., 2012. Multi-temporal sub-pixel Landsat ETM+ classification of isolated wetlands in Cuyahoga County, Ohio, USA. Wetlands 32, 289–299. doi:10.1007/s13157-011-0254-8

Gain, A.K., Immerzeel, W.W., Sperna Weiland, F.C., Bierkens, M.F.P., 2011. Impact of climate change on the stream flow of the lower Brahmaputra: trends in high and low flows based on discharge-weighted ensemble modelling. Hydrol. Earth Syst. Sci. 15, 1537–1545. doi:10.5194/hess-15-1537-2011

Garrote, L., Bras, R.L., 1995. A distributed model for real-time flood forecasting using digital elevation models. J. Hydrol. 167, 279–306. doi:10.1016/0022-1694(94)02592-Y

Gassman, P.W., Arnold, J.G., Srinivasan, R., Reyes, M., 2010. The worldwide use of the SWAT Model: Technological drivers, networking impacts, and simulation trends, in: 21st Century Watershed Technology: Improving Water Quality and Environment. ASABE.

Gassman, P.W., Reyes, M.R., Green, C.H., Arnold, J.G., 2007. The Soil and Water Assessment Tool: Historical development, applications, and future research directions. Trans. ASABE 50, 1211–1250.

Gentine, P., Troy, T.J., Lintner, B.R., Findell, K.L., 2012. Scaling in surface hydrology: progress and challenges. J. Contemp. Water Res. Educ. 147, 28–40. doi:10.1111/j.1936-704X.2012.03105.x

Ghosh, S., Das, D., Kao, S., Ganguly, A.R., 2012. Lack of uniform trends but increasing spatial variability in observed Indian rainfall extremes. Nat. Clim. Chang. 2, 86–91. doi:10.1038/NCLIMATE1327

Gibson, S.A., Pasternack, G.B., 2016. Selecting between one-dimensional and two-dimensional hydrodynamic models for ecohydraulic analysis. River Res. Appl. 32, 1365–1381. doi:10.1002/rra

Githui, F., Mutua, F., Bauwens, W., 2009. Estimating the impacts of land-cover change on runoff using the soil and water assessment tool (SWAT): case

study of Nzoia catchment, Kenya. Hydrol. Sci. J. 54, 899–908. doi:10.1623/hysj.54.5.899

Giudice, G.D., Padulano, R., Rasulo, G., 2014. Spatial prediction of the runoff coefficient in Southern Peninsular Italy for the index flood estimation. Hydrol. Res. 45, 263–281. doi:10.2166/nh

Giudice, G.D., Padulano, R., Rasulo, G., 2012. Factors affecting the runoff coefficient. Hydrol. Earth Syst. Sci. Discuss. 9, 4919–4941. doi:10.5194/hessd-9-4919-2012

Golden, H.E., Lane, C.R., Amatya, D.M., Bandilla, K.W., Raanan Kiperwas, H., Knightes, C.D., Ssegane, H., 2014. Hydrologic connectivity between geographically isolated wetlands and surface water systems: A review of select modeling methods. Environ. Model. Softw. 53, 190–206. doi:10.1016/j.envsoft.2013.12.004

Gonçalves, T.D., Fischer, T., Gräbe, A., Kolditz, O., Weiss, H., 2013. Groundwater flow model of the Pipiripau watershed, Federal District of Brazil. Environ. Earth Sci. 69, 617–631. doi:10.1007/s12665-013-2400-5

Gopal, B., 2013. Future of wetlands in tropical and subtropical Asia, especially in the face of climate change. Aquat. Sci. 75, 39–61. doi:10.1007/s00027-011-0247-y

Green, W.H., Ampt, G.A., 1911. Studies on soil physics, Part I- The flow of air and water through soils. J. Agric. Sci. 4, 1–24.

Greenberg, C.H., Goodrick, S., Austin, J.D., Parresol, B.R., 2015. Hydroregime prediction models for ephemeral groundwater-driven sinkhole wetlands: a planning tool for climate change and amphibian conservation. Wetlands 35, 899–911. doi:10.1007/s13157-015-0680-0

Guo, H., Hu, Q., Jiang, T., 2008. Annual and seasonal streamflow responses to climate and land-cover changes in the Poyang Lake basin, China. J. Hydrol. 355, 106–122. doi:10.1016/j.jhydrol.2008.03.020

Gupta, A.D., Babel, M.S., Albert, X., Mark, O., 2005. Water sector of Bangladesh in the context of Integrated Water Resources Management: A review. Int. J. Water Resour. Dev. 21, 385–398. doi:10.1080/07900620500037818

Gupta, P.K., Panigrahy, S., Parihar, J.S., 2011. Impact of climate change on runoff of the major river basins of India using Global Circulation Model (HadCM3) projected data. J. Indian Soc. Remote Sens. 39, 337–344.

doi:10.1007/s12524-011-0101-7

Gupta, P.K., Singh, R., Raghuwanshi, N.S., Dutta, S., Panigrahy, S., 2008. Effect of remotely sensed data on the performance of a distributed hydrological model : Case Study. J. Hydrol. Eng. 13, 939–947.

Guse, B., Reusser, D.E., Fohrer, N., 2014. How to improve the representation of hydrological processes in SWAT for a lowland catchment - temporal analysis of parameter sensitivity and model performance. Hydrol. Process. 28, 2651–2670. doi:10.1002/hyp.9777

Hammer, D.E., Kadlec, R.H., 1986. A model for wetland surface water dynamics. Water Resour. Res. 22, 1951–1958.

Hanasaki, N., Kanae, S., Oki, T., Masuda, K., Motoya, K., Shirakawa, N., Shen, Y., Tanaka, K., 2008a. An integrated model for the assessment of global water resources – Part 1 : Model description and input meteorological forcing. Hydrol. Earth Syst. Sci. 12, 1007–1025. doi:10.5194/hess-12-1027-2008

Hanasaki, N., Kanae, S., Oki, T., Masuda, K., Motoya, K., Shirakawa, N., Shen, Y., Tanaka, K., 2008b. An integrated model for the assessment of global water resources – Part 2: Applications and assessments. Hydrol. Earth Syst. Sci. 12, 1027–1037. doi:10.5194/hess-12-1027-2008

Hansen, M.C., Defries, R.S., Townshend, J.R.G., Sohlberg, R., 2000. Global land cover classification at 1 km spatial resolution using a classification tree approach. Int. J. Remote Sens. 21, 1331–1364.

Harding, R.J., Weedon, G.P., van Lanen, H.A.J., Clark, D.B., 2014. The future for global water assessment. J. Hydrol. 518, 186–193. doi:10.1016/j.jhydrol.2014.05.014

Hargreaves, G.L., Hargreaves, G.H., Riley, J.P., 1985. Agricultural benefits for Senegal River Basin. J. Irrig. Drain. Eng. 111, 113–124.

Harris, I., Jones, P.D., Osborn, T.J., Lister, D.H., 2014. Updated high-resolution grids of monthly climatic observations - the CRU TS3.10 Dataset. Int. J. Climatol. 34, 623–642. doi:10.1002/joc.3711

Harvey, K.R., Hill, G.J.E., 2001. Vegetation mapping of a tropical freshwater swamp in the Northern Territory, Australia: a comparison of aerial photography, Landsat TM and SPOT satellite imagery. Int. J. Remote Sens. 22, 2911–2925.

Hattermann, F.F., Krysanova, V., Habeck, a., Bronstert, a., 2006. Integrating wetlands and riparian zones in river basin modelling. Ecol. Modell. 199, 379–392. doi:10.1016/j.ecolmodel.2005.06.012

Hattermann, F.F., Krysanova, V., Hesse, C., 2008. Modelling wetland processes in regional applications. Hydrol. Sci. J. 53, 1001–1012.

Haverkamp, S., Fohrer, N., Frede, H.-G., 2005. Assessment of the effect of land use patterns on hydrologic landscape functions: a comprehensive GIS-based tool to minimize model uncertainty resulting from spatial aggregation. Hydrol. Process. 19, 715–727. doi:10.1002/hyp.5626

Hayashi, M., van der Kamp, G., 2000. Simple equations to represent the volume–area–depth relations of shallow wetlands in small topographic depressions. J. Hydrol. 237, 74–85. doi:10.1016/S0022-1694(00)00300-0

Heimann, D.C., Krempa, H.M., 2011. Cumulative effects of impoundments on the hydrology of riparian wetlands along the Marmaton River, West-Central Missouri, USA. Wetlands 31, 135–146. doi:10.1007/s13157-010-0121-z

Hidayat, H., Vermeulen, B., Sassi, M.G., Torfs, P.J.J.F., Hoitink, a. J.F., 2011. Discharge estimation in a backwater affected meandering river. Hydrol. Earth Syst. Sci. 15, 2717–2728. doi:10.5194/hess-15-2717-2011

Hirabayashi, Y., Mahendran, R., Koirala, S., Konoshima, L., Yamazaki, D., Watanabe, S., Kim, H., Kanae, S., 2013. Global flood risk under climate change. Nat. Clim. Chang. 3, 1–6. doi:10.1038/NCLIMATE1911

Ho, J.T., Thompson, J.R., Brierley, C., 2016. Projections of hydrology in the Tocantins-Araguaia Basin, Brazil: uncertainty assessment using the CMIP5 ensemble. Hydrol. Sci. J. 61, 551–567. doi:10.1080/02626667.2015.1057513

Hofer, T., Messerli, B., 2006. Floods in Bangladesh: history, dynamics and rethinking the role of Himalayas. United Nationas University Press.

Hollis, G.E., Thompson, J.R., 1998. Hydrological data for wetland management. J. Chart. Inst. Water Environ. Manag. 12, 9–17.

Hoque, R., Nakayama, D., Matsuyama, H., Matsumoto, J., 2011. Flood monitoring, mapping and assessing capabilities using RADARSAT remote sensing, GIS and ground data for Bangladesh. Nat. Hazards 57, 525–548. doi:10.1007/s11069-010-9638-y

Hossain, M.A., 2011. An overview on shifting cultivation with reference to

Bangladesh. Sci. Res. Essays 6, 6509–6514. doi:10.5897/SRE11.1282

Hsu, K., Gupta, H.V., Sorooshian, S., 1995. Artificial neural network modeling of the rainfall-runoff process. Water Resour. Res. 31, 2517–2530.

Huang, G., 2006. Physics based, integrated modeling of hydrology and hydraulics at watershed scales. PhD Thesis. The Pennsylvania State University.

Hwang, S., Graham, W.D., 2014. Assessment of alternative methods for statistically downscaling daily GCM precipitation outputs to simulate regional streamflow. J. Am. Water Resour. Assoc. 50, 1010–1032. doi:10.1111/jawr.12154

IFAD, 2011. BANGLADESH: Haor Infrastructure and livelihood improvement project.

Immerzeel, W., 2008. Historical trends and future predictions of climate variability in the Brahmaputra basin. Int. J. Climatol. 28, 243–254. doi:10.1002/joc

Ines, A.V.M., Hansen, J.W., 2006. Bias correction of daily GCM rainfall for crop simulation studies. Agric. For. Meteorol. 138, 44–53. doi:10.1016/j.agrformet.2006.03.009

IPCC, 2013. Climate Change 2013: The Physical Science Basis. Contribution of Working Group I to the Fifth Assessment Report of the Intergovernmental Panel on Climate Change. Cambridge University Press, Cambridge, United Kingdom and New York, NY, USA.

Islam, A.S., Haque, A., Bala, S.K., 2010. Hydrologic characteristics of floods in Ganges–Brahmaputra–Meghna (GBM) delta. Nat. Hazards 54, 797–811. doi:10.1007/s11069-010-9504-y

Islam, M.R., Begum, S.F., Yamaguchi, Y., 1999. The Ganges and Brahmaputra rivers in Bangladesh : basin denudation and sedimentation. Hydrol. Process. 13, 2907–2923.

Islam, M.S., Hasan, G.M.J., Chowdhury, M.A.I., 2006. Destroying hills in the northeastern part of Bangladesh: a qualitative assessment of extent of the problem and its probable impact. Int. J. Environ. Sci. Technol. 2, 301–308. doi:10.1007/BF03325890

Islam, S.N., 2010. Threatened wetlands and ecologically sensitive ecosystems management in Bangladesh. Front. Earth Sci. China 4, 438–448. doi:10.1007/s11707-010-0127-0

Ivanov, V.Y., Vivoni, E.R., Bras, R.L., Entekhabi, D., 2004. Preserving high-resolution surface and rainfall data in operational-scale basin hydrology: a fully-distributed physically-based approach. J. Hydrol. 298, 80–111. doi:10.1016/j.jhydrol.2004.03.041

Ivanov, V.Y., Vivoni, E.R., Bras, R.L., Entekhabi, D., 2004. Catchment hydrologic response with a fully distributed triangulated irregular network model. Water Resour. Res. 40, 1–23. doi:10.1029/2004WR003218

Jaber, F.H., Shukla, S., 2012. MIKE SHE: Model use, calibration, and validation. Trans. ASABE 55, 1479–1489.

Jaber, F.H., Shukla, S., 2005. Hydrodynamic modeling approaches for agricultural storm water impoundments. J. Irrig. Drain. Eng. 131, 307–315.

Jain, M.K., Singh, V.P., 2005. DEM-based modelling of surface runoff using diffusion wave equation. J. Hydrol. 302, 107–126. doi:10.1016/j.jhydrol.2004.06.042

Jain, S.K., Sudheer, K.P., 2008. Fitting of hydrologic models : A close look at the Nash–Sutcliffe index. J. Hydrol. Eng. 13, 981–986.

Jankowfsky, S., Branger, F., Braud, I., Rodriguez, F., Debionne, S., Viallet, P., 2014. Assessing anthropogenic influence on the hydrology of small peri-urban catchments: development of the object-oriented PUMMA model by integrating urban and rural hydrological models. J. Hydrol. 517, 1056–1071. doi:10.1016/j.jhydrol.2014.06.034

Javaheri, A., Babbar-sebens, M., 2014. On comparison of peak flow reductions, flood inundation maps, and velocity maps in evaluating effects of restored wetlands on channel flooding. Ecol. Eng. 73, 132–145.

Jeong, D.-I., Kim, Y.-O., 2005. Rainfall-runoff models using artificial neural networks for ensemble streamflow prediction. Hydrol. Process. 19, 3819–3835. doi:10.1002/hyp.5983

Jhajharia, D., Dinpashoh, Y., Kahya, E., Singh, V.P., Fakheri-Fard, A., 2012. Trends in reference evapotranspiration in the humid region of northeast India. Hydrol. Process. 26, 421–435. doi:10.1002/hyp.8140

Jing, L., Chen, B., 2011. Hydrological modeling of subartic wetlands: comparison between SLURP and WATFLOOD. Environ. Eng. Sci. 28, 521–533. doi:10.1089/ees.2010.0277

Johnson, W.C., Werner, B., Guntenspergen, G.R., Voldseth, R. a., Millett, B.,

Naugle, D.E., Tulbure, M., Carroll, R.W.H., Tracy, J., Olawsky, C., 2010. Prairie wetland complexes as landscape functional units in a changing climate. Bioscience 60, 128–140. doi:10.1525/bio.2010.60.2.7

Julien, P.Y., Saghafian, B., Ogden, F.L., 1995. Raster-based hydrologic modeling of spatially-varied surface runoff. Water Resour. Bull. 31, 523–536.

Jung, M., Reichstein, M., Ciais, P., Seneviratne, S.I., Sheffield, J., Goulden, M.L., Bonan, G., Cescatti, A., Chen, J., de Jeu, R., Dolman, a J., Eugster, W., Gerten, D., Gianelle, D., Gobron, N., Heinke, J., Kimball, J., Law, B.E., Montagnani, L., Mu, Q., Mueller, B., Oleson, K., Papale, D., Richardson, A.D., Roupsard, O., Running, S., Tomelleri, E., Viovy, N., Weber, U., Williams, C., Wood, E., Zaehle, S., Zhang, K., 2010. Recent decline in the global land evapotranspiration trend due to limited moisture supply. Nature 467, 951–954. doi:10.1038/nature09396

Junk, W.J., An, S., Finlayson, C.M., Gopal, B., Květ, J., Mitchell, S. a., Mitsch, W.J., Robarts, R.D., 2013. Current state of knowledge regarding the world's wetlands and their future under global climate change: a synthesis. Aquat. Sci. 75, 151–167. doi:10.1007/s00027-012-0278-z

Kadlec, R.H., Wallace, S.D., 2009. Treatment wetlands, Second. ed. CRC Press, Taylor & Francis Group.

Kalin, L., Hantush, M.H., 2006. Comparative assessment of two distributed watershed models with application to a small watershed. Hydrol. Process. 20, 2285–2307. doi:10.1002/hyp.6063

Kalin, L., Hantush, M.M., 2014. Assessment of two physically-based watershed models based on their performances of simulataing water and sediment movement [WWW Document]. URL http://cfpub.epa.gov/si/si_public_file_download.cfm?p_download_id=441554

Kalteh, A.M., 2008. Rainfall-runoff modelling using artificial (ANNs): modelling and understanding. Casp. J. Environ. Sci. 6, 53–58.

Kampf, S.K., Burges, S.J., 2007. A framework for classifying and comparing distributed hillslope and catchment hydrologic models. Water Resour. Res. 43, 1–24. doi:10.1029/2006WR005370

Karim, F., Dutta, D., Marvanek, S., Petheram, C., Ticehurst, C., Lerat, J., Kim, S., Yang, A., 2015. Assessing the impacts of climate change and dams on

floodplain inundation and wetland connectivity in the wet-dry tropics of northern Australia. J. Hydrol. 522, 80–94. doi:10.1016/j.jhydrol.2014.12.005

Karim, F., Kinsey-Henderson, A., Wallace, J., Arthington, A.H., Pearson, R.G., 2012. Modelling wetland connectivity during overbank flooding in a tropical floodplain in north Queensland, Australia. Hydrol. Process. 26, 2710–2723. doi:10.1002/hyp.8364

Karim, F., Petheram, C., Marvanek, S., Ticehurst, C., Wallace, J., Hasan, M., 2016. Impact of climate change on floodplain inundation and hydrological connectivity between wetlands and rivers in a tropical river catchment. Hydrol. Earth Syst. Sci. 30, 1574–1593. doi:10.1002/hyp.10714

Kavvas, M.L., Chen, Z.Q., Dogrul, C., Yoon, J.Y., Ohara, N., Liang, L., Aksoy, H., Anderson, M.L., Yoshitani, J., Fukami, K., Matsuura, T., 2004. Watershed Environmental Hydrology (WEHY) model based on upscaled conservation equations : Hydrologic Module. J. Hydrol. Eng. 9, 450–464.

Kazezyılmaz-Alhan, C.M., Medina, M. a., Richardson, C.J., 2007. A wetland hydrology and water quality model incorporating surface water/groundwater interactions. Water Resour. Res. 43, 1–16. doi:10.1029/2006WR005003

Khan, A.S., Masud, A.S., Palash, W., 2005. Hydrological impact study of Tipaimukh Dam Project of India on Bangladesh. Dhaka, Bangladesh.

Khan, M.N.H., Mia, M.Y., Hossain, M.R., 2012. Impacts of flood on crop production in haor areas of two upazillas in Kishoregonj. J. Environ. Sci. Nat. Resour. 5, 193–198.

Khandu, Forootan, E., Schumacher, M., Awange, J.L., Schmied, H.M., 2016. Exploring the influence of precipitation extremes and human water use on total water storage (TWS) changes in the Ganges-Brahmaputra-Meghna River Basin. Water Resour. Res. 52, 2240–2258. doi:10.1002/2014WR015716

Kim, N.W., Chung, I.M., Kim, C., Lee, J., Lee, J.E., 2009. Development and applications of SWAT-K (Korea), in: Arnold, J., Srinivasan, R., Neitsch, S., George, C., Abbaspour, K., Hao, F.H., van Griensven, A., Gosain, A., Debels, P., Kim, N.W., Somura, H., Ella, V.B., Leon, L., Jintrawet, A., Reyes, M., Sombatpanit, S. (Eds.), Soil and Water Assessment Tool (SWAT) Global Applications. World Association of Soil and Water Conservation (WASWAC), Bangkok, pp. 223–252.

Kim, N.W., Chung, I.M., Won, Y.S., Arnold, J.G., 2008. Development and application of the integrated SWAT–MODFLOW model. J. Hydrol. 356, 1–16. doi:10.1016/j.jhydrol.2008.02.024

King, K.W., Arnold, J.G., Bingner, R.L., 1999. Comparison of Green-Ampt and Curve Number methods on Goodwin Creek watershed usign SWAT. Trans. ASAE 42, 919–925.

Kirkby, M., 1988. Hillslope runoff processes and models. J. Hydrol. 100, 315–339.

Kite, G., 2001. Modelling the Mekong: hydrological simulation for environmental impact studies. J. Hydrol. 253, 1–13. doi:10.1016/S0022-1694(01)00396-1

Kite, G., Droogers, P., 2000. Integrated basin modeling. Colombo, Sri Lanka.

Kling, H., Gupta, H., 2009. On the development of regionalization relationships for lumped watershed models: The impact of ignoring sub-basin scale variability. J. Hydrol. 373, 337–351. doi:10.1016/j.jhydrol.2009.04.031

Knight, D.W., Shamseldin, A.Y., 2005. River Basin Modelling for Flood Risk Mitigation. CRC Press, Taylor & Francis Group.

Knisel, W.G., 1980. CREAMS, a field-scale model for chemicals, runoff, and erosion from agricultural management systems. Dept. of Agriculture, Science and Eduction Administration, Washington.

Kouwen, N., 2013. WATFLOOD/ WATROUTE Hydrological model routing & flow forecasting system. University of Waterloo, Ontario, Canada.

Kouwen, N., 1988. WATFLOOD: a micro-computer based flood forecasting system based on real-time weather radar. Can. Water Resour. J. 13, 62–77. doi:10.4296/cwrj1301062

Krasnostein, A.L., Oldham, C.E., 2004. Predicting wetland water storage. Water Resour. Res. 40. doi:10.1029/2003WR002899

Krause, P., Boyle, D.P., Bäse, F., 2005. Comparison of different efficiency criteria for hydrological model assessment. Adv. Geosci. 5, 89–97.

Krause, S., Bronstert, A., Zehe, E., 2007. Groundwater–surface water interactions in a North German lowland floodplain – Implications for the river discharge dynamics and riparian water balance. J. Hydrol. 347, 404–417. doi:10.1016/j.jhydrol.2007.09.028

Kristensen, K.J., Jensen, S.E., 1975. A model for estimating actual evapotranspiration from potential evapotranspiration. Nord. Hydrol. 6, 170–

188.

Krysanova, V., Arnold, J.G., 2008. Advances in ecohydrological modelling with SWAT — a review. Hydrol. Sci. J. 53, 939–947.

Krysanova, V., Hatterman, F., Wechsung, F., 2005. Development of the ecohydrological model SWIM for regional impact studies and vulnerability assessment. Hydrol. Process. 19, 763–783.

Kulawardhana, R.W., Thenkabail, P.S., Vithanage, J., Biradar, C., Islam, M.A., Gunasinghe, S., Alankara, R., 2007. Evaluation of the wetland mapping methods using Landsat ETM+ and SRTM data. J. Spat. Hydrol. 7, 62–96.

Kumar, V., Jain, S.K., Singh, Y., 2010. Analysis of long-term rainfall trends in India. Hydrol. Sci. J. 55, 484–496. doi:10.1080/02626667.2010.481373

Kushwaha, A., Jain, M.K., 2013. Hydrological simulation in a forest dominated watershed in Himalayan region using SWAT model. Water Resour. Manag. 27, 3005–3023. doi:10.1007/s11269-013-0329-9

Lai, X., Jiang, J., Liang, Q., Huang, Q., 2013. Large-scale hydrodynamic modeling of the middle Yangtze River Basin with complex river–lake interactions. J. Hydrol. 492, 228–243. doi:10.1016/j.jhydrol.2013.03.049

Lai, Y.G., 2009. Watershed runoff and erosion modeling with a hybrid mesh model. J. Hydrol. Eng. 14, 15–26.

Laskar, A.A., Phukon, P., 2013. Structural control on landscape development of Barak Valley , Northeast India. J. Geol. Soc. India 81, 232–240.

Leander, R., Buishand, T.A., 2007. Resampling of regional climate model output for the simulation of extreme river flows. J. Hydrol. 332, 487–496. doi:10.1016/j.jhydrol.2006.08.006

Legates, D.R., McCabe Jr, G.J., 1999. Evaluating the use of “goodness-of-fit” measures in hydrologic and hydroclimatic model validation. Water Resour. Res. 35, 233–241.

Lehner, B., 2005. HydroSHEDS technical documentation, Version 1.0. Washington.

Leonard, R.A., Knisel, W.G., Still, D.A., 1987. GLEAMS: Groundwater loading effects of agricultural management systems. Trans. ASAE 30, 1403–1418.

Li, J., Wong, D.W.S., 2010. Effects of DEM sources on hydrologic applications. Comput. Environ. Urban Syst. 34, 251–261. doi:10.1016/j.compenvurbsys.2009.11.002

Li, M., Ma, Z., Du, J., 2010. Regional soil moisture simulation for Shaanxi Province using SWAT model validation and trend analysis. Sci. China Earth Sci. 53, 575–590. doi:10.1007/s11430-010-0031-1

Li, Q., Wang, S., Lee, D.K., Tang, J., Niu, X., Hui, P., Gutowski, W.J., Dairaku, K., Mcgregor, J.L., Katzfey, J., Gao, X., Wu, J., Hong, S.-Y., Wang, Y., Sasaki, H., 2016. Building Asian climate change scenario by multi-regional climate models ensemble. Part II: mean precipitation. Int. J. Climatol. doi:10.1002/joc.4633

Liang, X., Lettenmaier, D.P., Wood, E.F., Burges, S.J., 1994. A simple hydrologically based model of land surface water and energy fluxes for general circulation models. J. Geophys. Res. 99, 14415–14428.

Lindsay, J.B., Creed, I.F., 2005. Sensitivity of digital landscapes to artifact depressions in remotely-sensed DEMs. Photogramm. Eng. Remote Sens. 71, 1029–1036. doi:10.14358/PERS.71.9.1029

Lindsay, J.B., Creed, I.F., Beall, F.D., 2004. Drainage basin morphometrics for depressional landscapes. Water Resour. Res. 40, 1–9. doi:10.1029/2004WR003322

Liong, S., Lim, W., Kojiri, T., Hori, T., 2000. Advance food forecasting for food stricken Bangladesh with a fuzzy reasoning method. Hydrol. Process. 14, 431–448.

Liu, J., Williams, J.R., Wang, X., Yang, H., 2009. Using MODAWEC to generate daily weather data for the EPIC model. Environ. Model. Softw. 24, 655–664. doi:10.1016/j.envsoft.2008.10.008

Liu, Y., Yang, W., Wang, X., 2008. Development of a SWAT extension module to simulate riparian wetland hydrologic processes at a watershed scale. Hydrol. Process. 22, 2901–2915. doi:10.1002/hyp

Lobligeois, F., Andréassian, V., Perrin, C., Tabary, P., Loumagne, C., 2013. When does higher spatial resolution rainfall information improve streamflow simulation? An evaluation on 3620 flood events. Hydrol. Earth Syst. Sci. Discuss. 10, 12485–12536. doi:10.5194/hessd-10-12485-2013

Lund, J.R., Scheierling, S.M., Milne, G., 2010. Modeling for watershed management: a practioner’s guide. Washington DC.

Luo, Y., Su, B., Yuan, J., Li, H., Zhang, Q., 2011. GIS techniques for watershed delineation of SWAT model in plain polders. Procedia Environ. Sci. 10,

2050–2057. doi:10.1016/j.proenv.2011.09.321

Lutz, A.F., ter Maat, H.W., Biemans, H., Shrestha, A.B., Wester, P., Immerzeel, W.W., 2016. Selecting representative climate models for climate change impact studies: An advanced envelope-based selection approach. Int. J. Climatol. doi:10.1002/joc.4608

Ma, Y., Feng, S., Zhan, H., Liu, X., Su, D., Kang, S., Song, X., 2011. Water infiltration in layered soils with air entrapment : modified Green-Ampt model and experimental validation. J. Hydrol. Eng. 16, 628–638. doi:10.1061/(ASCE)HE.1943-5584.0000360.

Malone, S.L., Starr, G., Staudhammer, C.L., Ryan, M.G., 2013. Effects of simulated drought on the carbon balance of Everglades short-hydroperiod marsh. Glob. Chang. Biol. 19, 2511–2523. doi:10.1111/gcb.12211

Mansell, R.S., Bloom, S.A., Sun, G., 2000. A model for wetland hydrology: Description and validation. Soil Sci. 165, 384–397.

Markstrom, S.L., Niswonger, R.G., Regan, R.S., Prudic, D.E., Barlow, P.M., 2008. GSFLOW—Coupled groundwater and surface-water flow model based on the integration of the Precipitation-Runoff Modeling System (PRMS) and the Modular Ground-Water Flow Model (MODFLOW-2005), in: U.S. Geological Survey Techniques and Methods. U.S. Geological Survey, Virginia, p. 240.

Marsik, M., Waylen, P., 2006. An application of the distributed hydrologic model CASC2D to a tropical montane watershed. J. Hydrol. 330, 481–495. doi:10.1016/j.jhydrol.2006.04.003

Martinez-Martinez, E., Nejadhashemi, A.P., Woznicki, S.A., Love, B.J., 2014. Modeling the hydrological significance of wetland restoration scenarios. J. Environ. Manage. 133, 121–34. doi:10.1016/j.jenvman.2013.11.046

Masood, M., Takeuchi, K., 2016. Climate change impacts and its implications on future water resource management in the Meghna Basin. Futures 78–79, 1–18. doi:10.1016/j.futures.2016.03.001

Masood, M., Yeh, P.J.-F., Hanasaki, N., Takeuchi, K., 2015. Model study of the impacts of future climate change on the hydrology of Ganges-Brahmaputra-Meghna basin. Hydrol. Earth Syst. Sci. 19, 747–770. doi:10.5194/hess-19-747-2015

Maxa, M., Bolstad, P., 2009. Mapping northern wetlands with high resolution satellite images and LiDAR. Wetlands 29, 248–260.

McCarthy, G.-T., 1939. The Unit Hydrograph and Flood Routing, in: Conference North Atlantic Division. US Army Corporation of Engineers.

McCutcheon, S.C., 2003. Hydrologic evaluation of the Curve Number method for forest management in West Virginia. Charleston, West Virginia.

McDonald, M.G., Harbaugh, A.W., 1988. A modular three-dimensional finite-difference ground-water flow model, in: Book 6: Modeling Techniques, in Techniques of Water Resources Investigations of the United States Geological Survey. U.S. Geological Survey, Washington.

McIntyre, N., Al-Qurashi, A., Wheater, H., 2007. Regression analysis of rainfall–runoff data from an arid catchment in Oman. Hydrol. Sci. J. 52, 1103–1118. doi:10.1623/hysj.52.6.1103

Mein, R.G., Larson, C.L., 1973. Modelign infiltration during a steady rain. Water Resour. Res. 9, 384–394.

Mendoza-Sanchez, I., Phanikumar, M.S., Niu, J., Masoner, J.R., Cozzarelli, I.M., McGuire, J.T., 2013. Quantifying wetland–aquifer interactions in a humid subtropical climate region: An integrated approach. J. Hydrol. 498, 237–253. doi:10.1016/j.jhydrol.2013.06.022

Menon, A., Levermann, A., Schewe, J., 2013. Enhanced future variability during India's rainy season. Geophys. Res. Lett. 40, 3242–3247. doi:10.1002/grl.50583

Meselhe, E.A., Habib, E.H., Oche, O.C., Gautam, S., 2009. Sensitivity of conceptual and physically based hydrologic models to temporal and spatial rainfall sampling. J. Hydrol. Eng. 14, 711–720.

Metcalf & Eddy Inc., 1971. Storm Water Management Model, Volume I – Final Report. Washington.

Metcalfe, I., 2003. Environmental concerns for Bangladesh. South Asia J. South Asian Stud. 26, 423–438. doi:10.1080/0085640032000178961

Migliaccio, K.W., Chaubey, I., 2008. Spatial distributions and stochastic parameter influences on SWAT flow and sediment predictions. J. Hydrol. Eng. 13, 258–269. doi:10.1061/(ASCE)1084-0699(2008)13:4(258)

Miller, S.N., Semmens, D.J., Goodrich, D.C., Hernandez, M., Miller, R.C., Kepner, W.G., Guertin, D.P., 2007. The Automated Geospatial Watershed Assessment tool. Environ. Model. Softw. 22, 365–377. doi:10.1016/j.envsoft.2005.12.004

Min, J.-H., Perkins, D.B., Jawitz, J.W., 2010. Wetland-groundwater interactions in subtropical depressional wetlands. Wetlands 30, 997–1006. doi:10.1007/s13157-010-0043-9

Mirza, M.M.Q., Warrick, R. a., Ericksen, N.J., Kenny, G.J., 2001. Are floods getting worse in the Ganges, Brahmaputra and Meghna basins? Environ. Hazards 3, 37–48. doi:10.3763/ehaz.2001.0305

Mirzaee, S., Zolfaghari, A.A., Gorji, M., Dyck, M., Dashtaki, S.G., 2014. Evaluation of infiltration models with different numbers of fitting parameters in different soil texture classes. Arch. Agron. Soil Sci. 60, 681–693. doi:10.1080/03650340.2013.823477

Mishra, A., Kar, S., 2012. Modeling hydrologic processes and NPS pollution in a small watershed in subhumid subtropics using SWAT. J. Hydrol. Eng. 17, 445–454. doi:10.1061/(ASCE)HE.1943-5584.0000458.

Mishra, S.K., Kumar, S.R., Singh, V.P., 1999. Calibration and validation of a general infiltration model. Hydrol. Process. 13, 1691–1718. doi:10.1002/(SICI)1099-1085(19990815)13:11<1691::AID-HYP818>3.0.CO;2-W

Mishra, S.K., Singh, V.P., 2004. Validity and extension of the SCS-CN method for computing infiltration and rainfall-excess rates. Hydrol. Process. 18, 3323–3345. doi:10.1002/hyp.1223

Mishra, S.K., Tyagi, J. V., Singh, V.P., 2003. Comparison of infiltration models. Hydrol. Process. 17, 2629–2652. doi:10.1002/hyp.1257

Moffitt, C.B., Hossain, F., Adler, R.F., Yilmaz, K.K., Pierce, H.F., 2011. Validation of a TRMM-based global Flood Detection System in Bangladesh. Int. J. Appl. Earth Obs. Geoinf. 13, 165–177. doi:10.1016/j.jag.2010.11.003

Mohamed, Y., Savenije, H.H.G., 2014. Impact of climate variability on the hydrology of the Sudd wetland: signals derived from long term (1900-2000) water balance computations. Wetl. Ecol. Manag. 22, 191–198. doi:10.1007/s11273-014-9337-7

Molden, D., Sakthivadivel, R., Habib, Z., 2001. Basin-level use and productivity of water: Examples from South Asia. Colombo, Sri Lanka.

Monteith, J.L., 1965. Evaporation and the environment, in: The State and Movement of Water in Living Organisms. Cambridge University Press, London, pp. 205–234.

Montroull, N.B., Saurral, R.I., Camilloni, I. a., Grimson, R., Vasquez, P., 2013. Assessment of climate change on the future water levels of the Iberá wetlands, Argentina, during the twenty-first century. Int. J. River Basin Manag. 11, 401–410. doi:10.1080/15715124.2013.819807

Moriasi, D.N., Arnold, J.G., Liew, M.W. Van, Bingner, R.L., Harmel, R.D., Veith, T.L., 2007. Model evaluation guidelines for systematic quatification of accuracy in watershed simulations. Trans. ASABE 50, 885–900.

Morison, J.I.L., 1987. Intercellular CO2 concentration and stomatal response to CO2, in: Zeiger, E., Farquhar, G.D., Cowan, I.R. (Eds.), Stomatal Function. Palo Alto, CA, pp. 229–251.

MPO, 1991. Description of Groundwater Model Programs. Dhaka, Bangladesh.

Mukherjee, A., Fryar, A.E., Thomas, W.A., 2009. Geologic, geomorphic and hydrologic framework and evolution of the Bengal basin, India and Bangladesh. J. Asian Earth Sci. 34, 227–244. doi:10.1016/j.jseaes.2008.05.011

Murphy, P.N.C., Ogilvie, J., Connor, K., Arp, P. a., 2007. Mapping wetlands: A comparison of two different approaches for New Brunswick, Canada. Wetlands 27, 846–854. doi:10.1672/0277-5212(2007)27[846:MWACOT]2.0.CO;2

Murphy, P.N.C., Ogilvie, J., Meng, F., Arp, P., 2008. Stream network modelling using lidar and photogrammetric digital elevation models : a comparison and field verification. Hydrol. Process. 22, 1747–1754. doi:10.1002/hyp

Murray, S.J., Foster, P.N., Prentice, I.C., 2012. Future global water resources with respect to climate change and water withdrawals as estimated by a dynamic global vegetation model. J. Hydrol. 448–449, 14–29. doi:10.1016/j.jhydrol.2012.02.044

Mutlu, E., Chaubey, I., Hexmoor, H., Bajwa, S.G., 2008. Comparison of artificial neural network models for hydrologic predictions at multiple gauging stations in an agricultural watershed. Hydrol. Process. 22, 5097–5106. doi:10.1002/hyp

Naidu, C. V., Durgalakshmi, K., Muni Krishna, K., Ramalingeswara Rao, S., Satyanarayana, G.C., Lakshminarayana, P., Malleswara Rao, L., 2009. Is summer monsoon rainfall decreasing over India in the global warming era? J. Geophys. Res. 114, 1–16. doi:10.1029/2008JD011288

Narasimhan, B., Srinivasan, R., Bednarz, S.T., Ernst, M.R., Allen, P.M., 2010. A comprehensive modeling approach for reservoir water quality assessment and management due to point and nonpoint source pollution. Trans. ASABE 53, 1605–1617.

Nash, J.E., Sutcliffe, J. V., 1970. River flow forecasting through conceptual models. Part I: a discussion of principles. J. Hydrol. 10, 282–290.

Neitsch, S.L., Arnold, J.G., Kiniry, J.R., Williams, J.R., 2011. Soil and Water Assessment Tool, Theoretical Documentation, Version 2009. Grassland, Soil and Water Research, College Station.

Nejadhashemi, A.P., Woznicki, S.A., Douglas-Mankin, K.R., 2011. Comparison of four models (STEPL, PLOAD, L-THIA, AND SWAT) in simulating sediment, nitrogen, and phosphorus loads and pollutant source areas. Trans. ASABE 54, 875–890.

Nilsson, K.A., Ross, M.A., Trout, K.E., 2008. Analytic method to derive wetland stage-storage relationships using GIS areas. J. Hydrol. Eng. 13, 278–282.

Niraula, R., Kalin, L., Wang, R., Srivastava, P., 2012. Determining nutrient and sediment crtical source areas with SWAT: effect of lumped calibration. Trans. ASABE 55, 137–147.

Nishat, B., Rahman, S.M.M., 2009. Water resources modeling of the Ganges-Brahmaputra-Meghna River Basins using satellite remote sensing data. J. Am. Water Resour. Assoc. 45, 1313–1327. doi:10.1111/j.1752-1688.2009.00374.x

Noguchi, S., Rahim Nik, A., Kasran, B., Tani, M., Sammori, T., Morisada, K., 1997. Soil physical properties and preferential flow pathways in tropical rain forest, Bukit Tarek, Peninsular Malaysia. J. For. Res. 2, 115–120. doi:10.1007/BF02348479

Nungesser, M., Saunders, C., Coronado-Molina, C., Obeysekera, J., Johnson, J., McVoy, C., Benscoter, B., 2015. Potential effects of climate change on Florida's Everglades. Environ. Manage. 55, 824–835. doi:10.1007/s00267-014-0417-5

Nyarko, B.K., 2007. Floodplain wetland-river flow synergy in the White Volta River basin, Ghana.

O'Sullivan, J.J., Ahilan, S., Bruen, M., 2012. A modified Muskingum routing approach for floodplain flows: Theory and practice. J. Hydrol. 470–471, 239–

254. doi:10.1016/j.jhydrol.2012.09.007

Office of the Registrar General & Census Commissioner India, 2011. Population Enumeration Data (Final Population) [WWW Document]. Census India 2011. URL http://www.censusindia.gov.in/2011census/population_enumeration.aspx

Ogawa, H., Male, J.W., 1986. Simulating the flood mitigation role of wetlands. J. Water Resour. Plan. Manag. 112, 114–128. doi:10.1061/(ASCE)0733-9496(1986)112:1(114)

Ogden, F.L., Sagafian, B., 1997. Green and Ampt infiltration with redistribution. J. Irrig. Drain. Eng. 123, 386–393.

Ojha, C.S.P., Berndtsson, R., Bhunya, P., 2008. Engineering hydrology. Oxford University Press.

Oka, T., Iguchi, M., Ahmed, S.M.U., Bala, S.K., 2013. Numerical simulation of flood lake behavior in Northeastern Bangladesh [WWW Document]. URL http://www.hydro-soft.co.jp/image/report/iguchimk/iguchimk04.pdf

Oki, T., Kanae, S., 2006. Global hydrological cycles and world water resources. Science (80-.). 313, 1068–1072.

Olivera, F., Valenzuela, M., Srinivasan, R., Choi, J., Cho, H., Koka, S., Agwawal, A., 2006. ArcGIS-SWAT : A geodata model and GIS interface for SWAT. J. Am. Water Resour. Assoc. 42, 295–309.

Ouessar, M., Bruggeman, A., Abdelli, F., Mohtar, R.H., Gabriels, D., Cornelis, W.M., 2009. Modelling water-harvesting systems in the arid south of Tunisia using SWAT. Hydrol. Earth Syst. Sci. 13, 2003–2021.

Öztürk, M., Copty, N.K., Saysel, A.K., 2013. Modeling the impact of land use change on the hydrology of a rural watershed. J. Hydrol. 497, 97–109. doi:10.1016/j.jhydrol.2013.05.022

Paiva, R.C.D., Collischonn, W., Tucci, C.E.M., 2011. Large scale hydrologic and hydrodynamic modeling using limited data and a GIS based approach. J. Hydrol. 406, 170–181. doi:10.1016/j.jhydrol.2011.06.007

Palmer, M.A., Liermann, C.A.R., Nilsson, C., Flörke, M., Alcamo, J., Lake, P.S., Bond, N., 2008. Climate change and the world's river basins: anticipating management options. Front. Ecol. Environ. 6, 81–89. doi:10.1890/060148

Pan, S., Tian, H., Dangal, S.R.S., Yang, Q., Yang, J., Lu, C., Tao, B., Ren, W., Ouyang, Z., 2015. Responses of global terrestrial evapotranspiration to

climate change and increasing atmospheric CO2 in the 21st century. Earth' s Futur. 3, 15–35. doi:10.1002/2014EF000263.Received

Panday, S., Huyakorn, P.S., 2004. A fully coupled physically-based spatially-distributed model for evaluating surface/subsurface flow. Adv. Water Resour. 27, 361–382. doi:10.1016/j.advwatres.2004.02.016

Parajuli, P.B., 2012. Evaluation of spatial variability on hydrology and nutrient source loads at watershed scale using a modeling approach. Hydrol. Res. 43, 808–821. doi:10.2166/nh.2012.013

Parlange, J.-Y., 1971. Theory of water movement in soils. 2. One-dimensional infiltration. Soil Sci. 113, 170–174.

Pathiraja, S., Westra, S., Sharma, A., 2012. Why continuous simulation? The role of antecedent moisture in design flood estimation. Water Resour. Res. 48, 1–15. doi:10.1029/2011WR010997

Pattanaik, D.R., 2007. Analysis of rainfall over different homogeneous regions of India in relation to variability in westward movement frequency of monsoon depressions. Nat. Hazards 40, 635–646. doi:10.1007/s11069-006-9014-0

Paz, A.R., Bravo, J.M., Allasia, D., Collischonn, W., Tucci, C.E.M., 2010. Large-scale hydrodynamic modeling of a complex river network and floodplains. J. Hydrol. Eng. 14, 152–165.

Paz, A.R., Collischonn, W., 2007. River reach length and slope estimates for large-scale hydrological models based on a relatively high-resolution digital elevation model. J. Hydrol. 343, 127–139. doi:10.1016/j.jhydrol.2007.06.006

Pechlivanidis, I.G., Jackson, B.M., Mcintyre, N.R., Wheater, H.S., 2011. Catchment scale hydrological modelling: A review of model types, calibration approaches and uncertainty analysis methods in the context of recent developments in technology and applications. Glob. NEST J. 13, 193–214.

Penman, H.L., 1961. Weather, plant and soil factors in hydrology. Weather 16, 207–219. doi:10.1002/j.1477-8696.1961.tb01934.x

Phan, D.B., Wu, C.C., Hsieh, S.C., 2011. Impact of climate change on stream discharge and sediment yield in Northern Viet Nam. Water Resour. 38, 827–836. doi:10.1134/S0097807811060133

Philip, J.R., 1991. Hillslope infiltration: planar slopes. Water Resour. Res. 27, 109–117.

Philip, J.R., 1957. Theory of Infiltration. Soil Sci. 83, 345–357.

Pitchford, J.L., Wu, C., Lin, L., Petty, A.T., Thomas, R., Veselka, W.E., Welsch, D., Zegre, N., Anderson, J.T., 2012. Climate change effects on hydrology and ecology of wetlands in the mid-atlantic highlands. Wetlands 32, 21–33. doi:10.1007/s13157-011-0259-3

Pitman, J.I., 1989. Rainfall interception by bracken in open habitats relations between leaf area, canopy storage and drainage rate. J. Hydrol. 105, 317–334.

Plate, E.J., 2009. HESS Opinions “Classification of hydrological models for flood management.” Hydrol. Sci. J. 13, 1939–1951.

Poggio, L., Soille, P., 2011. A probabilistic approach to river network detection in digital elevation models. Catena 87, 341–350. doi:10.1016/j.catena.2011.07.001

Pohlert, T., Huisman, J.A., Breuer, L., Freude, H.-G., 2007. Integration of a detailed biogeochemical model into SWAT for improved nitrogen predictions—Model development, sensitivity, and GLUE analysis. Ecol. Modell. 203, 215–228.

Poiani, K.A., Johnson, W.C., 1993. A spatial simulation model of hydrology and vegetation dynamics in semi-permanent prairie wetlands. Ecol. Appl. 3, 279–293.

Pokhrel, Y., Hanasaki, N., Koirala, S., Cho, J., Yeh, P.J.-F., Kim, H., Kanae, S., Oki, T., 2012. Incorporating anthropogenic water regulation modules into a land surface model. J. Hydrometeorol. 13, 255–269. doi:10.1175/JHM-D-11-013.1

Ponce, V.M., 1996. Engineering Hydrology: Principles and Practices. Prentice Hall.

Ponce, V.M., Hawkins, R.H., 1996. Runoff curve number: Has it reached maturity? J. Hydrol. Eng. 1, 11–19.

Popescu, I., Cioaca, E., Pan, Q., Jonoski, A., Hanganu, J., 2015. Use of hydrodynamic models for the management of the Danube Delta wetlands : The case study of Sontea-Fortuna ecosystem. Environ. Sci. Policy 46, 48–56.

Powell, S.J., Letcher, R.A., Croke, B.F.W., 2008. Modelling floodplain inundation for environmental flows: Gwydir wetlands, Australia. Ecol. Modell. 211, 350–362. doi:10.1016/j.ecolmodel.2007.09.013

Priestley, C.H.B., Taylor, R.J., 1972. On the assessment of surface heat flux and evaporation using large-scale parameters. Mon. Weather Rev. 100, 81–92.

Putty, M.R.Y., 2009. Curve-Number-Based watershed model incorporating quick subsurface runoff, with applications in the Western Ghats, South India. J. Hydrol. Eng. 14, 876–881.

Pyzoha, J.E., Callahan, T.J., Sun, G., Trettin, C.C., Miwa, M., 2008. A conceptual hydrologic model for a forested Carolina bay depressional wetland on the Coastal Plain of South Carolina, USA. Hydrol. Process. 22, 2689–2698. doi:10.1002/hyp

Qi, Y., Qian, C., Yan, Z., 2017. An alternative multi-model ensemble mean approach for near-term projection. Int. J. Climatol. 37, 109–122. doi:10.1002/joc.4690

Quinton, W.L., Roulet, N.T., 1998. Spring and summer runoff hydrology of a subarctic patterned wetland. Arctic, Antarct. Alp. Rsearch 30, 285–294.

Raghunath, H.M., 2006. Hydrology. New Age International (P) Ltd., New Delhi.

Rahman, M.M., 2011. Application of SWAT for impact analysis of subsurface drainage on streamflows in a snow dominated watershed. North Dakota State University.

Rahman, M.M., Arya, D.S., Goel, N.K., 2010. Limitation of 90 m SRTM DEM in drainage network delineation using D8 method—a case study in flat terrain of Bangladesh. Appl. Geomatics 2, 49–58. doi:10.1007/s12518-010-0020-2

Rahman, M.M., Lin, Z., Jia, X., Steele, D.D., DeSutter, T.M., 2014. Impact of subsurface drainage on streamflows in the Red River of the North basin. J. Hydrol. 511, 474–483. doi:10.1016/j.jhydrol.2014.01.070

Rahman, M.M., Singh Arya, D., Goel, N.K., Mitra, A.K., 2012. Rainfall statistics evaluation of ECMWF model and TRMM data over Bangladesh for flood related studies. Meteorol. Appl. 19, 501–512. doi:10.1002/met.293

Rahman, M.M., Thompson, J.R., Flower, R.J., 2016. An enhanced SWAT wetland module to quantify hydraulic interactions between riparian depressional wetlands, rivers and aquifers. Environ. Model. Softw. 84, 263–289. doi:10.1016/j.envsoft.2016.07.003

Rahman, R., Haque, A., Khan, S.A., Salehin, M., Bala, S.K., 2005. Investigation of hydrological aspects of flood-2004 with special emphasis on Dhaka City. Dhaka, Bangladesh.

Ramsar Convention Secretariat, 2013. The Ramsar Convention Manual: a guide to the Convention on Wetlands (Ramsar, Iran, 1971), 6th ed. Ramsar Convention Secretariat, Gland, Switzerland.

Raneesh, K.Y., Thampi Santosh, G., 2011. A study on the impact of climate change on streamflow at the watershed scale in the humid tropics. Hydrol. Sci. J. 56, 946–965. doi:10.1080/02626667.2011.595371

Rao, M., Fan, G., Thomas, J., Cherian, G., Chudiwale, V., Awawdeh, M., 2007. A web-based GIS Decision Support System for managing and planning USDA's Conservation Reserve Program (CRP). Environ. Model. Softw. 22, 1270–1280. doi:10.1016/j.envsoft.2006.08.003

Rashid, M.M., Beecham, S., Chowdhury, R.K., 2015. Statistical downscaling of CMIP5 outputs for projecting future changes in rainfall in the Onkaparinga catchment. Sci. Total Environ. 530–531, 171–182. doi:10.1016/j.scitotenv.2015.05.024

Reclamation, 2013. Downscaled CMIP3 and CMIP5 climate projections: Release of downscaled CMIP5 climate projections, comparison with preceding information, and summary of user needs. Denver, Colorado.

Refsgaard, J.C., 1996. Terminology, modelling protocol and classification of hydrological model codes, in: Abott, M.B., Refsgaard, J.C. (Eds.), Distributed Hydrological Modelling. Springer Netherlands, pp. 17–39.

Refsgaard, J.C., Storm, B., 1995. MIKE SHE, in: Singh, V.. (Ed.), Computer Models of Watershed Hydrology. Water Resources Publications, LLC, Highlands Ranch, pp. 809–846.

Restrepo, J.I., Montoya, A.M., Obeysekera, J., 1998. A wetland simulation module for the MODFLOW ground water model. Groundwater 36, 764–770.

Reusser, D.E., Blume, T., Schaefli, B., Zehe, E., 2009. Analysing the temporal dynamics of model performance for hydrological models. Hydrol. Earth Syst. Sci. 13, 999–1018. doi:10.5194/hess-13-999-2009

Reusser, D.E., Buytaert, W., Zehe, E., 2011. Temporal dynamics of model parameter sensitivity for computationally expensive models with the Fourier amplitude sensitivity test. Water Resour. Res. 47. doi:10.1029/2010WR009947

Reusser, D.E., Zehe, E., 2011. Inferring model structural deficits by analyzing temporal dynamics of model performance and parameter sensitivity. Water

Resour. Res. 47, 1–15. doi:10.1029/2010WR009946

Revadekar, J. V., Patwardhan, S.K., Rupa Kumar, K., 2011. Characteristic features of precipitation extremes over India in the warming scenarios. Adv. Meteorol. 2011, 1–11. doi:10.1155/2011/138425

Rezaeianzadeh, M., Stein, a., Tabari, H., Abghari, H., Jalalkamali, N., Hosseinipour, E.Z., Singh, V.P., 2013. Assessment of a conceptual hydrological model and artificial neural networks for daily outflows forecasting. Int. J. Environ. Sci. Technol. 10, 1181–1192. doi:10.1007/s13762-013-0209-0

Richards, L.A., 1931. Capillary conduction of liquids through porous mediums. J. Appl. Phys. 1, 318–333. doi:10.1063/1.1745010

Rochester, R.E., 2010. Uncertainty in hydrological modelling: A case study in the Tern Catchment, Shropshire, UK. University College London (UCL).

Rojas, R., Julien, P., Johnson, B., 2003. A 2-dimensional rainfall-runoff and sediment model. Colorado State University, USA, Fort Collins, Colorado.

Ross, M.A., Tara, P.D., Geurink, J.S., Stewart, M.T., 1997. FIPR hydrologic model users manual and technical documentation. Tampa, Florida.

Rostamian, R., Jaleh, A., Afyuni, M., Mousavi, S.F., Heidarpour, M., Jalalian, A., Abbaspour, K.C., 2008. Application of a SWAT model for estimating runoff and sediment in two mountainous basins in central Iran. Hydrol. Sci. J. 53, 997–988.

Rousseau, M., Cerdan, O., Delestre, O., Dupros, F., James, F., Cordier, S., 2012. Overland flow modelling with the Shallow Water Equation using a well balanced numerical scheme : Adding efficiency or just more complexity ?

Rozalis, S., Morin, E., Yair, Y., Price, C., 2010. Flash flood prediction using an uncalibrated hydrological model and radar rainfall data in a Mediterranean watershed under changing hydrological conditions. J. Hydrol. 394, 245–255. doi:10.1016/j.jhydrol.2010.03.021

RRCAP, 2001. State of the Envirionment Report: Bangladesh 2001. Klong Luang.

Rutter, A.A.J., Morton, A.J., Robins, P.C., 1975. A predictive model of interception in forests. 2. Generalization of the model and comparison with observations in some coniferous and hardwood stands. J. Appl. Ecol. 12, 367–380.

Rutter, A.J., Kershaw, K.A., Robins, P.C., Morton, A.J., 1971. A predictive model

of rainfall interception in forests: 1. Derivation of the model from observation in a plantation of Corsican pine. Agric. Meteorol. 9, 367–384.

Saleh, A., Du, B., 2004. Evaluation of SWAT and HSPF within BASINS program for the upper north Bosque River watershed in central Texas. Trans. ASABE 47, 1039–1050.

Saleh, A., Gallego, O., 2007. Application of SWAT and APEX using the SWAPP (SWAT-APEX) program for the Upper North Bosque River Watershed in Texas. Trans. ASABE 50, 1177–1187.

Saleh, F., Ducharne, a., Flipo, N., Oudin, L., Ledoux, E., 2013. Impact of river bed morphology on discharge and water levels simulated by a 1D Saint–Venant hydraulic model at regional scale. J. Hydrol. 476, 169–177. doi:10.1016/j.jhydrol.2012.10.027

Saxton, K.E., Willey, P.H., 2005. The SPAW model for a agricultural field and pond hydrologic simulation, in: Frevert, D.K., Singh, V.P. (Eds.), Watershed Models. CRC Press, pp. 400–435. doi:10.1201/9781420037432.ch17

Schaefli, B., Gupta, H. V, 2007. Do Nash values have value ? Hydrol. Process. 21, 2075–2080. doi:10.1002/hyp

Scharffenberg, W.A., 2013. Hydrologic modeling system HEC-HMS, user's manual. Washington.

Schneider, C., Laizé, C.L.R., Acreman, M.C., Flörke, M., 2013. How will climate change modify river flow regimes in Europe? Hydrol. Earth Syst. Sci. 17, 325–339. doi:10.5194/hess-17-325-2013

Schroeder, R., McDonald, K.C., Chan, S.K., Chapman, B., Podest, E., Bohn, T.J., Jones, L.A., Kimball, J., Zimmermann, R., Kppers, M., 2012. Development and Evaluation of a Global Wetland Data Record Derived from Combined Active/Passive Microwave Remote Sensing Data.

Shamsudduha, M., 2010. Groundwater dynamics and arsenic mobilisation in Bangladesh: a national-scale characterisation. University College London (UCL).

Sharma, P.K., Pantuwan, G., Ingram, K.T., De Datta, S.K., 1994. Rainfed low land rice roots:soil and hydrological effects, in: Kirk, G.J.D. (Ed.), Rice Roots:nutrient and Water Use. IRRI, Laguna, Philippines, pp. 55–66.

Sharpley, A.N., Williams, J.R., 1990. EPIC-Erosion Productivity Impact Calculator, 1. Model Documentation.

Sherwood, D.B., 2009. Community –Based wetland comanagement in Bangladesh, in: Moore, K.M. (Ed.), The Sciences and Art of Adaptive Management: Innovating for Sustainable Agriculture and Natural Resource Management. Soil and Water Conservation Society, Ankeny, IA.

Shi, X.Z., Yu, D.S., Warner, E.D., Pan, X.Z., Petersen, G.W., Gong, Z.G., Weindorf, D.C., 2004. Soil database of 1:1,000,000 Digital Soil Survey and Reference System of the Chinese Genetic Soil Classification System. Soil Surv. Horizons 45, 129–136.

Shih, D., Yeh, G., 2011. Identified model parameterization , calibration , and validation of the physically distributed hydrological model WASH123D in Taiwan. J. Hydrol. Eng. 16, 126–136.

Singh, C.R., 2010. Hydrological and hydraulic modelling for the restoration and management of Loktak Lake, northeast India. University College London (UCL).

Singh, C.R., Thompson, J.R., French, J.R., Kingston, D.G., Mackay, a. W., 2010. Modelling the impact of prescribed global warming on runoff from headwater catchments of the Irrawaddy River and their implications for the water level regime of Loktak Lake, northeast India. Hydrol. Earth Syst. Sci. 14, 1745–1765. doi:10.5194/hess-14-1745-2010

Singh, J., Knapp, H.V., Arnold, J.G., Demissie, M., 2005. Hydrological modeling of the Iroquois River watershed using HSPF and SWAT. J. Am. Water Resour. Assoc. 41, 343–360.

Singh, J., Knapp, H.V., Demissie, M., 2004. Hydrologic Modeling of the Iroquois River Watershed Using HSPF and SWAT.

Singh, V.., 1995. Watershed modeling, in: Singh, V.P. (Ed.), Computer Models of Watershed Hydrology. Water Resources Publications, LLC, Highlands Ranch.

Singh, V.P., 1988. Hydrologic Systems. Prentice Hall, Eaglewood Cliffs, NJ, USA.

Singh, V.P., Woolhiser, D. a., 2002. Mathematical modeling of watershed hydrology. J. Hydrol. Eng. 7, 270–292. doi:10.1061/(ASCE)1084-0699(2002)7:4(270)

Singh, H. V, Kalin, L., Asce, M., Srivastava, P., 2011. Effect of soil data resolution on identification of critical source areas of sediment. J. Hydrol. Eng. 16, 253–262. doi:10.1061/(ASCE)HE

Sloan, P.G., Moore, I.D., 1984. Modeling subsurface streamflow on steeply sloping forested watersheds. Water Resour. Res. 20, 1815–1822.

Sloan, P.G., Morre, I.D., Coltharp, G.B., Eigel, J.D., 1983. Modeling surface and subsurface streamflow on steeply-sloping forested watersheds. Lexignton.

Smith, R.D., Ammann, A., Bartoldus, C., Brinson, M.M., 1995. An approach for assessing wetland functions using hydrogeomorphic classifications, referene wetlands, and functional indices. Washington.

Smith, R.E., Parlange, J.-Y., 1978. A parameter-efficient hydrologic infiltration model. Water Resour. Res. 14, 533–538.

Sombroek, W.G., 1984. Towards a global soil resources inventory at scale 1:1 Million: discussion paper.

Song, X., Duan, Z., Kono, Y., Wang, M., 2011. Integration of remotely sensed C factor into SWAT for modelling sediment yield. Hydrol. Process. 25, 3387–3398. doi:10.1002/hyp.8066

Song, X., Zhan, C., Kong, F., Xia, J., 2011. Advances in the study of uncertainty quantification of large-scale hydrological modeling system. J. Geogr. Sci. 21, 801–819. doi:10.1007/s11442-011-0881-2

Sood, A., Mathukumalli, B.K.P., 2011. Managing international river basins: reviewing India–Bangladesh transboundary water issues. Int. J. River Basin Manag. 9, 43–52. doi:10.1080/15715124.2011.553832

Sophocleous, M., 2004. Global and regional water availability and demand : prospects for the future. Nat. Resour. Res. 13, 61–75. doi:10.1023/B:NARR.0000032644.16734.f5

Sophocleous, M., 2002. Interactions between groundwater and surface water: the state of the science. Hydrogeol. J. 10, 52–67.

Sophocleous, M.A., Koelliker, J.K., Govindaraju, R.S., Birdie, T., Ramireddygari, S.R., Perkins, S.P., 1999. Integrated numerical modeling for basin-wide water management: The case of the Rattlesnake Creek basin in south-central Kansas. J. Hydrol. 214, 179–196. doi:10.1016/S0022-1694(98)00289-3

Soulis, K.X., Valiantzas, J.D., Dercas, N., Londra, P.A., 2009. Analysis of the runo ff generation mechanism for the investigation of the SCS-CN method applicability to a partial area experimental watershed. Hydrol. Earth Syst. Sci. 6, 373–400.

Spruill, C.A., Workman, S.R., Taraba, J.L., 2000. Simulation of daily and monthly stream discharge from small watersheds usingtThe SWAT model. Trans. ASABE 43, 1431–1439.

Srinivasan, R., Arnold, J.G., 1994. Integration of a basin-scale water quality model with GIS. Water Resour. Bull. 30, 453–462.

Steinschneider, S., Yang, Y.-C.E., Brown, C., 2015. Combining regression and spatial proximity for catchment model regionalization: a comparative study. Hydrol. Sci. J. 60, 1026–1043. doi:10.1080/02626667.2014.899701

Sterling, S.M., Ducharne, A., Polcher, J., 2013. The impact of global land-cover change on the terrestrial water cycle. Nat. Clim. Chang. 3, 385–390. doi:10.1038/nclimate1690

Stisen, S., Jensen, K.H., Sandholt, I., Grimes, D.I.F., 2008. A remote sensing driven distributed hydrological model of the Senegal River basin. J. Hydrol. 354, 131–148. doi:10.1016/j.jhydrol.2008.03.006

Strzepek, K., McCluskey, A., Boehlert, B., Jacobsen, M., Fant IV, C., 2011. Climate variability and change: A basin scale indicator approach to understanding the risk to water resources development and management, World Bank. Washington DC.

Sulis, M., Paniconi, C., Marrocu, M., Huard, D., Chaumont, D., 2012. Hydrologic response to multimodel climate output using a physically based model of groundwater/surface water interactions. Water Resour. Res. 48, 1–18. doi:10.1029/2012WR012304

Sun, G., Callahan, T., Pyzoha, J.E., Trettin, C.C., Amatya, D.M., 2004. Modeling the hydrologic processes of a depressional forested wetland in South Carolina, U.S.A., in: Altinakar, M.S., Wang, S.S.Y., Holz, K.P., Kawahara, M. (Eds.), 6th International Conf. on Hydro-Science and Engineering. Brisbane, Australia, pp. 331–332.

Sun, G., Riekerk, H., Comerford, N.B., 1998. Modeling the hydrologic impacts of forest harvesting on florida FLATWOODS. J. Am. Water Resour. Assoc. 34, 843–854.

Sun, X., Bernard-Jannin, L., Garneau, C., Volk, M., Arnold, J.G., Srinivasan, R., Sauvage, S., Sánchez-Pérez, J.M., 2015. Improved simulation of river water and groundwater exchange in an alluvial plain using the SWAT model. Hydrol. Process. doi:10.1002/hyp.10575

Swain, E.D., Wexler, E.J., 1996. A coupled surface-water and ground-water flow model (MODBRANCH) for simulation of stream-aquifer interaction, in: Techniques of Water-Resource Investigation. U.S. Geological Survey.

Tang, J., Li, Q., Wang, S., Lee, D.K., Hui, P., Niu, X., Gutowski, W.J., Dairaku, K., Mcgregor, J., Katzfey, J., Gao, X., Wu, J., Hong, S.-Y., Wang, Y., Sasaki, H., 2016. Building Asian climate change scenario by multi-regional climate models ensemble. Part I: surface air temperature. Int. J. Climatol. doi:10.1002/joc.4628

Tang, Q., Lettenmaier, D.P., 2012. 21st century runoff sensitivities of major global river basins. Geophys. Res. Lett. 39, 1–5. doi:10.1029/2011GL050834

Taylor, K.E., Stouffer, R.J., Meehl, G.A., 2012. An overview of CMIP5 and the experiment design. Bull. Am. Meteorol. Soc. 93, 485–498. doi:10.1175/BAMS-D-11-00094.1

Tedela, N.H., Mccutcheon, S.C., Asce, M., Rasmussen, T.C., Hawkins, R.H., Asce, F., Swank, W.T., Campbell, J.L., Adams, M.B., Jackson, C.R., Tollner, E.W., 2012. Runoff curve numbers for 10 small forested watersheds in the mountains of the Eastern United States 17, 1188–1198. doi:10.1061/(ASCE)HE

TEEBcase by P. Thompson and T. Balasinorwala, 2010. Wetland management and conservation , Hail Haor, Bangladesh.

Thompson, J., 2004. Simulation of wetland water-level manipulation using coupled hydrological/hydraulic modeling. Phys. Geogr. 25, 39–67. doi:10.2747/0272-3646.25.1.39

Thompson, J.R., Crawley, A., Kingston, D.G., 2015. GCM-related uncertainty for river flows and inundation under climate change: the Inner Niger Delta. Hydrol. Sci. J. 61, 2325–2347. doi:10.1080/02626667.2015.1117173

Thompson, J.R., Gavin, H., Refsgaard, A., Sørenson, H.R., Gowing, D.J., 2009. Modelling the hydrological impacts of climate change on UK lowland wet grassland. Wetl. Ecol. Manag. 17, 503–523. doi:10.1007/s11273-008-9127-1

Thompson, J.R., Green, A.J., Kingston, D.G., 2014a. Potential evapotranspiration-related uncertainty in climate change impacts on river flow: An assessment for the Mekong River basin. J. Hydrol. 510, 259–279. doi:10.1016/j.jhydrol.2013.12.010

Thompson, J.R., Green, A.J., Kingston, D.G., Gosling, S.N., 2013. Assessment of uncertainty in river flow projections for the Mekong River using multiple GCMs and hydrological models. J. Hydrol. 486, 1–30. doi:10.1016/j.jhydrol.2013.01.029

Thompson, J.R., Laizé, C.L.R., Green, a. J., Acreman, M.C., Kingston, D.G., 2014b. Climate change uncertainty in environmental flows for the Mekong River. Hydrol. Sci. J. 59, 935–954. doi:10.1080/02626667.2013.842074

Thompson, J.R., Sørenson, H.R., Gavin, H., Refsgaard, a., 2004. Application of the coupled MIKE SHE/MIKE 11 modelling system to a lowland wet grassland in southeast England. J. Hydrol. 293, 151–179. doi:10.1016/j.jhydrol.2004.01.017

Thompson, P.M., 2014. Conserving and restoring the benefits from Bangladesh wetlands [WWW Document]. URL http://iasc2008.glos.ac.uk/conference papers/papers/T/Thompson_220701.pdf

Todini, E., 1988. Rainfall-runoff modeling-Past, present and future. J. Hydrol. 100, 341–352.

Townsend, P.A., Walsh, S.J., 2001. Remote sensing of forested wetlands: application of multitemporal and multispectral satellite imagery to determine plant community composition and structure in southeastern USA. Plant Ecol. 157, 129–149.

Trzaska, S., Schnarr, E., 2014. A review of downscaling methods for climate change projections. Burlington, Vermont, USA.

Tucker, G.E., Lancaster, S.T., Gasparini, N.M., Bras, R.L., Rybarczyk, S.M., 2001. An object-oriented framework for distributed hydrologic and geomorphic modeling using triangulated irregular networks. Comput. Geosci. 27, 959–973. doi:10.1016/S0098-3004(00)00134-5

Tuppad, P., Winchell, M.F., X.Wang, Srinivasan, R., Williams, J.R., 2009. ArcAPEX: ArcGIS interface for Agricultural Policy Environmental Extender (APEX) hydrology/water quality model. Int. Agric. Eng. J. 18, 59–71.

Turner, A.G., Annamalai, H., 2012. Climate change and the South Asian summer monsoon. Nat. Clim. Chang. 2, 587–595. doi:10.1038/NCLIMATE1495

Turner, E.R., 2006. Comparison of infiltration equations and their field validation with rainfall simulation. University of Maryland.

Uddin, M.J., Mohiuddin, A.S.M., Kamal, A.T.M.M., Hossain, M.A., 2012. The

Agricultural potentiality of some wetland soils under Sylhet Basin of Bangladesh. Dhaka Univ. J. Biol. Sci. 21, 39–46. doi:10.3329/dujbs.v21i1.9743

Uddin, M.R., Wade, L.J., Pyon, J.Y., Mazid, M.A., 2009. Rooting behavior of rice cultivars under different planting methods. J. Crop Sci. Biotechology 12, 17–24.

UN Water, 2014a. UN-Water thematic factsheets: water and disasters [WWW Document]. URL http://www.unwater.org/fileadmin/user_upload/unwater_new/docs/water_disasters.pdf

UN Water, 2014b. UN-Water thematic factsheets: water scarcity [WWW Document]. URL http://www.unwater.org/fileadmin/user_upload/unwater_new/docs/water_scarcity.pdf

UNESCO, 2013. Free flow - reaching water security through cooperation. United Nations Educational, Scientific and Cultural Organization, Paris, France.

USDA, 2004. Estimation of direct runoff from storm rainfall, in: National Engineering Handbook, Part 630: Hydrology. USDA, Washington.

van Griensven, A., Bauwens, W., 2005. Application and evaluation of ESWAT on the Dender basin and Wister Lake basin. Hydrol. Process. 19, 827–838.

van Griensven, A., Ndomba, P., Yalew, S., Kilonzo, F., 2012. Critical review of the application of SWAT in the upper Nile Basin countries. Hydrol. Earth Syst. Sci. Discuss. 16, 3761–3788. doi:10.5194/hessd-9-3761-2012

Vazquez-Amábile, G.G., Engel, B.A., 2005. Use of SWAT to compute groundwater table depth and streamflow in the Muscatatuck river watershed. Trans. ASABE 48, 991–1003.

Vegas Galdos, F., Álvarez, C., García, A., Revilla, J.A., 2012. Estimated distributed rainfall interception using a simple conceptual model and Moderate Resolution Imaging Spectroradiometer (MODIS). J. Hydrol. 468–469, 213–228. doi:10.1016/j.jhydrol.2012.08.043

Vivoni, E.R., Ivanov, V.Y., Bras, R.L., Entekhabi, D., 2004. Generation of Triangulated Irregular Networks based on hydrological similarity. J. Hydrol. Eng. 9, 288–302.

Voinov, A.A., Fitz, H.C., Costanza, R., 1998. Surface water flow in landscape

models : 1 . Everglades case study. Ecol. Modell. 108, 131–144.

Voldseth, R.A., Johnson, W.C., Gilmanov, T., Guntenspergen, G.R., Millett, B. V, 2007. Model estimation of land-use effects on water levels of northern prairie wetlands. Ecol. Appl. 17, 527–540.

Volk, M., Arnold, J.G., Bosch, D.D., Allen, P.M., Green, C.H., 2007. Watershed configuration and simulation of landscape processes with the SWAT model, in: Oxley, L., Kulasiri, D. (Eds.), IMODSIM 2007: Intl. Congress on Modelling and Simulation. Modelling and Simulation Society of Australia and New Zealand, pp. 2383–2389.

Wagner, P.D., Kumar, S., Fiener, P., Schneider, K., 2011. Hydrological modeling with SWAT in a monsoon-driven environment: Experience from the Western Ghats, India. Trans. ASABE 54, 1783–1790.

Walton, R., Chapman, R.S., Davis, J.E., 1996. Development and application of the wetlands Dynamic Water Budget Model. Wetlands 16, 347–357. doi:10.1007/BF03161325

Wang, M., Qin, D., Lu, C., Li, Y., 2010. Modeling anthropogenic impacts and hydrological processes on a wetland in China. Water Resour. Manag. 24, 2743–2757. doi:10.1007/s11269-010-9577-0

Wang, X., Shang, S., Qu, Z., Liu, T., Melesse, A.M., Yang, W., 2010. Simulated wetland conservation-restoration effects on water quantity and quality at watershed scale. J. Environ. Manage. 91, 1511–1525. doi:10.1016/j.jenvman.2010.02.023

Wang, X., Yang, W., Melesse, A.M., 2008. Using hydrologic equivalent wetland concept within SWAT to estimate streamflow in watersheds with numerous wetlands. Trans. ASABE 51, 55–72. doi:10.13031/2013.24227

WARPO, 2001. National Water Management Plan. Dhaka, Bangladesh.

WARPO, 2000. National Water Management Plan (NWMP). Dhaka, Bangladesh.

Watson, B.M., McKeown, R.A., Putz, G., MacDonald, J.D., 2008. Modification of SWAT for modelling streamflow from forested watersheds on the Canadian Boreal Plain. J. Environ. Eng. Sci. 7, 145–159. doi:10.1139/S09-003

Weill, S., Mouche, E., Patin, J., 2009. A generalized Richards equation for surface/subsurface flow modelling. J. Hydrol. 366, 9–20. doi:10.1016/j.jhydrol.2008.12.007

Wen, L., Macdonald, R., Morrison, T., Hameed, T., Saintilan, N., Ling, J., 2013.

From hydrodynamic to hydrological modelling: Investigating long-term hydrological regimes of key wetlands in the Macquarie Marshes, a semi-arid lowland floodplain in Australia. J. Hydrol. 500, 45–61. doi:10.1016/j.jhydrol.2013.07.015

Werner, A.T., Cannon, A.J., 2016. Hydrologic extremes – an intercomparison of multiple gridded statistical downscaling methods. Hydrol. Earth Syst. Sci. Discuss. 20, 1483–1508. doi:10.5194/hessd-12-6179-2015

White, E.D., Easton, Z.M., Fuka, D.R., Steenhuis, T.S., 2009. SWAT-WB User Manual.

Wilby, R.L., Abrahart, R.J., Dawson, C.W., 2003. Detection of conceptual model rainfall—runoff processes inside an artificial neural network. Hydrol. Sci. J. 48, 163–181. doi:10.1623/hysj.48.2.163.44699

Williams, J.R., Jones, C.A., Dyke, P.T., 1984. A modeling approach to determining the relationship between erosion and soil productivity. Trans. ASAE 27, 129–144.

Willmott, C.J., 1981. On the validation of models. Phys. Geogr. 2, 184–194.

Willmott, C.J., Robeson, S.M., Matsuura, K., 2012. A refined index of model performance. Int. J. Climatol. 32, 2088–2094. doi:10.1002/joc.2419

Wilsnack, M.M., Welter, D.E., Montoya, A.M., Rest, J.I., Obeysekera, J., 2001. Simulating flow in regional wetlands with the MODFLOW wetlands package. J. Am. Water Resour. Assoc. 37, 655–674.

Wohl, E., Barros, A., Brunsell, N., Chappell, N.A., Coe, M., Giambelluca, T., Goldsmith, S., Harmon, R., Hendrickx, J.M.H., Juvik, J., Mcdonnell, J., 2012. The hydrology of the humid tropics. Nat. Clim. Chang. 2, 655–662. doi:10.1038/NCLIMATE1556

Wong, T.S.W., 2006. Physically based approach in hydrology — what is the benefit ? J. Hydrol. Eng. 11, 293–295.

Woolhiser, D.A., Smith, R.E., Goodrich, D.C., 1990. KINEROS, a kinematic runoff and erosion model: documentation and User manual.

Workman, S.R., Skaggs, R.W., 1990. PREFLO: A water management model capable of simulating preferential flow. Trans. ASABE 33, 1939–1948.

World Bank, 2013. Turn down the heat: climate extremes, regional impacts, and the case of resilience. Washington DC.

Wu, C.L., Shukla, S., Shrestha, N.K., 2016. Evapotranspiration from drained

wetlands with different hydrologic regimes: Drivers, modeling, and storage functions. J. Hydrol. 538, 416–428. doi:10.1016/j.jhydrol.2016.04.027

Wu, H., Kimball, J.S., Li, H., Huang, M., Leung, L.R., Adler, R.F., 2012. A new global river network database for macroscale hydrologic modeling. Water Resour. Res. 48, 1–5. doi:10.1029/2012WR012313

Wu, K., Johnston, C.A., 2008. Hydrologic comparison between a forested and a wetland / lake dominated watershed using SWAT. Hydrol. Process. 22, 1431–1442. doi:10.1002/hyp

Wu, L., Long, T., Liu, X., Guo, J., 2012. Impacts of climate and land-use changes on the migration of non-point source nitrogen and phosphorus during rainfall-runoff in the Jialing River Watershed, China. J. Hydrol. 475, 26–41. doi:10.1016/j.jhydrol.2012.08.022

Wu, P., Christidis, N., Stott, P., 2013. Anthropogenic impact on Earth ' s hydrological cycle. Nat. Clim. Chang. 1–4. doi:10.1038/NCLIMATE1932

Xie, X., Cui, Y., 2011. Development and test of SWAT for modeling hydrological processes in irrigation districts with paddy rice. J. Hydrol. 396, 61–71. doi:10.1016/j.jhydrol.2010.10.032

Xu, C., 2002. Text Book of Hydrlogic Models. Uppsala University, Department of Earth Sciences Hydrology.

Yamazaki, D., Kanae, S., Kim, H., Oki, T., 2011. A physically based description of floodplain inundation dynamics in a global river routing model. Water Resour. Res. 47, 1–21. doi:10.1029/2010WR009726

Yang, Y.E., Yu, W., Brown, C.M., Savitsky, A., 2011. Sustainable water management in the major basins of South Asia, in: American Geophysical Union, Fall Meeting 2011. American Geophysical Union, San francisco, California, USA.

Yeh, G.-T., Cheng, H.-P., Cheng, J.-R., 1998. A numerical model simulating flow, contaminant, and sediment transport in watershed systems (WASH12D).

Yeh, G.-T., Shih, D.-S., Cheng, J.-R.C., 2011. An integrated media, integrated processes watershed model. Comput. Fluids 45, 2–13. doi:10.1016/j.compfluid.2010.11.018

Young, R.A., Onstad, C.A., Bosch, D.D., Anderson, W.P., 1989. AGNPS: a non-point source pollution model for evaluating agricultural watersheds. J. Soil Water Conserv. 44, 168–173.

Yu, Z., Schwartz, F.W., 1998. Application of an integrated basin-scale hydrologic model to simulate surface-water and ground-water interactions. J. Am. Water Resour. Assoc. 34, 409–425.

Zaslavsky, D., Sinai, G., 1981. Surface hydrology 3: Causes of lateral flow.

Zevenbergen, C., van Herk, S., Rijke, J., Kabat, P., Bloemen, P., Ashley, R., Speers, A., Gersonius, B., Veerbeek, W., 2013. Taming global flood disasters. Lessons learned from Dutch experience. Nat. Hazards 65, 1217–1225. doi:10.1007/s11069-012-0439-3

Zhang, B., Tang, J.L., Gao, C., Zepp, H., 2011. Subsurface lateral flow from hillslope and its contribution to nitrate loading in streams through an agricultural catchment during subtropical rainstorm events. Hydrol. Earth Syst. Sci. 15, 3153–3170. doi:10.5194/hess-15-3153-2011

Zhang, J.L., Li, Y.P., Huang, G.H., 2014. A robust simulation-optimization modeling system for effluent trading-a case study of nonpoint source pollution control. Environ. Sci. Pollut. Res. Int. 21, 5036–5053. doi:10.1007/s11356-013-2437-8

Zhang, L., Mitsch, W.J., 2005. Modelling hydrological processes in created freshwater wetlands: An integrated system approach. Environ. Model. Softw. 20, 935–946. doi:10.1016/j.envsoft.2004.03.020

Zhao, L., Xia, J., Xu, C., Wang, Z., Sobkowiak, L., Long, C., 2013. Evapotranspiration estimation methods in hydrological models. J. Geogr. Sci. 23, 359–369. doi:10.1007/s11442-013-1015-9

Zhu, Q., Zhang, X., Ma, C., Gao, C., Xu, Y.-P., 2016. Investigating the uncertainty and transferability of parameters in SWAT model under climate change. Hydrol. Sci. J. 61, 914–930. doi:10.1080/02626667.2014.1000915

Zi, T., Kumar, M., Kiely, G., Lewis, C., Albertson, J., 2016. Simulating the spatio-temporal dynamics of soil erosion, deposition, and yield using a coupled sediment dynamics and 3D distributed hydrologic model. Environ. Model. Softw. 83, 310–325. doi:10.1016/j.envsoft.2016.06.004

Appendices

A.1. Monthly rainfall (mm) for each of 28 gauging stations/grids used in the model.

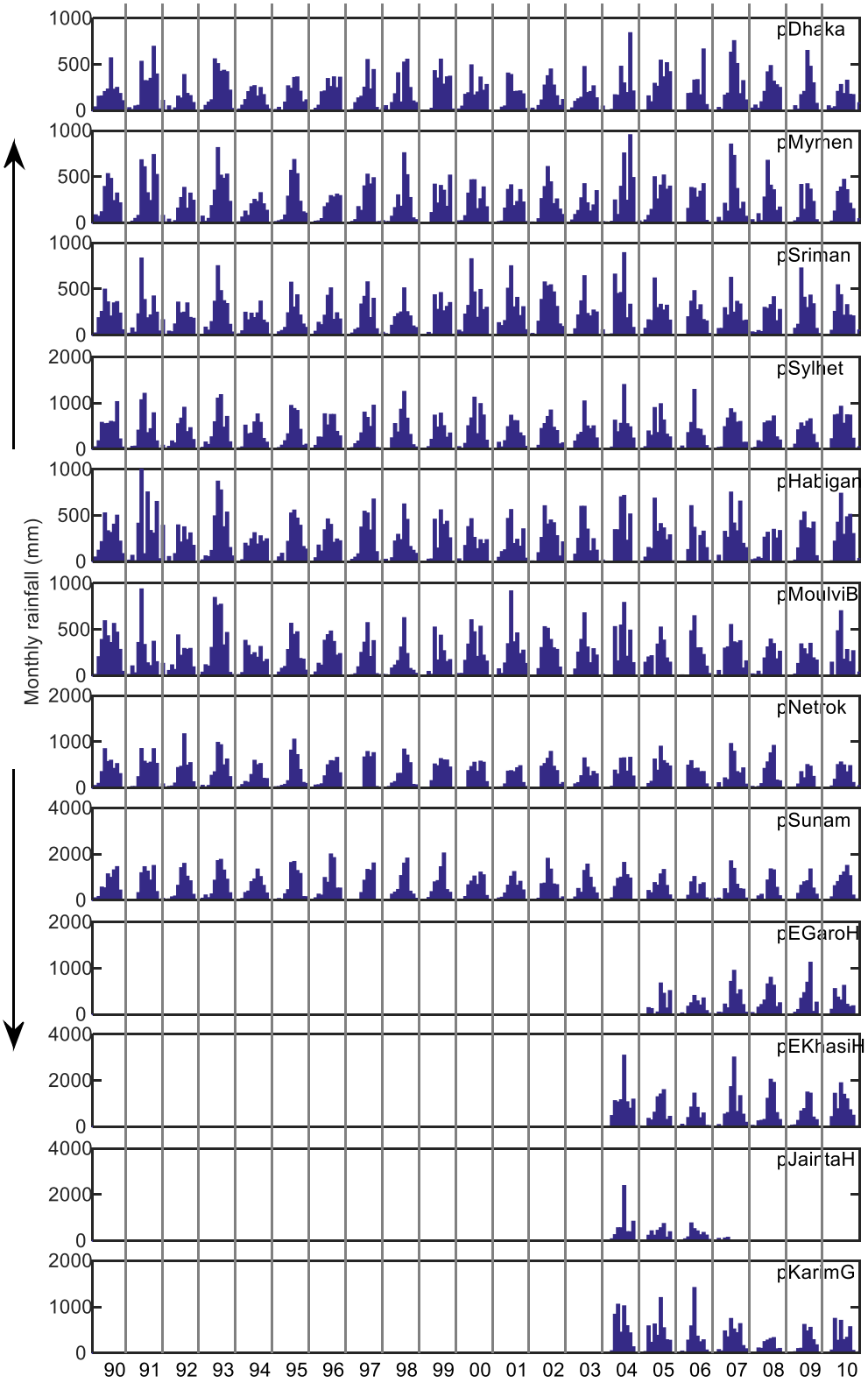

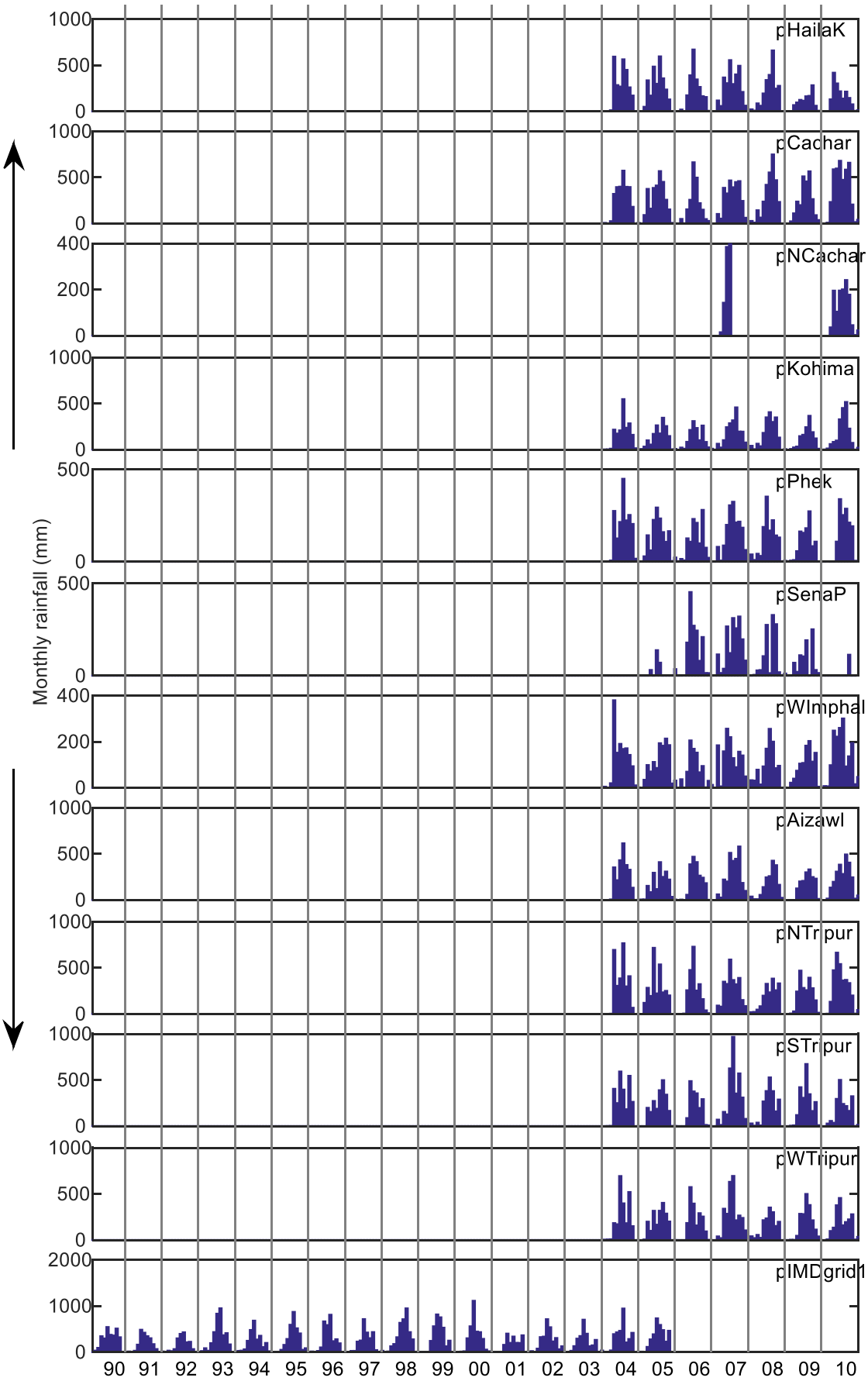
Monthly rainfall (mm)
pHailaK
pCachar
pNCachar
pKohima
pPhek
pSenaP
pWImphal
pAizawl
pNTripur
pSTripur
pWTripur
pIMDgrid1
90 91 92 93 94 95 96 97 98 99 00 01 02 03 04 05 06 07 08 09 10

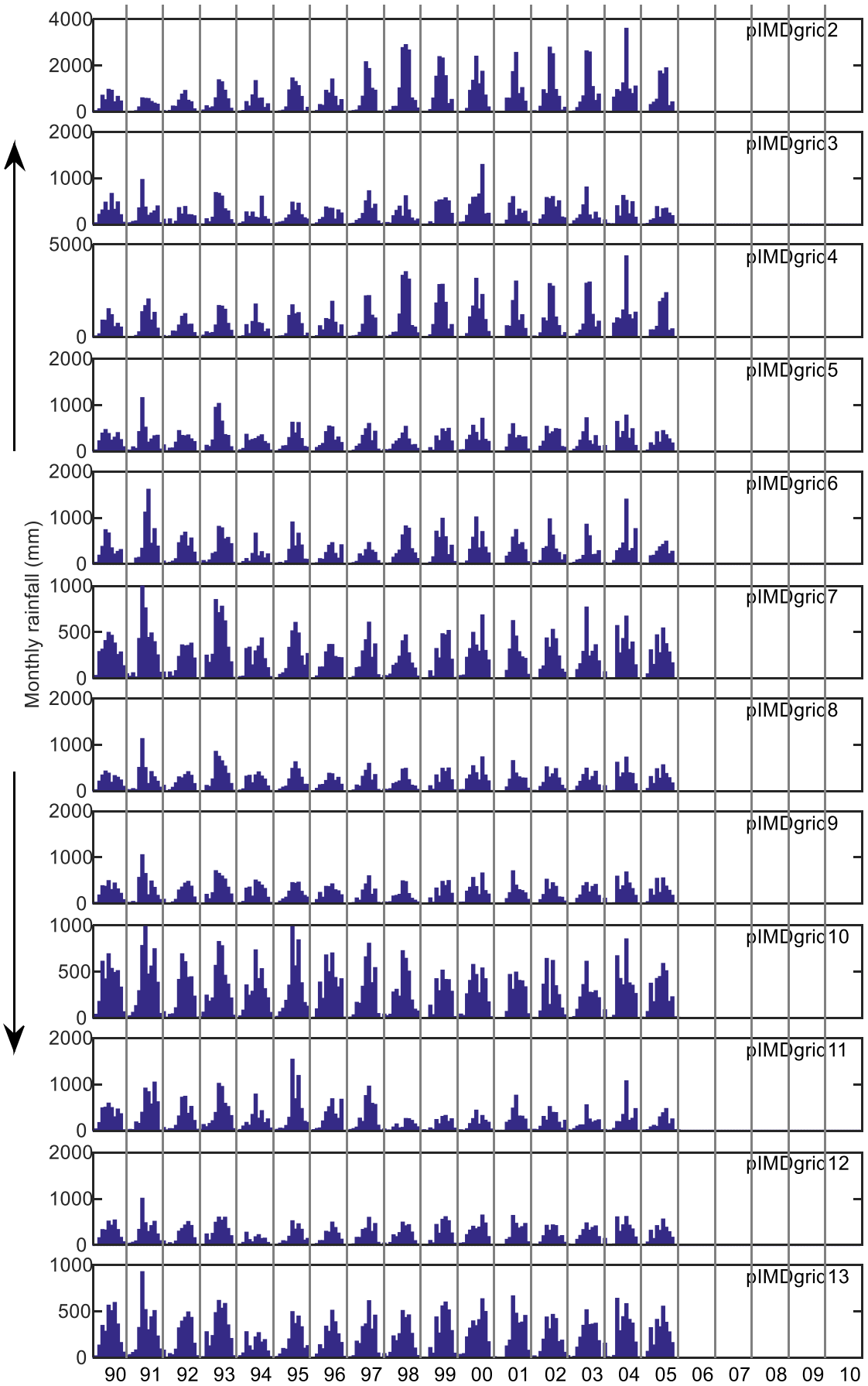
Monthly rainfall (mm)
pIMDgrid2
pIMDgrid3
pIMDgrid4
pIMDgrid5
pIMDgrid6
pIMDgrid7
pIMDgrid8
pIMDgrid9
pIMDgrid10
pIMDgrid11
pIMDgrid12
pIMDgrid13
90 91 92 93 94 95 96 97 98 99 00 01 02 03 04 05 06 07 08 09 10

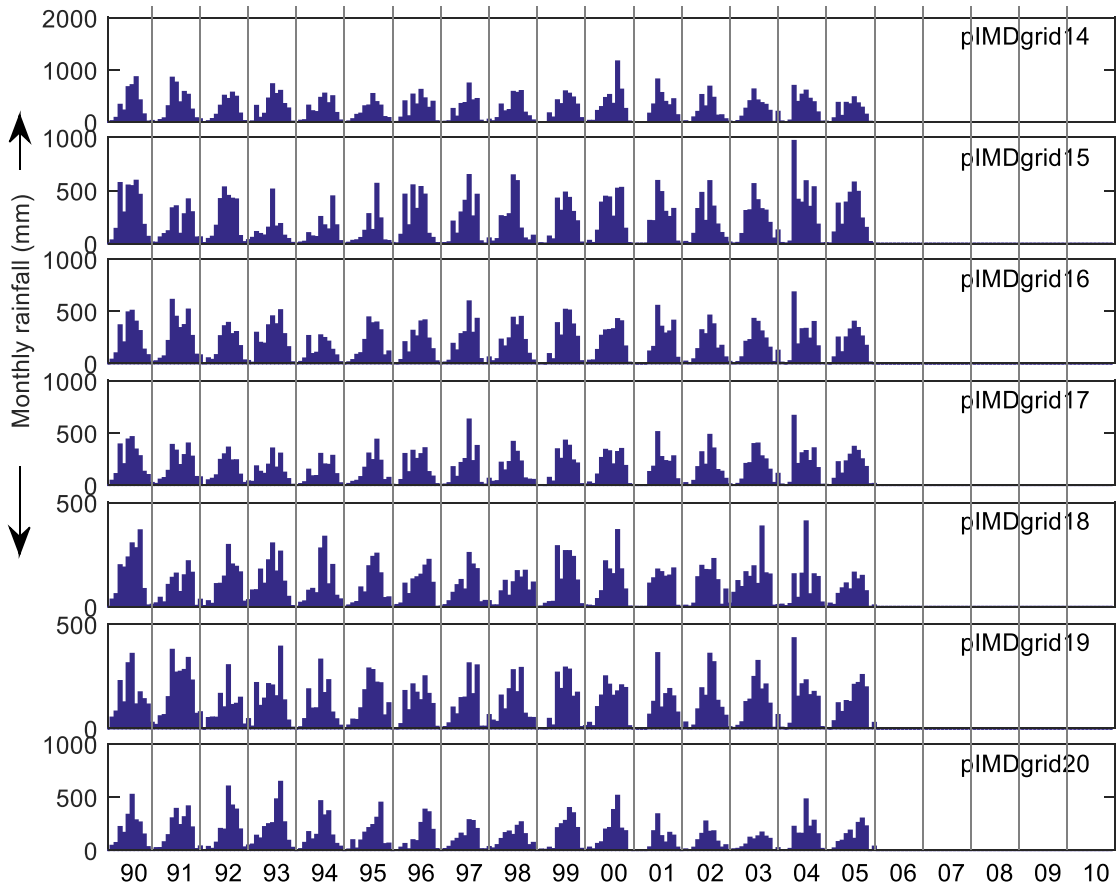
Monthly rainfall (mm)
pIMDgrid14
pIMDgrid15
pIMDgrid16
pIMDgrid17
pIMDgrid18
pIMDgrid19
pIMDgrid20
2000
1000
0
1000
500
0
1000
500
0
1000
500
0
500
0
500
0
1000
500
0
90 91 92 93 94 95 96 97 98 99 00 01 02 03 04 05 06 07 08 09 10